

Transportation
Kentucky Transportation Center Research
Report

University of Kentucky

Year 1991

Bearing Capacity Analysis of Pavements

Tommy C. Hopkins
University of Kentucky

**Research Report
KTC-91-8**

**BEARING CAPACITY ANALYSIS
OF
PAVEMENTS**

by

TOMMY C. HOPKINS

Chief Research Engineer
and
Head of Geotechnology

Kentucky Transportation Center
College of Engineering
University of Kentucky

in cooperation with
Transportation Cabinet
Commonwealth of Kentucky

and

Federal Highway Administration
U.S. Department of Transportation

The contents of this report reflect the views of the author, who is responsible for the facts and accuracy of the data presented herein. The contents do not necessarily reflect the official views or policies of the University of Kentucky, the Kentucky Transportation Cabinet, nor the Federal Highway Administration. This report does not constitute a standard, specification, or regulation.

June 1991
(Reprint October 1998)

1. Report No. KTC-91-8		2. Government Accession No.		3. Recipient's Catalog No.	
4. Title and Subtitle <i>Bearing Capacity Analysis of Pavements</i>				5. Report Date February 28, 1995	
				6. Performing Organization Code	
7. Author(s) Tommy C. Hopkins				8. Performing Organization Report No. KTC-91-8	
9. Performing Organization Name and Address Kentucky Transportation Center College of Engineering University of Kentucky Lexington, KY 40506-0043				10. Work Unit No. (TRAIS)	
				11. Contract or Grant No. KYHPR-88-121	
12. Sponsoring Agency Name and Address Kentucky Transportation Cabinet State Office Building				13. Type of Report and Period Covered Final Report	
				14. Sponsoring Agency Code	
15. Supplementary Notes Prepared in cooperation with the Federal Highway Administration, US Department of Transportation.					
16. Abstract A multilayered, mathematical model for analyzing the ultimate bearing capacity of soil subgrades and asphalt pavements is presented. Theoretical considerations and mathematical derivations of limit equilibrium equations, based on plasticity principles, for analyzing the ultimate bearing capacity of soil subgrades and partially completed asphalt pavements, and the extension of these equations to the analyses of asphalt pavements composed of multiple layers, are presented. The model is unique since shear strength parameters, ϕ and c , (the angle of internal friction and cohesion, respectively) are used to describe each layer of material of the pavement structure and a factor of safety against failure is calculated. Problems involving total stress and effective stress analyses may be solved using the new model. Theoretical derivations of the shear surface selected for the model analyses is presented. The theoretical failure mass consists of three failure zones -- active and passive wedges connected by a central wedge whose shear surface is a logarithmic spiral curve. Credibility of the model is established by solving three classes of pavement bearing capacity problems. Bearing capacity factors, N_e , N_q , and N_γ , are computed from the new theoretical model and compared to the classical bearing capacity factors (Prandtl). Solutions obtained from a two-layered, semi-empirical formula described by Vesic are compared to solutions obtained from the new mathematical model. Finally, factors of safety of asphalt pavements that failed during construction are analyzed. Factors of safety obtained from the model are compared to the failure factor of safety. These different analyses and comparisons show that the new model yields very reasonable solutions. Additionally, factors of safety of some 237 pavement sections of Loops 3, 4, 5, and 6 of the AASHO Road Test (1962) are computed and correlated to weighted, 18-kip, ESAL applications ($P = 2.0$). Analyses of the AASHO (flexible pavement) Road Test Equation (1962) and the 1981 Kentucky asphalt pavement curves using the new model show that there are situations where these design methods may yield pavement designs that may fail. Analyses of soil subgrades under typical construction traffic loadings using the model show that subgrade CBR-values should be in the range of about 6 to 8.5 to avoid bearing capacity failures during construction of subgrades and pavements. Several deficiencies of current design methods are identified and recommendations are made to correct these design and construction deficiencies.					
17. Key Words Safety Factors, Plasticity, Theory, Soils, Bearing Capacity, Stability, Asphalt, Design, Pavements, Correlations, Model, Construction			18. Distribution Statement Unlimited, with approval of the Kentucky Transportation Cabinet.		
19. Security Classif. (of this report)		20. Security Classif. (of this page)		21. No. of Pages 244	
				22. Price	



COMMONWEALTH OF KENTUCKY

TRANSPORTATION CABINET

FRANKFORT, KENTUCKY 40622

DON C. KELLY, P.E.
SECRETARY OF TRANSPORTATION

BRERETON C. JONES
GOVERNOR

JERRY D. ANGLIN
DEPUTY SECRETARY
AND
COMMISSIONER OF HIGHWAYS

February 28, 1995

Mr. Paul E. Toussaint
Division Administrator
Federal Highway Administration
330 West Broadway
Frankfort, Kentucky 40602-0526

Dear Mr. Toussaint:

SUBJECT: Implementation Statement: Research Study KYHPR 88-121,
Bearing Capacity Analysis of Pavements

This study originated from a desire to investigate what was considered premature failures of soil subgrades and resultant failure in flexible pavements during and shortly after completion of construction.

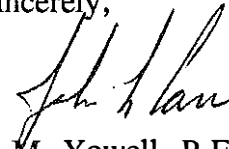
The study resulted in the development of a multilayered, mathematical model based on limited equilibrium (theory of plasticity) for analyzing the ultimate bearing capacity of soil subgrades and asphalt pavements. This complex model was programmed for a main frame computer. Practitioners having knowledge of geotechnical and pavement principles can use the bearing capacity program. Data entry and use of the program have been simplified as much as possible. Results obtained from the program are reasonably close to results obtained from classical bearing theory and other published theoretical solutions. Case studies involving failure of pavements and subgrades have been analyzed.

The model appears to have great potential for predicting the potential for premature flexible pavement failures related to soil bearing capacity during construction. With some adaptation, the program may be implemented by pavement design staff. The necessary revisions and modifications to the program for successful implementation by pavement design staff will be accomplished during the early phases of a newly funded research study: "Stresses in Highway Pavement Subgrades and Relationships Among Resilient Modulus and Soil Indices".

Pavement design, construction procedures, and conditions potentially contributing to premature failures of soil subgrades and subsequent failures of flexible pavements have been identified. Analyses using the newly developed model show that when the CBR-strength of a soil subgrade is six or lower, the subgrade is unstable under construction vehicular loading (tire contact stress equal to or greater than about 80 pounds per square inch). The subgrade should be stabilized, in this case. This important finding and recommendation has been implemented during the course of this study. Generally, this analysis has contributed to the current practice of stabilizing all subgrade soils with a soil CBR of six or less. Methods of stabilization include using either chemical admixtures or using mechanical methods.

In conclusion, the study has addressed the basic objectives of the study. Additional analyses are needed for calibration of these predictive models before full scale implementation can be accomplished. These calibrations will be accomplished during the course of work for the newly funded study: "Stress in Highway Pavement Subgrades and Relationships Among Resilient Modulus and Soil Indices".

Sincerely,


for J. M. Yowell, P.E.
State Highway Engineer

JMY:WRM:dkh

TABLE OF CONTENTS

LIST OF FIGURES	ix
LIST OF TABLES	xxi
EXECUTIVE SUMMARY	xxii
INTRODUCTION	1
Problem	1
Objectives	3
Scope	4
BACKGROUND	5
Plasticity and Elasticity Approaches	6
Principle of Effective Stress	9
Temperature of Asphalt Pavement	13
Geologic Setting and Soil Types	15
Physical Properties	18
<i>Compaction</i>	18
<i>Swelling</i>	20
<i>Moisture</i>	23
MATHEMATICAL MODEL EQUATIONS	24
Statical Indeterminacy	24
Basic Assumptions	25
Theoretical Equations	26
<i>Geometry</i>	28
<i>Definitions</i>	29
<i>Derivations</i>	31
<i>Solution of Equations</i>	39
Classes of Bearing Capacity Analysis	47
Shear Surface	48
<i>One, Homogeneous Layer</i>	48
<i>Multilayered Bearing Medium</i>	54

REASONABLENESS OF SOLUTIONS 59

Homogeneous Bearing Medium	59
Classical Bearing Capacity Equations and Factors	59
Bearing Capacity Factors -- HOPKIB Computer Model	61
Comparisons	63
Scenario 1 -- N_c - Bearing Capacity Factor	63
Scenario 2 -- N_q - Bearing Capacity Factor	66
Scenario 3 -- N_γ - Bearing Capacity Factor	68
Proposed methods	68
Theoretical comparisons	71
Experimental comparisons	71
Scenario 4--Combined Bearing Capacity Factors (N_c+N_γ)	81
Scenario 5--Combined Bearing Capacity Factors (N_q+N_γ)	83
Scenario 6--Combined Bearing Capacity Factors ($N_c+N_q+N_\gamma$)	85
Minimum subgrade strength	87
Undrained Shear Strength	87
CBR Bearing Strength - Theoretical	87
CBR Bearing Strength - Field Studies	96
Dynamic Modulus of Elasticity	99
Dynamic Cone Penetrometer Strengths	100
Two-Layered Problems	101
Typical Construction Situations and Analytical Approaches	101
Construction of Granular Bases	104
Subgrades Treated with Chemical Admixtures	108
Vesic's Method	108
Thompson's Approach (1988)	111
"Full-Depth[®]" Asphaltic Pavements	112

MULTILAYERED PAVEMENT ANALYSES--CASE STUDIES 122

Alexandria-Ashland Highway -- Sections 13 and 14	122
Site Conditions	122
Soils and Geology	122
Field Testing	124
Laboratory Shear Strengths	127
Analyses and Results	128
Great River Road -- State Route KY 94	131
Site Conditions	131
Soils and Geology	133
Field Study and Sampling	134

Laboratory Shear Strengths	134
Analyses and Results	136
Metropolitan City Streets	140
Analyses of Two Flexible Pavement Design Systems	143
1981 Kentucky Pavement Design Curves	143
AASHO Road Test -- Factors of Safety	147
<i>Subgrade Soils</i>	148
<i>Index properties</i>	148
<i>Bearing strengths</i>	148
<i>Analyses and Results</i>	150
<i>Factors of safety</i>	150
<i>Influence of the magnitude of contact tire stresses</i>	161
AASHO Road Test Equation -- Flexible Pavement	163
<i>Sensitivity of Stability to Changes in Subgrade Bearing Strength</i>	166
Critical Design Choices	166
Selection of Subgrade Strength	166
Subgrade Modification	174
Structural Credit of Modified Subgrades	174
 SUMMARY AND CONCLUSIONS	 182
 RECOMMENDATIONS AND IMPLEMENTATION	 186
 REFERENCES	 187
 APPENDIX A	 193

List of Figures

Figure 1.	<i>Stress as a Function of Strain-Elasticity Approach</i>	6
Figure 2.	<i>Stress as a Function of Strain-Plasticity Approach</i>	7
Figure 3.	<i>Comparison of Plasticity and Elasticity Approaches</i>	8
Figure 4.	<i>Shear Strength, c, of an Asphalt Pavement as a Function of Temperature</i>	8
Figure 5.	<i>Definition of Mobilized Shear Strength Parameters, ϕ_m, and c_m</i>	9
Figure 6.	<i>Variation of Temperature of an Asphalt Pavement and Unit Tire Contact Stress for Selected Values of Factor of Safety</i>	16
Figure 7.	<i>Exposure of Soil Subgrades to Flowing Water in a Granular Base</i>	17
Figure 8.	<i>Suggested Methods for Preventing the Contact of Water in a Granular Base with the Soil Subgrade.</i> <i>a) Partially encapsulated subgrade.</i> <i>b) Completely encapsulated subgrade</i>	19
Figure 9.	<i>Statistical Overview of the Types of Soils Located in Kentucky (Source: Kentucky Geotechnical Data Bank)</i>	20
Figure 10.	<i>Comparison of Soaked and Unsoaked Values of Kentucky CBR (KYCBR)</i>	21
Figure 11.	<i>Comparison of Soaked and Unsoaked Values of KYCBR for a Number of Selected, Typical Kentucky Shales</i>	22
Figure 12.	<i>Variation of Soaked and Unsoaked Values of KYCBR with Vertical Swell Measured During the KYCBR Test for Selected Kentucky Shales</i>	23
Figure 13.	<i>Relationships Between KYCBR Values and the Percent Finer than the 0.002-mm Size for Selected Kentucky Shales</i>	23
Figure 14.	<i>Division of Potential Failure Mass into Slices</i>	27
Figure 15.	<i>Forces Acting on Slice i</i>	27
Figure 16.	<i>Coordinate System</i>	28
Figure 17.	<i>Projections of the Forces dN and dS When $\theta > 0$ and $\theta < 0$</i>	30

Figure 18.	<i>Projections of Tensile Element Forces Acting at the Base of Slice i When $\theta > 0$ and $\theta < 0$..</i>	31
Figure 19.	<i>Relationship Between dx and dl ..</i>	33
Figure 20.	<i>Scheme for Estimating the Force, dW_b, for a Multilayered Bearing Medium ..</i>	40
Figure 21.	<i>Method for Describing Distributed Loads ..</i>	42
Figure 22.	<i>Scheme for Treating Distributed Loads ..</i>	43
Figure 23.	<i>Assumed Failure Pattern and Block Movements ..</i>	49
Figure 24.	<i>Entry and Exit Angles for a Homogeneous Bearing Media ..</i>	49
Figure 25.	<i>Geometric Quantities Defining the Shape of the Shear Surface in a Homogeneous Bearing Media ..</i>	51
Figure 26.	<i>Division of Theoretical Failure Mass into a Number of Slices and Method of Computing the Width of Each Slice ..</i>	52
Figure 27.	<i>Assumed Shear Surface of the Active Wedge in a Multilayered Bearing Media ..</i>	55
Figure 28.	<i>Assumed Shear Surface of the Passive Wedge in a Multilayered Bearing Media ..</i>	55
Figure 29.	<i>Method for Estimating the Effective Value of ϕ_{eff} ..</i>	56
Figure 30.	<i>Bearing Capacity of a Shallow Footing ..</i>	60
Figure 31.	<i>Bearing Capacity Factors as a Function of the Angle of Internal Friction ..</i>	61
Figure 32.	<i>Comparisons of the Bearing Capacity Factors, N_c, Obtained from the HOPKIB Model, Prandtl's Theory (1926), and Terzaghi's Method for a Range of ϕ Values ..</i>	63
Figure 33.	<i>Comparisons of the Ratios of the Bearing Capacity Factors, N_c, from the HOPKIB Model and Terzaghi's Method to N_c Values from Prandtl's Theory for a Range of ϕ Values ..</i>	64
Figure 34.	<i>Factors of Safety Obtained When Values of N_c from Terzaghi's Method and Prandtl's Theory are Inserted into the HOPKIB Model ..</i>	65
Figure 35.	<i>Comparisons of the Bearing Capacity Factors, N_q, Obtained</i>	

	<i>from the HOPKIB Model, Prandtl's Theory (1926), and Terzaghi's (1943) Method for a Range of ϕ Values</i>	65
Figure 36.	<i>Comparisons of the Ratios of the Bearing Capacity Factors, N_q, from the HOPKIB Model and Terzaghi's Method to N_q Values from Prandtl's Theory for a Range of ϕ Values</i>	66
Figure 37.	<i>Factors of Safety Obtained When Values of N_q, from Terzaghi's Method and Prandtl's Theory are Inserted into the HOPKIB Model</i>	67
Figure 38.	<i>Variations of the Bearing Capacity Factor, N_q, with Factor of Safety When ϕ Equals 35 Degrees</i>	67
Figure 39.	<i>Variations of Terzaghi's Values of the Coefficient of Passive Earth Pressure, K_{pp}, and ϕ</i>	69
Figure 40.	<i>Comparisons of N_γ Values Proposed by Terzaghi, Vesic', Caquot and Kerisel, and HOPKIB Model</i>	70
Figure 41.	<i>Comparisons of N_γ Values Proposed by Feda, deMello, and the HOPKIB Model</i>	73
Figure 42.	<i>Ratios of N_γ Values Proposed by Caquot and Kerisel, Terzaghi, and the HOPKIB Model to N_γ Values Proposed by Vesic' (c.f. 1975 Winterhorn and Fang)</i>	73
Figure 43.	<i>Ratios of N_γ Values Proposed by deMello, Feda, and the HOPKIB Model to N_γ Values Proposed by Vesic'</i>	74
Figure 44.	<i>Variation of the Factors of Safety with ϕ When N_γ Values Proposed by Terzaghi, Vesic', and Caquot and Kerisel are Used in the HOPKIB Model</i>	74
Figure 45.	<i>Variation of the Factors of Safety With ϕ When N_γ Values Proposed by Feda and deMello are Used in the HOPKIB Model</i>	75
Figure 46.	<i>Comparisons of the N_γ Factors from the HOPKIB Model, Terzaghi's, Vesic's, and Caquot and Kerisel's Methods and Experimental Values of N_γ Determined by DeBeer and Ladanyi (1961) from Model Footing Tests</i>	75
Figure 47.	<i>Variations of the Ratios of N_γ Bearing Capacity Factors Proposed by Terzaghi (1943); Vesic' (c.f. 1975 Winterhorn and Fang); Caquot and Kerisel (1961); and the HOPKIB Model to Experimental N_γ-Bearing Capacity Factors Obtained by DeBeer and Ladanyi (1961); as a Function of ϕ, the Angle of Internal Friction</i>	76
Figure 48.	<i>Variations of the Ratios of N_γ Bearing Capacity Factors Proposed by Feda</i>	

	<i>(1961); deMello (1969); and the HOPKIB Model to Experimental Values Obtained by DeBeer and Ladanyi (1961) as a Function of ϕ</i>	77
Figure 49.	<i>Comparison of $N\gamma$ Values from the HOPKIB Model and Experimental $N\gamma$ Values Obtained by Vesic' Using Rectangular Model Footings</i>	77
Figure 50.	<i>Comparison of $N\gamma$ Factors Proposed by Terzaghi, Vesic', Caquot and Kerisel, and the HOPKIB Model to $N\gamma$ Factors Determined Experimental by Vesic' Using Rectangular Model Footings</i>	78
Figure 51.	<i>Comparison of the $N\gamma$ Factors Obtained from the HOPKIB Model, Terzaghi's, Vesic's, and Caquot and Kerisel's Methods to Experimental $N\gamma$ factors Determined by Vesic's Circular, Model Footing Tests</i>	80
Figure 52.	<i>Comparisons of $N\gamma$ Factors (Corrected According to Shape of Footing) Obtained by DeBeer and Ladanyi (1961) and Vesic' (c.f. Lambe and Whitman (1969) from Model Footing Tests and $N\gamma$ Factors Proposed by Caquot and Kerisel (1953) and $N\gamma$ Factors from the HOPKIB Model</i>	81
Figure 53.	<i>Ratios of $N\gamma$ Factors Obtained from the HOPKIB Model and Caquot and Kerisel's Method to Experimental $N\gamma$ factors from Model Footing Tests</i>	82
Figure 54.	<i>Factors of Safety Obtained from the HOPKIB Model When Experimental Values of $N\gamma$--Corrected According to Shape-- Reported by DeBeer and Ladanyi, and Vesic' and Theoretical $N\gamma$ Values Reported by Caquot and Kerisel are Inserted into the HOPKIB Model</i>	82
Figure 55.	<i>Comparisons of $N_{c\gamma}$ (Sum of $N_c + N_{c\gamma}$) Proposed by Prandtl (N_c) and Vesic' ($N\gamma$) and $N\gamma$ Values Obtained from the HOPKIB Model</i>	84
Figure 56.	<i>Ratios of $N_{c\gamma}$ Factors from the HOPKIB Model to $N_{c\gamma}$ Factors from Prandtl's and Vesic's Equations</i>	84
Figure 57.	<i>Comparison of $N_{q\gamma}$ Factors ($N_q + N_{q\gamma}$) Obtained from the HOPKIB Model and $N_{q\gamma}$ Factors from Prandtl's and Vesic's Equations</i>	85
Figure 58.	<i>Ratios of $N_{q\gamma}$ Factors from the HOPKIB Model to $N_{q\gamma}$ Values Obtained from Prandtl's and Vesic's Equations</i>	85
Figure 59.	<i>Comparison of $N_{cq\gamma}$ Factors (Sum of N_c, N_q, and $N_{q\gamma}$) Obtained from the HOPKIB Model and $N_{cq\gamma}$ Values from Prandtl's and Vesic's Equations</i>	86

Figure 60.	<i>Ratios of the $N_{c_{qy}}$ Factors Obtained from the HOPKIB Model to $N_{c_{qy}}$ Factors Obtained from Prandtl's and Vesic' Equations</i>	86
Figure 61.	<i>Relationship Between Subgrade Undrained Shear Strength and Contact Tire Stress Obtained from the HOPKIB Model for a Factor of Safety Equal to 1.0</i>	88
Figure 62.	<i>Relationship Between Subgrade Undrained Shear Strength and Contact Tire Stress Obtained from the HOPKIB Model for a Factor of Safety Equal to 1.5</i> . . .	88
Figure 63.	<i>Theoretical Failure Pattern in the CBR Test</i>	89
Figure 64.	<i>Relationship Between CBR and Cohesion Based on S_c Equal to 1</i>	91
Figure 65.	<i>Variations of Dry Density and Undrained Shear Strength With Molding Water Content</i>	93
Figure 66.	<i>Variation of Dry Density and CBR With Molding Water Content</i>	94
Figure 67.	<i>Comparison of the Results of Silty Clay Tests and the CBR-Cohesion Relationship</i>	95
Figure 68.	<i>Relationship Between Subgrade CBR Strength and Tire Contact Stress Obtained from the HOPKIB Model at a Factor of Safety Equal to 1.0</i>	95
Figure 69.	<i>Relationship Between Subgrade CBR Strength and Contact Tire Stress Obtained from the HOPKIB Model at a Factor of Safety Equal to 1.5</i>	96
Figure 70.	<i>Soil Strength - Sinkage Relations for a 9-Kip Wheel Load (after Thompson, 1988)</i>	97
Figure 71.	<i>Relationship Between Subgrade CBR Strengths and Tire Sinkage for Tire Inflation Pressures Ranging from 50 to 80 psi (Data from Thompson 1988)</i> 97	
Figure 72.	<i>Tire Sinkage Compared to Factor of Safety</i>	98
Figure 73.	<i>Factor of Safety Obtained from the HOPKIB Model as a Function of Tire Sinkage</i>	98
Figure 74.	<i>Variation of the Dynamic Modulus of Elasticity and Contact Tire Stress Obtained from the HOPKIB Model at a Factor of Safety Equal to 1.5</i>	99
Figure 75.	<i>Relationship Between Dynamic Modulus of Elasticity and Contact Tire Stress Obtained from the HOPKIB Model at a Factor of Safety Equal to 1.0</i> . . .	99

Figure 76.	<i>Relationship Between the Dynamic Modulus of Elasticity and Contact Tire Stress Obtained from the HOPKIB Model at a Factor of Safety Equal to 1.5</i> . .	100
Figure 77.	<i>CBR as a Function of Dynamic Cone Penetrometer Values (DCP--after Thompson 1988 and Techion-Israel)</i>	101
Figure 78.	<i>Relationship Between Dynamic Cone Penetrometer (DCP) Value and Contact Tire Stress, T_c, Established from the HOPKIB Model for a Factor of Safety of 1.0</i>	101
Figure 79.	<i>Relationship Between Dynamic Cone Penetrometer (DCP) Value and Contact Stress, T_c, Established from the HOPKIB Model for a Factor of Safety of 1.5</i>	102
Figure 80.	<i>Three Pavement Situations Involving Two Layers of Different Materials.</i> a) <i>Granular Layer Resting on a Subgrade.</i> b) <i>Chemically Treated Layer Resting on a Subgrade.</i> c) <i>"Full-Depth[®]" Asphalt Bearing Directly on the Subgrade</i>	103
Figure 81.	<i>Problems that May Occur During the Construction of Pavements on Weak, Soft Subgrades</i>	104
Figure 82.	<i>Variation of the Thickness of a Granular Layer With Undrained Shear Strength f a Clayey Subgrade for Factors of Safety Equal to 1.0 and 1.5</i>	105
Figure 83.	<i>Relationship Between Thickness of Granular Base and CBR for Factors of Safety Equal to 1.0 and 1.5</i>	105
Figure 84.	<i>Comparisons of Thicknesses Obtained from Vesic's Method and the HOPKIB for a Factor of Safety of 1.5</i>	107
Figure 85.	<i>Comparison of Factors of Safety Obtained from the HOPKIB Model and Vesic's Approach for a Range of Values of CBR</i>	107
Figure 86.	<i>Required Thickness of Chemically Treated Subgrade and Granular Layer as a Function of Subgrade CBR (Data from Thompson 1988)</i>	111
Figure 87.	<i>Comparisons of Treated Subgrade Thicknesses Obtained from the HOPKIB Model, Vesic's Approach, and Thompson's Method.</i> a) <i>Factor of Safety Equals 1.25</i> b) <i>Factor of Safety Equals 1.5</i>	113
Figure 88.	<i>Arrangement of Triaxial Equipment Used to Test Asphalt Core Samples</i>	114
Figure 89.	<i>Close-Up View of Triaxial Chamber and Coiled Copper Tubing Used to Control Temperature of Asphalt Core</i>	114

Figure 90.	<i>Typical Results Obtained from Unconsolidated-Undrained Triaxial Compression Tests of Asphalt Core Specimen</i>	115
Figure 91.	<i>Cohesion of Asphalt Cores as a Function of Temperature</i>	116
Figure 92.	<i>Angle of Internal Friction, ϕ, of Asphalt Cores as a Function of Temperature</i>	116
Figure 93.	<i>Mechanical Behavior of Asphaltic-Granular Matrix at Low and High Temperatures</i>	117
Figure 94.	<i>Factor of Safety Obtained from the HOPKIB Model as a Function of the Temperature of an Asphalt Lift for Different CBR Values of the Subgrade</i>	117
Figure 95.	<i>Factor of Safety as a Function of Subgrade CBR for Asphalt Temperatures of 77°F and 140°F</i>	118
Figure 96.	<i>Dry Densities of Remolded Specimens Obtained from the KYCBR Testing Procedures as a Function of Maximum Dry Densities Obtained from AASHTO T-99</i>	119
Figure 97.	<i>Dry Densities of Soaked Specimens Obtained from the KYCBR Testing Procedure as a Function of Maximum Dry Densities Obtained from AASHTO T-99</i>	119
Figure 98.	<i>Factors of Safety of Different Thicknesses of "Full-Depth®" Asphalt Pavement as a Function of CBR</i>	120
Figure 99.	<i>Minimum Thickness of "Full-Depth®" Asphalt Pavement as a Function of CBR and Factor of Safety</i>	121
Figure 100.	<i>Values of CBR of Soils Located Along the Highway Corridor of Sections AA-13 and AA-14</i>	123
Figure 101.	<i>Relationship Between KYCBR and Time for Compacted Shales from the Kope Geological Formation</i>	124
Figure 102.	<i>Vertical Swell of Compacted Shales for the Kope Geological Formation as a Function of Time</i>	124
Figure 103.	<i>Design (and As-Built) Pavement Cross Section of Section AA-13 and AA-14</i> . . .	125
Figure 104.	<i>CBR as a Function of Moisture Content</i>	125
Figure 105.	<i>Values of Laboratory KYCBR</i>	126

Figure 106.	<i>Typical Triaxial Tests Results Obtained at a Temperature of 100°F</i>	126
Figure 107.	<i>Variation of the Total Stress Parameter, ϕ, With Temperature of Asphalt Pavement Core Specimens</i>	127
Figure 108.	<i>Variation of the Total Stress Parameter, ϕ, With Temperature of Asphalt Pavement Cores</i>	127
Figure 109.	<i>Variation of Temperature of Asphalt Pavement and Depth of Asphalt Pavement</i>	128
Figure 110.	<i>Parameters Used to Analyze Site Numbers 3, Station 2140, of Sections AA-13 and AA-14</i>	130
Figure 111.	<i>Factors of Safety of the Partially Completed Pavement Sections of Sections AA-13 and AA-14</i>	130
Figure 112.	<i>Factors of Safety of the Pavement Cross Sections of Sections AA-13 and AA-14</i>	131
Figure 113.	<i>Remedial Overlay Pavement Sections of Sections AA-13 and AA-14</i>	132
Figure 114.	<i>Remedial Overlay Pavement Sections</i>	132
Figure 115.	<i>Factors of Safety of Overlay Sections Obtained from the HOPKIB Computer Program for Sections AA-13 and AA-14</i>	133
Figure 116.	<i>Design Pavement Section of the Great River Road (KY 94) and the Pavement Section at the Time of Failure</i>	134
Figure 117.	<i>Effective Stress Parameters of Bank Gravel used to Construct the Base Cores of KY 94</i>	137
Figure 118.	<i>Percentages of Stable and Unstable Areas of the Great River Road (KY 94) Obtained from the HOPKIB Model</i>	138
Figure 119.	<i>Factors of Safety of the Partially Completed Pavement Sections of the Great River Road (KY 94)</i>	138
Figure 120.	<i>Factors of Safety of the Pavement Overlay Sections of the Great River Road (KY 94)</i>	139
Figure 121.	<i>In-situ Dry Density as a Function of Moisture Content--KY 94</i>	139
Figure 122.	<i>Factors of Safety at Locations on KY 94 During Construction that Were Described as "Visually Failed."</i>	140

Figure 123.	<i>Undrained Shear Strength as a Function of Moisture Content--KY 94</i>	140
Figure 124.	<i>Factors of Safety as a Function of Moisture Content--KY 94</i>	141
Figure 125.	<i>Typical Pavement Sections of Metropolitan City Streets for Low-Volume Traffic</i>	141
Figure 126.	<i>Factors of Safety of Section 1 Constructed on an Untreated Subgrade</i>	142
Figure 127.	<i>Factors of Safety of Section 2 Constructed on an Untreated Subgrade</i>	142
Figure 128.	<i>Factors of Safety of Section 3 Constructed on an Untreated Subgrade</i>	143
Figure 129.	<i>Factors of Safety of Section 1 and an Eight-Inch, Chemically Treated Subgrade Layer</i>	143
Figure 130.	<i>Factors of Safety of Section 2 and an Eight-Inch, Chemically Treated Subgrade Layer</i>	144
Figure 131.	<i>Factors of Safety of Section 3 and an Eight-Inch, Chemically Treated Subgrade Layer</i>	144
Figure 132.	<i>Examples of the 1981 KYCBR Curves Used in the Design of Flexible Pavements in Kentucky</i>	145
Figure 133.	<i>Factors of Safety Obtained from the HOPKIB Model as a Function of Total Pavement Thickness for CBR Values Ranging from 2 to 12</i>	145
Figure 134.	<i>Factor of Safety Obtained from the HOPKIB Model as a Function of Total Pavement Thickness for CBR Values Ranges from 2 to 12 and a Tire Contact Stress of 105 psi</i>	146
Figure 135.	<i>Comparison of Unsoaked and Soaked Values of KYCBR and the Percentage of Soaked Values of KYCBR Equal to or Lower than 3</i>	146
Figure 136.	<i>Minimum Pavement Thickness (One-Third Asphalt; Two-Thirds Granular Base) as a Function of CBR</i>	147
Figure 137.	<i>Comparison of Subgrade CBR Values Observed in the Summer of 1959 and the Spring of 1960 at the AASHO Road Test</i> ...	149
Figure 138.	<i>In-Situ CBR Values (Spring Months) of the AASHO Roadbed Soils as a Function of Moisture Contents</i>	149
Figure 139.	<i>Comparison of In-Situ Moisture Contents Observed in the Summer of 1959 and the Spring of 1960</i>	150

Figure 140.	<i>In-Situ CBR Values (Spring Months) of the AASHO Roadbed Soils as a Function of Dry Density</i>	150
Figure 141.	<i>In-Situ Dry Density of the AASHO Roadbed Soils as a Function of In-Situ Moisture Contents</i>	151
Figure 142.	<i>Typical AASHO Road Test Pavement Section Illustrating the Setup of Parameters for Analysis</i>	151
Figure 143.	<i>Factor of Safety as a Function of Weighted Equivalent Single-Axle Load Applications</i>	152
Figure 144.	<i>Factor of Safety Obtained from the HOPKIB Model as a Function of Weighted, ESAL Values Assuming the Temperature of the Pavement is 77° F Throughout</i>	154
Figure 145.	<i>Comparison of Factor of Safety - ESAL Curves Assuming Two Different Temperatures</i>	154
Figure 146.	<i>Pavement Thickness (One-Third Asphalt; Two-Thirds Granular Base) as a Function of the Factor of Safety</i>	155
Figure 147.	<i>Factors of Safety for Values of ESAL Less than 50,000</i>	156
Figure 148.	<i>Factors of Safety for Values of ESAL Between 50,000 and 200,000</i>	157
Figure 149.	<i>Factors of Safety for Values of ESAL Ranging from 200,000 to 500,000</i>	158
Figure 150.	<i>Factors of Safety for Values of ESAL Ranging from 500,000 to 1 Million</i>	159
Figure 151.	<i>Factors of Safety for Values of ESAL Ranging from 1 Million to 8 Million</i>	160
Figure 152.	<i>Factors of Safety for Sections that Remained for the Duration of the AASHO Road Test</i>	161
Figure 153.	<i>Relationships Between Values of Equivalent Single-Axle Load Applications and Factors of Safety for Two Different Pavement Temperatures</i>	161
Figure 154.	<i>Values of ESAL from the AASHO Road Test as a Function of Factor of Safety</i>	162
Figure 155.	<i>Effects of Unit Ground Contact Tire Stresses on the Values of ESAL</i>	162
Figure 156.	<i>Factor of Safety as a Function of Total Pavement Thickness and</i>	

	<i>Different Proportions of Asphalt and Granular Base</i>	165
Figure 157.	<i>Comparison of Factors of Safety for Two Different Values of CBR</i>	167
Figure 158.	<i>Comparison of Values of ESAL Based on Two Different Values of CBR</i>	167
Figure 159.	<i>Failures of Pavement Sections of (AASHO Road Test 1962) Loop 4 (Lane 1) During the Spring Months of 1960</i>	168
Figure 160.	<i>Relationships Between Cost Ratio and Percentile Test Values for Different Values of EAL (Equivalent Axle Load) and Coefficients of Variance (after Yoder 1965).</i>	
	a) <i>Coefficient of Variation Equals 10 Percent.</i>	
	b) <i>Coefficient of Variation Equals 30 Percent.</i>	
	c) <i>Coefficient of Variation Equals 50 Percent (Soaked Subgrades)</i>	169
Figure 161.	<i>Variation of Percentile Test Value and Subgrade CBR--Sections 13 and 14 on the Alexandria-Ashland Highway</i>	170
Figure 162.	<i>Factors of Safety Obtained When Different Design Values of CBR are Assumed</i>	171
Figure 163.	<i>Frequency of Occurrence as a Function of CBR--Sections 13 and 14</i>	171
Figure 164.	<i>Variation of Field and Laboratory Percentile Test Values With Values of CBR--Section 13 and 14</i>	172
Figure 165.	<i>Pavement Thickness Obtained When Different Design Values of CBR are Assumed--Sections 13 and 14</i>	173
Figure 166.	<i>Percentage of Sites Where Values of CBR are Less Than the Average Values of CBR and the Value of CBR at the 90th Percentile Test Value--Sections 13 and 14</i>	173
Figure 167.	<i>Comparison of the Average CBR Values of Selected Subgrades of the Alexandria-Ashland Highway and CBR Values Occurring at the 90th Percentile Test Value</i>	176
Figure 168.	<i>Comparison of Factors of Safety Obtained When the Average Subgrade CBR Values are Assumed to Factors of Safety Obtained When CBR Values Occurring at the 90th Percentile Test Value are Assumed</i>	177
Figure 169.	<i>Percentile Test Value as a Function of Field Values of CBR for Subgrade Soils Treated With Hydrated Lime</i>	178
Figure 170.	<i>Comparison of Factors of Safety Obtained When the Average CBR Values</i>	

	<i>of Selected Untreated Subgrades are Assumed to Factors of Safety Obtained When CBR Values Occurring at the 90th Percentile Test Value are Assumed</i> ..	178
Figure 171.	<i>Predicted Values of ESAL for Selected Pavement Sections Resting on Untreated Subgrades of the Alexandria-Ashland Highway</i>	179
Figure 172.	<i>Predicted Values of 18-Kip, ESAL Obtained for Selected Pavement of the Alexandria-Ashland Highway When the Strengths of Hydrated-Lime Treated Subgrades are Considered</i>	179
Figure 173.	<i>Typical Cross Section Used in the Analyses to Illustrate the Effects of the Variation of Tire Contact Stresses on Factor Safety and Predicted Values of ESAL</i>	180
Figure 174.	<i>Factors of Safety as a Function of Tire Contact Stress</i>	180
Figure 175.	<i>Relationship Between Tire Contact Stress and Predicted Values of ESAL</i>	181

List Of Tables

TABLE 1.	UNKNOWN AND EQUATIONS FOR n SLICES	25
TABLE 2.	JANBU'S (1954) APPROACH (UNKNOWN AND EQUATIONS FOR n SLICES)	26
TABLE 3.	COMPARISONS OF PROPOSED AND EXPERIMENTAL VALUES OF THE BEARING CAPACITY FACTOR, N_r	72
TABLE 4.	SUMMARY OF FACTORS OF SAFETY FOR ACTUAL PAVEMENT THICKNESSES AT TIME OF FAILURE AND ORIGINAL PAVEMENT SECTIONS-- AA-13 AND AA-14	129
TABLE 5.	SUMMARY OF FACTORS OF SAFETY FOR REMEDIAL PAVEMENT SECTIONS USED AT SECTIONS 13 AND 14 OF THE ALEXANDRIA- ASHLAND HIGHWAY	133
TABLE 6.	SUMMARY OF UNDRAINED SHEAR STRENGTHS OF THE SUBGRADE OF KY 94 AND FACTORS OF SAFETY	135
TABLE 7.	FACTORS OF SAFETY FOR AREAS ON KY 94 DESCRIBED AS VISUALLY FAILED	136
TABLE 1A.	SUMMARY OF AASHO ROAD TESTS DATA FOR LOOP 3 (FLEXIBLE PAVEMENT), LANE 1 AND 2 AND 12-KIP LOAD APPLICATIONS	194
TABLE 2A.	SUMMARY OF AASHO ROAD TEST DATA FOR LOOP 4 (FLEXIBLE PAVEMENT), LANE 1 AND 18-KIP LOAD APPLICATIONS	195
TABLE 3A.	SUMMARY OF AASHO ROAD TEST DATA FOR LOOP 4(FLEXIBLE PAVEMENT), LANE 2 AND 32-KIP LOAD APPLICATIONS	196
TABLE 4A.	SUMMARY OF AASHO ROAD TEST DATA FOR LOOP 5 (FLEXIBLE PAVEMENT), LANE 1 AND 22.4-KIP LOAD APPLICATIONS	197
TABLE 5A.	SUMMARY OF AASHO ROAD TEST DATA FOR LOOP 5 (FLEXIBLE PAVEMENT), LAND 2 AND 40-KIP LOAD APPLICATIONS	198
TABLE 6A.	SUMMARY OF AASHO ROAD TEST DATA FOR LOOP 6, (FLEXIBLE PAVEMENT), LANE 1 AND 2 AND 48-KIP LOAD APPLICATIONS	199
TABLE 7A.	SUMMARY OF AASHO ROAD TEST DATA FOR LOOP 6, (FLEXIBLE PAVEMENT), LANE 1 AND 2 AND 48-KIP APPLICATIONS	200

EXECUTIVE SUMMARY

Pavement subgrades must be stable during construction and perform throughout the design life of the pavement. Often, the subgrade is the weakest member of the pavement structure and is an important factor influencing pavement performance. The subgrade during construction must be sufficiently stable to prevent rutting, pushing, and shoving. The subgrade must also provide a sound platform so that the various pavement layers can be effectively and efficiently placed and compacted. The subgrade must serve as a "working platform," and possess strength so that large permanent deformations do not accumulate over a long period of time and affect the performance of the pavement.

Pavements are typically designed to support anticipated traffic loadings after the total pavement system is constructed. Usually, no consideration is given to the need to support heavily-loaded vehicles, such as gravel or concrete trucks, during construction. It is assumed that pavements can be constructed as designed. The question of constructability is frequently overlooked and left to the field and geotechnical engineers to confront (Hopkins 1987). A common assumption is made that if the soil subgrade is compacted to 95 percent of standard (AASHTO T 99) maximum dry density, and ± 2 percent of optimum moisture content, construction of the pavement, as designed, should not present a problem; that is, if proper compaction is obtained, then the bearing, or shear strength of the soil subgrade is sufficient to withstand construction traffic loadings. Compaction of soil subgrades is an essential element in the construction of pavements. This assumption fails to recognize that subgrade strength and stability varies during construction and throughout the life of the pavement and that subgrades, when constructed of weak soils, may not have adequate bearing strength to withstand construction traffic loadings. Damaged subgrades and partially completed pavements during construction may also lead to poor performance of the pavement after construction.

Observed differences (Hopkins 1987) between pavement design assumptions and actuality -- the actual conditions faced by the field construction engineer -- have led to many pavement construction problems. Many pavement problems, or premature pavement problems, have occurred after construction. As a sampling of these construction problems, from about May 1986 to November 1989 -- about 3.5 years -- the Geotechnical Branch (Division of Materials) of the Kentucky Department of Highways was involved in developing remedial plans at more than 40 highway construction sites. Personnel of the University of Kentucky Transportation Center have been involved in many pavement failures. Pavement construction problems may be classified as follows:

- failures of weak soil subgrades under construction traffic loadings;
- failures of granular base courses under construction traffic loadings;
- failures of partially completed pavement/base materials under, construction traffic loadings;
- premature failures of pavements shortly after construction; and
- difficulties in achieving proper compaction of granular base and pavement materials due to inadequate bearing strength of the soil subgrade.

Although current design methods and construction practices have apparently been successful in many cases, this success must be modulated and viewed cautiously when the number of failures is considered. That is, the problem of pavement failures continues to occur during pavement construction and after construction. This aspect prompted this study and shaped the objectives of this study. In examining

design methods currently available, it appeared that a new design approach was needed to examine the pavement problem from a different viewpoint or perspective. This study had three major objectives. These were as follows:

- develop a generalized, multi-layered, mathematical pavement model and equations using bearing capacity concepts based on limit equilibrium theories of plasticity;
- program the algorithms of the newly developed, pavement model for the computer to ease the use of the model; and
- identify designs, construction procedures, and conditions that may lead to premature failures during construction, or shortly after construction.

These three objectives were achieved and detailed aspects of these objectives are reported herein.

A general discussion of how the principle of effective stress may be used to view and explain the behavior of flexible pavements under wheel loadings, the interaction of stresses induced by traffic wheel loadings, and pore waters in pavement layers is presented. Factors that influence the behavior of subgrades and partially completed pavements during and after construction are discussed. Theoretical considerations and mathematical derivations of limit equilibrium equations for analyzing the ultimate bearing capacity of soil subgrades and partially completed pavements, and the extension of these equations to the analyses of pavements composed of multiple layers, are presented. Bituminous pavements consisting of as many as 25 -- an arbitrarily selected value -- layers may be analyzed. Various types of shear surfaces are considered and the theoretical derivation of equations of one type of shear surface selected for use in the bearing capacity model is presented. To facilitate the use of the newly developed bearing capacity model, the limit equilibrium equations were programmed for the computer model; a brief description of the bearing capacity computer model (called the HOPKIB model) and program is given.

To verify and evaluate the reasonableness of solutions obtained from the HOPKIB bearing capacity model and computer program, three different classes of problems are solved. Solutions obtained from the bearing capacity computer program are compared to solutions obtained from other theoretical or empirical methods. The different bearing capacity classes included problems that involve one homogenous layer of material, two layers of different materials, and two case studies of actual pavement failures that occurred during construction. The case studies involved multiple layers of materials. Regarding the first class of examples, bearing capacity factors are computed from the HOPKIB computer program and compared to bearing capacity factors obtained from classical bearing capacity theory (Prandtl 1920; Terzaghi 1943; and Vesic' 1963). These comparisons show that the newly developed, bearing capacity model yields bearing capacity factors that are nearly identical to the classical bearing factors. These comparisons aid in establishing the theoretical credibility of the model.

Relationships between the undrained shear strength of soil subgrades and contact wheel stresses for various factors of safety obtained from the HOPKIB bearing capacity computer program are computed and included in the first class of problems. Similar relationships between California Bearing Ratio (CBR) of soil subgrade and contact wheel stresses for various factors of safety are included. From these relationships, the minimum undrained shear strength, or CBR value, which corresponds to a selected value of factor of safety (against failure) and contact wheel stress may be obtained. Relationships between sinkage (or rutting) of a subgrade and different values of CBR (and undrained shear strength)

published by Thompson in 1988, and Taylor and Thompson in 1977, are analyzed using the HOPKIB model to find the minimum factor of safety (for a given contact wheel stress) that corresponds to a minimum sinkage value. As shown by model analyses, when the CBR value of the subgrade is below about 6 percent, the subgrade is subject to fail under typical construction traffic. This result was verified by field data published by Thompson (1988). It was recommended that when this condition exists, the subgrade should be modified. This important finding was carried out by the Kentucky Department of Highways during this study.

In the second class of bearing capacity problems, subgrades involving two layers are analyzed using the HOPKIB bearing capacity computer program and the bearing capacity model proposed by Vesic' (c.f. Winterhorn and Fang, 1963). Results obtained from these models are compared to show the reasonableness of solutions obtained from the HOPKIB model. Results obtained from the HOPKIB computer program are used to illustrate how this model may be used to devise a simple approach for designing the thickness of a soil subgrade treated with chemical admixtures. Based on the results of these analyses, three alternative methods are discussed for designing the thicknesses of soil subgrades treated with chemical admixtures. A relationship developed and published by Thompson (1988), to predict the required thickness of treated subgrade and the CBR value of underlying soil subgrade, is also analyzed using the HOPKIB program.

Comparisons of the results obtained from the three different methods show that reasonable results may be obtained from the HOPKIB model. As shown by the analyses, "full depth" asphalt pavements, or granular base courses, should not be constructed on clayey subgrades that have CBR values of less than about nine. Subgrade strengths of this size are required to avoid failure during construction of the first lift of asphalt pavement, or the first lift of a granular base course.

Many pavement problems have developed during and after construction because of the low bearing strength of Kentucky soils. As determined by the Kentucky geotechnical soils data bank (Hopkins and Tollner 1991), about 86 percent of Kentucky soils consist (statistically) of fat clays and clays. Approximately 40 percent of Kentucky soils have very low bearing strengths -- that is, the soaked CBR is less than six. About 20 percent of Kentucky soils have soaked CBR values that are less than three. Because of these low bearing strengths, subgrade modification is highly desirable in these cases to insure stability during and long after construction.

Although a pavement may be designed, the issue of whether the pavement may be constructed has often been ignored. Ignoring this issue leads to failures during construction and premature failures after construction. The concept of designing a pavement should involve more than merely obtaining the total thickness of the pavement. The issue of constructability should be addressed during the design phase. The design should consist of examining the bearing strengths of soils used to construct the pavement and determining the stability of the subgrade under anticipated construction traffic to avoid failure of the subgrade. The stability of each pavement lift should be analyzed to insure that each structural lift (especially the first lift) will not fail and to insure that each structural lift can be adequately compacted. When failure occurs during any phase of construction, a permanently weakened shear zone is built-in which may lead to future pavement cracking and premature failures. Once a pavement cracks, problems will persist throughout the life of the pavement since reflective cracking will occur in overlays. The HOPKIB model may be used to conveniently and efficiently examine both the stability of each phase of construction and the stability of the pavement after construction.

In an effort to illustrate the reasonableness of solutions obtained from the HOPKIB computer model and program, and to demonstrate that the model can be used to analyze flexible pavements consisting of multiple layers, detailed analyses of two case studies are presented. In each of these cases, the flexible pavements failed during construction under construction traffic loadings. The factors of safety of these pavements were near or equal to 1.0. Factors of safety obtained from the HOPKIB model should be near 1.0. Factors of safety were computed in those cases for the pavements having overlays. Unconsolidated-undrained triaxial tests were done on specimens obtained from the flexible pavement, granular base, and soil subgrade at each site. Using these data, stability analyses were performed for different construction stages -- soil subgrade only; soil subgrade in combination with the granular base; the combination of soil subgrade, granular base, and flexible pavement; and the combination (4 layers) of bituminous overlay, the original flexible pavement, the granular base, and soil subgrade. These analyses show that the HOPKIB model was a good predictor of failure in the cases analyzed.

To develop some design guidelines regarding the factor of safety obtained from the HOPKIB bearing capacity model, pavement sections (lanes one and two) of loops 3, 4, 5, and six of the AASHO Road Test (1962) were analyzed. These analyses involved 237 pavement sections. A correlation between factors of safety obtained from these analyses and weighted values of 18-kip, equivalent single-axle loads were developed. These analyses show that when the factor of safety of a flexible pavement is greater than about 1.5 - 1.6, the pavement will sustain large values of 18-kip, equivalent single-axle loads. The analyses indicate that flexible pavements should not be designed for a factor of safety below about 1.2 or 1.3 however small the value of predicted ESAL may be.

Analyses of the 1981 Kentucky flexible pavement design curves (Havens, et al.) were performed using the newly developed model. CBR curves ranging from two to 12 were analyzed. Results show that for low-bearing soils (CBR equal to two or three), factors of safety equal to or less than 1.0 were obtained in most cases of ESAL values. From these analyses, certain design thicknesses may be obtained from the design curves that may be unstable. This aspect is particularly important for thin metropolitan streets that are usually designed for low values of ESALs. This situation is not trivial since hundreds of miles of highways in Kentucky exist on soil subgrades having CBR values of two or three. Flexible pavement thicknesses obtained from these design curves should receive a critical review when the factor of safety is less than 1.3 (as determined from the HOPKIB model) or when the CBR strength of the subgrade is below about six. When large factors of safety ($> \approx 3$) are computed for pavement thicknesses obtained from the 1981 design curves, then the design should be reviewed critically since the pavement may be overdesigned.

Model analyses show that increasing tire contact stresses from 68 psi to 105 psi causes very significant decreases in the values of 18-kip, equivalent single-axle loads that a pavement may withstand. The life of the pavement decreases dramatically. Decreasing the tire contact stress from 68 psi to 50 psi causes very significant increases in values of allowable ESAL. Significant increases in pavement life occur for this condition. Tire contact stresses, or unit stresses of tires, at the AASHO Road Test (1962) averaged about 68 psi, although different types of loaded vehicles were used in this field test. Consideration should be given to studying the tire contact stresses of vehicles currently operating on highway pavements since significant changes have occurred in the design of tires from 1962 to 1991. Such studies could be conducted conveniently at weigh stations. These data are needed to assess current design practices and policies and to assess likely damage to a given pavement. Model analyses show that gross loads are not necessarily the determinant factor causing pavement damage but that the magnitude of tire contact

stresses is the more significant factor.

Tire contact stresses should be regulated to reduce pavement damage. Regulating gross load limits may not necessarily regulate tire contact stresses on the pavement. Pressure to increase gross loads will continue -- an understandable situation from their point of view. An equally understandable viewpoint is that the public's interest must be protected to prevent costly, premature failures of pavements. When this condition occurs, neither the public's interests nor commercial interests are served. Both interests may better be served by considering new approaches to the weigh-limit problem. For example, building structurally stronger roadways having thicker pavements would only moderately increase initial costs. As one means of building thicker pavements, the use of chemical admixtures to increase the strength of soil subgrades would add modestly to initial costs. By increasing the number of axles of commercial vehicles, tire contact stresses are reduced. With structurally tougher pavements and reduced tire contact stresses, the values of ESALs increase dramatically as shown by the HOPKIB model analysis (see Figure 155 in this report). With an increase in values of ESAL, there is an increase in pavement life and, therefore, a reduction in maintenance costs (For example, Small et. al. 1989, of the Brookings Institute estimates that,

"The total annual savings from operating trucks having more axles on more durable highways would run about nine billion dollars, with added construction costs offsetting just 1.3 billion. Adjusted to reflect costs, user fees collected would fall about 600 million dollars."

That would leave a net dividend of about seven billion dollars. By reducing maintenance costs, user fees could be realigned, perhaps reduced, or the rate of increase of user fees could eventually diminish.

An important aspect of this study has been done by the Kentucky Department of Highways, that is, when the CBR strength of the soil subgrade is below 6 percent, the subgrade is modified or strengthened. The Department has embarked on a program to build structurally tougher pavements.

There is much past and continuing discussion of the correct approach for selecting the design strength, or CBR strength, of soil subgrades. Some engineers advocate using the lowest CBR value of the data set while others advocate using the average value of the data set. Others advocate using values obtained from reliability theory based on the assumption that the data set is normally distributed. This problem is examined in some detail in this report. Use of the lowest value may lead to a pavement thickness overdesigned and uneconomical. Using the average CBR value of data sets does not seem to be an appropriate approach since about one half the pavement will be undersigned while the other half will be overdesigned. Using values from reliability theory may not be wise since the CBR-data set may not be normally distributed as shown by an analysis of a case study. Equations of reliability theory cannot be used when the data set is abnormally distributed. When this condition exists, results from reliability theory may yield pavement thicknesses that may be underdesigned. Based on the analysis shown herein, the most appropriate approach for selecting a design CBR is a method proposed by Yoder (1975). Details of this approach have been published by Yoder (1969) and the use of the method is illustrated herein. Attractive features of Yoder's approach are that the method is based on least-cost analysis and optimization concepts. The approach involves constructing a percentile test value - CBR curve. Yoder relates the cost ratio -- defined as the unit maintenance cost to the initial unit construction cost -- to values of 18-kip, equivalent single-axle loads, percentile test values, and the coefficient of variance of the CBR data set. Based on values of ESAL, coefficient of variance, and cost ratio, a percentile test value

may be determined. Using this value, the design CBR value may be determined from the percentile test value - CBR curve obtained by analyzing the CBR data set. To simplify the use of this approach, the method has been programmed for the desktop computer. This program will be made available to the Kentucky Department of Highways. It is strongly recommended that this method be given consideration in future designs of pavements for new highway projects -- at least on a trial basis.

INTRODUCTION

Problem

Pavements are typically designed to support anticipated traffic loadings after the total pavement system is constructed. Design schemes of this sort normally consider failure by fatigue, or the tendency of the structural components of the pavement to break under repeated, traffic wheel loadings. Usually, no consideration is given to the need to support heavily-loaded vehicles, such as gravel or concrete trucks, during construction. Often, it is assumed that pavements, as designed, can be constructed. The question of constructability is frequently overlooked and left to the field engineer to confront (Hopkins 1986). Frequently, pavements are designed and specified to bear on very weak soil subgrades -- that is, CBR values equal to or less than six. The low values of CBR or some type of elastic subgrade modulus are incorporated into the design scheme to obtain the total pavement thickness; the construction aspect is somehow ignored, although the soils used in the subgrade may be too weak to adequately support construction traffic. A common assumption is made that if the soil subgrade is compacted to 95 percent of standard (ASTM D 698 or AASHTO T 99) maximum dry density and ± 2 percent of optimum moisture content, then construction of the pavement, as designed, should not present a problem, that is, if proper compaction is obtained, then the shear, or bearing, strength of the soil subgrade is sufficient to withstand construction traffic loadings. This assumption fails to recognize that subgrade strength and stability varies during construction (and after construction) and that subgrades when constructed of weak soils may not have adequate bearing strength to withstand construction traffic loadings.

Observed differences (Hopkins 1987) between pavement design assumptions and actuality -- the actual conditions faced by the field construction engineer -- have led to many pavement construction problems. As a sampling of these problems, from May 1986 to November 1989, personnel of the Geotechnical Branch (Division of Materials) of the Kentucky Transportation Cabinet were involved in developing remedial plans at more than 40 construction sites (Smith 1989). Personnel of the Kentucky Transportation Center have been involved in many pavement failure investigations (Sharpe and Deen 1987; Sharpe 1988; Hopkins and Sharpe 1985; Hopkins and Hunsucker, November 1990; Hopkins and Allen 1986; Hopkins, et. al., October 1988; Drake and Havens, 1959; Baker and Drake 1948; Allen and Graves, November 1990; Allen and Graves, December 1990; Allen and Graves, October 1990; Havens, et. al., August 1981; Southgate, et. al., 1981). Pavement subgrade instability is not unique to Kentucky but is nationwide in scope (for example, Thompson 1988; Terrell, et. al., 1979; Traylor and Thompson 1977; Hammitt 1970; The AASHTO Road Test 1962).

Pavement construction problems may be classified as follows:

- failures of weak soil subgrades under construction traffic loadings;
- failures of granular bases under construction traffic loadings;
- failures of partially completed pavement/base materials under construction traffic loadings;
- premature failures of pavements shortly after construction; and
- difficulties in achieving proper compaction of granular base and pavement materials due to inadequate bearing strength of the soil subgrade.

The actual importance of the subgrade problem is unknown because the problem is usually solved by the geotechnical engineer and the field construction engineer and the problem oftentimes is not formally

reported.

Most pavement design methods are based on empirical, or semi-empirical, approaches, or use, in some fashion, the theory of elasticity. Empirical methods, such as the AASHO (1962) -- American Association of State Highway Officials -- procedure, or the method (Baker and Drake 1949; Drake and Havens 1959) used over the past four decades in Kentucky rely on experience, observation, and a trial-and-error procedure without due regard to system and theory. The first rational approach to pavement design was introduced by Burmister in 1943. Each layer or component of the pavement -- subgrade, base course, and pavement -- is assumed to consist of perfectly elastic material. Required thickness of a flexible pavement may be found for any measured or assumed modulus of elasticity for each structural layer and for any specified deflection of the surface of the pavement under the applied load within the elastic range (McLeod 1953). Many hybrid methods (for example, Michelow 1963; Southgate, et al., 1981) currently in use have evolved from Burmister's original concept. Multi-layered, elastic analysis of flexible pavements is commonly used to design pavement thickness. Hundreds of papers -- too numerous to cite in this report -- dealing with this approach and various aspects of this approach have been published.

The use of multi-layered, elastic analysis has certain short-comings. For example, most researchers and pavement engineers recognize that water in pavements is an undesirable condition that may lead to failure under wheel stresses. Thousands of miles of highways have been fitted with side or edge drains in an attempt to intercept and remove surface and subsurface waters. Free-draining base courses are increasingly being used to remove waters from pavement layers. Methods based on elasticity principles cannot be used conveniently and do not provide a means to view the mechanistic behavior and interaction of water and stresses induced by wheel loads. It is commonly assumed that the presence of water in pavements is detrimental but the fundamental question of why it is detrimental cannot readily be explained by multi-layered, elastic approaches. If drainage systems performed perfectly, and continuously removed excessive amounts of water from the pavement layers, then the elasticity concept would not need to explain or consider the interaction of waters in pavement layers and stresses induced by wheel loads.

In Burmister's theory and other approaches that rely on the use of elasticity principles, the principle assumption that the subgrade, base course, subbase course, and pavement behave in a perfectly elastic manner is certainly questionable (McLeod 1953). The actual behavior of materials in the pavement system may be far from elastic. For very small strain levels, the system may approximate elastic behavior, depending on actual stress levels and stiffness of the components of the pavement system. In performing elastic analysis, a question arises concerning how moduli are selected for the different layers of the flexible pavement. There are several ways of defining modulus. The modulus has been determined using laboratory tests and/or field procedures. When laboratory tests are used, the modulus may be defined by the secant modulus, initial tangent modulus, or resilient modulus. In the past few years, field nondestructive testing equipment, such as the Road Rater (Southgate, et. al. 1982) and the Falling Weight Deflectometer (Bohn, et. al. 1972), have been developed and are intended to provide a fast and reliable system for determining the structural response and adequacy of pavements. Efforts have been made to simulate actual load magnitudes in developing this equipment. Field load-deflection data obtained from nondestructive testing equipment are used in back-calculation methods to obtain modulus of the structural layers of the pavement. Because of the closeness of the spacing of the deflection sensors of present equipment, erroneous or variable results may be obtained (TRB -- Committee Number 2B05, 1990). Many research studies are being conducted to learn the most suitable means of determining the

most appropriate modulus of the pavement layers.

Elastic analysis also requires that a critical surface deflection or critical compressive strain or/and critical tensile strain at the bottom of the flexible pavement be arbitrarily assumed or determined in some manner from laboratory tests, field tests or observations. These methods require the use of an adequate thickness of base course and bituminous surface so that the specified deflection at the surface or specified tensile strain at the bottom of the bituminous layer is not exceeded. The possibility exists that those values may be exceeded. Elastic methods may indicate that the critical values are beyond the elastic range, or that the moduli of the base course and surface course is less than the elastic method required to prevent failure. Since the modulus of bituminous materials varies widely with changes in temperatures, the likelihood that critical strains, deflections, or tensile strains in the bituminous layer may be exceeded, especially at elevated temperatures, is very real. The pavement designer must accept, in some manner, that critical values may be exceeded at times during the year due to temperature variations (and variations in properties) of the bituminous layer. The factor of safety against failure is unknown in methods based on elasticity principles or trial-and-error procedures.

Objectives

The foregoing discussion is not intended as an indictment of the multi-layered, elastic analysis or trial-and-error procedures but rather to focus attention on the need to refine and improve such methods, to emphasize the need to analyze construction conditions, and to seek, or explore, alternative approaches for analyzing pavement construction conditions and the design of flexible pavements. The major objectives of this study were to:

- identify designs, construction procedures, and conditions that may lead to premature failures during or shortly after construction;
- develop a generalized, multi-layered, mathematical pavement model and equations using bearing capacity models and concepts based on limit equilibrium theories of plasticity; and
- program the algorithms of the newly developed, pavement model for the computer.

Few, if any, current pavement design methods are based on limit equilibrium theory of plasticity. McLeod in 1953 attempted to use classical bearing capacity theory (Terzaghi 1943; Prandtl 1920) to analyze and determine the ultimate bearing capacity of two layers (surface and base) by determining ϕ and c values of an equivalent homogenous material having the same ultimate strength as the layered system of the flexible pavement. The ultimate strength of the equivalent homogenous material was then calculated on the basis of a logarithmic-spiral shear surface. This approach apparently was not pursued by many researchers; rather, pavement researchers generally pursued methods based on empirical approaches or the approach developed by Burmister (1943). One reason for a lack of interest in plastic limit equilibrium was due to the fact that classical bearing capacity is only applicable to one layer of material. Attempts to use this approach to analyze pavements having multiple layers presented difficulties in formulating a rational design method and interest apparently waned over the past decades. The major intent of this report is an effort to develop (and explore) the use of the limit equilibrium approach for analyzing pavements having multiple layers of materials. The approach is essentially a method of slices and the original mathematical model equations (Hopkins 1986) were developed for analyzing the stability of earthen slopes. The method makes use of the ultimate strengths of the various components of a layered pavement system. This is analogous, for example in steel structures, to using

the ultimate strength of steel. For many years, steel structures were designed using the working stress method, or elasticity concepts. Elastic pavement design methods that are currently used widely are based on the working-stress approach. The method proposed herein is based on the ultimate strength approach. Basically, in applying the limit equilibrium method to analyzing the bearing capacity of pavements, the problem is statically indeterminate; that is, there are more unknown quantities than known quantities. However, by assuming certain unknowns, the problem and the equations can be made to become statically determinate. A mathematical bearing capacity model can be devised; a factor of safety against failure may be calculated.

Scope

A general discussion of how the principle of effective stress may be used to view and explain the behavior of flexible pavements under wheel loadings and the interaction of stresses induced by traffic wheel loadings and pore waters in pavement layers is presented. Factors that influence the behavior of subgrades and partially completed pavements during construction and completed pavements are discussed. Theoretical considerations and mathematical derivations of limit equilibrium equations for analyzing the ultimate bearing capacity of soil subgrades and partially completed pavements, and the extension of these equations to the analyses of pavements composed of multiple layers are presented. Bituminous pavements consisting of as many as 25 -- an arbitrarily selected value -- layers may be analyzed. Various types of shear surfaces are considered and the theoretical derivation of equations of one type of shear surface selected for use in the bearing capacity model is presented. To facilitate the use of the newly developed, bearing capacity model, the limit equilibrium equations were programmed for the computer; a brief description of the bearing capacity computer model (referred herein as the HOPKIB model) and program is given.

To verify and evaluate the reasonableness of solutions obtained from the HOPKIB bearing capacity model and computer program, three different classes of problems are solved. Solutions obtained from the bearing capacity computer program are compared to solutions obtained from other theoretical or empirical methods. The different bearing capacity classes included problems that involve one homogenous layer of material, two layers of different materials, and case studies of actual pavement failures that occurred during construction. The case studies involved multiple layers of materials. Regarding the first class of examples, bearing capacity factors are computed from the HOPKIB computer program and compared to bearing capacity factors obtained from classical bearing capacity theory (Prandtl 1920; Terzaghi 1943; and Vesic' 1963). Relationships between the undrained shear strength of soil subgrades and contact wheel stresses for various factors of safety obtained from the HOPKIB bearing capacity computer program are computed and included in the first class of problems. Similar relationships between CBR of soil subgrade and contact wheel stresses for various factors of safety are included. From these relationships, the minimum undrained shear strength, or CBR value, which corresponds to a selected value of factor of safety (against failure) and contact wheel stress may be obtained. Relationships between sinkage (or rutting) of a subgrade and different values of CBR (and undrained shear strength) published by Thompson in 1988 and Traylor and Thompson in 1977 are analyzed using the HOPKIB model in an effort to determine the minimum factor of safety (for a given contact wheel stress) that corresponds to a minimum sinkage value.

In the second class of bearing capacity problems, subgrades involving two layers are analyzed using the HOPKIB bearing capacity computer program and the bearing capacity model proposed by Vesic' (c.f.

Winterhorn and Fang 1963). Results obtained from these models are compared in an effort to demonstrate the reasonableness of solutions obtained from the HOPKIB model. Results obtained from the HOPKIB computer program are used to illustrate how this model may be used to devise a simple approach for designing the thickness of a soil subgrade treated with chemical admixtures. Based on the results of these analyses, three alternative methods are discussed for designing the thicknesses of soil subgrades treated with chemical admixtures. A relationship, developed and published by Thompson (1988), that predicts the required thickness of treated subgrade and the CBR value of underlying soil subgrade is also analyzed using the HOPKIB program. This particular relationship was developed by Thompson based on the assumptions that the improved portion of the subgrade had a CBR value of 8 to 10 and the treated and untreated portions of the soil subgrade were subjected to a 32 kip, dual axle, tandem load. Thompson assumed 500 coverages and used multi-layered, elastic analysis to develop the relationship between the required treated subgrade thicknesses and values of CBR of the untreated portion of the soil subgrade -- that is the portion underlying the treated portion of soil subgrade.

In an effort to illustrate the reasonableness of solutions obtained from the HOPKIB computer model and program and to demonstrate that the model can be used to analyze flexible pavements consisting of multiple layers, detailed analyses of two case studies are presented. In each of these cases, the flexible pavements failed during construction under construction traffic loadings. The factors of safety of these pavements were near or equal to 1.0. Factors of safety obtained from the HOPKIB model should be near 1.0. In each case, nondestructive testing and back-calculation methods based on elastic analysis were used to obtain individual modulus of the pavement layers and to determine remedial overlay thicknesses. Factors of safety were computed in those cases for the pavements having overlays. Unconsolidated-undrained triaxial tests were performed on specimens obtained from the flexible pavement, granular base, and soil subgrade at each site. Using these data, stability analyses were performed for different construction stages -- soil subgrade only, soil subgrade in combination with the granular base; the combination of soil subgrade; granular base, and flexible pavement; and the combination (4 layers) of bituminous overlay, the original flexible pavement, the granular base, and soil subgrade. In an effort to develop some design guidelines with regard to the factor of safety obtained from the HOPKIB bearing capacity, pavement sections (lanes 1 and 2) of loops 3, 4, 5, and 6 of the AASHO Road Test (1962) were analyzed. These analyses involved some 237 pavement sections.

BACKGROUND

Attempts to explain the mechanical behavior of flexible pavements and subgrades may broadly be divided into two groups. Burmister (1943) used elasticity principles in an effort to explain the mechanical behavior of pavements. In 1953, McLeod attempted to use classical bearing capacity theory based on plasticity principles.

In viewing the behavior of flexible pavements during construction and after construction, the principle of effective stress is very useful in visualizing the mechanical behavior of the pavement under wheel traffic loadings and in developing a mathematical model that attempts to simulate, or model, the interaction of stresses imposed by traffic and pavement layers. The mechanical behavior of the pavement is strongly influenced by such factors as:

- temperature of the asphalt pavement;
- geologic setting of the pavement and types of soils used to construct the pavement subgrade; and
- physical properties, such as compaction, swelling, and moisture of the bituminous pavement, granular base courses, and soil subgrades.

Plasticity and Elasticity Approaches

Pavement design models that rely on the theory of elasticity use in some form the relationship between compressive stress or tensile stress, σ , and the mobilized strain, ϵ , as shown in Figure 1, or

$$\sigma = E\epsilon, \quad (1)$$

where E = modulus of elasticity. When considering the limit equilibrium approach based on the theory of plasticity (Figure 2), the relationship between the shear stress, τ , and the failure shear stress, τ_f is used, or

$$\tau = \left(\frac{1}{F}\right) \tau_f, \quad (2)$$

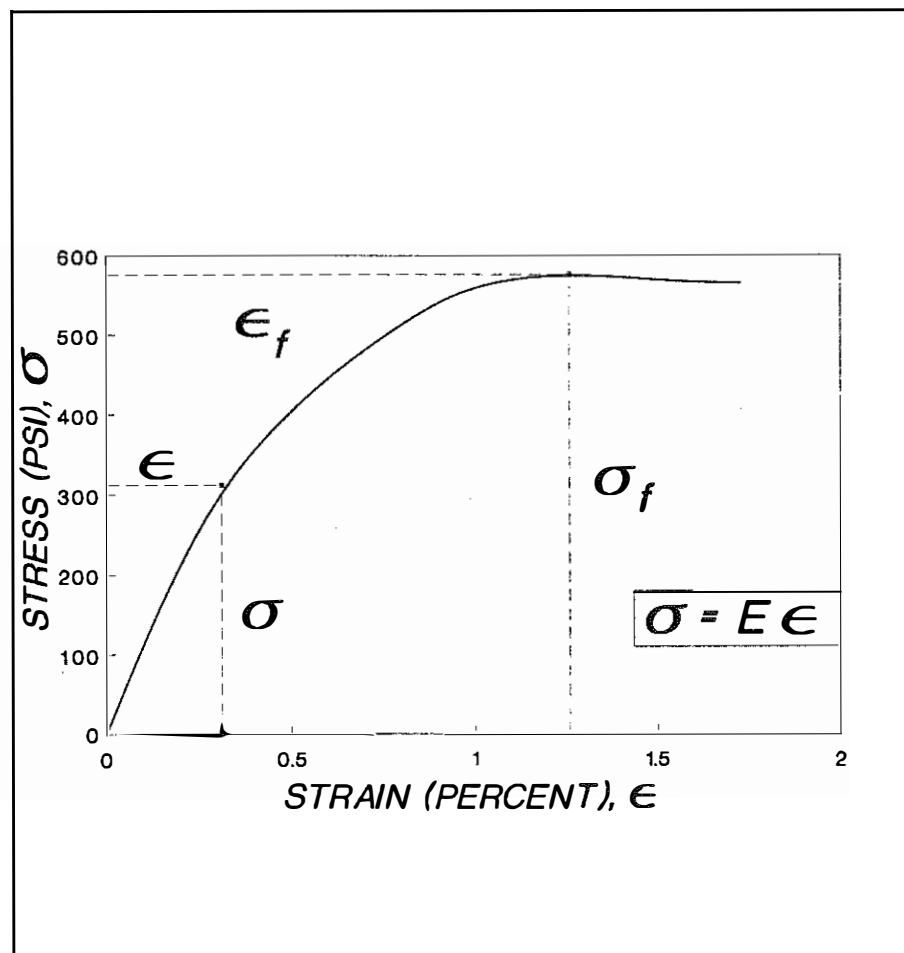


Figure 1. Stress as a Function of Strain-Elasticity Approach.

where $1/F$ is the degree of mobilization and F is the factor of safety.

The two different approaches are compared in Figure 3. In this comparison, the shear stress, τ , is analogous to the tensile or compressive stress, σ ; the degree of mobilization, $1/F$, is analogous to the mobilized strain, ϵ ; and the failure shear stress, τ_f , is analogous to the modulus of elasticity, E . At a state of failure, the minimum factor of safety is equal to 1 in the plasticity approach, or

$$F_{\min.} = 1, \quad (3)$$

while in the elasticity

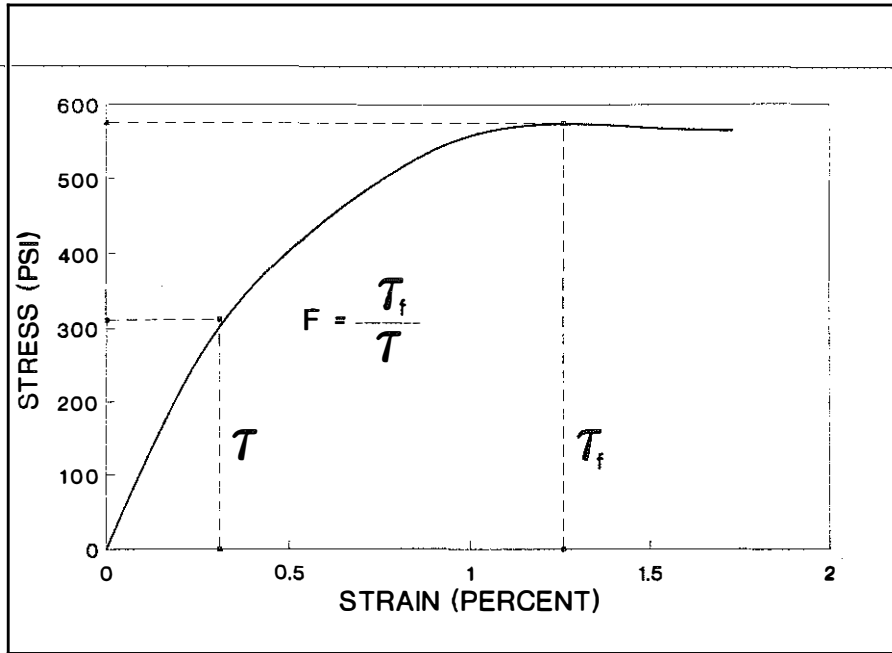


Figure 2. *Stress as a Function of Strain-Plasticity Approach*

then the modulus of elasticity must vary with depth of pavement. However, to the knowledge of this author, the use of different values of elastic modulus to describe different layers of the asphalt pavement is not assumed in multi-layered, elastic analysis. Normally, one value of modulus is ascribed to the asphalt pavement in performing these analyses. In the method proposed herein, the shear strength of each layer of the pavement system is defined by either effective stress parameters, ϕ' and c' , (or total stress parameters, ϕ and c), or the undrained-shear strength parameter, S_u (or c). In the latter case, the material is assumed to be saturated and ϕ equals zero. The approach described herein calculates a factor of safety against failure, as depicted in Figure 2. Since

$$F = \frac{\tau_f}{\tau}, \quad (5)$$

then

$$\tau = \frac{\tau_f}{F} = \frac{c'}{F} + \frac{\sigma'_n \tan \phi'}{F} = c'_m + \sigma'_n \tan \phi'_m \quad (6)$$

where (Figure 5),

$$\tan \phi'_m = \frac{\tan \phi'}{F}, \text{ and} \quad (7)$$

$$c'_m = \frac{c'}{F}. \quad (8)$$

approach, the mobilized strain is greater than or equal to, the failure strain, ϵ_f , or

$$\epsilon \geq \epsilon_f \quad (4)$$

In pavement problems involving multiple layers of different materials, a modulus of elasticity of each layer must be defined when using a multi-layered, elastic approach. Since the strength of an asphalt-granular matrix varies with temperature (Figure 4) and the temperature of an asphalt pavement varies with the depth of the pavement,

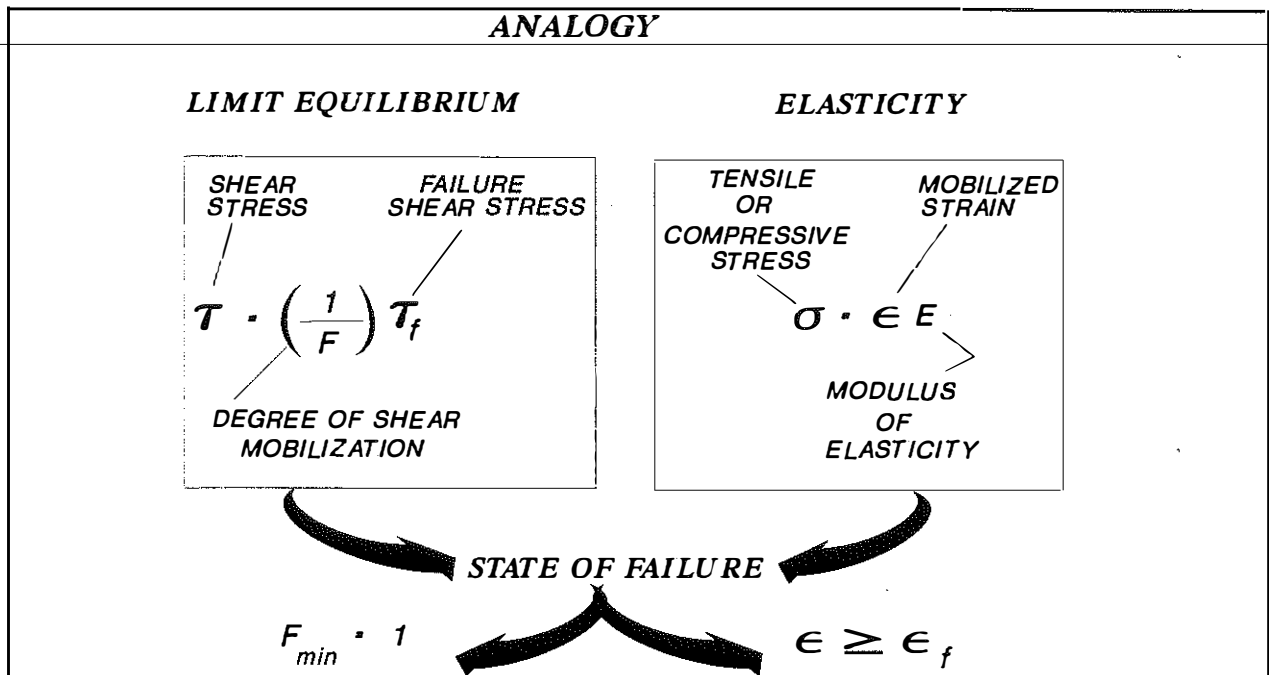
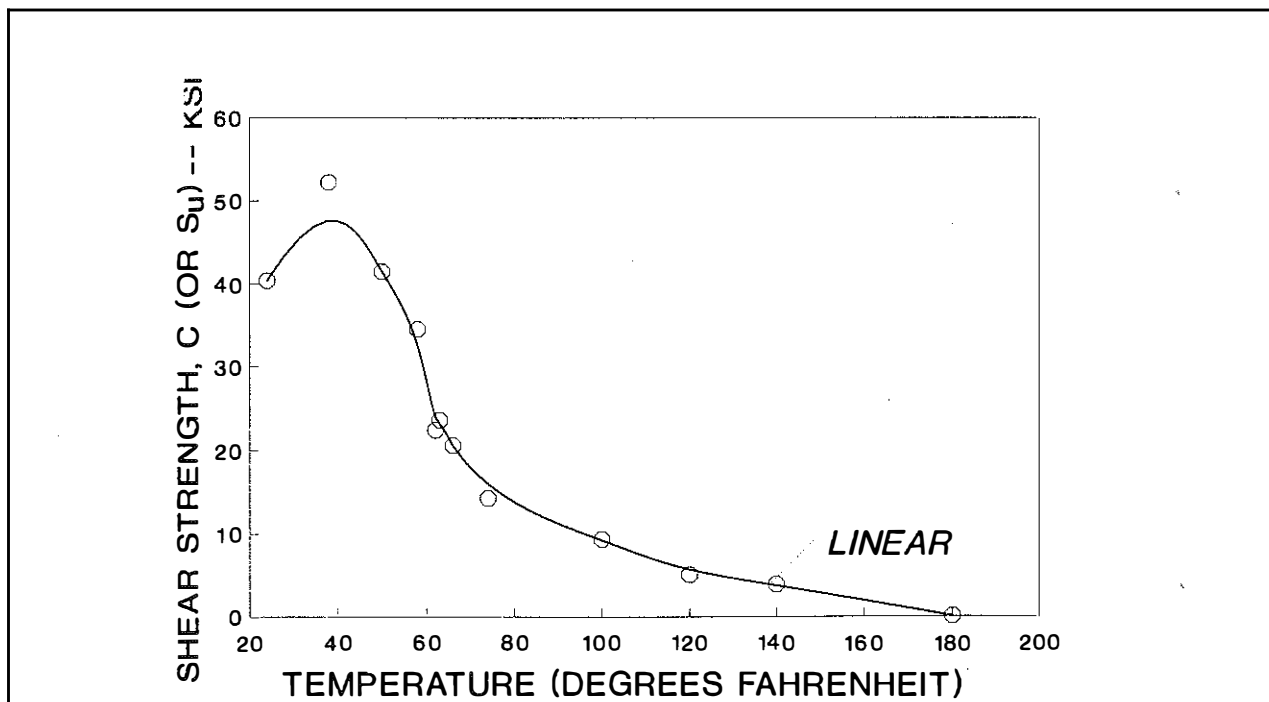


Figure 3. Comparison of Plasticity and Elasticity Approaches

Figure 4. Shear Strength, c , of an Asphalt Pavement as a Function of Temperature.

Principle of Effective Stress

The principle of effective stress (Terzaghi 1943) is very useful in viewing the mechanical behavior of pavements under traffic loadings. Simply stated, the principle is as follows:

$$\sigma'_n = \sigma_n - u \quad (9)$$

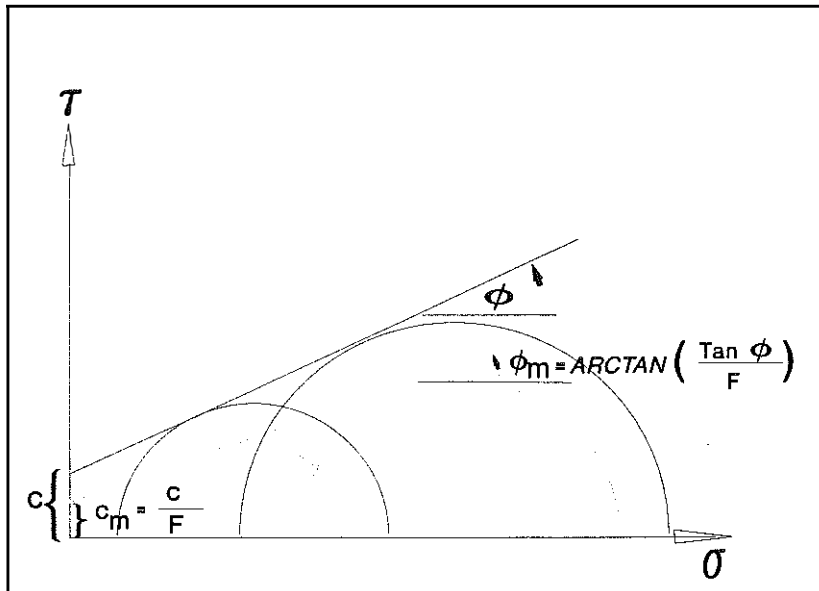


Figure 5. Definition of Mobilized Shear Strength Parameters, ϕ_m and c_m

or, the effective normal stress, σ'_n , acting on a potential shear surface, is equal to the total normal stress acting on the shear plane minus the pore water pressure. The shear strength, τ , available to resist failure under traffic loadings is (assuming a Mohr-Coulomb failure envelope -- Terzaghi 1943),

$$\tau = c' + \sigma'_n \tan \phi', \text{ or} \quad (10)$$

$$\tau = c' + (\sigma - u)_n \tan \phi'. \quad (11)$$

where

τ = shear strength, or stress, of the bearing media;

c' = effective stress parameter, cohesion;

σ'_n = effective normal stress;

σ_n = total normal stress;

u = total pore water pressure; and

ϕ' = effective stress parameter, the angle of internal friction.

As shown by Equation 11, the shear strengths of the pavement layers (bituminous layer, granular base, and soil subgrade) consist of two parts -- the cohesion, which is not a function of pore water pressure, and the internal friction, which is a function of pore water pressure. Effective stresses, or pressures, are transmitted through the points of contact between the particles whereas the pore water pressures, or neutral stresses are transmitted through the pore water occupying space between particles.

Stability of subgrades, for example, during construction is controlled by the magnitude, or level, of stresses imposed by traffic wheel loadings and the shear strength, τ , of the subgrade available to resist failure. As shown by Equation 11, the available shear strength is a function of the magnitudes of ϕ' and c' and the pore water pressure acting within the subgrade media. The total pore water pressure acting within the subgrade media may be viewed as consisting of three parts, or

$$u = u_s + u_{ss} + \Delta u, \quad (12)$$

where

u = total pore water pressure;

u_s = static pore water pressure;

u_{ss} = pore water pressure due to flow or artisan flow; and

Δu = hydrostatic, or excess, pore pressure at a selected point in the subgrade due to transmitted stresses induced by the applied traffic stresses.

In most cases, u_s and u_{ss} are small (however, u_{ss} may become large at the bottom of long, steep highway grades). Typically, the major part of the total pore water pressure is due to the excess pore water pressure created by applied wheel stresses. If Δu is large, then the shear strength available to resist failure may be reduced significantly, as shown by Equation 11; that is, since Δu is large, the term, $(\sigma_n - \Delta u) \tan \phi'$, in Equation 11 decreases, and, consequently, the available shear strength, τ , decreases. Instability of the subgrade may occur. Even when Δu equals zero, instability may still occur if the imposed stresses, or driving stresses, are larger than the available, or resisting shear strengths, or stresses. Similar arguments can be made in cases involving more than one layer of material. In these cases, the shear strengths available to resist failure are controlled by the ϕ' and c' values of each individual layer and the pore water pressures acting within each layer of material.

Consider, for example, the conditions that may exist if the bituminous pavement becomes saturated. This condition may occur during prolonged periods of rainfall, or when there is an upward flow of ground water into the bituminous pavement for certain types of asphalt pavements that are permeable. When the asphalt pavement becomes saturated and is subjected to large wheel stresses, the shear strength, τ , available to resist failure decreases as shown by Equation 11, or

$$\tau = c'_a + (\sigma_n - \Delta u) \tan \phi'_a, \quad (13)$$

where ϕ'_a and c'_a are the effective stress strength parameters of the asphalt-granular matrix.

Because of the large increase in the hydrostatic pore pressure, Δu , due to the induced stresses of the wheel loadings and the relatively low permeability of the asphalt pavement, the term $(\sigma_n - \Delta u) \tan \phi'_a$ decreases. The shear strength, τ , available to resist failure decreases. The pore pressure, Δu , may become large enough to "strip" the asphalt from the aggregate. When the pavement is dry, or partially saturated, the pore pressure, Δu , is very small or zero. There is no change in the shear strength, τ , available to resist

failure.

At elevated temperatures, the behavior of the asphalt in the asphalt-granular matrix begins to behave more like a fluid than a solid. If the asphalt-granular matrix located directly under large wheel loads compresses and the air voids approach zero, or if the voids are filled with water, then excess pore asphaltic pressures may develop in the pavement at the elevated temperatures. In this situation, the shear strength of the asphalt pavement becomes:

$$\tau = c_a' + (\sigma_n - \Delta u_a - \Delta u) \tan \phi_a' \quad (14)$$

where

c_a' = effective stress parameter, cohesion of the asphalt-granular matrix;

σ_n = total normal stress;

Δu_a = excess pore asphaltic pressure, or stress, due to stresses transmitted by traffic loads;

Δu = excess pore water pressure due to stresses transmitted by traffic loads; and

ϕ_a' = effective stress parameter, angle of internal friction of the asphalt-granular matrix.

The shear strength and behavior of asphalt pavements is controlled by two different excess pore pressures -- Δu_a and Δu . The so-called bleeding of asphalt pavements occur when

- excessive amounts of asphalt are present in the mix;
- the asphalt-granular matrix is subjected to high temperatures; or
- the voids are filled with water; or
- the air voids in the matrix approach zero due to compression under wheel stresses.

When these conditions occur, the asphalt moves to the surface of the pavement as the pore asphaltic pressures dissipate. Since the excess pore pressures, Δu_a and/or Δu , increase, the terms $(\sigma_n - \Delta u_a - \Delta u)$, decrease, as shown by Equation 14, and the shear strength available to resist failure decreases. If the wheel stresses are sufficiently large, then failure or rutting may occur because of the decrease of the shear strength under wheel stresses. When the pavement contains air voids that are not filled with water, the excess pore pressures, Δu_a and Δu , are zero. The shear strength remains the same at a given temperature, or

$$\tau = c_a' + \sigma_n \tan \phi_a' \quad (15)$$

Constructing asphalt pavements having about 4 percent air voids appears sufficient to avoid the build-up of excess pore pressures, Δu_a and Δu .

For crushed stone that contains no fines (percent passing the number 200 sieve is less than 5 percent), the shear strength, τ , may be expressed as:

$$\tau = (\sigma_n - \Delta u) \tan \phi_s' \quad (16)$$

where ϕ_s is the effective stress strength parameter, the angle of internal friction. The cohesive component of shear strength, c_s , is equal to zero. When the stone is saturated -- a condition that may occur due to prolonged periods of rainfall or snow melt, or to a continuous flow or seepage into the crushed stone from shallow drainage ditches that parallel the roadway -- the pore water pressures may become moderate to relatively high due to the instantaneous loading of traffic. There is a reduction in the available shear strength since Δu increases and the term, $(\sigma_n - \Delta u) \tan \phi'_s$, decreases. When the crushed stone contains excessive amounts of fine material (greater than 5 percent passing the number 200 sieve), the build-up of excess pore water pressure in the base (and subbase) course may be sufficient to cause lateral movement of the fines away from the area located directly under wheeled traffic. Some support of the asphalt pavement may be gradually reduced.

The build-up of excess pore pressures is partly controlled by the nature of the pavement components and by the amount of wheel stresses applied to the pavement. Types of soils often used to construct pavement subgrades are sands, silts, and clays, or combinations of these soil types. The permeability of these types of materials are several orders of magnitude lower than the permeability of crushed stone. When these materials are subjected to large wheel stresses, very large excess pore pressures may build-up because of the low permeability of these types of materials. Sufficient time must elapse for the dissipation of excess pore pressures. Although sands are fairly permeable, excess pore pressures may build-up because of the instantaneous loadings imparted by large, wheeled traffic. The shear strength available to resist failure for sands may be defined by Equation 11. Sands do not generally possess a cohesive component of strength. Since Δu may increase when sands are saturated, the term, $(\sigma_n - \Delta u) \tan \phi_s$, decreases and the shear strength available to resist failure decreases. In thin pavement sections subjected to large, wheeled stresses, excess pore pressures may become so large that the term, $(\sigma_n - \Delta u)$, may become equal to zero. In this case, the shear strength may approach or equal zero and the sand liquefies under the large wheel stresses. Where joints exist in the pavement, there is a tendency for the fine material of the sand particles to move upward (and also laterally) through the joint as the excess pore water pressures dissipate. There may be a loss of support for the pavement, and failure of the joint may occur.

The shear strength, τ , for silts may be expressed by Equation 16. Silts usually do not possess cohesion since the permeability of silts is usually very small (smaller than sands). Excess pore pressures may build up to relatively large values when this material is subjected to large wheel stresses. These materials are very susceptible to liquefy since the term, $(\phi_n - \Delta u)$, may become zero. When this occurs -- this condition has been described as pumping -- soil particles may move laterally and upward through joints as the excess pore water pressures dissipate. Movement of the soil particles is away from an area located directly under the wheel paths.

The shear strength of clays may be defined by Equation 11. Here, the clay soils of the subgrade possess a cohesive component of strength when they exist in a compactive state. Since the permeability of saturated clays is extremely small, very large excess pore water pressures may build up under wheel stresses. Since the term, Δu , in Equation 11 becomes large, the term, $(\phi_n - \Delta u)$, decreases. If Δu is sufficiently large, then the term, $(\sigma_n - \Delta u)$, may approach zero. The shear strength available to resist failure may be approximated by:

$$\tau \approx c. \quad (17)$$

Under repeated loadings and the build-up of excess pore pressures, the cohesive component of shear strength in clays may be destroyed. Now, the shear strength may approach zero and the clay may liquefy.

At pavement joints, soil particles may move upward and laterally from an area located under the wheel paths as the excess pore water dissipates. Cavities may be created and cause a collapse of the pavement or the failure of a joint. When the clay is in an unsaturated state, the term, Δu , does not build up and the shear strength remains unchanged.

Under repeated loadings, an unsaturated clay or silt (or sand) may approach a saturated condition because the material directly under the wheel loadings compresses; i.e., the volume decreases. Here, excess pore pressures may build up and cause a decrease in the shear strength available to resist failure, as shown by examining Equation 11. This condition commonly occurs when clay or silt subgrades are placed at a moisture content that surpasses the optimum moisture content. Although the subgrade may not be completely saturated initially, the portions of the subgrade located directly under the wheel paths may become saturated when the volume of material decreases due to compression under the wheel stresses. When the material under the wheel paths becomes saturated, the excess pore pressures build up and the shear strength available to resist failure decreases; thus stability decreases, and rutting may develop.

Based on the discussion above, the following simple observations may be made:

- The stability of highway subgrades and pavements is not static, but is dependent on the degree of saturation in each layer of the pavement system.
- The subgrade is normally the weakest member of the pavement system since it is usually constructed of materials that have much lower shear strengths than those used to construct the asphalt or concrete base and subbase courses. The behavior of the subgrade greatly affects the stability of the pavement.
- When layers of the pavement system become saturated, there is a reduction in the stability under wheeled traffic because there is an increase in the excess pore pressures and a decrease in the shear strength available to resist failure.
- Providing good drainage in pavements is essential to reduce the opportunity for excess build-up of pore water pressures. However, providing good drainage does not necessarily guarantee that pavement and subgrade problems will not occur.

Temperature of Asphalt Pavement

As shown in Figure 4, the shear strength of asphalt pavements is very dependent on temperature. In this series of tests, unconfined compression tests were done on several core specimens from Interstate 65 near Elizabethtown, Kentucky. The tests were performed at different selected temperatures. Each specimen was immersed in a water bath and allowed to reach a selected temperature. After about two to three hours, the specimen was removed from the water bath, and an unconfined compression test was done immediately. As shown in Figure 4, the shear strength of the asphalt core specimens begin to decrease dramatically for temperatures ranging from about 40° to 100°F. From 100° to 180°F, the shear strength-temperature relationship is linear. In this range, the asphalt in the asphalt-granular matrix begins to behave more like a fluid than a solid. A simple analysis may be performed to examine the bearing capacity of the asphalt-granular matrix. In these analyses, the asphalt pavement is assumed to be

infinitely thick. Based on a total stress analysis, the ultimate bearing capacity, q_u , may be defined as (cf Vesic-- Winterhorn and Fang 1975):

$$q_u = cN_c, \quad (18)$$

where

c = cohesion

N_c = bearing capacity factor (when $\phi = 0$; $N_c = 5.14$).

At a temperature of 77°F, the ultimate bearing capacity is

$$q_u = 14.275 \frac{\text{Kips}}{\text{FT}^2} \times \frac{\text{FT}^2}{144 \text{ in}^2} \times \frac{1000 \text{ lb}}{\text{Kips}} \times 5.14 = 509.5 \text{ psi}. \quad (19)$$

If the applied unit tire contact stress, q_a , is 68 psi, then, by definition:

$$F = \frac{q_u}{q_a} = 7.55. \quad (20)$$

The factor of safety is very large. Assume that the temperature of the asphalt pavement is in the linear range of the relationship shown in Figure 4. This linear portion of the relationship may be expressed as:

$$c = 134.35 - 0.758T. \text{ (in psi) } (100 \leq T \leq 180^\circ\text{F}) \quad (21)$$

Solving for T,

$$T = \frac{134.35 - c}{0.758}. \quad (22)$$

Since $q_u = cN_c$, and

$$c = \frac{q_u}{N_c}, \quad (23)$$

then

$$T = \frac{134.35 - \frac{q_u}{N_c}}{0.758} \quad (24)$$

Rearranging the terms of Equation 20, noting that

$$q_u = q_a F,$$

and substituting this expression into Equation 24, then

$$T = \frac{134.35 - \frac{q_a F}{N_c}}{0.758} = 177.2 - 0.257 q_a F. \quad (25)$$

If the unit contact tire stress is 68 psi, and for an assumed factor of safety of 1.0, then

$$T = 177.1 - 0.257 (68)(1.0) = 159.7. \quad (26)$$

For a tire contact stress of 68 psi, the asphalt-granular matrix fails at a temperature of 160° F. Surface temperatures of asphalt pavements reportedly reach values of 140 - 160° F during the warm months in Kentucky.

In Figure 6, relationships between temperature and tire contact stresses for three different factors of safety are shown. These relationships are based on Equation 25. At a temperature of 150°F, tire contact stresses of about 70, 81 and 106 psi correspond to factors of safety of 1.5, 1.3, and 1.0. As these data show, tire stresses should be limited to about 80 psi to avoid serious rutting and shoving. At intersections and steep grades, limiting the stresses to 80 psi is difficult because of the dynamic loads and stresses that occur when heavy vehicles stop, decelerate, or accelerate. Shoving and pushing of asphalt pavements at intersections and steep grades is commonly observed.

Geologic Setting and Soil Types

Soils and geology influence the behavior and performance of highway pavements. This observation is generally recognized by many engineers; however, this aspect is often ignored. The types of soils usually located in a given geologic setting are used to construct the pavement subgrades. The types of soils at a given highway site are usually controlled by the type of geological formations existing at a given location. For example, in certain locations in Kentucky, pavements constructed on compacted, clayey shales or residual soils from such geologic units as the Kope and Crab Orchard frequently undulate and show very visible signs of distress. Often, the pavements fail prematurely. Residual soils derived from the Kope geologic unit in the northern portion of Kentucky are highly plastic and swell when exposed to water.

Bearing capacity failures of many city streets located in this portion of Kentucky are extensive. In these townships, specifications permit placing four or 5 inches of concrete directly on subgrades constructed of the highly plastic, weak residual soils of the Kope geologic unit. When concrete is used, no drainage

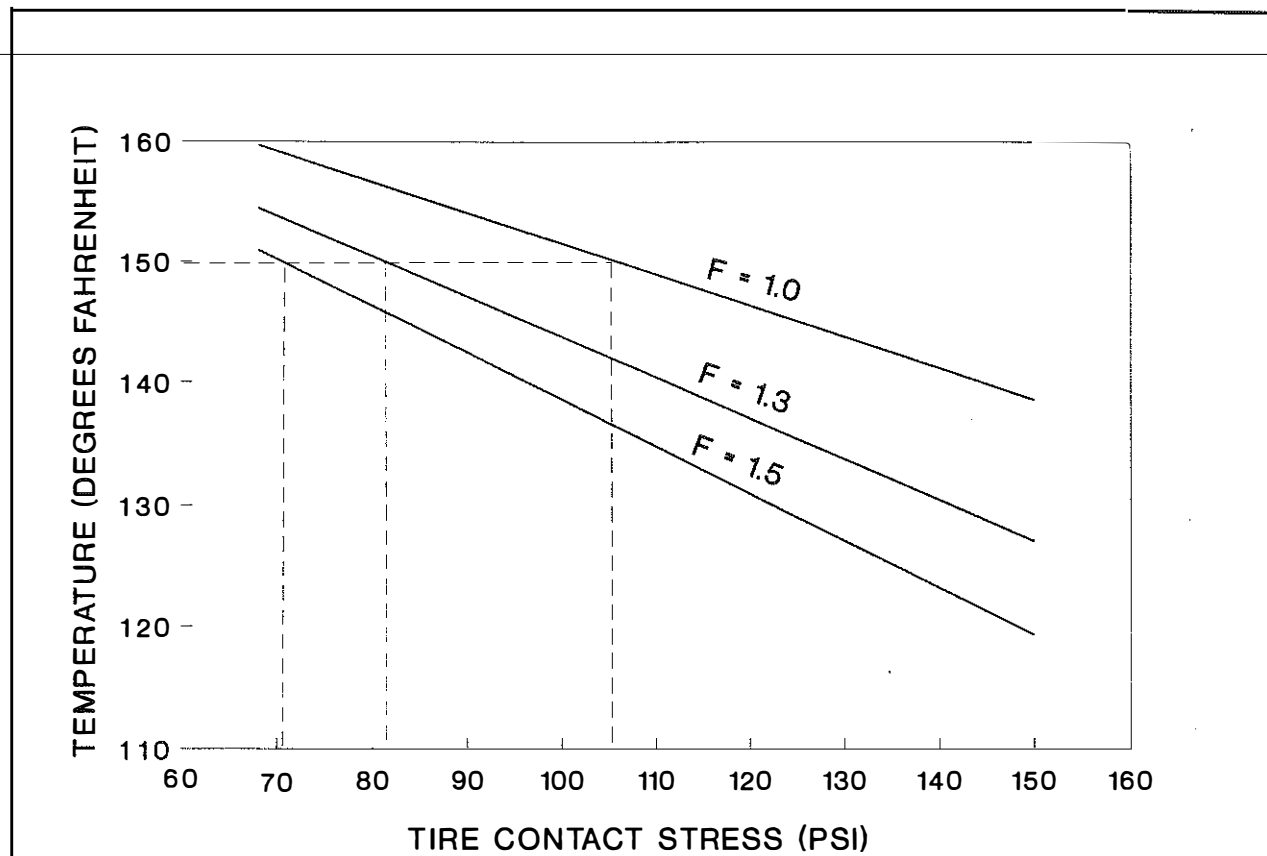


Figure 6. Variation of Temperature of an Asphalt Pavement and Unit Tire Contact Stress for Selected Values of Factor of Safety.

courses or granular base materials are specified. Sections of these concrete city streets were observed to have completely collapsed. The compacted, highly plastic, clayey shales or residual soils derived from the shale formations of this area absorb water, swell, and become saturated (the pores of the compacted clays are completely filled with water). Collapse of sections of the concrete streets in this area occurred because of three conditions. When the subgrade soils swell and change volume, the shear strength of the soil decreases. Secondly, when the subgrades become saturated and the thin, concrete pavements are loaded with large wheel stresses (due to heavy garbage trucks, concrete trucks, etc.), large excess pore pressures, Δu , build up under the wheel stresses. According to Equation 11, with an increase in Δu , the shear strength decreases and promotes instability. With a build up of large excess pore pressures, a condition is created under which the dissipation of the excess pore pressures move clay particles outward from beneath the concrete pavement, or the excess pore pressures move clay particles upward at joints in the concrete pavement. With a loss of clay particles or material supporting the pavement, voids are created and the pavement collapses. The pavements eventually collapse due to a loss of support. Even pavements of Interstate 75 that pass through the area have required large remedial expenditures. Pavements of this interstate route that pass through this area were characteristically undulated and were distressed, bumpy, and contained failures at joints (collapses) in the concrete sections before a thick bituminous overlay was placed.

Similar situations occur at other locations in Kentucky where pavements have been placed on highly plastic, clayey shales and residual clays from such geologic units as the Crab Orchard, Clays Ferry, and New Providence. The highly plastic clays of areas (residual soils derived from limestone and shale geologic formations) around Elizabethtown (mid-western Kentucky) have caused many pavement problems before, and after construction. In a recent study (Hopkins and Sharpe 1985), a section (southbound lanes) of Interstate 65 that passes through this area failed during construction under

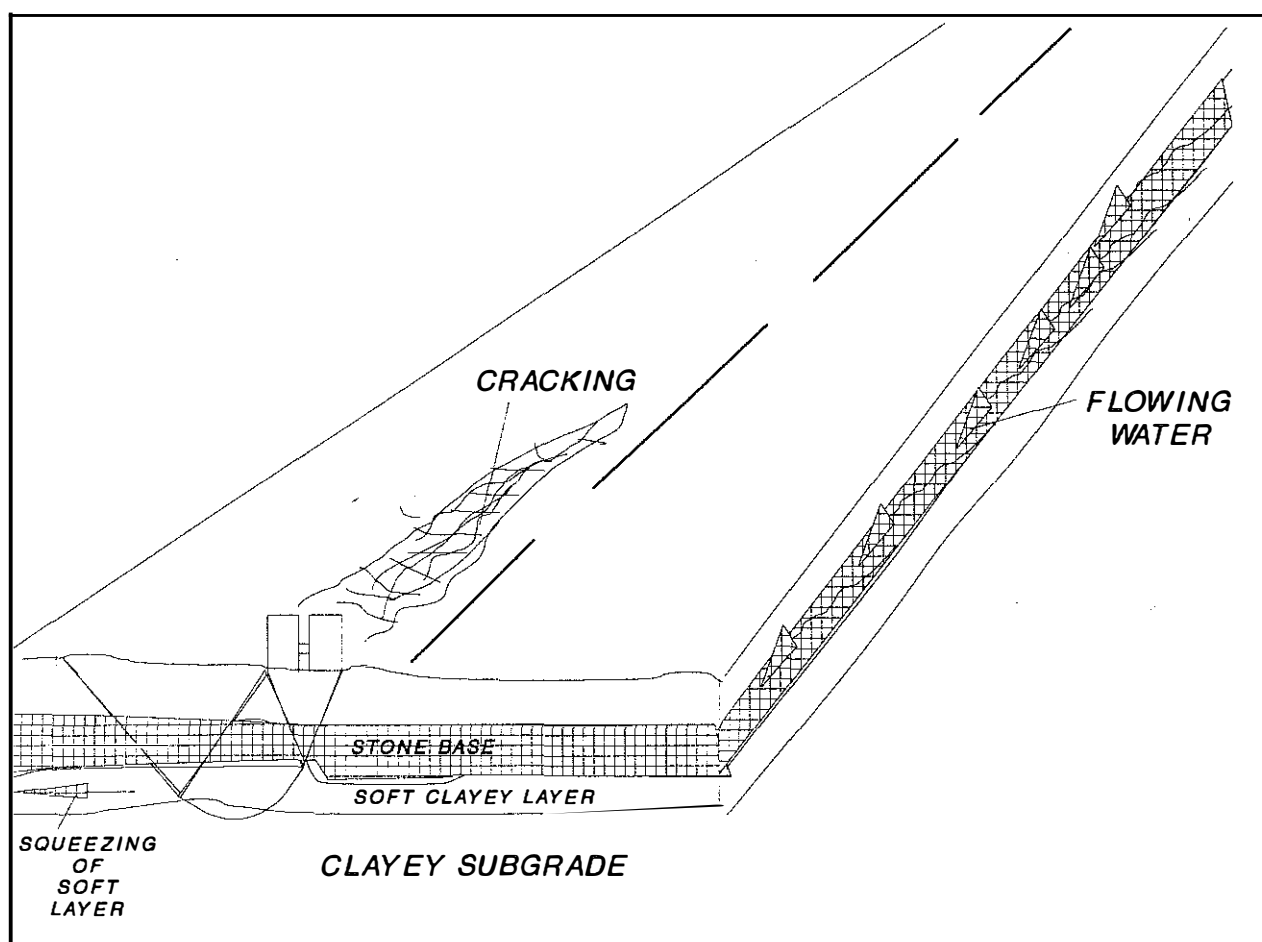


Figure 7. *Exposure of Soil Subgrades to Flowing Water in a Granular Base.*

construction traffic loading (gravel trucks). The partially completed pavement and dense graded aggregate (DGA) cracked, rutted, and deformed under construction traffic. Large deflections were observed shortly after a portion of the pavement was placed. Analyses showed that failure occurred because of a bearing capacity failure of the plastic clayey subgrade. Values of undrained shear strengths were as low as 850 pounds per square foot and averaged 1,250 pounds per square foot. Careful examination of several specimens (thin-walled, tube samples) obtained from the subgrade of the southbound lanes showed that the top three to 5 inches of the clayey subgrade was extremely soft -- the material was easily indented with the finger. Material below the soft zone was very firm. Preconsolidation stresses obtained from consolidation tests of soil specimens from the soft zone were

extremely low. Estimated stresses due to traffic loadings and the weight of material above the clayey subgrade showed that the preconsolidation pressures of the soft soils were smaller than the imposed stresses at the elevation of the soft layer of subgrade. Both bearing capacity failure and punching shear failure occurred. Case studies such as this emphasize the need to analyze the bearing capacity of pavements during construction to determine their constructability. Such cases illustrate the important role that geology and soil types play in the performance of pavements. Moreover, the consolidation characteristics of subgrades need to be examined. Other case studies similar to this case history will be examined in depth later in this report.

Although granular base courses are used to drain water from the pavement structure, the flow of water in the granular base, as shown in Figure 7, is usually in contact with the soil subgrade since the base rests directly on the subgrade. This condition exposes the subgrade soils to water, part of which seeps into the subgrade and is absorbed. During periods of flow, the soils of the subgrade have an opportunity to swell and soften, and there is a loss of shear strength. The top portion of the subgrade becomes saturated. When this occurs and the pavement is subjected to traffic stresses, the excess pore pressures build up. The shear strength available to resist failure decreases as shown by Equation 11. (One method that might be tried -- at least on an experimental basis -- to prevent the water from coming into contact with clay subgrades involves spraying the finished subgrade with an asphalt emulsion, or using a geomembrane, as illustrated in Figure 8. Currently, asphalt emulsion coatings are used to cure chemically-treated subgrades).

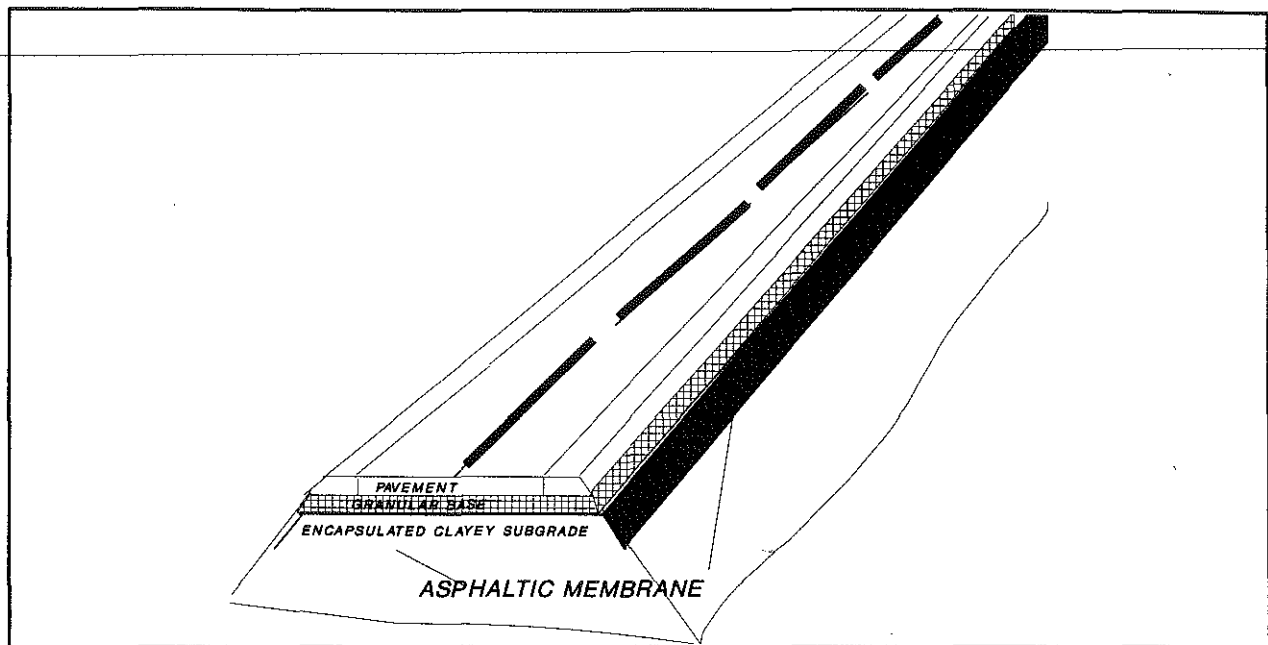
To develop a view of the types of soils found in Kentucky and the types of soils that are most likely to be used to construct pavement subgrades in this state, use may be made of engineering soils data contained in a soils data bank developed for Kentucky (Hopkins, et al. 1991). These data are the result of basic geotechnical tests done on specimens obtained throughout Kentucky. The data bank contains some 20,000 records. These data have been accumulated over the past four decades. Examination of data in this data bank show (statistically) that about 70 percent of the soils in Kentucky classify as clays and silts, as shown in Figure 9. About 16 percent of the soils are fat clays and silts. Only about 14 percent of the soils in Kentucky consist of clayey, silty sands and sands, or clayey, silty gravel or gravels. About 86 percent of soils in this state are materials of poor engineering quality and the likelihood of these poor engineering soils being used to construct pavement subgrades is very high. The likelihood of pavement construction problems occurring in Kentucky is considerably high. This problem occurs in many other areas of the country where clayey soils exist.

Physical Properties

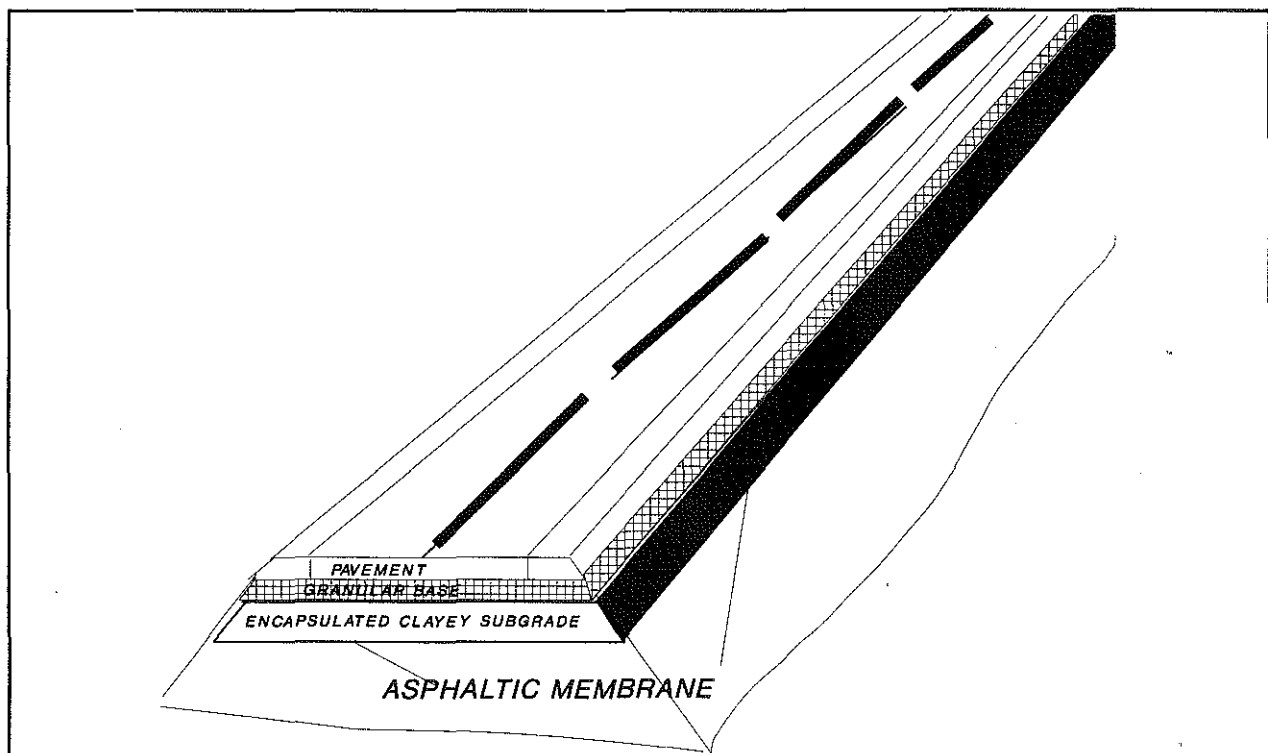
The mechanical behavior and performance of pavements are controlled by the physical properties of the materials used to construct the individual layers of the pavement structure. Some important physical properties include compaction, swelling, and moisture content. These factors affect the shear strength of the materials that is available to resist stresses imposed by traffic loadings.

Compaction

Generally, many engineers assume that if a subgrade constructed of a fine-grained soil, is compacted to 95 percent of standard maximum dry density and close to optimum moisture content (AASHTO T 99



a) Partially encapsulated subgrade



b) Completely encapsulated subgrade

Figure 8. Suggested Methods for Preventing the Contact of Water in a Granular Base with the Soil Subgrade.

or ASTM D 698), pavement constructability problems will not be encountered, or future pavement problems will not occur. Generally, this may be true in many situations. Compaction increases the shear strength of soils. As the compactive effort increases, the cohesive component increases; the angle of internal friction increases slightly (Hopkins, January 1988). When fine-grained soils, such as clays or silts, are compacted in the subgrade, the degree of saturation of the compacted material is approximately 80 to 85 percent. The degree of saturation indicates the portion of void spaces in a soil mass filled with water -- the ratio of the volume of water to the volume of voids. When a subgrade is initially compacted to standard conditions and there is no change in the volume of compacted subgrade under wheel stresses, the build up of excess pore water pressure cannot occur, that is $\Delta u = 0$, since the degree of saturation is below 100 percent. As shown by Equation 11, the shear strength available to resist failure (and the imposed loads) remains constant and the stability remains constant. Instability may still occur if the wheel stresses (driving stresses) are greater than the shear strength given by Equation 11. If the number of traffic load applications are increased, and the size of induced stresses is sufficiently large, then the fine-grained subgrade may reduce volume, or compress. With a reduction in volume of material located under the wheel stresses, the degree of saturation increases and eventually may reach 100 percent. When

this occurs, the situation is created under which large, excess pore water pressures (Δu) increase, and the shear strength available to resist failure decreases rapidly since the term, $(\sigma_n - \Delta u) \tan \phi'$, decreases.

The available strength essentially decreases. Under repeated loadings, the cyclic action of excess pore pressures created by repeated loadings eventually destroys, or decreases, the cohesive component and the available shear strength to resist failure tends to zero. As a result, the subgrade may fail

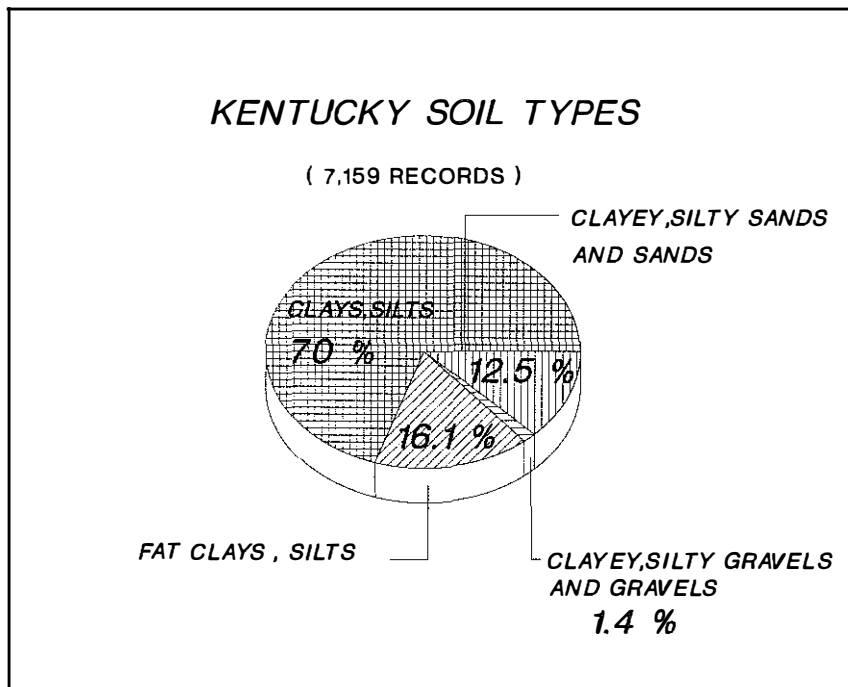


Figure 9. Statistical Overview of the Types of Soils Located in Kentucky (Source: Kentucky Geotechnical Data Bank).

Swelling

Although a subgrade constructed of fine-grained soils may be compacted according to specifications, there is no assurance that the subgrade soils will remain in the same state as they were originally compacted. The likelihood that the original compactive state will change with increasing time and load applications is very probable. Fine-grained soils, especially clayey soils, in a compacted state have a large potential to absorb water and swell. When a compacted soil swells, the volume increases and the shear strength available to resist failure decreases. Swelling lowers the size of the cohesive component rapidly and causes large decreases in this portion of resisting strength (Equation 11). The angle of internal friction is slightly lowered. The total shear

strength available to resist failure is lowered. The shear strength available at sometime after compaction may be much lower than the strength available at the time of initial compaction. Most clayey soils existing in a compacted state swell when exposed to a source of moisture.

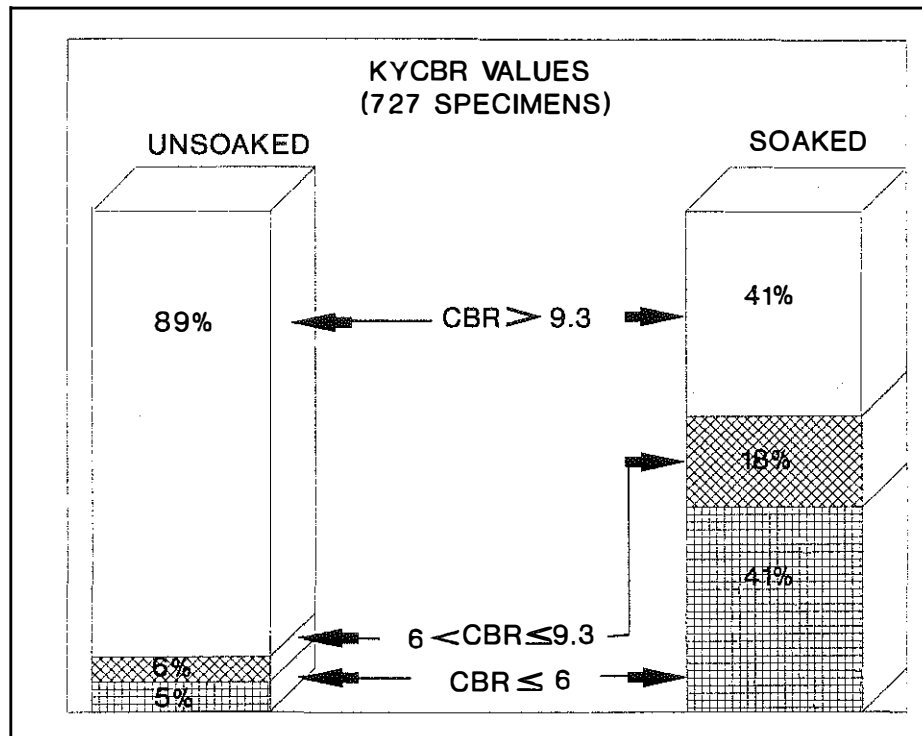


Figure 10. Comparison of Soaked and Unsoaked Values of Kentucky CBR (KYCBR).

tests, each specimen was penetrated before and after soaking. Before soaking, 95 percent of the 727 test specimens had KYCBR values greater than six; only 5 percent of the specimens had values of KYCBR less than 6. After soaking (specimens in the KYCBR test are allowed to swell until successive, measured values of deflection are less than 0.003 inches), only 59 percent of the test specimens had KYCBR values greater than six; 41 percent of the specimens had KYCBR values less than 6. The percentage of specimens having KYCBR values less than six increased 36 percent after soaking. Many pavement problems have occurred on soils that have soaked KYCBR values less than six. Bearing strengths of many specimens decreased significantly after soaking.

The effect of swelling on bearing strength is also illustrated by data shown in Figure 11 (Hopkins 1984; Hopkins 1988). The values of CBR of unsoaked specimens of a number of different types of compacted shales are compared to CBR values of the same specimens soaked and given full opportunity to swell. Except the specimens identified as "New Albany," "Hance", and "Drakes," there was a significant decrease in the value of CBR for each specimen after soaking. Various types of shales represented in Figure 11 have been used often in Kentucky to construct pavement subgrades and have caused numerous pavement problems. A significant aspect of the data in Figure 11 is the large values of KYCBR of the compacted shales in an unsoaked state. The unsoaked values ranged from about 15 to 42. Materials that have bearing strengths of this size could easily withstand most construction traffic loadings without serious rutting or failure. When materials of this nature are initially compacted, serious problems are not normally encountered as long as

The effect of swelling on the bearing, or shear, strength of clayey soils due to absorption of water is illustrated by the data presented in Figure 10. These data were obtained from the Kentucky Geotechnical Data Bank (Hopkins, et al. 1991) and illustrate how the bearing strength of many soils may be reduced when soaked and allowed to swell. In this figure, the KYCBR (Drake and Havens, 1959; Kentucky Methods Manual 1987) values of unsoaked and soaked specimens are compared. Some 727 values of unsoaked and soaked values of KYCBR were available for comparison. In all these

they remain in this initial compactive state and the placement water content is near or lower than the optimum water content. After soaking, the KYCBR values of the specimens range from about 0.5 to 6 percent if the specimens identified as New Albany, Hance, and Drakes are excluded. These three shales are very sandy and silty and do not degrade when exposed to water. The other specimens are clayey shales and degrade into flakes when exposed to water. Particles of these shales have a great affinity for water.

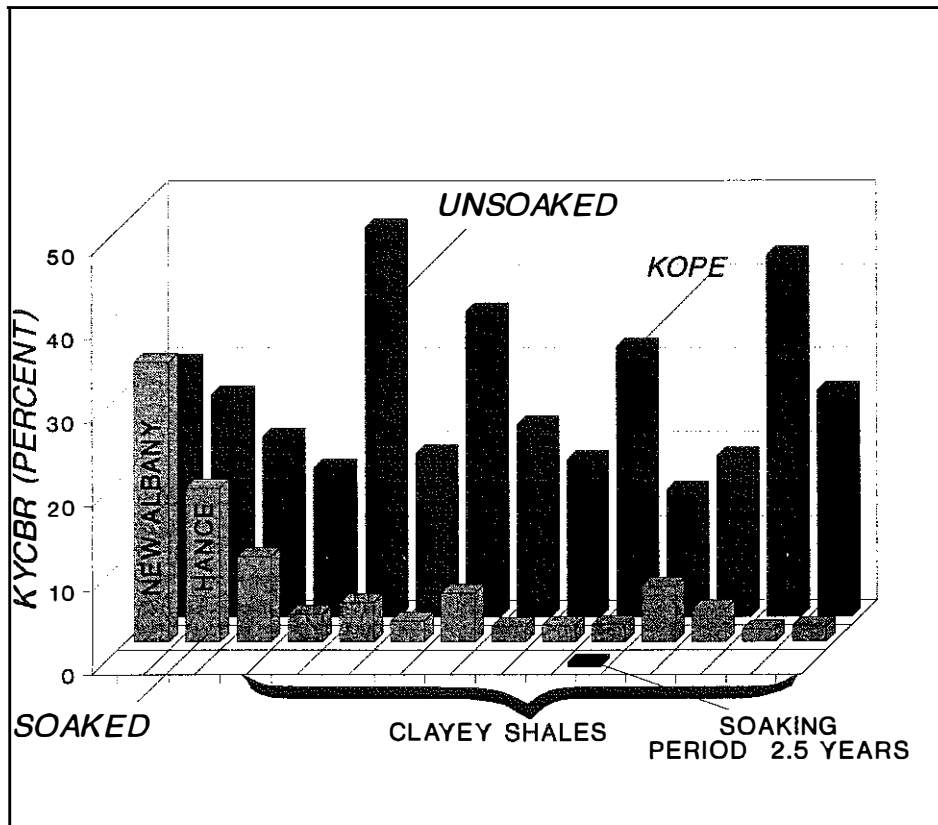


Figure 11. Comparison of Soaked and Unsoaked Values of KYCBR for a Number of Selected, Typical Kentucky Shales.

size particles, as shown in Figure 13. As the percent finer than 0.002-mm size particles increase, both unsoaked and soaked values of CBR decrease. If the percent of clay-size particles finer than the 0.002-mm size is less than about 10-15 percent or the value of swell is less than about 2 percent, it appears that the soaked CBR value does not change significantly after soaking. The size of the KYCBR value is probably sufficient to withstand most construction traffic loadings without failure.

When a compacted shale or clayey soil absorbs water, the degree of saturation approaches 100 percent. If a source of water is readily available for a substantial period, the swelling soil eventually becomes completely saturated and the shear strength is lowered in two ways. First, as the soil swells, the volume increases as the moisture content increases. The cohesive component of strength (Equation 11) decreases. A slight change also occurs in the angle of internal friction. Secondly, when construction traffic loads clayey subgrades, sufficiently large, excess pore water pressures occur and the shear strength is further reduced as illustrated by Equation 11. Normally, granular bases and bituminous layers of the pavement do not swell, this aspect does not affect their shear strength.

The enormous decrease in the CBR values after soaking appears to be a function of the magnitudes of vertical swell (or strain) -- as measured in the CBR test -- and the clay-size particles smaller than 0.002 mm as shown in Figures 12 and 13, respectively. As shown in Figure 12, the trend of unsoaked values of CBR remains essentially constant or increases slightly as the vertical swell increases. After soaking, the soaked value of KYCBR decreases as the vertical swell increases. The magnitudes of KYCBR values of the compacted shales seem closely related to the percent finer than 0.002-mm

Moisture

Water may enter pavement layers in several ways. Surface water from rainfall or snow melt seep into layers through surface cracks, joints, through the unpaved portions at the edges of shoulders, and through the pavement itself. Water may enter the pavement layers by subsurface seepage from water bearing rock strata in cut-and-fill transitional zones. Although the water table may be located at some elevation lower than the bottom of the base courses, the clay subgrade may increase in moisture content because of capillary rise. It is generally recognized that water in pavement layers is detrimental to the performance of the pavement.

The most critical period for the development of damage to the subgrade, and the future source of damage to the pavement, occurs during construction. During this critical period, the subgrade remains exposed to rainfall, or snow melt, which seeps into the subgrade. If rainy periods or heavy snowfalls occur during construction, the exposed subgrade, especially a clayey subgrade (which are frequently constructed), has the opportunity to absorb water and swell. With an increase in moisture content and volume, the degree of saturation approaches 100 percent. Both the cohesive shear strength component and angle of internal friction decrease, that is, the bearing strength is lowered. When the degree of saturation is 100 percent and the subgrade is

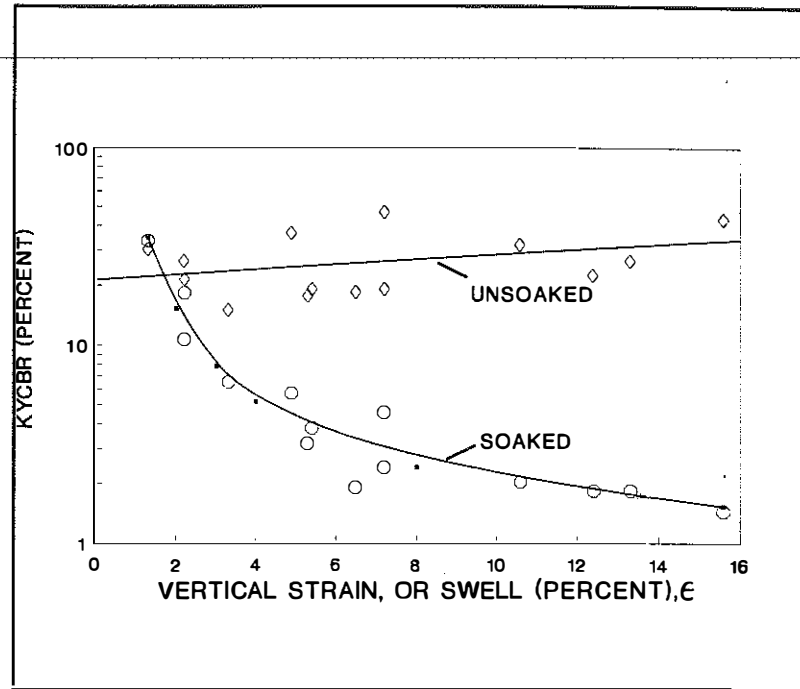


Figure 12. Variation of Soaked and Unsoaked Values of KYCBR with Vertical Swell Measured During the KYCBR Test for Selected Kentucky Shales.

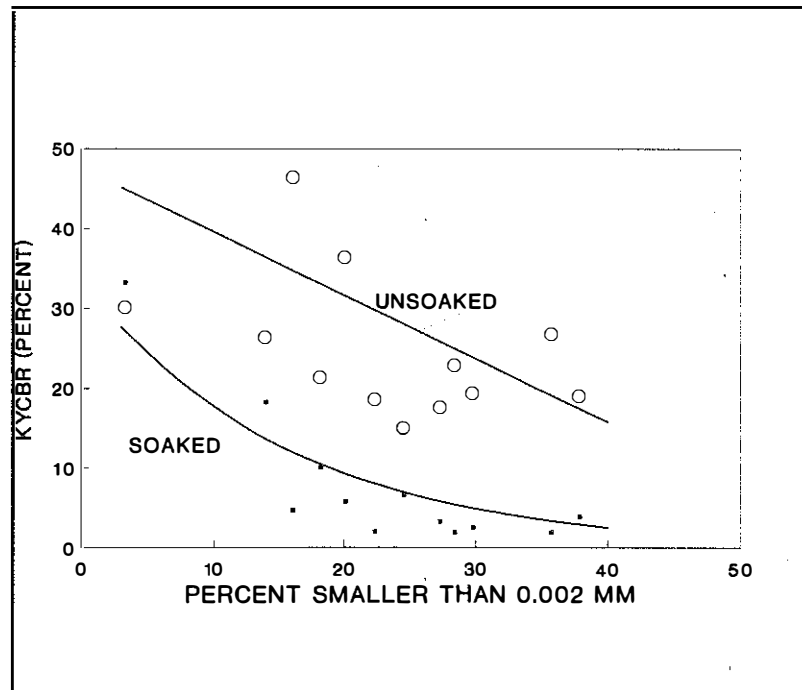


Figure 13. Relationships Between KYCBR Values and the Percent Finer Than the 0.002-mm Size for Selected Kentucky Shales.

loaded with construction traffic, excess pore pressures build up and, according to Equation 11, the shear strength available to resist failure is lowered. The stability of the subgrade is lowered. This situation occurs quite often when clayey subgrades remain exposed during the winter, or when heavy rainfalls (or/and snow melt) occur before placement of the pavement (many subgrades requiring remedial measures and inspected by personnel of the Geotechnical staff of the Kentucky Transportation Cabinet are of this nature -- Smith 1989). There is a tendency for the degree of saturation to increase from the initial state of 80-85 percent to some value higher than the initial value.

Attempts to construct granular base courses and bituminous courses on subgrades that have increased in moisture content and saturation presents compactive problems. Difficulties are encountered in achieving proper compaction of the granular base and bituminous layers because of the weakened or soft condition of the subgrade. Stresses due to heavy compactors are transmitted through the pavement layers to the saturated subgrade. These stresses cause an instantaneous increase in excess pore water pressure in the subgrade. As shown by Equation 11, there is a decrease in the shear strength available to resist failure.

MATHEMATICAL MODEL EQUATIONS

The pavement bearing capacity model developed during this research study and used to calculate the factor of safety against failure is a generalized limit equilibrium procedure of slices. The pavement mathematical model is an adaptation of a slope stability model developed by Hopkins in 1986. The mathematical model has been formulated in such a manner that the factor of safety of a multi-layered flexible pavement system may be calculated. The factor of safety of a pavement system containing as many as 25 (arbitrarily selected) different layers may be found. In the procedure, the potential failure mass is divided into a series of vertical slices; the equilibrium of each slice and the equilibrium of the entire mass is considered. In the approach used in the model, the ultimate strength of the materials in each pavement layer is used. Algorithms were developed to simulate any given contact tire stress. The theoretical equations presented herein were programmed for the IBM 3091. The computer program was written in the FORTRAN language and it is referred to herein as the HOPKIB computer program. Development of the pavement bearing capacity mathematical model is presented as follows.

Statical Indeterminacy

Determining the stability of a potentially unstable mass based on a limit equilibrium approach is indeterminate as shown in Table 1. There are more unknown quantities than known quantities. To make the pavement stability problem determinate, certain assumptions must be made. Known quantities and assumptions required to achieve statical equilibrium of the pavement bearing capacity model are summarized in Table 2. The location of the line passing through the points of action of the interslice forces, or the line of thrust (Bishop 1955; Janbu 1954) is assumed. This assumption is unique. In other limit equilibrium procedures of slices, such as those by Morgenstern and Price (1965), Spencer (1967), Spencer (1973), and Hardin (1984), the locations of the points of action of the interslice forces are computed as part of the solution. Although variation of the interslice points of location on the sides of slices causes changes in computed values of the factor of safety, the slight variations do not appear to affect the reasonableness of solutions obtained from the model analyses.

TABLE 1. UNKNOWNNS AND EQUATIONS FOR n SLICES

UNKNOWNNS ASSOCIATED WITH FORCE EQUILIBRIUM		
1	Factor of Safety	
n	Normal Forces (dN_i) on the Base of Each Slice	Resultant Forces (Z_i) of E_i and (or) T_i on Each Interface Between Slices
$n-1$	Normal Forces (E_i) on Each Interface Between Slices	
$n-1$	Shear Forces (T_i) on Each Interface Between Slices	Angles -- Which Express the Relationships between E_i and on Each Interface

UNKNOWNNS ASSOCIATED WITH MOMENT EQUILIBRIUM		
n	Coordinates b_i Locating the Normal Forces on the Base of Each Slice	
$n-1$	Coordinates a_i Locating the Normal Forces E_i on Each Interface Between Slices	

$2n-1$	Unknowns Versus n Equations	
Total Unknowns		
$5n-2$	Unknowns Versus $3n$ Equations	

Basic Assumptions

Fundamental assumptions made in the formulation of the pavement bearing capacity model are as follows:

- A line, or thrust line (Bishop 1954), passing the points of action of the interslice forces is known or assumed.
- The materials forming the layers of the pavement of the potentially unstable mass conform to the Terzaghi-Coulomb shear strength formula (Terzaghi 1943).
- For each pavement cross section, the stability problem is treated as two dimensional (plain strain).
- The shear strength of the materials in the pavement layers may be expressed in terms of effective stress or total stress (Terzaghi 1943).
- The factor of safety of the cohesive component of strength and the frictional component are equal.

TABLE 2. JANBU'S (1954) APPROACH (UNKNOWN AND EQUATIONS FOR n SLICES)

UNKNOWN ASSOCIATED WITH FORCE EQUILIBRIUM	
1	Factor of Safety
n	Normal Forces (N_i) on the Base of Each Slice
$n-1$	Normal Forces (E_i) on Each Interface Between Slices
Assume (Initially) $T_i = 0$	Shear Forces (T_i) on each Interface Between Slices

2n	Unknowns Versus 2n Equations
UNKNOWN ASSOCIATED WITH MOMENT EQUILIBRIUM	
n	Coordinates b_i Locating the Normal Forces on the Base of Each Slice
Assume	Coordinates A_i Locating the Normal Force E_i on Each Interface Between Slices

n	Unknowns Versus n Equations
Total Unknowns	

3n	Unknowns Versus 3n Equations

- The factor of safety is the same for all slices. It is expressed as the ratio of the total shear strength available on the shear surface to the total shear strength mobilized to maintain statical equilibrium (Bishop 1954). This assumption implies there is mutual support between adjacent slices. It implies the existence of interslice forces.
- Since vehicles are normally in motion, the assumption is made that contact tire stresses are in motion and that the imposed contact stresses act similar to an infinitely long strip loading. While this assumption may not be strictly correct, this assumption is considered to be conservative in nature since end effects of the loaded area are not included. Forces due to acceleration, a , or deceleration are not considered in this study ($a = 0$).

Theoretical Equations

A cross section of a pavement subgrade showing the external loading of wheel loads and the potential failure mass and bearing capacity shear surface is shown in Figure 14. The potential failure mass located between the potential failure surface and grade elevation is divided into slices by vertical lines. The forces acting on the four boundaries of an individual slice are shown in Figure 15. The sign convention used in formulating equations is shown in the upper right portion of this figure.

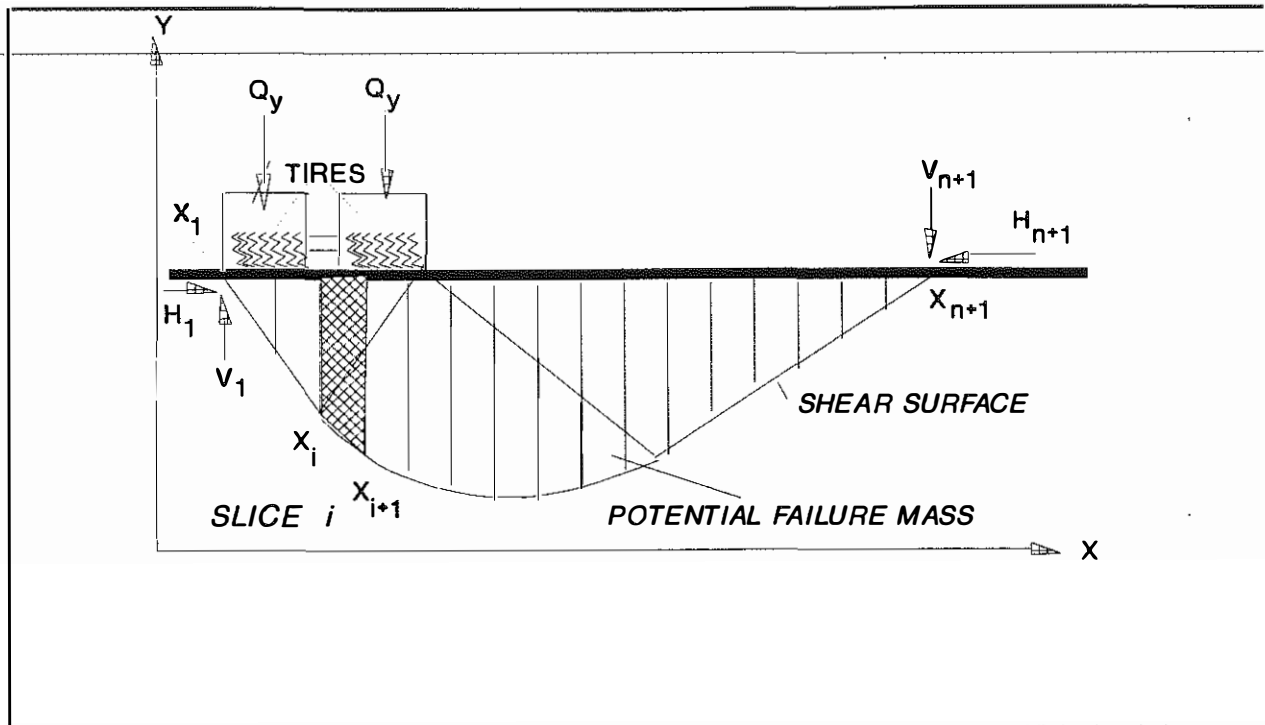


Figure 14. Division of Potential Failure Mass Into Slices.

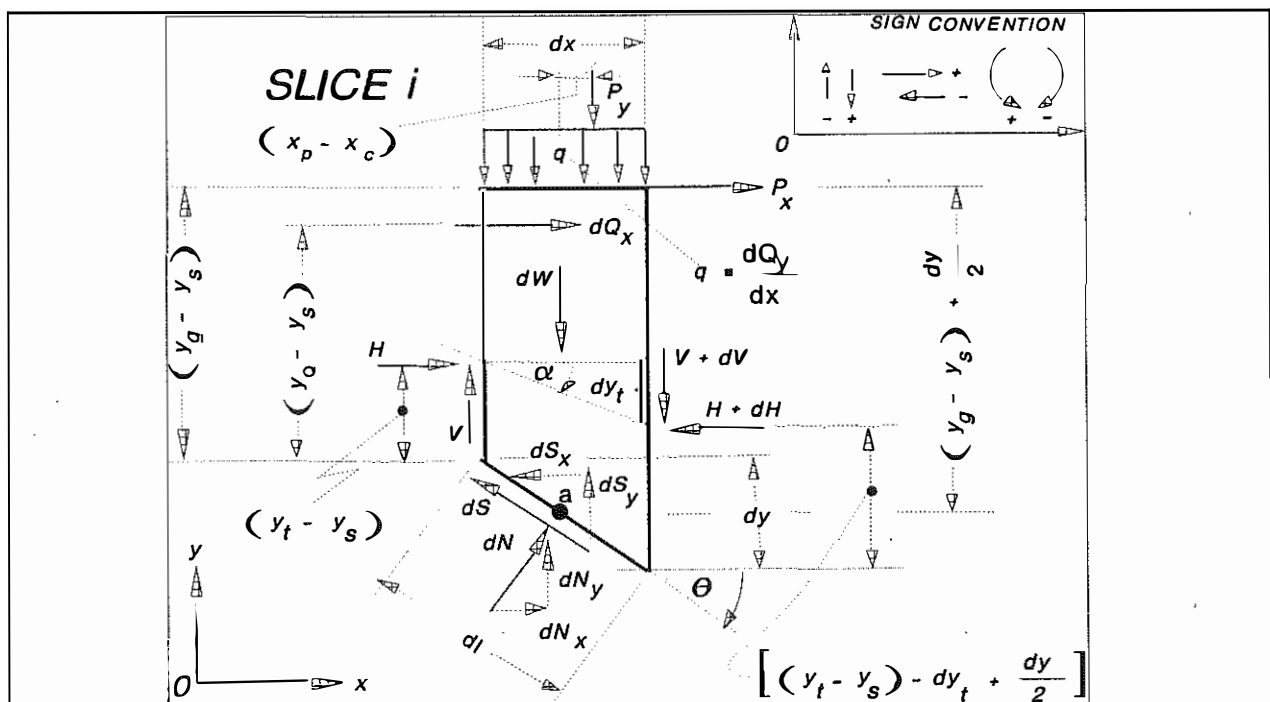


Figure 15. Forces Acting on Slice i .

Geometry

The method used to describe the geometry of a pavement section and the arrangements of different types of layers is illustrated in Figure 16. Only two-dimensional problems may be solved by the computer program. Geometry of the section is defined by x- and y- coordinates and line segments. The x- coordinate direction must be horizontal and increases positively from left to right. The y- coordinate direction is vertical and must increase positively from bottom to top. The origin of the coordinate system is located to the left and below the section.

The entire cross section is approximated by straight-line segments. This applies to the ground line surface, layer boundary interfaces, water table surface, or piezometric lines, shear surface, and thrust line (Bishop 1954). The uppermost line segments are identified in the computer solution as the ground line surface (grade elevation). In the example shown in Figure 16, the ground line is defined by x- and y- coordinates of points a, b, and c. Layer number 1 lies between the line segments of the ground line surface and line segments of boundary interface number 1. Boundary interface number 1 is described

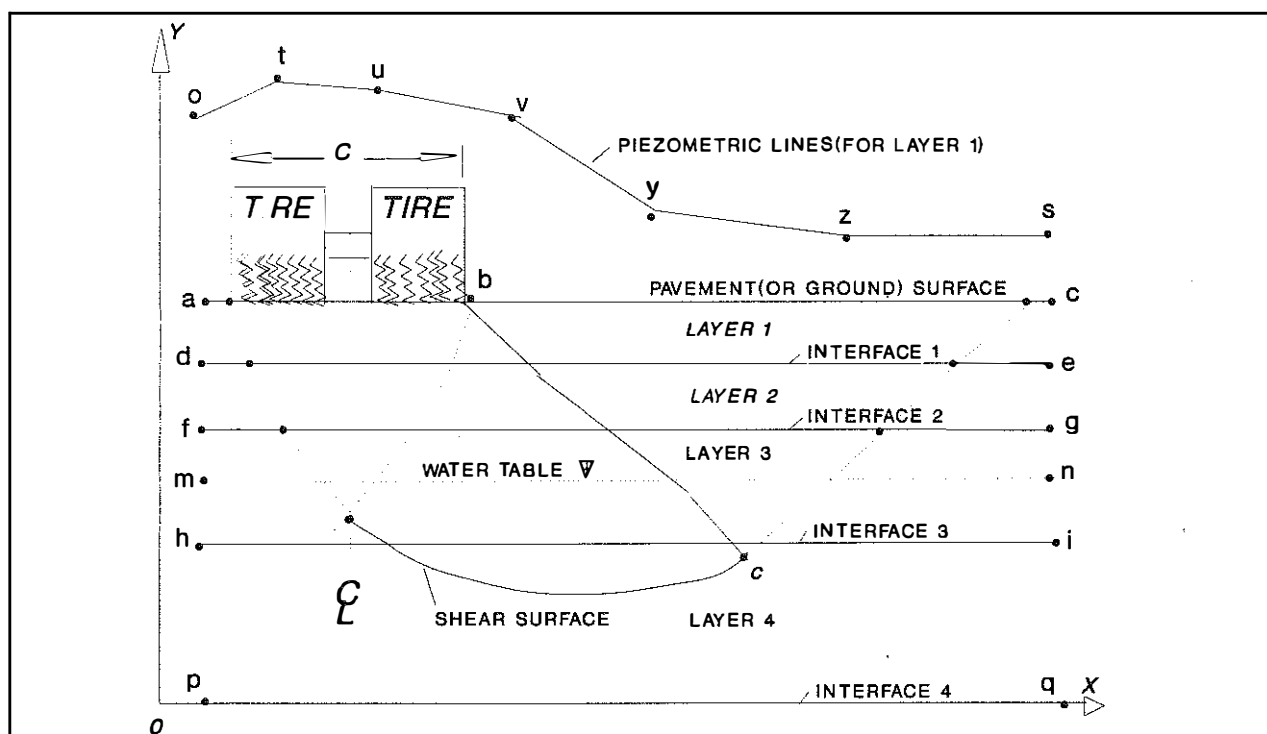


Figure 16. *Coordinate System.*

by x- and y- coordinates of Points d and e. Layer number 2 lies between boundary interface number 1 (Points d and e) and boundary interface number 2. This interface is described by x- and y- coordinates of Points f and g in the example. Layer number 3 lies between boundary interface number 2 and boundary interface number 3. Interface number 3 is described by x- and y- coordinates of Points h and i. For additional layers of material, this pattern is repeated. In the present version of the computer model (HOPKIB, version 1.0), a maximum of 25 (arbitrarily selected) layers of material may be specified.

Additionally, the ground surface and all boundary interfaces must be horizontal -- this condition does not seriously affect the solution since most pavement layers are essentially horizontal (subsequent versions of the computer model will remove this condition).

As shown in Figure 16, the water table is defined by x- and y- coordinates of Points m and n. Alternatively, the pore pressures in any given layer of material may be defined by x- and y- piezometric coordinates (identified as Points o, t, u, v, y, z and s in Figure 16). As another option, pore pressures may be defined for each layer of material using a pore pressure ratio (Daehn and Hilt 1951),

$$r_u = \frac{u}{\sigma_v}. \quad (27)$$

The pore pressure ratio, r_u , is a dimensionless parameter. This parameter is the ratio of the pore pressure, u , to the vertical stress, σ_v , above the element under consideration. In the computer solution, pore pressures in one layer may be defined by piezometric coordinates while in another layer they may be defined by specifying a value of r_u . Line segments of the water table, piezometric coordinates, thrust line, or shear surface need not be horizontal. A maximum of twenty-five coordinates may be used to describe a given piezometric level or water table. A set of piezometric lines may be used to define the pore pressures for each layer of material. Piezometric lines and pore pressure ratios may be intermixed.

Definitions

A summary and definitions of the forces acting on an individual slice (Figure 15) are as follows:

dx	=	finite width of slice i
P_y	=	external vertical point load acting on the surface of slice i
P_x	=	horizontal external point load acting at the surface of slice i
dQ_x	=	horizontal force acting at the surface or in the interior of the soil mass (earthquake force)
dQ_y	=	vertical force acting at the surface or in the interior of the soil mass (in the analysis performed herein, $dQ_y (= qdx)$ is assumed to be the force acting on a single tire).
dW_y	=	denotes the weight of the slice
dN	=	normal force acting perpendicular to the base of slice i (see Figures 15 and 17)
dN_y	=	normal force component acting vertically at the base of slice i
dN_x	=	normal force component acting horizontally at the base of slice i
dS	=	shear force acting along the base of slice i (see Figures 15 and 17)
dS_y	=	component of the shear force acting vertically at the base of slice i
dS_x	=	component of the shear force acting horizontally at the base of slice i
H	=	resultant of the total horizontal interslice force
V	=	resultant of the total vertical interslice force
dl	=	length of slice i along its base
S_c	=	seismic coefficient
$\tan \alpha$	=	slope of line of thrust
$\tan \theta$	=	slope of shear surface

$(y_t - y_s)$	=	vertical distance between shear surface and line of thrust
dy	=	vertical distance between the shear surface at the left side of slice i and the shear surface at the right side of slice i
$(y_Q - y_s)$	=	distance that dQ_x acts above the assumed shear surface
$(y_g - y_s)$	=	distance that P_x acts above the assumed shear surface (also, the vertical distance between ground surface and shear surface at the side of slice i)
σ	=	normal stress acting perpendicular to the base of slice i
τ	=	shear stress acting along the shear surface
F	=	average factor of safety
C	=	tensile element resultant force acting at the base of slice i (see Figure 18).
C_x	=	tensile element component force acting horizontal at the base of slice i
C_y	=	tensile element component force acting vertical at the base of slice i

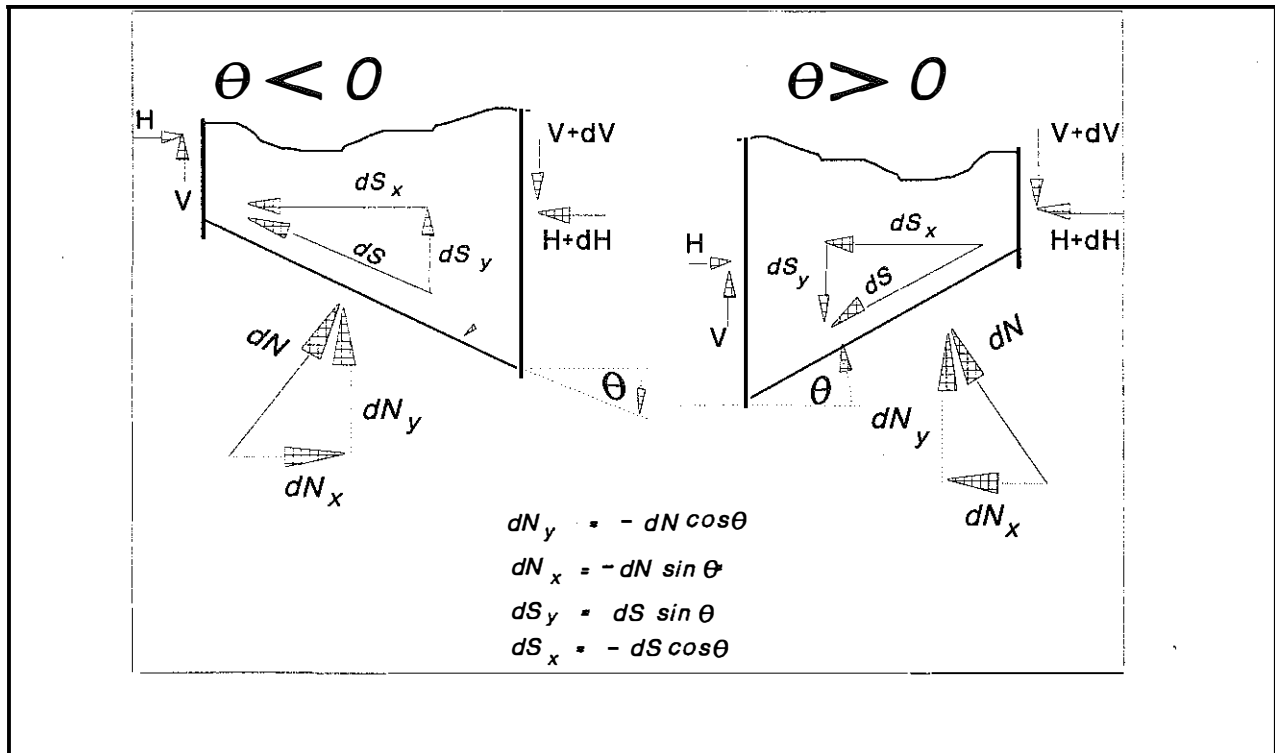


Figure 17. Projections of the Forces dN and dS When $\theta > 0$ and $\theta < 0$.

Projections of the forces, dN and dS , when θ is greater than zero and when θ is less than zero are shown in Figure 17. The tensile element force, C , acting at the base of slice i and projections of this force, C_x and C_y , are considered in Figure 18. The directions of the force C when θ is greater than zero and when θ is less than zero are shown in Figure 18. When θ is less than zero, the force C acts at some angle, η (as shown in the left portion of Figure 18) where η is assumed to be some value between $180 + \theta$ and 180 degrees. When θ is greater than zero, the force C is assumed to act at angle, η , that lies between $180 + \theta$ degrees and 270 degrees, as shown in the right portion of Figure 18 (equations have been derived that relate the direction -- or angle η -- of force C in terms of the angle θ and the failure strain, E_f , or a selected value of E , of the tensile element that intersects the base of slice i).

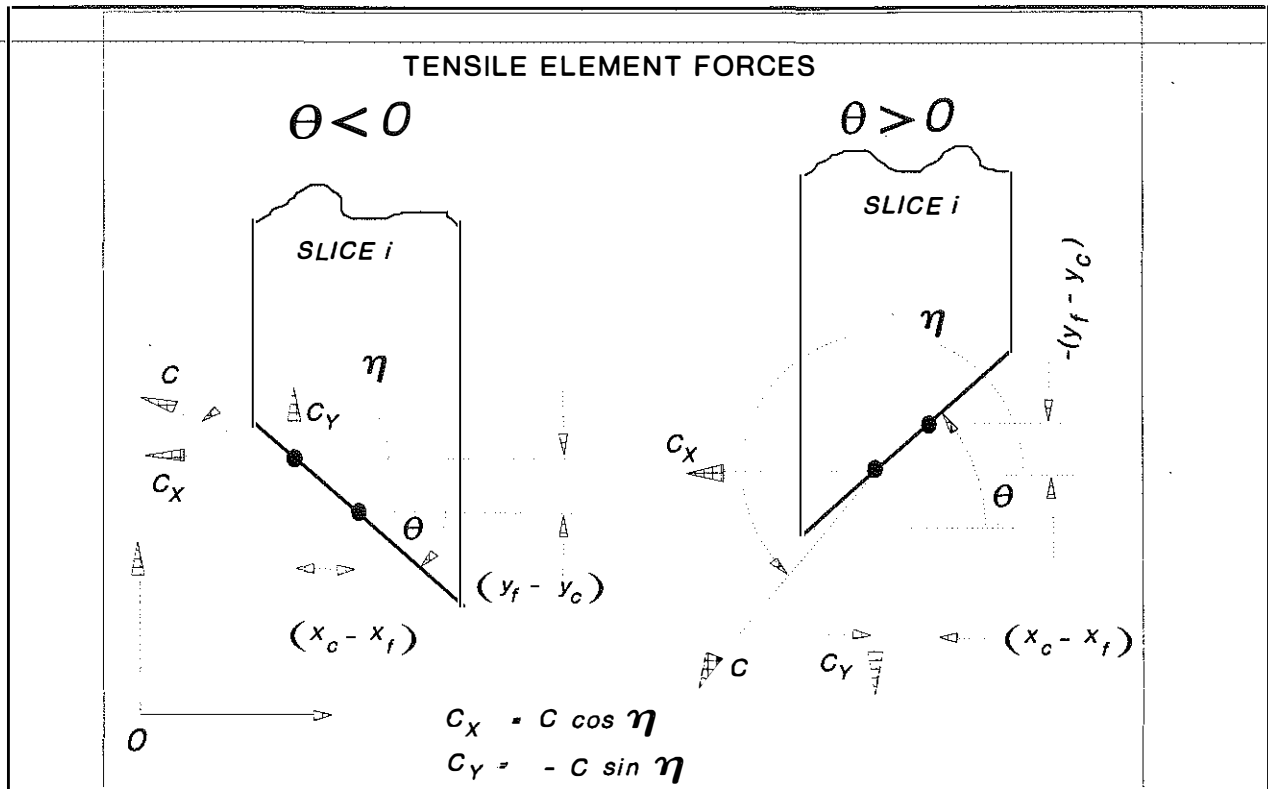


Figure 18. Projections of Tensile Element Forces Acting at the Base of Slice i When $\theta > 0$ and $\theta < 0$.

Presentation of these equations and a full treatment of the algorithms associated with tensile elements is beyond the objectives and scope of this research study; a complete discussion of these relationships will be given in a future research study (Hopkins 1991) that currently is in progress. Although the derivations given below consider the force C , the HOPKIB bearing capacity computer model does not include these algorithms.

Derivations

The equation of equilibrium in the horizontal direction (see Figure 15) is:

$$\Sigma \text{ HORIZONTAL FORCES} = 0:$$

$$H - (H + dH) + dN_x + dS_x + dQ_x + P_x + C_x = 0 \quad (28)$$

$$H - H - dH + dN_x + dS_x + dQ_x + P_x + C_x = 0. \quad (29)$$

Solving for dN_x ,

$$dN_x = dH - dS_x - dQ_x - P_x - C_x. \quad (30)$$

The equation of equilibrium in the vertical direction is:

Σ VERTICAL FORCES = 0:

$$dQ_y + P_y + dW - V + (V + dV) + dS_y + dN_y + C_y = 0. \quad (31)$$

Solving for dN_y

$$dN_y = -dQ_y - P_y - dW - dV - dS_y - C_y. \quad (32)$$

Equation 31 may be used to develop an expression for the normal stress, σ , which acts perpendicular to the base of slice i . Since

$$dN_y = -dN \cos \theta, \text{ and} \quad (33)$$

$$dS_y = dS \sin \theta, \text{ then} \quad (34)$$

$$-dN \cos \theta = -dQ_y - P_y - dW - dV - dS \sin \theta + C \sin \eta \quad (35)$$

$$dN \cos \theta = dQ_y + P_y + dW + dV + dS \sin \theta - C \sin \eta \quad (36)$$

$$dN = [dQ_y + P_y + dW + dV - C \sin \eta] \sec \theta + dS \tan \theta \quad (37)$$

(See Figure 19), then

$$dN = \sigma dl = \sigma dx \sec \theta, \text{ and} \quad (38)$$

$$dS = \tau dl = \tau dx \sec \theta, \text{ then} \quad (39)$$

$$\sigma dx \sec \theta = [dQ_y + P_y + dW + dV - C \sin \eta] \sec \theta + \tau dx \sec \theta \tan \theta. \quad (40)$$

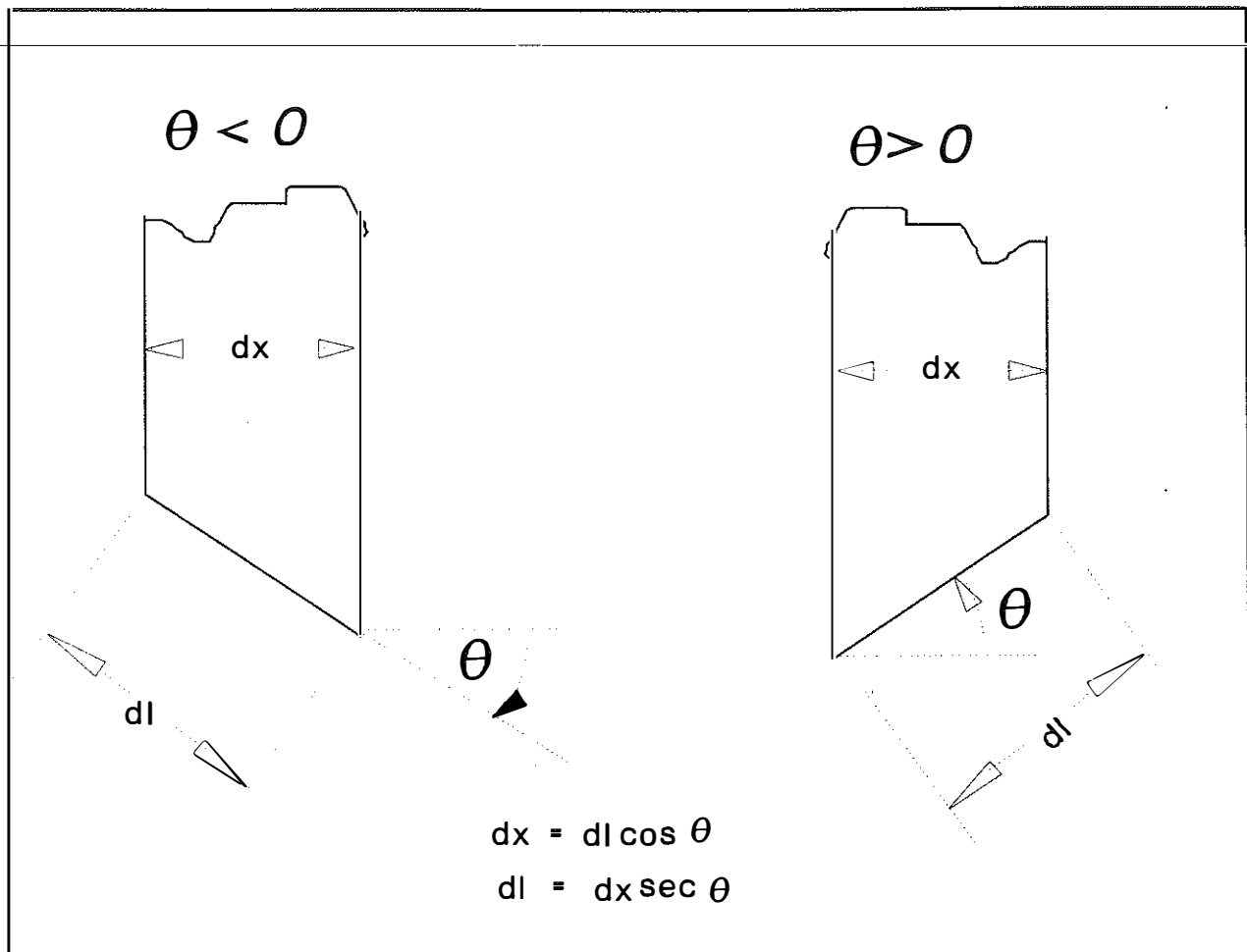


Figure 19. Relationship Between dx and dl .

Solving for σ ,

$$\sigma = \frac{[dQ_y + P_y + dW + dV - C \sin \eta] \sec \theta}{dx \sec \theta} + \frac{\tau dx \sec \theta \tan \theta}{dx \sec \theta} \quad (41)$$

$$\sigma = \left[\frac{dQ_y}{dx} + \frac{P_y}{dx} + \frac{dW}{dx} + \frac{dV}{dx} - \frac{C \sin \eta}{dx} \right] + \tau \tan \theta \quad (42)$$

By definition, the equation defining limit equilibrium and the mobilized shear stress, τ is:

$$\tau = \frac{c'}{F} + \frac{(\sigma - u)\tan\phi'}{F} \quad (43)$$

By introducing Equation 42 into Equation 43, an expression for τ is:

$$\tau = \frac{c'}{F} + \left(\left[\frac{dQ_y}{dx} + \frac{P_y}{dx} + \frac{dW}{dx} + \frac{dV}{dx} - \frac{C\sin\eta}{dx} \right] + \tau\tan\theta - u \right) \frac{\tan\phi'}{F}. \quad (44)$$

Let

$$M = \left[\frac{dQ_y}{dx} + \frac{P_y}{dx} + \frac{dW}{dx} + \frac{dV}{dx} - \frac{C\sin\eta}{dx} \right], \quad (45)$$

then

$$\tau = \frac{c'}{F} + \frac{M\tan\phi'}{F} - u\frac{\tan\phi'}{F} + \frac{\tau\tan\theta\tan\phi'}{F} \quad (46)$$

$$\tau = \frac{c'}{F} + [(M + \tau\tan\theta) - u]\frac{\tan\phi'}{F} \quad (47)$$

$$\tau - \frac{\tau\tan\theta\tan\phi'}{F} = \frac{c'}{F} + \frac{M\tan\phi'}{F} - u\frac{\tan\phi'}{F} \quad (48)$$

Equations 30 and 32 may be used to obtain an expression for the differential horizontal force, dH , by eliminating dN . By making the substitution,

$$dN_x = -dN\sin\theta, \quad (49)$$

$$\tau \left(1 - \frac{\tan\theta\tan\phi'}{F} \right) = \frac{c'}{F} + \frac{M\tan\phi'}{F} - u\frac{\tan\phi'}{F} \quad (50)$$

$$\tau_f = \frac{c' + \left(\left[\frac{dQ_y}{dx} + \frac{P_y}{dx} + \frac{dW}{dx} + \frac{dV}{dx} - \frac{C \sin \eta}{dx} \right] - u \right) \tan \phi'}{\left(1 - \frac{\tan \theta \tan \phi'}{F} \right)} \quad (51)$$

Equation 30 becomes:

$$dN_x = -dN \sin \theta = dH - dS_x - dQ_x - P_x - C_x \quad (52)$$

$$dN = (-dH + dS_x + dQ_x + P_x + C_x) \csc \theta. \quad (53)$$

Making the substitution,

$$dN_y = -dN \cos \theta, \quad (54)$$

Equation 32 becomes:

$$dN_y = -dN \cos \theta = -dQ_y - P_y - dW - dV - dS_y - C_y \quad (55)$$

$$dN = (dQ_y + P_y + dW + dV + dS_y + C_y) \sec \theta \quad (56)$$

Setting Equation 53 equal to Equation 56, an expression for the differential interslice horizontal forces may be developed as follows:

$$(-dH + dS_x + dQ_x + P_x + C_x) \csc \theta = (dQ_y + P_y + dW + dV + dS_y + C_y) \sec \theta \quad (57)$$

$$(-dH + dS_x + dQ_x + P_x + C_x) = (dQ_y + P_y + dW + dV + dS_y + C_y) \tan \theta \quad (58)$$

$$-dH = (-dS_x - dQ_x - P_x - C_x) + (dQ_y + P_y + dW + dV + dS_y + C_y) \tan \theta \quad (59)$$

$$-dH = -dS_x + dS_y \tan \theta - dQ_x - P_x - C_x + (dQ_y + P_y + dW + dV + C_y) \tan \theta \quad (60)$$

$$-dH = dS \cos \theta + dS \sin \theta \tan \theta - dQ_x - P_x - C_x + (dQ_y + P_y + dW + dV + C_y) \tan \theta \quad (61)$$

$$-dH = \tau dx \sec \theta \cos \theta + \tau dx \sec \theta \sin \theta \tan \theta - dQ_x - P_x - C_x + (dQ_y + P_y + dW + dV + C_y) \tan \theta \quad (62)$$

$$-dH = \tau dx (\sec \theta \cos \theta + \sec \theta \sin \theta \tan \theta) - dQ_x - P_x - C_x + (dQ_y + P_y + dW + dV + C_y) \tan \theta \quad (63)$$

$$-dH = \tau dx (1 + \tan^2 \theta) - dQ_x - P_x - C_x + (dQ_y + P_y + dW + dV + C_y) \tan \theta \quad (64)$$

$$-dH = \tau dx \sec^2 \theta - dQ_x - P_x - C_x + (dQ_y + P_y + dW + dV + C_y) \tan \theta \quad (65)$$

At any interface, x_i , as shown in Figure 14 and 15, the side force, H_i , at any distance from x_1 , may be calculated in the following manner:

$$H_i - H_1 = \int_{x_1}^{x_i} dH \quad (66)$$

or (introducing Equation 65 into Equation 66),

$$H_i = H_1 - \int_{x_1}^{x_i} \tau dx (\sec^2 \theta) - dQ_x - P_x - C \cos \eta + \left(\frac{dQ_y}{dx} + \frac{P_y}{dx} + \frac{dW}{dx} + \frac{dV}{dX} - \frac{C \sin \eta}{dx} \right) dx \tan \theta \quad (67)$$

An expression for calculating the vertical shear force, at any interface, x_i , may be obtained by considering moment equilibrium about point a of slice i, as shown in Figure 15. Moment equilibrium about the assumed point of application (point a in Figure 15) of the normal force, dN , is:

$$\Sigma \text{ MOMENTS} = 0$$

$$\begin{aligned} & H \left[(Y_t - y_s) - \frac{dxtan\theta}{2} \right] - (H + dH) \left[(y_t - y_s) + dxtan\alpha - \frac{dxtan\theta}{2} \right] + \\ & V_i \frac{dx}{2} + (V_i + dV) \frac{dx}{2} + P_x \left[(y_g - y_s) - \frac{dxtan\theta}{2} \right] + \\ & dQ_x (Y_g - y_s) - \frac{dQ_x dxtan\theta}{2} + P_y (X_p - x_c) - C_y (x_c - x_f) + \\ & C_x (Y_f - y_c) = 0. \end{aligned} \quad (68)$$

Multiplying terms,

$$\begin{aligned} & H(Y_t - y_s) - H \frac{dxtan\theta}{2} - H \left[(y_t - y_s) + dxtan\alpha - \frac{dxtan\theta}{2} \right] - \\ & dH \left[(y_t - y_s) + dxtan\alpha - \frac{dxtan\theta}{2} \right] + V_i \frac{dx}{2} + V_i \frac{dx}{2} + dV \frac{dx}{2} + \\ & P_x \left[(y_g - y_s) - \frac{dxtan\theta}{2} \right] + dQ_x (y_g - y_s) - \frac{dQ_x dxtan\theta}{2} + P_y (x_p - x_c) + \\ & C \cos \eta (y_f - y_c) + C \sin \eta (x_c - x_f) = 0. \end{aligned} \quad (69)$$

Rearranging terms, Equation 69 may be written as:

$$\begin{aligned} & H(y_t - y_s) - H \frac{dxtan\theta}{2} - H(y_t - y_s) - Hdxtan\alpha + H \frac{dxtan\theta}{2} - \\ & dH(y_t - y_s) - dHdxtan\alpha + dH \frac{dxtan\theta}{2} + V_i \frac{dx}{2} + V_i \frac{dx}{2} + dV \frac{dx}{2} + \\ & P_x \left[(y_g - y_s) - \frac{dxtan\theta}{2} \right] + dQ_x (y_g - y_s) - \frac{dQ_x dxtan\theta}{2} + P_y (x_p - x_c) + \\ & C \cos \eta (y_f - y_c) + C \sin \eta (x_c - x_f) = 0. \end{aligned} \quad (70)$$

Neglecting the second-order term, $dQ_x dx \tan \theta / 2$, Equation 70 becomes:

$$\begin{aligned}
 & -H dx \tan \alpha - dH(y_i - Y_s) - dH dx \tan \alpha + dH \frac{dx \tan \theta}{2} + dV \frac{dx}{2} \\
 & + V_i dx + P_x(y_g - Y_s) - P_x \frac{dx \tan \theta}{2} + dQ_x(y_q - y_s) + P_y(x_p - x_c) \\
 & + C \cos \eta (y_f - y_e) + C \sin \eta (x_c - x_p) = 0.
 \end{aligned} \tag{71}$$

When concentrated loads are not considered ($P_x = P_y = C_x = C_y = 0$), the values of dH and dV are of the same order as dx . Here, Equation 71 can be further simplified and an expression for V_i is:

$$V_i = H \tan \alpha + \frac{dH}{dx} (y_i - y_s) - \frac{dQ_x}{dx} (y_q - y_s). \tag{72}$$

At any interface, x_i , as shown in Figures 14 and 15, the differential vertical force dV , at any distance from x_i , may be calculated as follows:

$$\int_{x_i}^{x_1} dV = V_1 - V_i. \tag{73}$$

When concentrated loads are present, an expression for dV can be obtained by solving the system of Equations 71, 65, and 50 with respect to dH and dV .

An expression for the average factor of safety may be developed from the equation for overall horizontal equilibrium, or

$$H_{n+1} - H_1 = \int_{x_1}^{x_{n+1}} dH. \tag{74}$$

Substituting the expression, Equation 65, for the differential horizontal interslice forces, Equation 74 becomes:

$$H_1 - H_{n+1} = \int_{x_1}^{x_{n+1}} \frac{\tau_f}{F} dx (1 + \tan^2 \theta) - dQ_x - P_x - C_x + (dQ_y + P_y + dW + dV + C_y) \tan \theta \tag{75}$$

Rearranging terms,

$$H_1 - H_{n+1} + \int_{x_1}^{x_{n+1}} dQ_x + P_x + C_x - \left(\frac{dQ_y}{dx} + \frac{P_y}{dx} + \frac{dW}{dx} + \frac{dV}{dx} + \frac{C_y}{dx} \right) dx \tan \theta = \frac{1}{F} \int_{x_1}^{x_{n+1}} \tau_f dx (1 + \tan^2 \theta), \quad (76)$$

and solving for the average factor of safety, or

$$F = \frac{\int_{x_1}^{x_{n+1}} \tau_f dx (1 + \tan^2 \theta)}{H_1 - H_{n+1} + \int_{x_1}^{x_{n+1}} dQ_x + P_x + C_x - \left(\frac{dQ_y}{dx} + \frac{P_y}{dx} + \frac{dW}{dx} + \frac{dV}{dx} + \frac{C_y}{dx} \right) dx \tan \theta}. \quad (77)$$

Substituting the expression for τ_f (Equation 50), Equation 77 becomes:

$$F = \frac{\int_{x_1}^{x_{n+1}} \left(c' + \left[\frac{dQ_y}{dx} + \frac{P_y}{dx} + \frac{dW}{dx} + \frac{dV}{dx} - \frac{C \sin \eta}{dx} \right] - u \right) \tan \phi' dx (1 + \tan^2 \theta)}{\left(1 - \frac{\tan \theta \tan \phi'}{F} \right) \left(H_1 - H_{n+1} + \int_{x_1}^{x_{n+1}} dQ_x + P_x + C \cos \eta - \left(\frac{dQ_y}{dx} + \frac{P_y}{dx} + \frac{dW}{dx} + \frac{dV}{dx} - \frac{C \sin \eta}{dx} \right) dx \tan \theta \right)}. \quad (78)$$

Solution of Equations

There are many considerations and steps involved in calculating the factor of safety from Equation 78. A full description and complete details of the solution are much beyond the scope of this report. Many details and geometric considerations have been given elsewhere (Hopkins 1985). A brief summary of the steps necessary to solve Equation 78 is described below.

The force, dW , may be approximated as shown in Figure 20 and the expressions

$$dW^i \approx \Delta W_i \approx dW_1 + dW_2 + \dots + dW_{K-1} + dW_K \quad (79)$$

$$\approx \gamma_1 a_1 + \gamma_2 a_2 + \dots + \gamma_{K-1} a_{K-1} + \gamma_K a_K \quad (80)$$

$$\approx \gamma_1 dx(y_g - y_1) + \gamma_2 dx(y_1 - y_2) + \dots + \gamma_{K-1} dx(y_{K-2} - y_{K-1}) + \gamma_K dx(y_{K-1} - y_K), \quad (81)$$

where $y_g, y_1, \dots, y_{K-2}, y_{K-1}$, and $y_K = y$ - coordinates at the intersections of the center of slice i and the bottom of each layer of material and $\gamma_1, \gamma_2, \dots, \gamma_{K-1}$, and $\gamma_K =$ unit weights of Layers 1, 2, ..., $K-1, K$ (K is equal to the total number of layers of the bearing media).

The actual areas bounded by the boundary layer interfaces and the x - coordinates of the sides of the slices are approximated by rectangles. For example, in Figure 20 the actual area identified as $abcd$ (Layer 1) is approximated by the rectangular area identified as $a'b'd'e'$. Similarly, the actual area (Layer 2) identified as $cdef$ is approximated by the rectangular area $c'd'e'f'$. Although this scheme introduces some error in calculating the actual area of a slice (and the force dW), the error becomes essentially insignificant when a large number of slices are used (in solutions shown herein, the potential failure

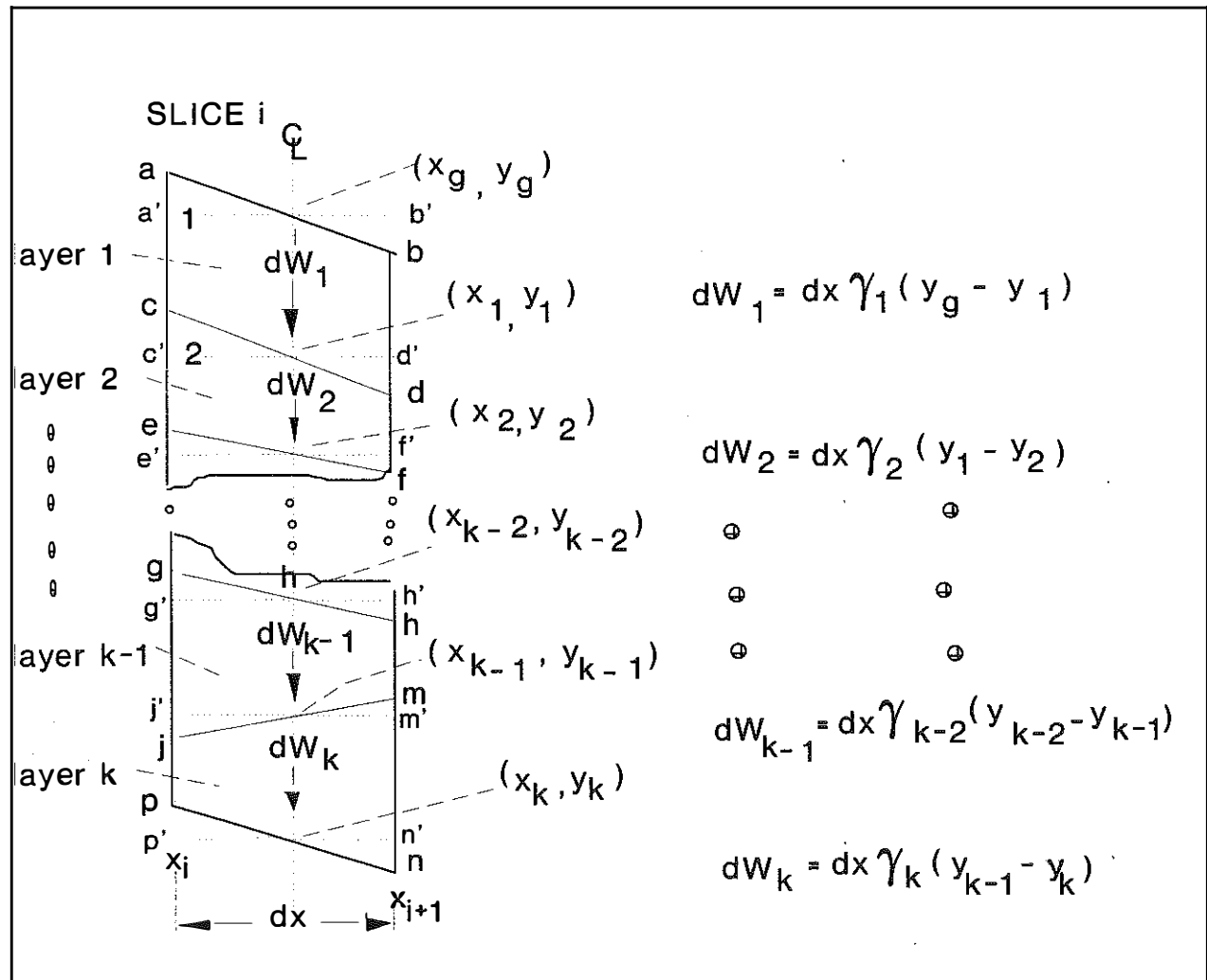


Figure 20. Scheme for Estimating the Force, dW , for a Multilayered Bearing Medium.

masses were divided into 598 slices). The derivative, dW/dx , may be approximated from the following expression:

$$\frac{dW^i}{dx} \approx \frac{\Delta W^i}{\Delta x}, \quad (82)$$

where $\Delta x = x_{i+1} - x_i$.

The scheme for considering distributed loads due to the tire force, dQ_y , is illustrated in Figures 21 and 22. The contact area of the tire resting on the pavement is assumed to be essentially a square. It is assumed that the length of the contact area is infinitely long since the vehicle is normally in motion. The distributed stress may be computed from the relationship:

$$q = \frac{Q_y}{a_c}, \quad (83)$$

where

q = tire contact stress,
 a_c = unit ground contact area.

For example, in the AASHO Road Test (1962), the gross tire unit contact area for the vehicles on lane one, loop four, (18-Kip single-axle loads) was 67.8 pounds per square inches (For loops 3, 4, 5, and six of the AASHO Road Test, the unit tire contact stress was about 87 to 90 percent of the tire inflation pressure). The force (dQ_y) per tire was 4,580 pounds. The unit stress was

$$q_u = \frac{4580 \text{ lbs}}{67.8 \text{ in}^2} = 67.5 \text{ lb/in}^2. \quad (84)$$

In the computer analyses shown herein, the stress, q_u , was assumed to be uniformly distributed as shown in Figure 21. While this assumption is not strictly correct, the assumption simplifies the setup of the equations. Uniformly distributed load (or stress) was assumed to extend the width of the tire and to extend 1 inch into the page (perpendicular to the section). Hence, the distributed load is 67.5 lb/inch(inch) (note: other units may be used). The units of all data entered into the computer model must be consistent. The numerical value and units specified for the unit weight of water control the units of all other input data. For example, if the unit weight of water is specified to be 0.0361 pounds per cubic inch, then x - and y - coordinates must be in inches; values of the strength component, cohesion, c , must be in pounds per square inch; and unit weights of layer materials must be specified as pounds per cubic inch. These units were used in all problems shown herein since these units are convenient to use when

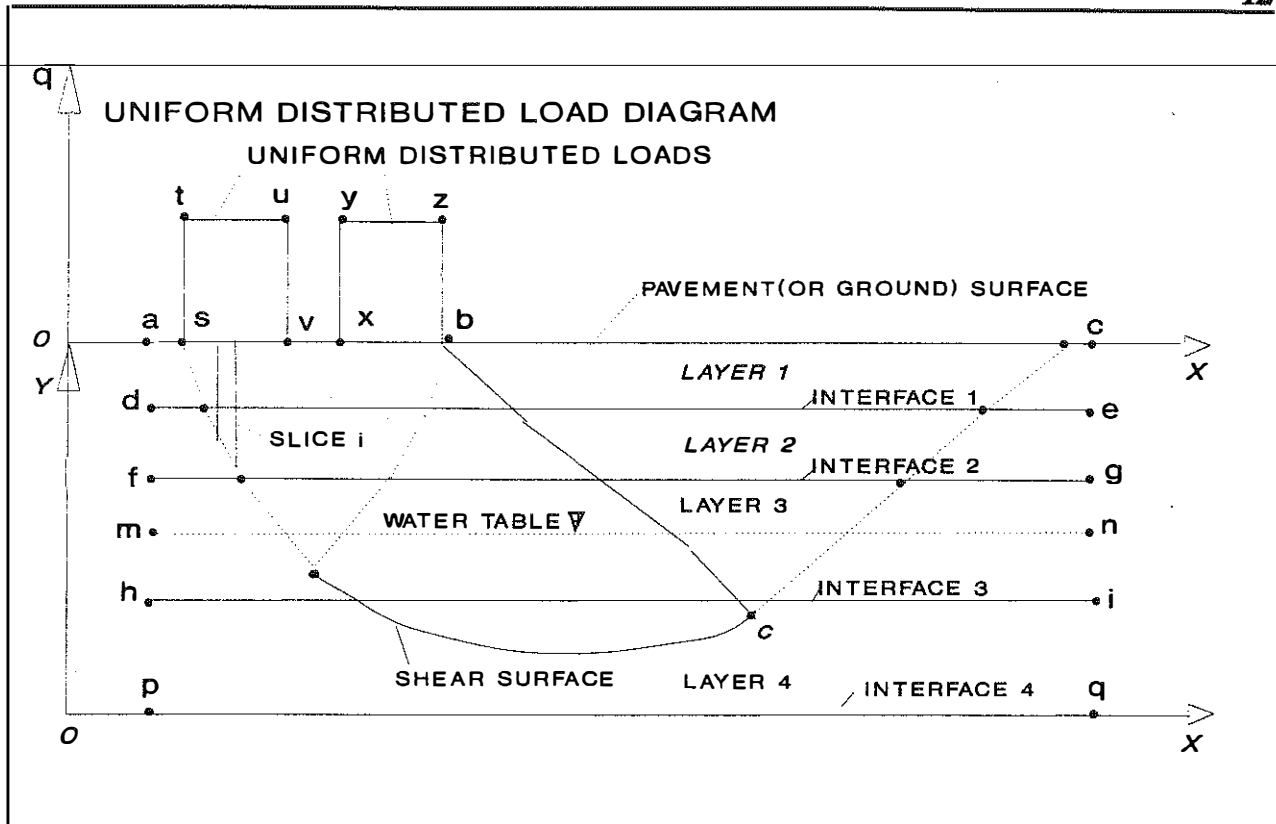


Figure 21. Method for Describing Distributed Loads.

working with pavement layers and considering that thicknesses of pavement layers and tire inflation pressures are usually stated in units of inches and pounds per square inch, respectively.

As shown in Figure 21, the externally-acting distributed loads, q , due to wheel loadings are entered into the computer model by specifying values of q at specified values of the x -coordinate. For example, the distributed load in the example in Figure 21 is described by q - and x - coordinates of Points $a, s, t, u, v, x, y, z, b$, and c . For instance, if q equals 67.5, then the following coordinates would be entered (the q_u - x coordinates must extend the full length of the ground line surface):

x_a	00.0
x_s	00.0
x_t	67.5
x_u	67.5
x_v	00.0
x_x	00.0
x_y	67.5
x_z	67.5
x_b	00.0
x_c	00.0

Internally, in the computer program, for each slice located between the end points, x_i and x_{i+1} , the portion

of the load diagram lying immediately above slice i is divided into ten slices (an arbitrarily selected value), as illustrated in Figure 22, or

$$\Delta X_{si} = \frac{x_{i+1} - x_i}{10} \quad (85)$$

For each small slice, ΔX_{si} , point loads, $P_{\Delta xs}$, are computed from:

$$P_{\Delta xs} = q \cdot \Delta x_s \quad (86)$$

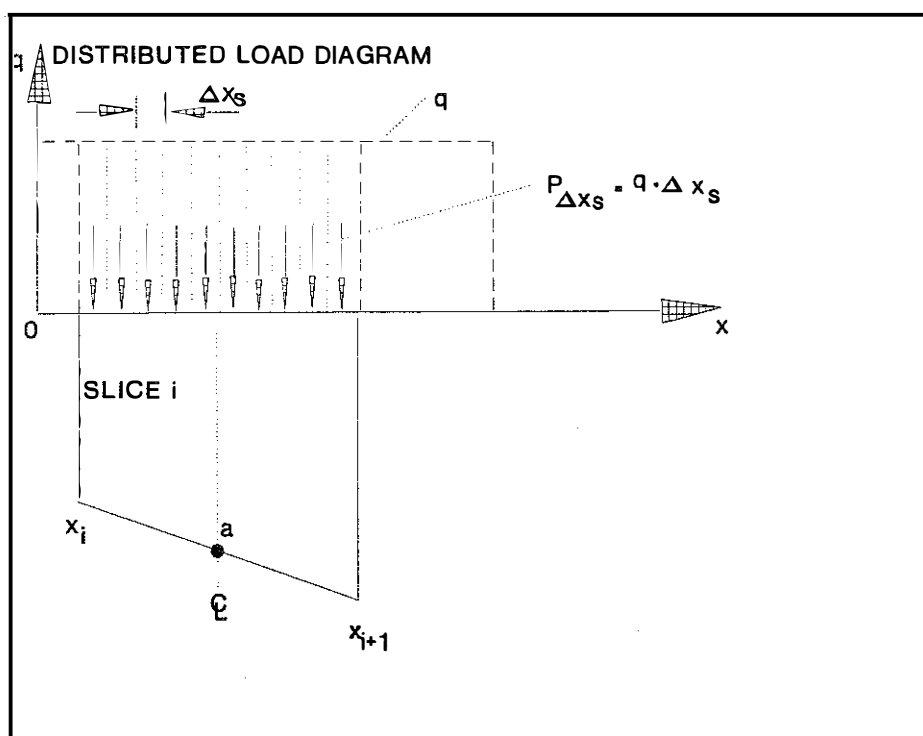


Figure 22. Scheme for Treating Distributed Loads.

using a large number of slices (Note: by formulating the scheme in the manner described above, irregularly-shaped distributed loads, q , may be solved; however, in the present version-- HOPKIB 1.0 -- of the computer solution, only uniformly distributed loads may be solved since the moments due to $P_{\Delta xs}$ are not considered in the present version. When irregularly-shaped distributed loads are used, the unbalanced moments need to be considered. Future versions will rectify this situation so that irregularly-shaped distributed loads may be considered). The derivative dQ_y/dx is

$$\frac{dQ_y}{dx} = q. \quad (87)$$

Since $P_{\Delta xs}$ values occur on both sides of the center of slice i at the base (point a in Figure 22), there are moments about point Q . For a given slice, the moments due to the $P_{\Delta xs}$ forces to the left of Point a and moments to the right of Point a cancel each other, since the area of a given slice is approximated by a rectangle. At the ends of the load ($q > 0$) and in the case where the loaded portion does not coincide with the x -coordinate, x_i or x_{i+1} , there are unbalanced moments. There is some error introduced, but it may be made small by

The force, Q_x (considered herein as an earthquake force acting at the side of each slice), may be approximated from the expression:

$$dQ_x \approx dW \cdot S_c \quad (88)$$

The force dQ_x for each slice is plotted as a function of x_i for each slice. Numerical differentiation is used to obtain a value of dQ_x/dx at the side (x_i - coordinate) of each slice (these calculations are performed internally in the computer model solution).

The end boundary forces, H_1 , H_{n+1} , V_1 , and V_{n+1} are assumed to be known quantities (these quantities, when known or estimated, may be entered into the computer program). In the analyses shown herein, these forces are assumed equal to zero.

The forces, P_y , P_x , and dQ_y are assumed to be known quantities. The derivative, dQ_y/dx , is approximated as follows:

$$\frac{dQ_y}{dx} \approx \frac{\Delta Q_y}{\Delta x} \quad (89)$$

The quantity, P_x/dx (or P_y/dx), containing concentrated load, P_x (or P_y), does not represent a real derivative. This is a generalized δ -function that makes sense only under the integral sign:

$$\left. \begin{aligned} \int_{a_x}^{b_x} \frac{P_x}{dx} dx &= \int_{a_x}^{b_x} P_x \delta(X-C_x) dx = P_x \\ \int_{a_y}^{b_y} \frac{P_y}{dx} dx &= \int_{a_y}^{b_y} P_y \delta(X-C_y) dx = P_y \end{aligned} \right\} \quad (90)$$

where (a_x, B_x) or (a_y, B_y) is any interval containing the point C_x (or C_y) of application of the concentrated load P_x (or P_y).

The value of the tensile element force, C , is assumed to be known. Angle, η , must be assumed. This angle ranges between the angles $180 + \theta$ (see Figure 18) and 180 degrees for $\theta < 0$, and between $180 + 0$ and 270 degrees for $\theta > 0$. The terms, $C \sin \eta/dx$, and $C \cos \eta/dx$ are of the same nature as P_x and P_y , so they are estimated as follows:

$$\int_{a_c}^{b_c} \frac{C \sin \eta}{dx} dx = C \sin \eta \quad (91)$$

and

$$\int_{a_c}^{b_c} \frac{C \cos \eta}{dx} dx = C \cos \eta, \quad (92)$$

where (a_c, b_c) is any interval, containing the point of application of the tensile force C .

(The present version of the HOPKIB computer program (version 1.0) does not contain these algorithms. Future versions will consider tensile element forces.) The values of ϕ' and c' (or the total stress parameters, ϕ and c) must be determined for each layer of the multi-layered bearing medium.

Location of the points of action (thrust line -- Bishop 1954) of the interslice forces on the sides of the slices is assumed. In the computer model solution, only one parameter, λ , needs to be entered. The parameter, λ , is defined as follows (see Figure 15):

$$\lambda = \frac{Y_t - y_s}{Y_g - y_s}, \quad (93)$$

$$(y_t - y_s) = \lambda(y_g - y_s). \quad (94)$$

In the solutions shown herein, a value of 0.33 was assumed for λ .

The quantities $\tan \theta$ and $\tan \alpha$ are computed from geometric considerations. The factor of safety, F , must be obtained by iteration since the factor of safety appears on both sides of Equation 78. The derivative, dv/dx , appearing in Equation 78 for each slice is unknown. The values of V_i cannot be defined until values of the derivative, dH/dx , and H_i are known. To obtain estimates of the derivatives, dV/dx and dH/dx , and the quantities V_i and H_i , the following procedure may be used. Let

$$N = \frac{1 - \frac{\tan \theta \tan \phi'}{F}}{1 + \tan^2 \theta}, \quad (95)$$

$$dM = \left(C' + \left[\frac{dQ_y}{dx} + \frac{P_y}{dx} + \frac{dW}{dx} + \frac{dV}{dx} - \frac{C \sin \eta}{dx} \right] - u \right) \tan \phi' \frac{dx}{N}, \quad (96)$$

$$dL = dQ_x + P_x + C \cos \eta - \left(\frac{dQ_y}{dx} + \frac{P_y}{dx} + \frac{dW}{dx} + \frac{dv}{dx} - \frac{c \sin \eta}{dx} \right) dx \tan \theta. \quad (97)$$

Equation 78 becomes:

$$F = \frac{\int_{x_1}^{x_{n+1}} dM}{H_1 - H_{n+1} + \int_{x_1}^{x_{n+1}} dL} \quad (98)$$

Using the new variables, M and L, Equation 50 may be rewritten

$$\tau_f = \frac{\frac{dM}{dx}}{1 + \tan^2 \theta} \quad (99)$$

Since, by definition

$$\tau = \frac{\tau_f}{F}, \quad (100)$$

then Equation 65 for the differential horizontal interslice forces, dH, is

$$dH = dL - \frac{dM}{F} \quad (101)$$

An expression may be developed for computing the differential horizontal interslice forces. The vertical interslice forces, V_i , and the derivatives, dv/dx , are unknown in Equation 101. Iteration may be used to obtain a first approximation of the factor of safety, F_0 . This operation is done by setting the derivatives, dv/dx , equal to zero. Iteration is performed on Equation 98 by first assuming that values of dv/dx are equal to zero and by using an assumed value of F_0 . Iteration is completed when the condition,

$$|F_0^{n+1} - F_0^n| \leq \epsilon, \quad (102)$$

is satisfied. The parameter, ϵ , is a selected error. In all computations shown herein, ϵ is set equal to 0.001. That is, the iteration is considered successful when the absolute difference in successive factors of safety is equal to or less than 0.001. Convergence of the solution to the factor of safety, F_0 , usually occurs in three to six iterations.

The second stage of the computations involves the introduction of interslice forces, H_i and V_i , and the derivatives, dv/dx and dH/dx , into the equations and performing iteration on Equation 98. Using F_0 , the first set of the horizontal interslice force differentials, dH , may be computed from Equation 101 for each

slice. At any interslice boundary x_i , the horizontal force may be computed from the expression:

$$H_i = H_1 + \int_{x_1}^{x_i} dH. \quad (103)$$

The values of H_i are plotted as functions of the values of x_i . Based on this curve, numerical differentiation may be used to compute the derivative, dH/dx , at a selected value of x_i . Using the computed derivative at a selected value of x_i , the vertical interslice force, V_i , may be computed from Equations 71 or 72. Values V_i are plotted as a function of x_i . Based on this relationship, the derivative dv/dx may be computed using numerical differentiation techniques. Using the computed values of dv/dx , a new factor of safety is computed -- F_1 . Based on F_1 , the process is repeated: new values of dH , dH/dX , V_i , and dV/dX are obtained. Based on these subsequent sets of values, a new safety factor is obtained. The iterative scheme is continued until the condition,

$$|F_{n+1} - F_n| \leq \epsilon, \quad (104)$$

is satisfied.

Classes of Bearing Capacity Analysis

Bearing capacity analyses of pavements and soil subgrades may be divided into two main classes of problems. In the first class, the pore pressures acting within each structural layer of pavement (asphaltic concrete, base, subbase, and soil subgrade) are independent of the magnitude of total stresses acting in each layer of the pavement regime. The pore pressures are independent variables and the analyses are performed in terms of effective stress using the shear strength parameters, ϕ' and c' . The values of ϕ' and c' may be obtained from consolidated-drained triaxial tests (Bishop and Henkel 1964) or consolidated-undrained triaxial tests with pore pressure measurements. To analyze the stability of pavements using the effective stress approach requires a knowledge of the pore pressures acting within each layer of material. To conduct this type of analysis would require estimating pore pressures using (perhaps) methods proposed by Skempton (1954); or Ching and Fredlund (1983); Fredlund and Rahardjo (1985); Fredlund (1985) -- future versions will consider methods involving unsaturated soils.

In the second class of analyses, the pore pressures acting in each layer are a function of stress changes within each layer. The analyses are conducted in terms of total stress using the total stress parameters, ϕ_u and c_u . The values of ϕ_u and c_u are obtained from unconsolidated-undrained triaxial tests. If the soil subgrade is saturated, then the total stress parameters of the soil may be obtained from the unconfined triaxial (ASTM) compression test -- a form of the unconsolidated-undrained triaxial compression test. In this case, the total stress parameter, ϕ_u , is zero and the undrained strength is defined as c_u .

At the present stage in the development of the HOPKIB pavement bearing capacity computer model, the stability analyses shown herein were performed using total stress analyses. Unconsolidated-undrained triaxial compression tests were done on the asphaltic concrete and base (and subbase) to define the total stress parameters, ϕ_u and c_u . Unconfined compression tests were used to define the shear strength of the soil subgrade (when these were available). Alternately, a relationship developed during

the course of this study between the CBR strength and the undrained shear strength, c_u , or S_u , was used to define the undrained shear strength when CBR data were available (although total stress analyses were used herein, the bearing capacity problem may be solved using the effective stress technique). Use of this method of analyses was beyond the scope of this study because of the complexity of determining values of pore pressures. Perhaps, in future research, an examination of techniques necessary to define pore pressures in each pavement layer could be made. For example, consolidated-undrained triaxial compression tests with pore pressure measurements could be performed on saturated specimens of asphaltic concrete to define the effective stress parameters, ϕ' and c' . Additionally, consolidated-undrained triaxial compression tests with pore pressure measurements could be performed on base (and subbase materials), and the subgrade soils to define the effective stress parameters, ϕ' and c' . To perform the analysis in terms of effective stress, pore pressures acting within each pavement layer and subgrade could be estimated or measured -- a complex task.

More sophisticated techniques of shear strength testing than used herein could be examined to define the shear strengths of the different pavement components. For example, consolidated-drained, or consolidated-undrained triaxial compression tests with pore pressure measurements could be used to estimate the effective stress parameters, ϕ_a and c_a , for the portion of the shear surface along the active wedge. Simple shear tests, torsional tests, or direct shear tests could be performed to estimate the shear strength along the portion of the shear surface of the central wedge. Triaxial extension tests could be done to define the shear strength along the portion of the shear surface of the passive wedge. These series of tests would be performed on each member or layer of the pavement regime. To a certain degree, the research version of the HOPKIB model has been developed to consider this approach. However, full development of this approach is much beyond the scope of this study.

Shear Surface

Shear surfaces of various shapes or failure patterns may be assumed in performing bearing capacity analysis. For example, circular and wedge-type shear surfaces may be used. However, basic bearing capacity solutions by Prandtl in 1921 and Reissner in 1924 show that the failure pattern should consist of three distinctive zones as shown in Figure 23. These three zones are identified as zones 1, 2, and 3. Zone 1 is an active Rankine zone. This zone pushes the radial Prandtl Zone 2 sideways and the passive Rankine Zone 3 in an upward direction as shown in Figure 23. The basic Prandtl-type failure pattern was assumed in developing the pavement bearing capacity mathematical model. Basic failure patterns and equations for one, homogeneous layer and a multi-layered system are described as follows.

One, Homogenous Layer

The shear surface assumed in the model analysis for a homogeneous layer of material consists of a lower boundary, identified on the previous page in Figure 24, as **abcd**. This surface consists of two straight lines, **ab** and **cd**. The portion of the shear surface shown as line **ab** is inclined at an angle, α_1 to the horizontal, or

$$\alpha_1 = 45 + \frac{\phi}{2} \quad (105)$$

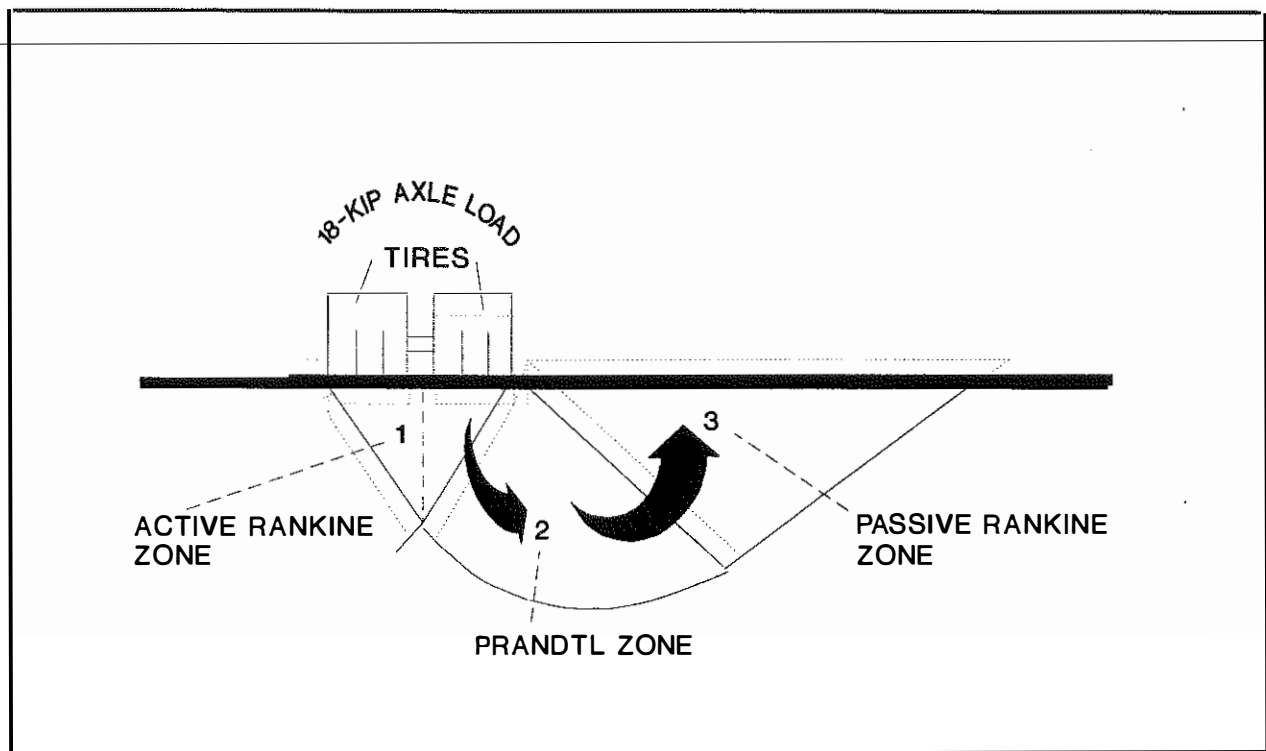


Figure 23. Assumed Failure Pattern and Block Movements.

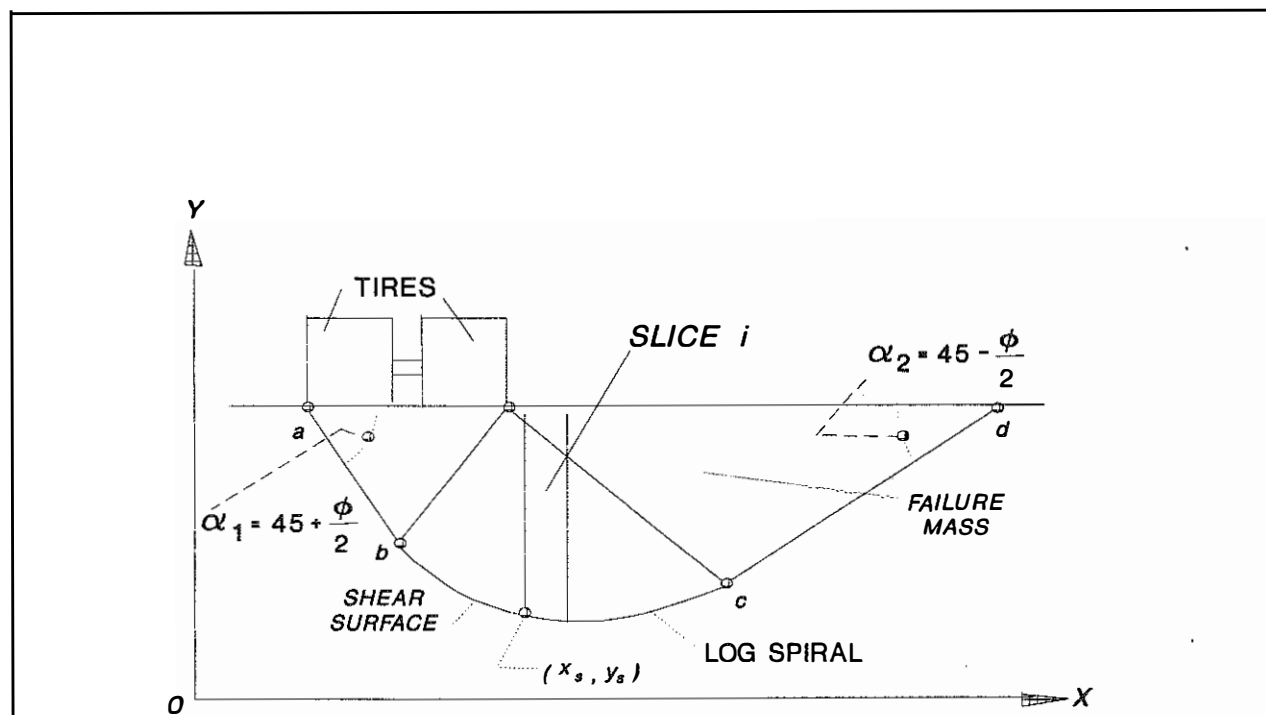


Figure 24. Entry and Exit Angles for a Homogeneous Bearing Medium.

while line **cd** is inclined at an angle, α_2 to the horizontal, or

$$\alpha_2 = 45 - \frac{\phi}{2}. \quad (105)$$

According to Vesic' (cf. Winterhorn 1975), the shape of curve **bc** connecting the two straight lines of the shear surface depends on the angle of internal friction, ϕ , and the ratio, $\gamma C/q$, where

- γ = unit weight of the bearing layer of material,
- C = width of the loaded area, or footing, and
- q = distributed load acting on the surface of the bearing layer.

When the ratio $\gamma C/q$ approaches a value of zero, the connecting curve becomes a logarithmic spiral in which γ equal zero degenerates into a circle. If the term, γC , is not zero, the connecting curve lies between a spiral and between a circle when the value of ϕ is not zero. If the soil is frictionless (ϕ equal to zero), then the connecting curve is a circle. According to Vesic' (cf. Winterhorn and Fang 1975), these findings have been confirmed experimentally.

To describe the shape of the shear surface **abcd** in Figure 25 for use in the pavement bearing capacity computer model, the x- and y- coordinates of points **a**, **o**, **b**, **c**, and **d** must be established. After these points have been defined, the coordinates, x_s (the x-coordinates of the sides of the slices) and y_s (the y-coordinates of the shear surface at the sides of the slices) may be determined. The coordinates of point **a**, x_a , and y_a are assumed. The x- coordinate of point (**o**, x_o) is assumed and depends on the width of the footing, C , or

$$C = x_o - x_a, \text{ and} \quad (107)$$

$$x_o = C + x_a. \quad (108)$$

The y- coordinate, y_o , is arbitrarily selected, or assumed. The coordinates of point **b**, x_m , y_m , may be defined by first computing the radius, r_1 , of the spiral,

$$r_1 = \frac{C \cdot \sin \alpha_1}{\sin \Psi}, \quad (109)$$

where $\Psi = 90 - \phi$. Line **ab** is assumed to be tangent to the log spiral curve at point **b**. After determining

$$r_2 = r_o \cdot e^{(180 - \Omega_2) \cdot \tan \phi}, \quad (114)$$

where

$$\Omega_2 = \Psi - \alpha_2. \quad (115)$$

Coordinates of point c may now be defined by the following expressions:

$$x_{tm} = x_o + r_2 \cdot \cos(\Omega_2), \quad (116)$$

and

$$y_{tm} = y_o + r_2 \cdot \sin(\Omega_2). \quad (117)$$

The x-coordinate, x_d , of the point d may be determined by first computing the value of r_2 in Equation 114 (Figure 25). After r_2 is determined, the distance B may be calculated using the law of sines, or

$$B = \frac{r_2 \cdot \sin(180 - \Psi)}{\sin \alpha_2}. \quad (118)$$

Hence,

$$x_d = x_o + B. \quad (119)$$

The y-coordinate, y_d , may be found from the following expression:

$$y_d = y_{tm} + (x_d - x_{tm}) \tan \alpha_2. \quad (120)$$

After the coordinates a, b, c, and d are defined, the y-coordinate, y_s , of the intersection of the x-coordinate of the side of any given slice i and the shear surface may be determined. The potential failure mass is divided into a selected number of slices, n, as shown in Figure 26, or

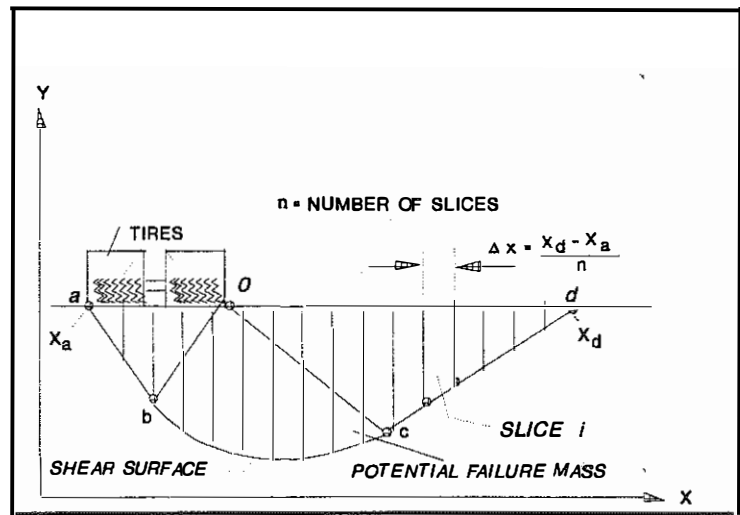


Figure 26. Division of Theoretical Failure Mass Into a Number of Slices and Method of Computing the Width of Each Slice.

$$\Delta x = \frac{x_a - x_d}{n}, \quad (121)$$

where Δx is equal to the width of each slice. For the x-coordinates, x_s , at the sides of slices that lie between points a and b, the y-coordinates, y_s , may be computed from the expression:

$$y_s = y_a - (y_{tm} - y_o) \tan \alpha_1 \quad (x_a < x_i < x_{tm}) \quad (122)$$

Similarly, for the x-coordinates, x_s , at the sides of slices that lie between x_{tm} and x_b , the y-coordinates, y_s , located on the shear surface may be computed from the expression:

$$y_s = y_{tm} + (x_b - x_{tm}) \tan \delta_2 \quad (x_{tm} < x_i < x_{tn}) \quad (123)$$

For the x-coordinates at sides of slices that intersect the shear surface between points b and c (the connecting logarithmic spiral), the corresponding y-coordinates, y_s , cannot be computed straightforwardly since the angle, ω_{xi} , corresponding to a given x-coordinate of the side of slice i is unknown. The problem may be solved by using an iterative scheme. The iterative scheme is performed by assuming, initially, a value of the angle, ω_{xi} , and a value of y_{si} . To start the iteration for the first x-coordinate, x_s , which lies between x_{t1} and x_{tm} , the following assumptions are made

$$y_s = y_{tm}, \quad (124)$$

and

$$\Omega_n = \Psi_1. \quad (125)$$

Iteration is performed on the following expression:

$$\Omega_{(n+1)} = \Omega_n - \frac{(x_o - x_s) - \left[e^{(\Omega_1 \tan \phi)} \right] r_o \cos \Omega_1}{r_o \left[e^{\Omega_1 \tan \phi} \right] \left[\sin \Omega_1 - \cos \Omega_1 \tan \phi \right]} \quad (126)$$

When

$$\left| \left[(x_o - x_s) - \left[e^{(\Omega_n \tan \phi)} \right] r_o \cos \Omega_n \right] \right| \leq \Delta, \quad (127)$$

where Δ = a selected value, then

$$\Omega_{(n+1)} \approx \Omega_n, \text{ and} \quad (128)$$

the correct angle, ω_{xi} , is found that corresponds to the x-coordinate of slice i. A selected value of 0.0001 is used for Δ in the bearing capacity computer program. The y-coordinate, y_s , may be computed from the following expression:

$$y_s = y_o - \left[r_o e^{(\Omega_{(n+1)} \tan \phi)} \right] \sin \Omega_{n+1}. \quad (129)$$

For each x-coordinate of the side of each slice that lies between the x-coordinates, x_{in} and x_{un} , the iterative scheme is repeated so that corresponding y-coordinates, y_s , may be determined. Convergence is very rapid using this scheme.

Multilayered Bearing Medium

Bearing capacity calculations involve a certain degree of uncertainty and complexity when the problem involves more than one layer of material. The failure pattern, or the shape of the shear surface, of a multilayered medium is not as evident as the shear surface shape associated with only one layer of material. No bearing capacity, experimental information concerning the failure patterns of multilayered systems could be located in published literature. An approach was assumed, as shown in Figures 27 through 29. The approach adopted for approximating the failure pattern, or shear surface, of the multilayered medium is based partly on theoretical considerations. For a given multilayered bearing medium, the shear surfaces, identified as lines $aa_1, \dots, a_{m-1}a_m$, and a_mb in Figure 27, are assumed to lie at angles to the horizontal as follows:

$$\theta_{a1} = 45 + \frac{\phi_1}{2} \quad (\text{Line } aa_1), \quad (130)$$

$$\theta_{a2} = 45 + \frac{\phi_2}{2} \quad (\text{Line } a_1a_2), \quad (131)$$

$$\theta_{a_{(m-1)}} = 45 + \frac{\phi_{(m-1)}}{2} \quad (\text{Line } a_{(m-1)}a_m), \quad (132)$$

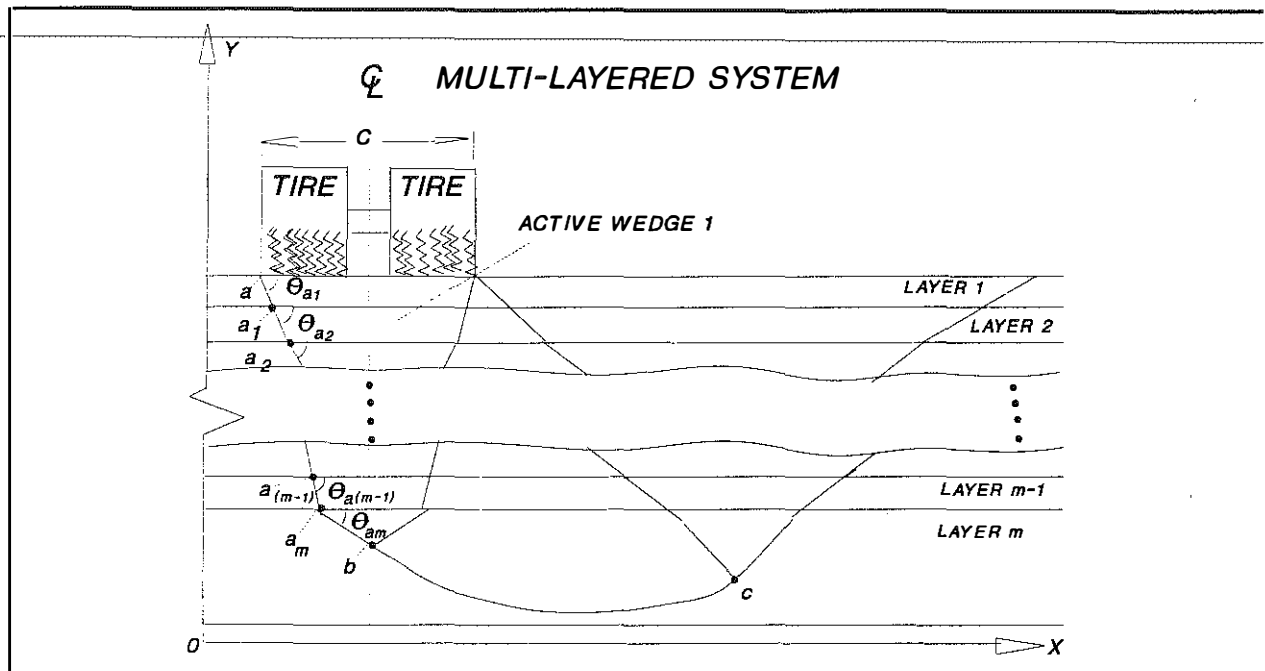


Figure 27. Assumed Shear Surface of the Active Wedge in a Multilayered Bearing Media.

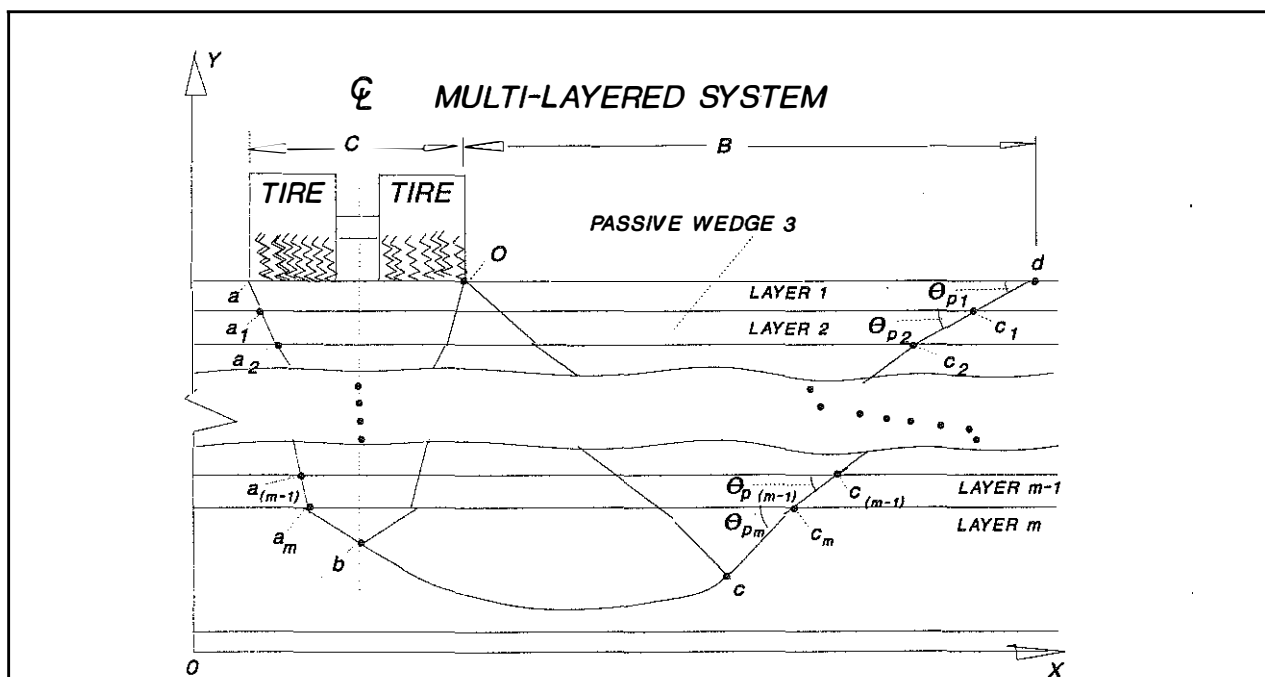


Figure 28. Assumed Shear Surface of the Passive Wedge in a Multilayered Bearing Media.

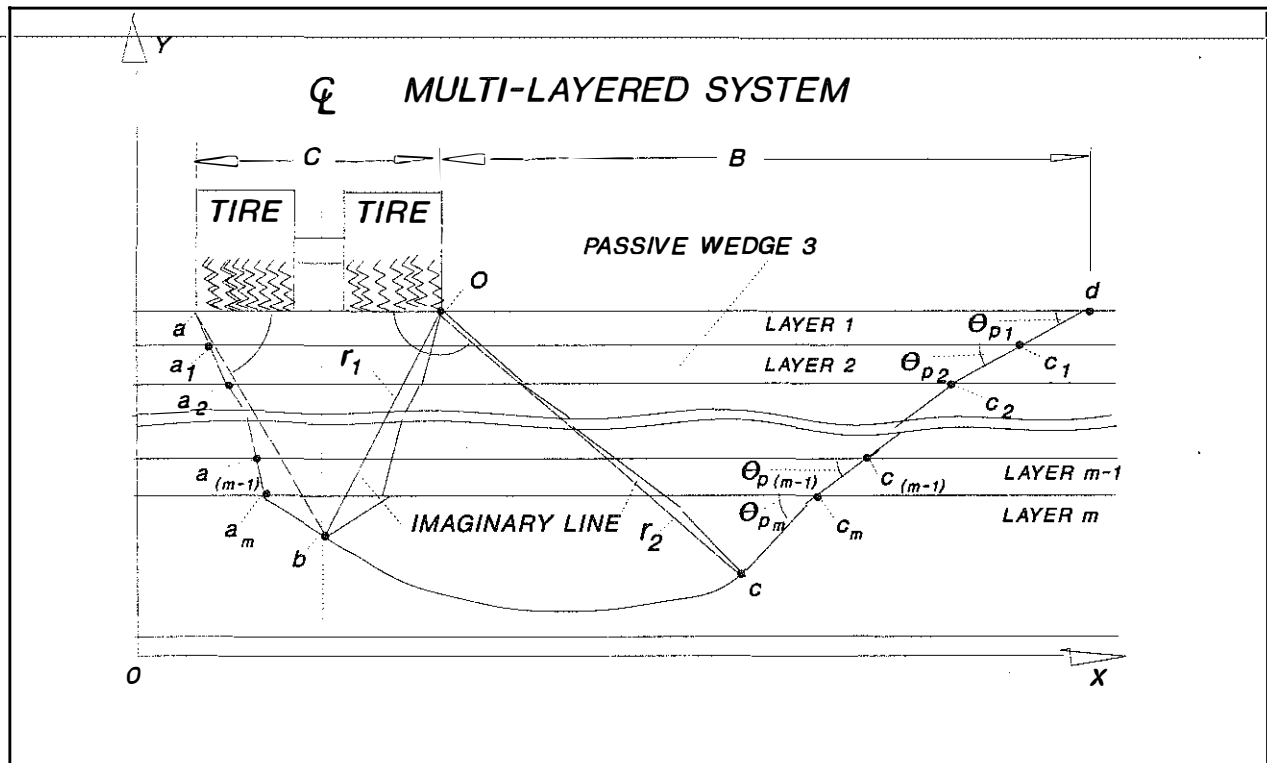


Figure 29. Method for Estimating the Effective Value of ϕ_{eff}

and

$$\theta_{am} = 45 + \frac{\phi_m}{2} \quad (\text{Line } a_m b), \quad (133)$$

where m is the total number of layers of the multi-layered bearing medium and $\phi_1, \phi_2, \dots, \phi_{(m-1)}$, and ϕ_m are the angles of internal friction of the individual layers, respectively, of the bearing medium. The angles, $\theta_1, \theta_2, \dots, \theta_{(m-1)}$, and θ_m are the entry angles of the shear surface of the active block (number 1 in Figure 27).

At point a , the x - and y -coordinates are known, or assumed. The problem consists of determining the points of intersections (points $a_1, a_2, \dots, a_{(m-1)}$) of the shear surfaces passing through the individual layers and the boundary layer lines. The y -coordinates of these points of intersections are known since the elevations of the boundary layer lines are known. Boundary layer lines are assumed to be horizontal. The x -coordinates of the points of intersection may be determined from the following equations:

$$x_{a1} = \frac{y_a - y_{a1} + \tan \theta_{a1}}{\tan \theta_{a1}} \quad (134)$$

$$x_{a2} = \frac{y_{a1} - y_{a2} + \tan\theta_{a2}}{\tan\theta_{a1}} \quad (135)$$

$$x_m = \frac{y_{m-1} - y_n + \tan\theta_{(m-1)}}{\tan\theta_{(m-1)}}. \quad (136)$$

Since the active block is assumed to be symmetrical, the x-coordinate of point **b** is determined from Equation 136. The y-coordinate of point **b** is decided from the following equation:

$$y_b = y_{tn} = y_n + (x_n - x_{tn})\tan\theta_{am}. \quad (137)$$

The points (identified as c_m , $c_{(m-1)}$,, c_2 , and c_1 , in Figure 28) of the intersection of the shear surface (passive wedge 3) passing through each layer of the bearing medium and the boundary layer lines cannot be defined until the x-and y-coordinates of point **c** are determined. Although the assumption is made that points **b** and **c** are connected by a logarithmic spiral, the spiral terminating at point **c** cannot be computed since it is uncertain which ϕ value should be used to compute the spiral radius, r_2 . There may be several different ϕ values in a multi-layered medium. To overcome this problem, and for approximating the size of the passive wedge, an effective ϕ value is calculated and used to compute the coordinates of point **c** in Figure 28. This value, ϕ_{eff} , is an angle between an imaginary line connecting points **a** and **b** and the horizontal line and is estimated in the following manner (see Figure 29):

$$\theta_{eff} = 45 + \frac{\phi_{eff}}{2}, \quad (138)$$

and, rearranging terms,

$$\phi_{eff} = 2(\theta_{eff} - 45) = \tan^{-1} \left(\frac{y_{tn} - y_a}{x_{tn} - x_a} \right). \quad (139)$$

After computing ϕ_{eff} , r_o and r_1 may be determined from Equations 109 through 114. The ϕ_{eff} value obtained from Equation 139 is used in these equations. The radius, r_2 (an imaginary line connecting Points **o** and **c**) is computed from Equation 114 using the value of ϕ_{eff} . After r_2 is found, the x-and y-coordinates of Point **c** are calculated from Equations 119 and 120. Starting at Point **c**, the x-and y-coordinates of c_m , c_{m-1} ,, c_2 , c_1 may be computed. The y-coordinates of these points are known since the boundary layer lines are assumed to be horizontal and the elevations of these points are the same as the elevations of boundary layer lines. The x-coordinates of Points c_m , c_{m-1} ,, c_2 , and c_1 may be

computed from the following expressions:

$$x_{cm} = \frac{(y_{cm} - y_{tm}) + x_{tm} \tan \theta_{pm}}{\tan \theta_m}, (\text{line } cc_m) \quad (140)$$

$$x_{c(m-1)} = \frac{(y_{c(m-1)} - y_{c(m-2)}) + x_c \tan \theta_{p(m-1)}}{\tan \theta_{p(m-1)}}, (\text{Line } C_m C_{m-1}) \quad (141)$$

$$x_1 = \frac{(y_{c1} - y_{c2}) + x_{c2} \tan \theta_{p2}}{\tan \theta_{p2}}, (\text{Line } C_2 C_1) \quad (142)$$

$$x_d = \frac{(y_d - y_{c1}) + x_{c1} \tan \theta_{p1}}{\tan \theta_{p1}}, (\text{Line } c_1 d). \quad (143)$$

Equations 130 through 143 are used to determine the x-and y-coordinates at Points $a_1, a_2, \dots, a_{(m-1)}, a_m, b, c, c_m, c_{m-1}, \dots, c_2, c_1$, and d and to define the general shape of the shear surface passing through the multilayered bearing medium. After these coordinates are determined, the potential failure mass is divided into a selected number of slices, n , or

$$n = \frac{x_d - x_a}{\Delta x}, \quad (144)$$

and

$$x_{si} = x_a + \Delta x \cdot n, \quad (145)$$

where x_{si} is defined as the side of any given slice i . After the sides of the slices are defined, the y-coordinates, y_s , which lie on the shear surface at the intersection of the sides of the slice, x_s , and the shear surface may be computed in a fashion similar to the one described previously for the homogeneous case. Each segment of the shear surface passing through each layer is considered. Since the potential failure mass is divided into rectangular slices and considering that the thicknesses of individual layers of the multilayered medium may be very thin, a large number of slices are used. In the analyses shown herein, the potential failure masses were divided into 598 slices (any even number of slices may be used).

REASONABLENESS OF SOLUTIONS

Creditability and reasonableness of results were established by solving and comparing solutions from the proposed bearing capacity model and solutions from other theoretical, or empirical, mathematical models for different classes of bearing capacity problems. The classes of problems are as follows:

- one homogeneous layer of bearing medium,
- a bearing medium composed of two different layers of material, and
- a multilayered, bearing medium -- case studies.

Solutions of the various classes of selected bearing capacity problems are discussed as follows.

Homogeneous Bearing Medium

Classical Bearing Capacity Equations and Factors

Although a closed analytical solution has not been found for determining the maximum unit load, q_u , that a foundation can support, Prandtl (1921) and Reissner (1924 -- Vesic', cf. Winterhorn and Fang), using methods of the Theory of Plasticity, found that for weightless soils ($\gamma = 0$):

$$q_u = \frac{Q_u}{BL} = cN_c + qN_q, \quad (146)$$

where (see Figure 30)

q_u	=	ultimate stress which the footing can withstand without failure,
Q_u	=	ultimate load which the footing can withstand without failure,
B	=	width of footing,
L	=	length of footing,
γ	=	unit weight of the bearing medium,
c	=	cohesion,
D	=	depth of footing below the surface,
q	=	uniformly distributed surcharge due to the overburden stress = $\gamma.D$, and
N_c, N_q	=	dimensionless bearing capacity factors.

From solutions provided by Prandtl (1921) and Reissner (1924),

$$N_q = e^{\pi \tan \phi} \tan^2 \left(\frac{\pi}{4} + \frac{\phi}{2} \right) \quad (147)$$

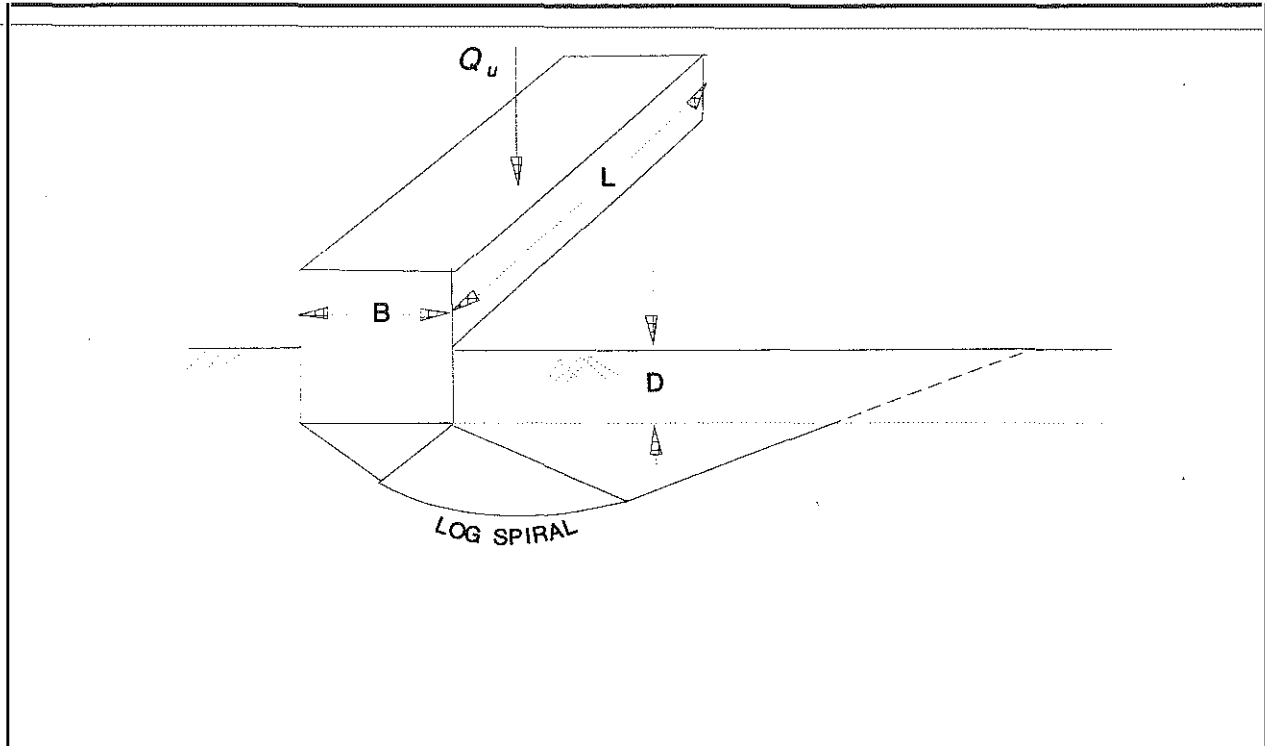


Figure 30. *Bearing Capacity of a Shallow Footing.*

and

$$N_c = (N_q - 1) \cot \phi. \quad (148)$$

Values of the bearing capacity factors, N_c and N_q , are shown in Figure 31 as a function of ϕ . According to Vesic' (cf. Winterhorn and Fang 1975), it can be shown that for a cohesionless soil ($c = 0$; $q = 0$): where N_γ is a dimensionless bearing capacity factor that must be evaluated numerically (see Caquot and

$$q_u = \frac{1}{2} \gamma B N_\gamma, \quad (149)$$

Kerisel, 1953). Also, Vesic' presents an analytical expression,

$$N_\gamma \approx 2(N_q + 1) \tan \phi, \quad (150)$$

for approximating this bearing capacity factor. The N_γ value as a function of ϕ is shown in Figure 31.

Based on superposition, which is not strictly correct, the ultimate bearing capacity of a footing may be approximated by the expression

$$q_u = cN_c + qN_q + (0.5)B\gamma N_\gamma \quad (151)$$

This expression may be referred to as the classical bearing capacity equation and is often referred to as the Buismann-Terzaghi equation (Buismann 1940; Terzaghi 1943). This equation in this form applies strictly to footings of an infinite length (strip loading). Bearing capacity factors shown in Figure 31 were developed from theoretical considerations for the shear surface shown in Figure 30. Terzaghi (1943) also developed values of the bearing capacity factors, N_c , N_q , and N_γ assuming a different failure pattern, or shear surface, than that shown in Figure 30. According to Vesic' (cf. Winterhorn and Fang 1975), the Terzaghi bearing capacity factors, although numerically there are substantially small differences, are being abandoned and the trend among engineers is to retain the Prandtl-Reissner and Caquot-Kerisel factors.

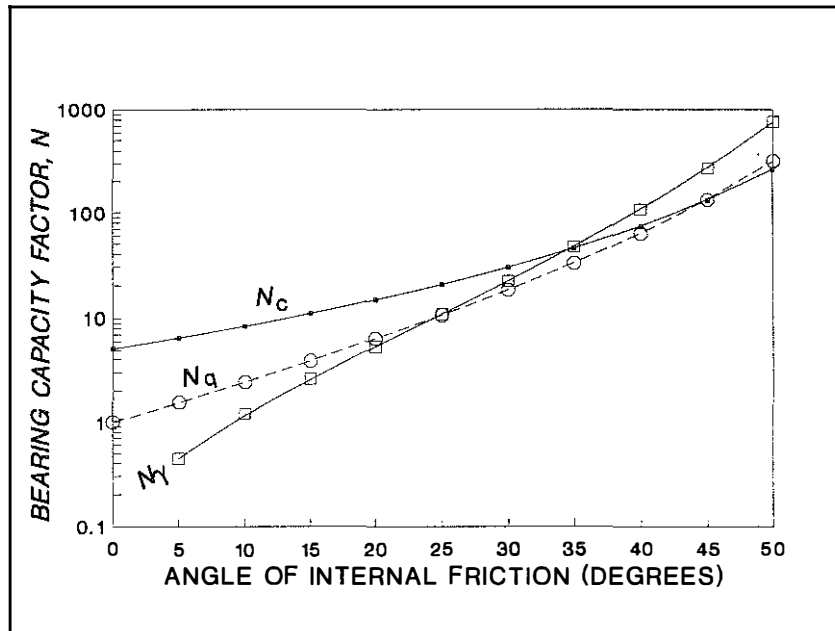


Figure 31. *Bearing Capacity Factors as a Function of the Angle of Internal Friction.*

The ultimate bearing capacity obtained from Equation 151 may be applied only for solving problems involving a single, homogeneous bearing medium and in footings that are infinitely long (strip loading) --

plane strain problems. The problem, from a theoretical viewpoint, becomes exceedingly complex when the foundation shape is something other than a long rectangular shape. The expression generally used in practice, which is semi-empirical and based on comparative loading tests with footings of different shapes, is

$$q_u = cN_c S_c + qN_q S_q + (0.5)\gamma B N_\gamma S_\gamma \quad (152)$$

where S_c , S_q , and S_γ are dimensionless shape factors, or parameters. These values change with foundation shape; they may be obtained from DeBeer, 1967 and Vesic', 1975 (cf. Winterhorn and Fang).

Bearing Capacity Factors -- HOPKIB Computer Model

The bearing capacity factors, N_c , N_q , and N_γ , may be calculated from the HOPKIB bearing capacity computer model and the mathematical algorithms. Bearing capacity factors computed from the HOPKIB model may then be compared to factors obtained from classical bearing capacity theory. The factors

obtained from the HOPKIB model may be judged for their reasonableness and creditability -- at least for a single, homogeneous bearing medium. Consequently, such a procedure is useful in establishing the creditability of the HOPKIB pavement bearing capacity model and computer program. For example, to determine the value of N_c when ϕ equals zero, the following procedure may be used:

Let

$$\begin{aligned} q &= 0, \\ \gamma &= 0, \text{ and} \\ S_c &= 1, \end{aligned}$$

then Equation 152 becomes:

$$q_u = cN_c. \quad (153)$$

Also, let c equal to one, then

$$q_u = N_c, \quad (154)$$

that is, the ultimate bearing stress is equal to the bearing capacity factor, N_c . Values inserted into the bearing capacity computer program for this example are as follows:

- q_u = an initial value is assumed
- γ = unit weight of the bearing medium = 0
- c = 1
- B = width of footing (an assumed value; independent variable) = 10
- S_c = 1 (an infinite strip is assumed)
- q = 0 (no overburden stress is used; $D = 0$)
- y_g = elevation of ground surface is assumed
- ϕ = an assumed value -- varied in the analyses.

A trial and error procedure is used. For example, let ϕ equal zero and q_u equal 4.00. Values of other parameters are shown above. The factor of safety obtained from the HOPKIB computer is 1.227. However, the problem involves determining the value of q_u when the factor of safety is equal to one. When the factor of safety is 1.227, the value of q_u is too small. Increasing the value to 5.14 psi yields a factor of safety of 0.956. The assumed value of 5.14 is too large. When the assumed value is 4.91, the factor of safety is 1.000. Since q_u equals N_c , the bearing capacity factor, N_c , from the computer program is 4.91. For this case ($\phi = 0$), the Prandtl value is 5.14. The bearing capacity factor obtained from the HOPKIB model for ϕ equal to zero is about 4 percent lower than Prandtl's value given by Equations 145 and 146. Various scenarios may be formulated so that the bearing capacity factors, N_c , N_q , N_γ , and combinations of these factors may be computed from the proposed bearing capacity model. Several scenarios are described below and bearing capacity factors obtained from the HOPKIB model are compared to bearing capacity factors presented by Vesic' (1975, cf. Winterhorn and Fang), Terzaghi (1943), and Caquot and Kerisel (1953).

Comparisons

Scenario 1 -- N_c - Bearing Capacity Factor

Let

$$\begin{aligned} c &= 1 \\ q &= 0 \\ \gamma &= 0 \text{ (weightless medium),} \\ S_c &= S_\gamma = S_q = 1 \end{aligned}$$

then (Equation 152)

$$q_u = cN_c S_c + qN_q S_q + (0.5)\gamma B N_\gamma S_\gamma \quad (155)$$

$$q_u = (1)N_c(1) + (0)N_q(1) + (0.5)(0)BN_\gamma S_\gamma \quad (156)$$

$$q_u = N_c \quad (157)$$

Inserting the above parameters and varying ϕ from zero to 50 degrees, N_c factors are computed from the HOPKIB model using a trial and error procedure described previously. Values of N_c obtained from the proposed model are shown as a function of ϕ in Figure 32. They also are compared to N_c factors proposed by Prandtl (1921; Equations 147 and 148) and Terzaghi (1943). In Figure 33, the ratios of HOPKIB N_c factors to Prandtl's N_c factors are compared. Terzaghi's N_c percent higher than Prandtl's N_c factors when

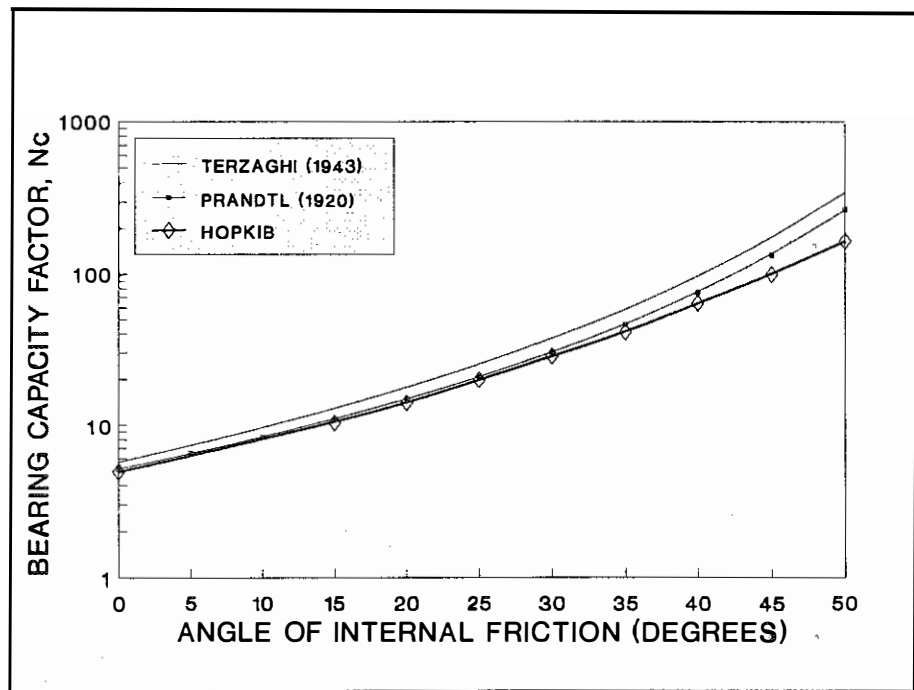


Figure 32. Comparisons of the Bearing Capacity Factors, N_c , Obtained from the HOPKIB Model, Prandtl's Theory (1926), and Terzaghi's Method for a Range of ϕ Values.

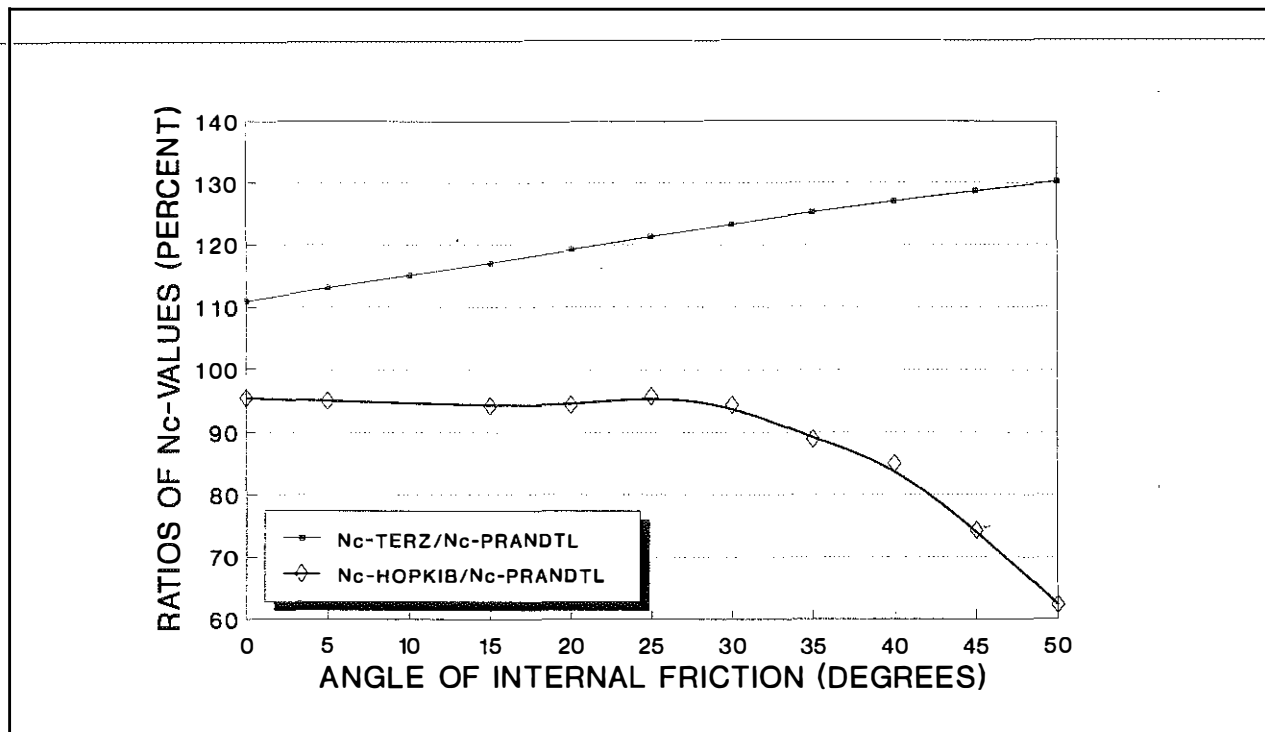


Figure 33. Comparisons of the Ratios of the Bearing Capacity Factors, N_c , from the HOPKIB Model and Terzaghi's Method to N_c Values from Prandtl's Theory for a Range of ϕ Values.

ϕ ranges from zero to 50 degrees. The HOPKIB N_c factors range from 62 to 95 percent of Prandtl's N_c factors when ϕ ranges from zero to 50 degrees. When ϕ ranges from zero to about 40 degrees, the HOPKIB N_c factors range from 85 to 96 percent of Prandtl's N_c factors. Viewed in another manner, what factors of safety would be obtained if the Prandtl and Terzaghi N_c factors were entered into the HOPKIB computer program? Factors of safety obtained from the proposed model when Prandtl's and Terzaghi's N_c factors are used as the ultimate bearing capacity stress (Equation 152) are shown in Figure 34 as a function of ϕ . Using Prandtl's N_c factors, the HOPKIB model gives factors of safety decreasing from 0.96 to 0.90 as ϕ ranges from zero to 50 degrees, respectively. For ϕ -values ranging from zero to about 45 degrees, the factors of safety range from about 0.96 to 0.93. Using Terzaghi's N_c factors, factors of safety range from 0.92 to 0.86.

Scenario 2 -- N_q - Bearing Capacity Factor

Let

$$\begin{aligned} c &= 0, \\ q &= 1, \\ \gamma &= 0, \text{ and} \\ S_c &= S_q = S_\gamma = 1, \end{aligned}$$

then

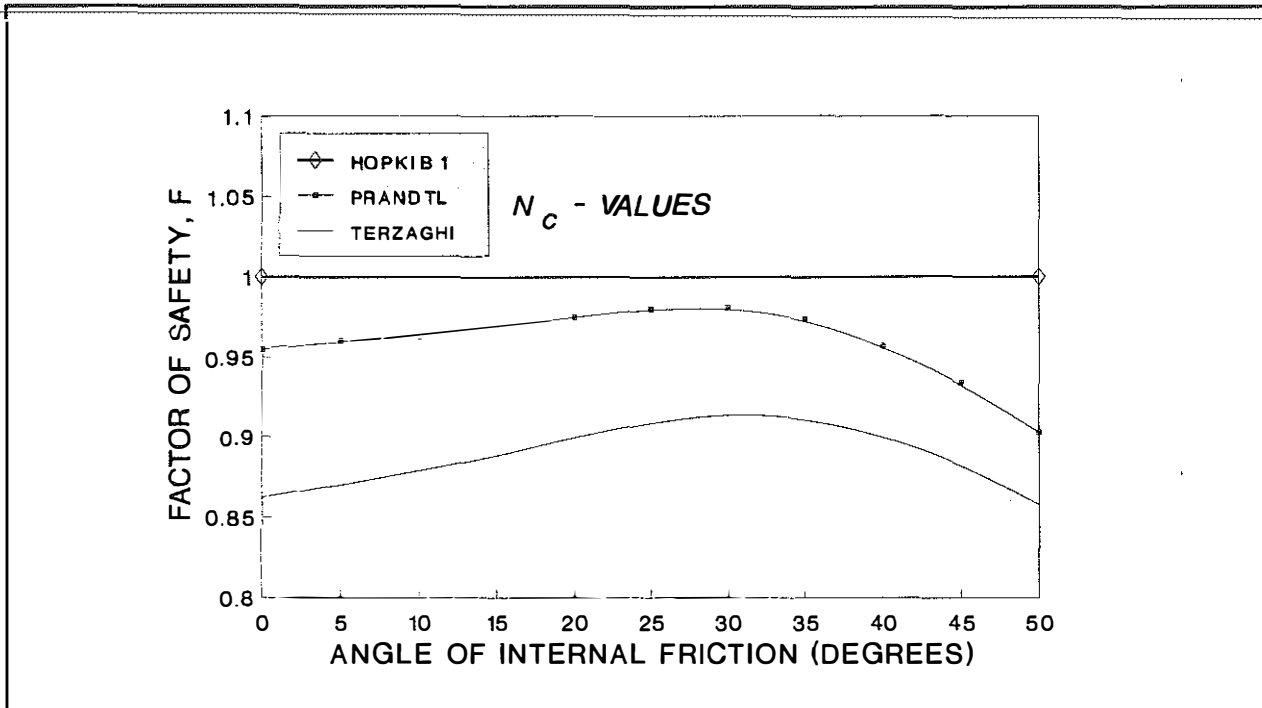


Figure 34. Factors of Safety Obtained When Values of N_c from Terzaghi's Method and Prandtl's Theory Are Inserted Into the HOPKIB Model.

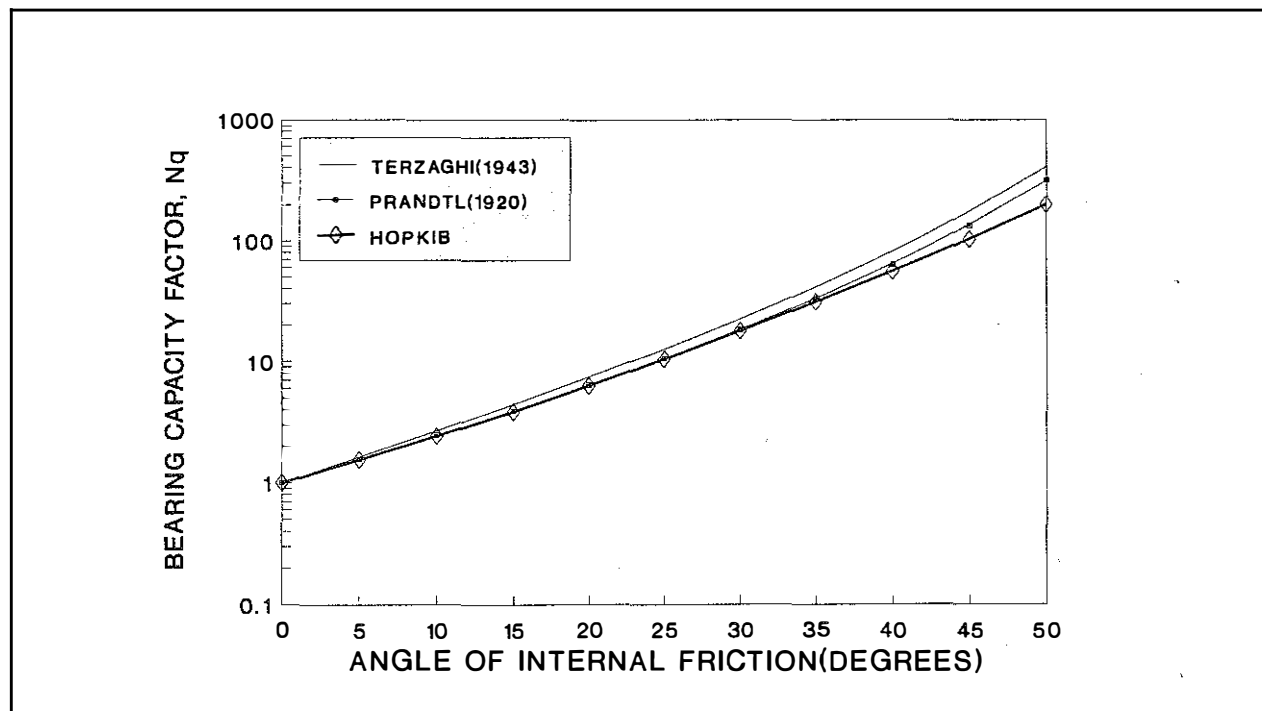


Figure 35. Comparisons of the Bearing Capacity Factors, N_q , Obtained From the HOPKIB Model, Prandtl's Theory (1926), and Terzaghi's (1943) Method for a Range of ϕ Values.

$$q_u = cN_c S_c + qN_q S_q + (0.5)\gamma B N_\gamma S_c \quad (158)$$

$$q_u = (0)N_c(1) + (1)N_q(1) + (0.5)(0)BN_\gamma(1) \quad (159)$$

$$q_u = N_q \quad (160)$$

By inserting the above parameters and varying ϕ from zero to 50 degrees, N_q factors may be computed from the HOPKIB model. The N_q bearing capacity factors obtained from the HOPKIB model are shown in Figure 35 as a function of ϕ and compared to N_q factors proposed by Prandtl and Terzaghi. The ratios of Terzaghi's N_q factors to Prandtl's N_q factors and the ratios of the HOPKIB N_q factors to Prandtl's N_q factors are compared in Figure 36. When ϕ ranges from five to 50 degrees, the Terzaghi N_q values are some 105 to 130 percent larger than the Prandtl N_q factors. The HOPKIB factors are about 99 to 63 percent of Prandtl's N_q factors when ϕ ranges from five to 50 degrees. However, between ϕ values of five to about 43 degrees, the HOPKIB N_q factors are only 99 to about 83 percent of Prandtl's N_q values.

Viewed in another sense, when Prandtl's N_q factors are inserted into the HOPKIB model, the factors of safety (Figure 37) range from 0.99 to 0.90 for ϕ -values ranging from 5 to 50 degrees. For ϕ values ranging from five to about 43 degrees, the factor of safety ranges from 0.99 to 0.95. As shown in Figure 38, a large change in the value of N_q does not cause a large change in the factor of safety when ϕ is held constant. For example, at ϕ equal to 35 degrees, increasing the N_q value from 27.5 to 37.5 -- an increase of 36 percent -- decreases the factor of safety obtained from the HOPKIB model by only about 10 percent; i.e., the factor of safety decreases from 1.05 to 0.95.

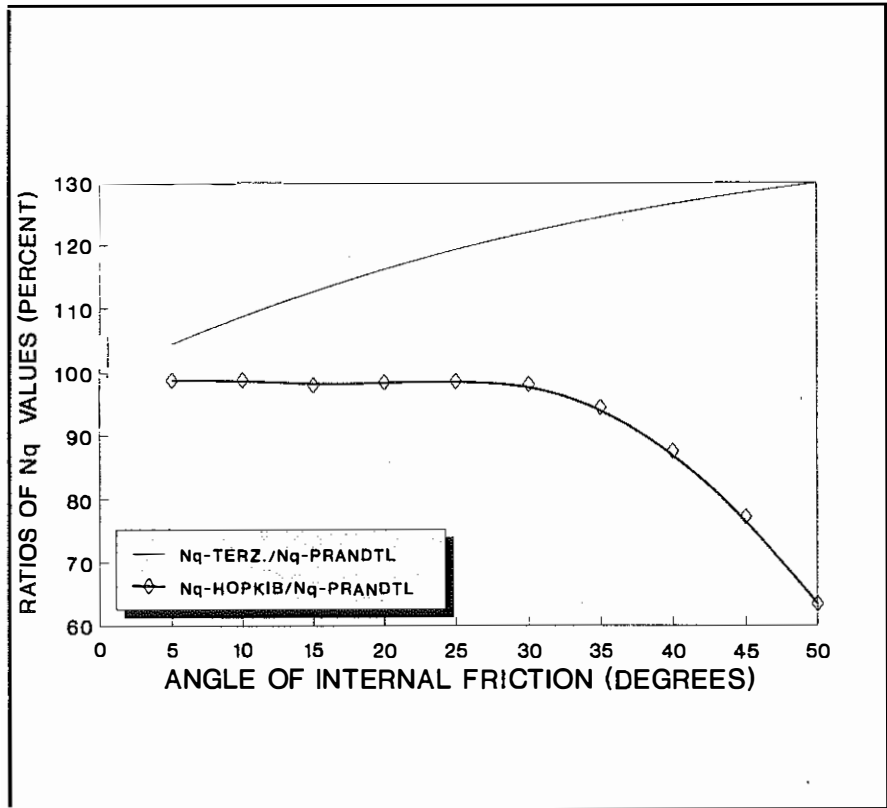


Figure 36. Comparisons of the Ratios of the Bearing Capacity Factors, N_q , from the HOPKIB Model and Terzaghi's Method to N_q Values from Prandtl's Theory for a Range of ϕ Values.

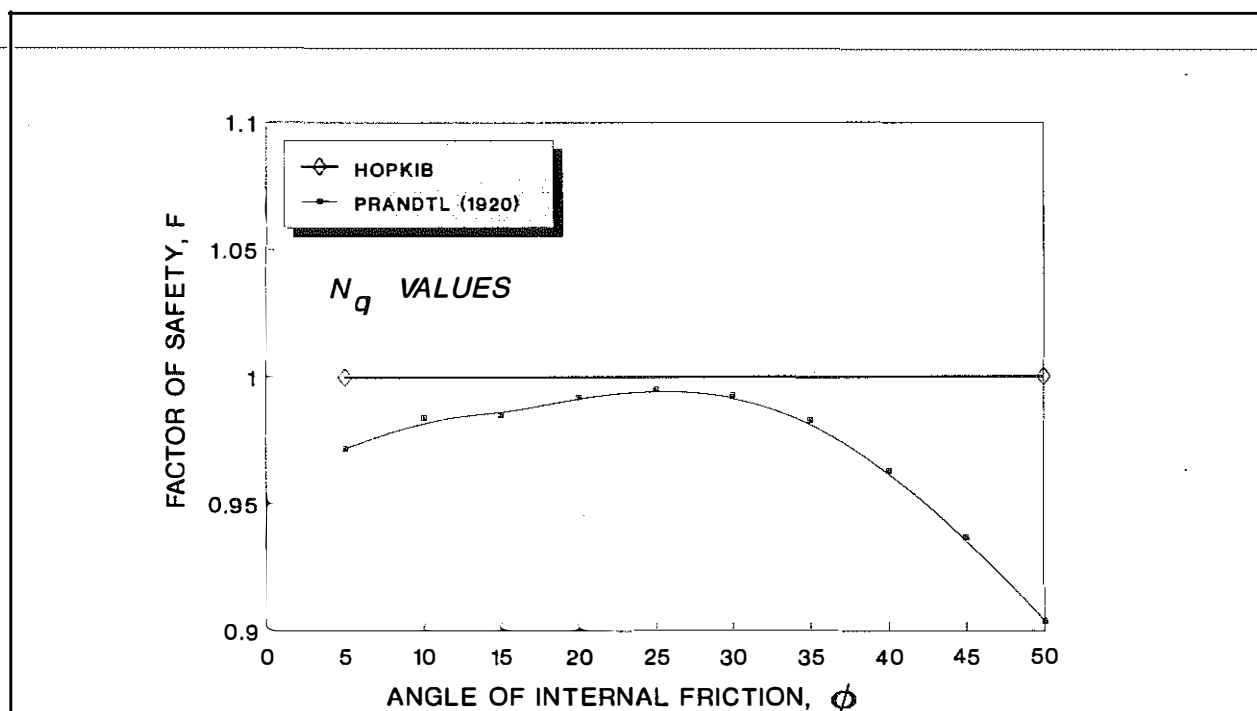


Figure 37. Factors of Safety Obtained When Values of N_q from Terzaghi's Method and Prandtl's Theory are Inserted Into the HOPKIB Model.

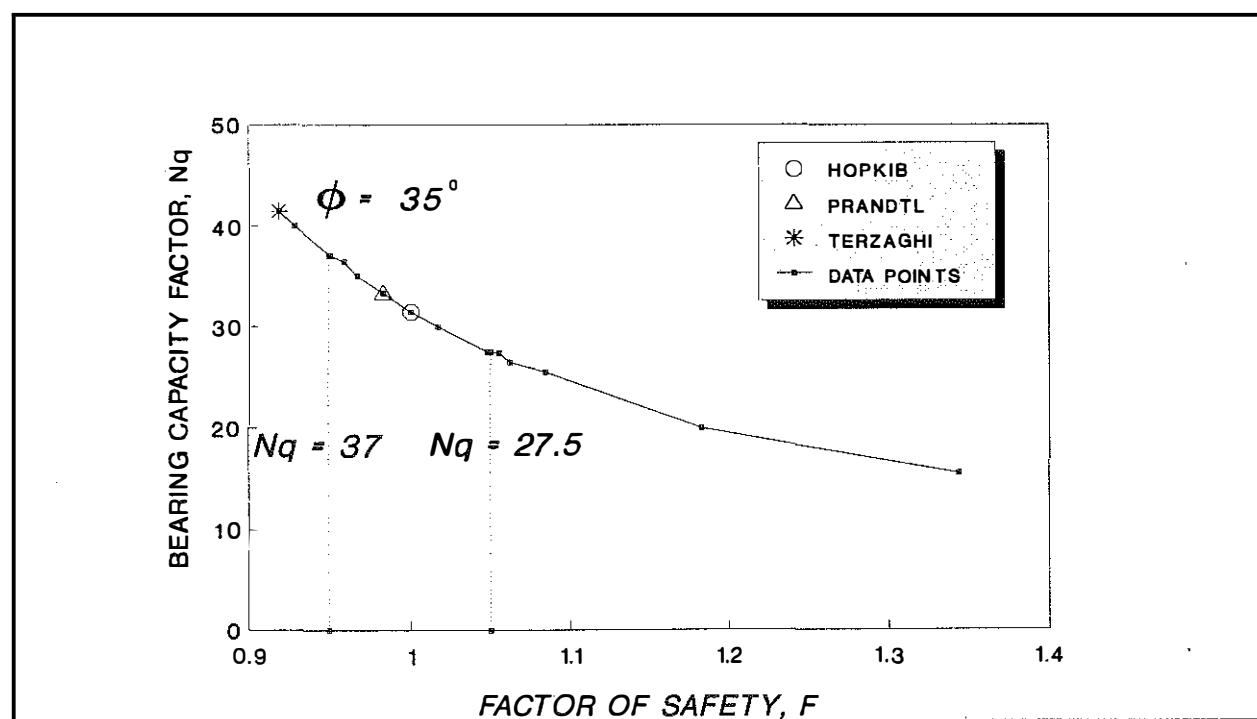


Figure 38. Variations of the Bearing Capacity Factor, N_q , with Factor of Safety When ϕ Equals 35 Degrees.

Scenario 3 -- N_γ - Bearing Capacity Factor*Proposed methods*

Several methods have been proposed for determining the values of the bearing capacity factor, N_γ (Terzaghi, 1943; Caquot and Kerisel, 1953; deMello 1969; Feda, 1961; and Vesic', 1970). Many different values of N_γ have been proposed and correct values of this bearing capacity factor remain very much unsettled. Terzaghi (1943) proposed the following expression for calculating the value of N_γ :

$$N_\gamma = \frac{1}{2} \tan \phi \left[\frac{K_{p\gamma}}{\cos^2 \phi} - 1 \right], \quad (161)$$

where $K_{p\gamma}$ is the coefficient of passive earth pressure (the failure pattern assumed to obtain this relationship is presented in the 1943 reference). As noted by Terzaghi, the value of N_γ depends only on the value of ϕ . Values of $K_{p\gamma}$ may be computed from the logarithmic spiral method (Terzaghi 1943) or the friction circle method (Taylor 1948). Although values of $K_{p\gamma}$ and N_γ were computed by Terzaghi (1943), he displays values of N_γ as a function of ϕ in graphical form. Unfortunately, obtaining numerical values of N_γ from the graphical presentation is not exact due to difficulties in reading Terzaghi's graph.

Terzaghi has shown three numerical values of N_γ . These were 36, 260, and 780 which correspond to values of ϕ of 34, 44, and 48 degrees, respectively. A few other numerical values of N_γ were published by deMello 1969. These values of N_γ were 0, 1.2, 4.7, 21, 130, and 330 and correspond to ϕ -values of 0, 10, 20, 40, and 45 degrees, respectively. Although values of N_γ may be computed for any given ϕ -value following Terzaghi's procedure, the approach is time consuming. As one approach to computing Terzaghi's values of N_γ for any given value of ϕ , the terms in Equation 161 were rearranged as follows:

$$K_{p\gamma} = \cos^2 \phi \left[\frac{2N_\gamma}{\tan \phi} - 1 \right]. \quad (162)$$

Using the few numerical values of N_γ published by Terzaghi (and other values shown by deMello 1969), values of $K_{p\gamma}$ (computed from Equation 162) were plotted as a function of ϕ values. Using a regression scheme, an expression relating Terzaghi's $K_{p\gamma}$ values and ϕ values was developed. This expression is as follows (Figure 39):

$$K_{p\gamma} = 12.7 e^{\phi(0.0017\phi - 0.00546)}. \quad (163)$$

For any given value of ϕ , a value of $K_{p\gamma}$ may be computed from Equation 163. Therefore, a value of N_γ (based on Terzaghi's assumed failure pattern) may be computed from Equation 161, or, alternatively,

$$N_\gamma = \frac{1}{2} \tan \phi \left[\frac{2[12.7e^{\phi(0.00177\phi - 0.00546)}]}{\cos^2 \phi} - 1 \right] \quad (164)$$

Values of N_γ proposed by Terzaghi assumes that the base of the footing is rough.

Values of N_γ for different values of ϕ were approximated by Vesic' (1975; cf. Winterhorn and Fang) using an analytical expression:

$$N_\gamma \approx 2(N_q + 1) \tan \phi, \quad (165)$$

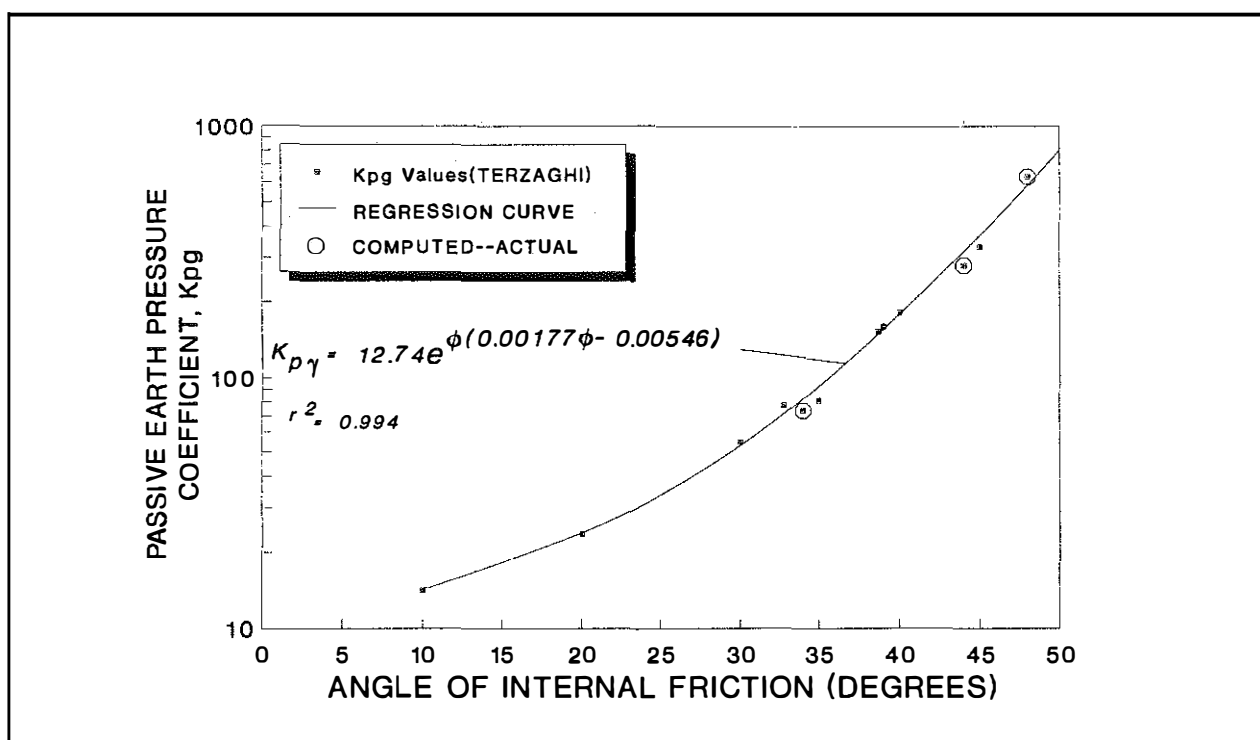


Figure 39. Variations of Terzaghi's Values of the Coefficient of Passive Earth Pressure, K_{pg} and ϕ .

where N_q is defined by Equation 147 (Prandtl, 1921). These values are based on the assumption that the base of the footing is frictionless. Caquot and Kerisel (1953) derived values of N_γ based on the assumption that θ_a is equal to $45^\circ + \phi/2$, or

$$N_\gamma \approx (N_q - 1) \tan(1.4\phi), \quad (166)$$

where N_q is defined by Equation 147 (Prandtl 1921).

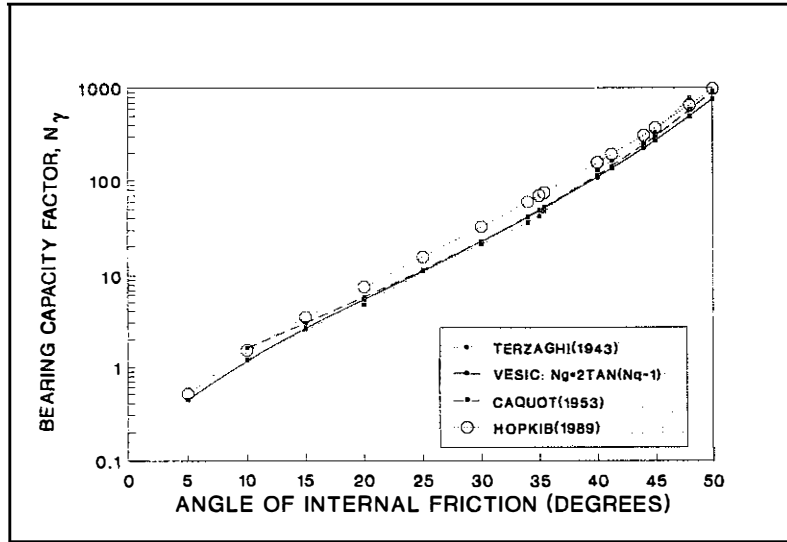


Figure 40. Comparisons of N_γ Values Proposed By Terzaghi, Vesic', Caquot and Kerisel, and HOPKIB Model.

$$\begin{aligned} q &= 0 \\ \gamma &= 1 \\ B &= 2 \\ S_c &= S_q = S_\gamma = 1, \end{aligned}$$

then

$$q_u = CN_c S_c + q N_q S_q + (0.5) \gamma B N_\gamma S_\gamma \quad (168)$$

$$q_u = (0) N_c (1) + (0) N_q (1) + (0.5) (1) (2) (1) \quad (169)$$

$$q_u = N_\gamma \quad (170)$$

The factor of safety is defined by the equation

$$F = \frac{q_u}{q_a} = 1 \text{ (at failure)} \quad (171)$$

where q_a is the allowable, applied stress. By setting F equal to 1, then

$$q_u = q_a = N_\gamma \quad (172)$$

Based on experimental work of his own and others and comparisons of theoretical values, Fedd (1961) proposed an empirical equation for determining values of N_γ . This expression is:

$$N_\gamma = 0.01 e^{0.25 \phi} \quad (167)$$

Values of N_γ may also be computed from the HOPKIB mathematical bearing capacity computer model. These calculations are based on the assumed failure pattern in Figure 23.

Let

$$c = 0$$

The problem is reduced to one of assuming a value of the applied load. Inserting the above values into the HOPKIB model and assuming a value of q_u (or q_{tu}), a factor of safety may be computed. If the factor of safety, as computed from the computer model, is not equal to one, then a new value of q_u is assumed and a new factor of safety is computed. The procedure is repeated until the computed factor of safety is equal to one. When this occurs, Equation 172 is satisfied.

Theoretical comparisons

Values of N_γ determined from the HOPKIB model are shown in Table 3 and compared to values proposed by Terzaghi, Vesic', Caquot and Kerisel, de Mello, and Feda. In Figure 40, values of N_γ obtained from the HOPKIB model are compared graphically to values proposed by Terzaghi, Vesic', and Caquot and Kerisel. In Figure 41, the HOPKIB N_γ values are compared to values proposed by de Mello and Feda. As shown graphically, considerable differences exist among the proposed values of N_γ . In Figure 42, the ratios of Terzaghi's, Caquot and Kerisel's, and HOPKIB models' N_γ values to N_γ values obtained from Vesic's analytical equation (number 165) are compared. For ϕ values ranging from 10 to 48 degrees, Terzaghi's values are about 87 to 121 percent of Vesic's values. Values proposed by Caquot and Kerisel are about 101 to 132 percent higher than Vesic's values. Values of N_γ computed from the HOPKIB model are 116 to 146 percent higher than Vesic's values. As shown in Figure 43, values of N_γ proposed by de Mello (smooth footing) range from about 16 percent to 115 percent of Vesic's values, and for a rough footing de Mello's, values range from 18 to 149 percent. Values of N_γ proposed by Feda are some eight to 352 percent of Vesic's values. Hence, there are considerable differences among the proposed values of N_γ .

Viewed in another sense, factors of safety obtained from the HOPKIB model using values of N_γ proposed by Terzaghi, Vesic', Caquot and Kerisel, de Mello, and Feda are compared in Figures 44 and 45. Based on Vesic's N_γ values, factors of safety obtained from the HOPKIB model range from 1.17 to 1.07 for ϕ values ranging from five to 50 degrees. Using Terzaghi's values, the factors of safety range from 0.93 to 1.27 while factors of safety range from 0.97 to 1.15 when Caquot and Kerisel's N_γ values are used in the HOPKIB model. Using the N_γ values of Terzaghi, Vesic', or Caquot and Kerisel yield factors of safety that generally range from 0.93 to 1.27. When Feda's N_γ values are used in the model, the factors of safety range from 0.82 to values greater than five. For a smooth footing, de Mello's values yield factors of safety that range from 5.5 to 1.03 as shown in Figure 45.

Experimental comparisons

Theoretical and empirical values of N_γ are compared in Figure 46 to experimental results obtained by DeBeer and Ladanyi (1961) from model footing tests (strip loading) using a uniform sand as the bearing medium. Experimental results obtained from those tests indicated that N_γ values for ϕ values equal to 25, 30, 35 and 40 degrees were 14, 33, 83, and 210, respectively. In model footing tests conducted by Feda (1961), an experimental value of N_γ equal to 170 was obtained. The bearing medium in Feda's experiments consisted of a coarser and less uniform sand than the sand used in DeBeer and Ladanyi's experiments. The ϕ value of Feda's bearing medium was 40 degrees. For the range of ϕ equal to 25 to 40 degrees, the experimental results obtained by DeBeer and Ladanyi may be approximated by the following expression:

$$N_\gamma = (0.149)10^{(0.0786\phi)}. \quad (173)$$

TABLE 3. COMPARISONS OF PROPOSED AND EXPERIMENTAL VALUES OF THE BEARING CAPACITY FACTOR, N_1

Angle of internal friction, ϕ (Degrees)	Terzaghi (1943-- Rough)	Prandtl (1920--cf Vesic' 1970)	Caquot/Kerisel (1953-- Rough)	de Mello (1969-- Smooth)	de Mello (1969-- Rough)	Feda (1961-- Empirical Formula)	Feda (1961-- Exp. Results)	DeBeer/Ladanyi (1961-- Exp. Results)	H O P K I B (1989)
0	0	0	0	0	0	0			0
5	0.57	0.45	---	0.07	0.08	0.035			0.52
10	1.20	1.22	1.604	0.37	0.42	0.122			1.524
15	2.58	2.65	2.98	1.13	1.32	0.425			3.47
20	4.70	5.39	5.69	2.87	3.42	1.484			7.38
25	10.98	10.88	11.22	6.77	8.21	5.18		14.00	15.40
30	21.00	22.40	22.69	16.57	19.31	18.08		33.00	32.50
34	36.00	41.06	41.70	37.00	38.88	49.15			60.00
35	42.10	48.06	49.10	37.16	46.52	63.11		83.00	70.20
35.43	47.74	51.44	52.87	40.13	50.31	70.32			75.20
40	130.00	109.41	114.00	93.70	119.01	220.26	170.00	210.00	157.00
40.04	131.10	110.21	115.00	94.46	119.95	222.59			158.00
41.25	164.25	136.08	144.25	119.80	152.68	301.07			193.60
44	260.00	224.64	245.00	211.41	273.23	598.74			310.00
45	330.00	271.76	300.00	338.12	338.12	768.80			371.00
48	780.00	496.01	577.00	682.40	682.40	1627.55			655.00
50	1167.24	762.89	916.00	1137.86	1137.86	2683.37			976.00
35.13									71.75
42.89									255.83

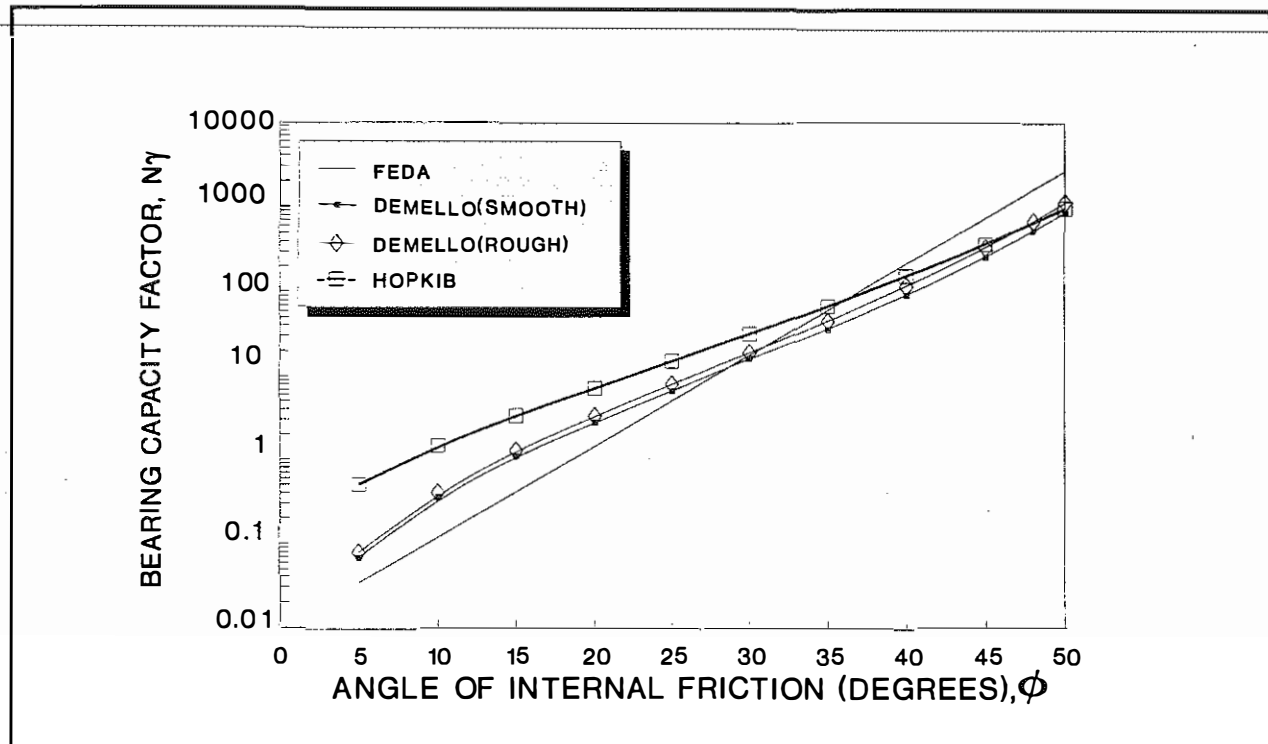


Figure 41. Comparisons of N_γ Values Proposed by Feda, deMello, and the HOPKIB Model.

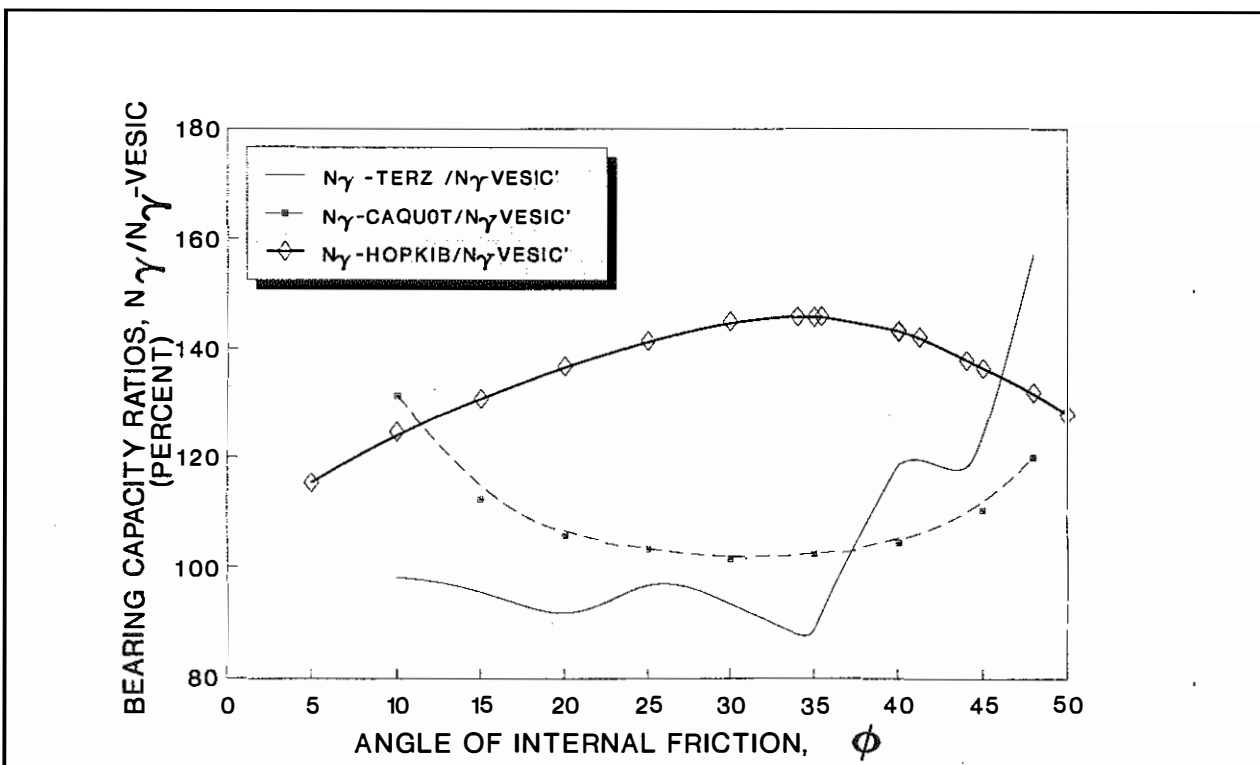


Figure 42. Ratios of N_γ Values Proposed By Caquot and Kerisel, Terzaghi, and the HOPKIB Model to N_γ Values Proposed by Vesic' (c.f. 1975 Winterhorn and Fang).

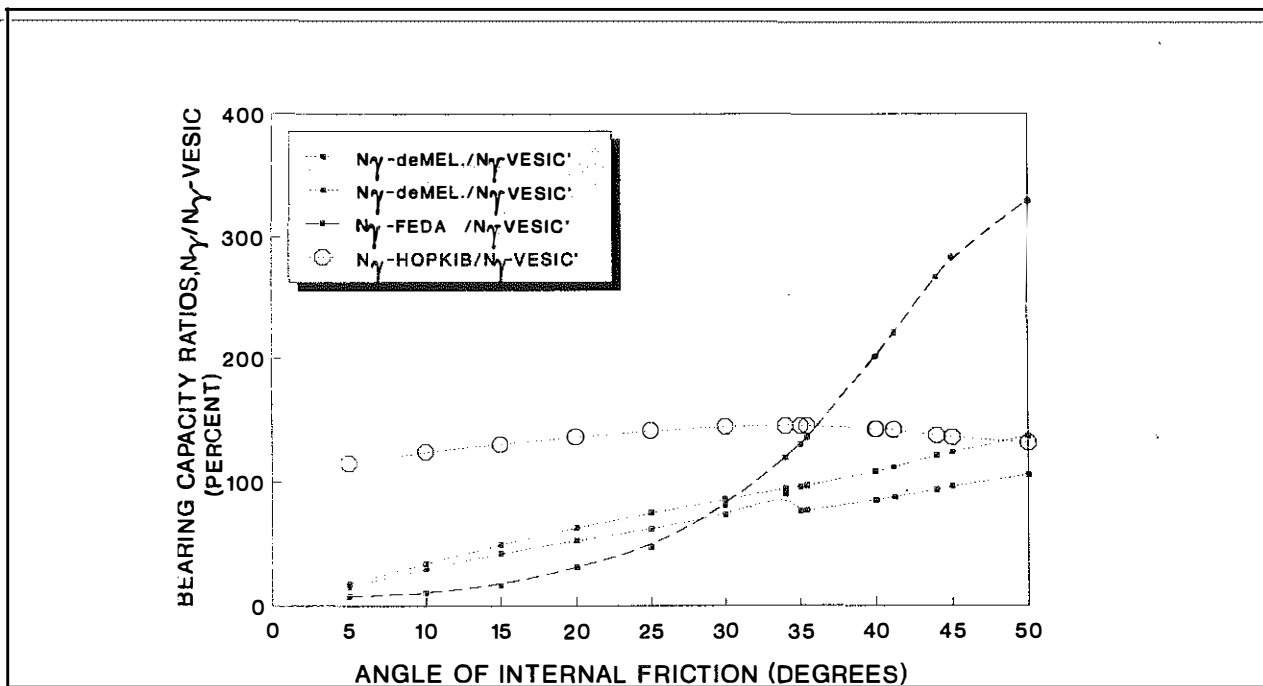


Figure 43. Ratios of N_{γ} Values Proposed By deMello, Feda, and the HOPKIB Model to N_{γ} Values Proposed By Vesic'.

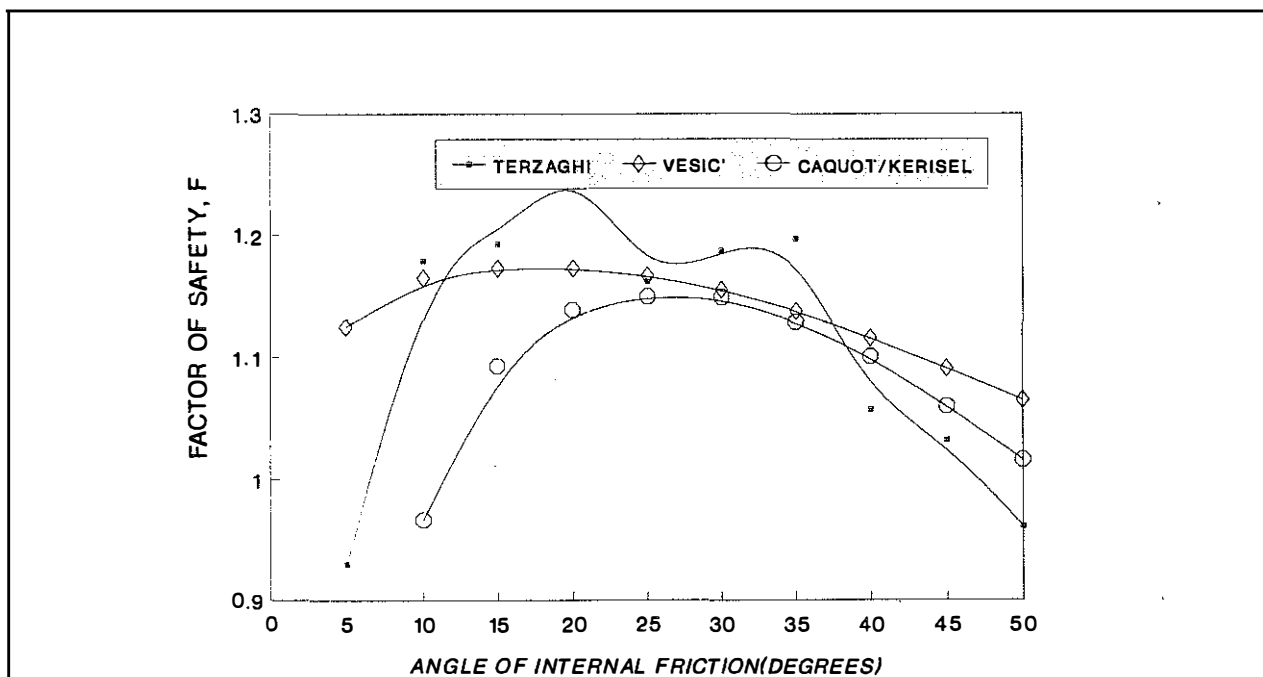


Figure 44. Variation of the Factors of Safety with ϕ When N_{γ} Values Proposed by Terzaghi, Vesic', and Caquot and Kerisel are Used in the HOPKIB Model.

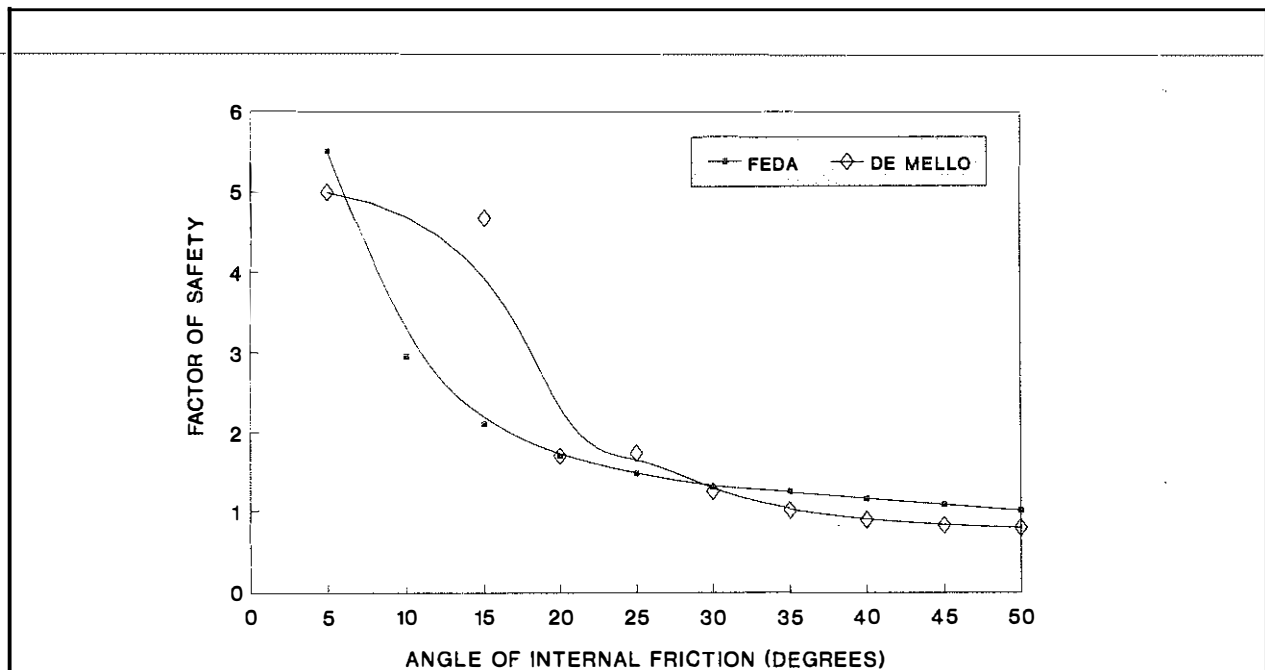


Figure 45. Variation of the Factors of Safety With ϕ When $N\gamma$ Values Proposed by Feda and deMello are Used in the HOPKIB Model.

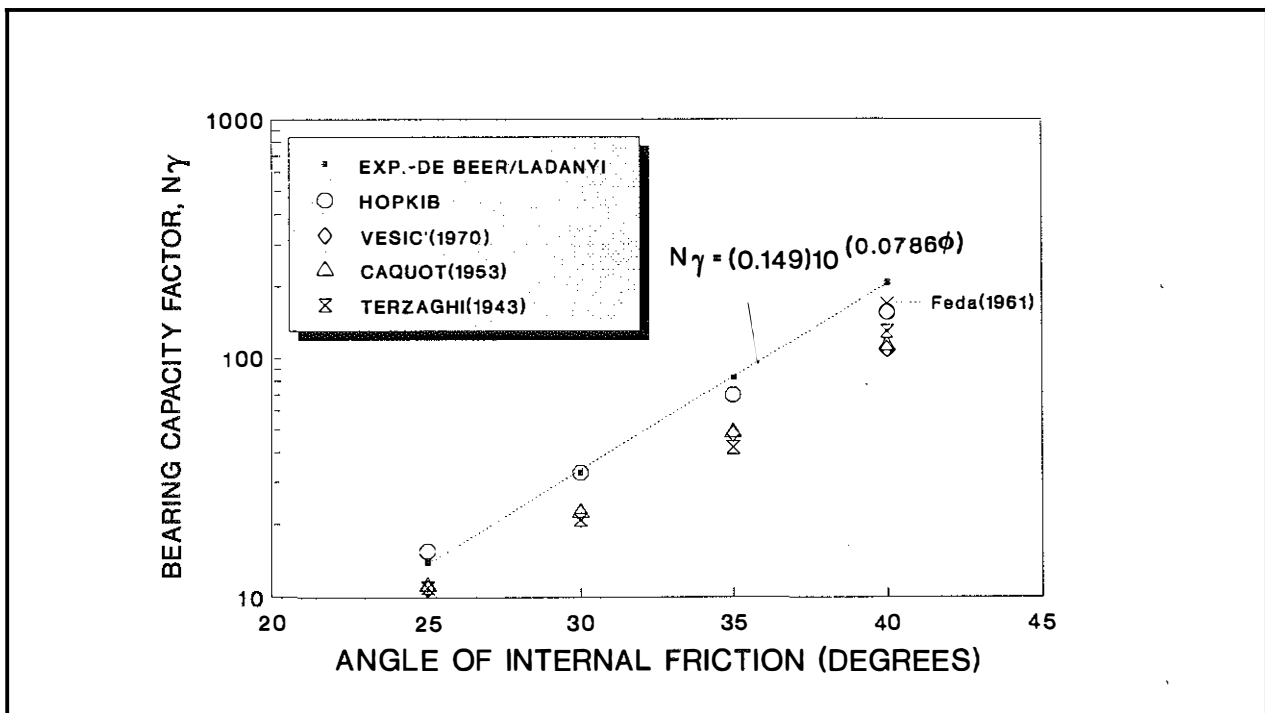


Figure 46. Comparisons of the $N\gamma$ Factors from the HOPKIB Model, Terzaghi's, Vesic's, and Caquot and Kerisel's Methods and Experimental Values of $N\gamma$ Determined by DeBeer and Ladanyi (1961) from Model Footing Tests.

Theoretical N_γ values obtained from the HOPKIB model are in better agreement with the experimental values reported by DeBeer and Ladanyi (1961) than theoretical N_γ values proposed by Terzaghi, Vesic' (analytical equation), Caquot and Kerisel, or the empirical values proposed by de Mello. This is also illustrated in Figures 47 and 48. As shown in Figure 47, the N_γ values obtained from the HOPKIB model range from about 78 to 110 percent of the experimental N_γ values. Values of N_γ proposed by Terzaghi, Vesic', Caquot and Kerisel are about 50 to 80 percent of the experimental N_γ values. Values of N_γ proposed by de Mello are only 48 to 60 percent (Figure 48) of the experimental values. Fedas's empirical equation yields N_γ values that are about 37 to 100 percent of the experimental values.

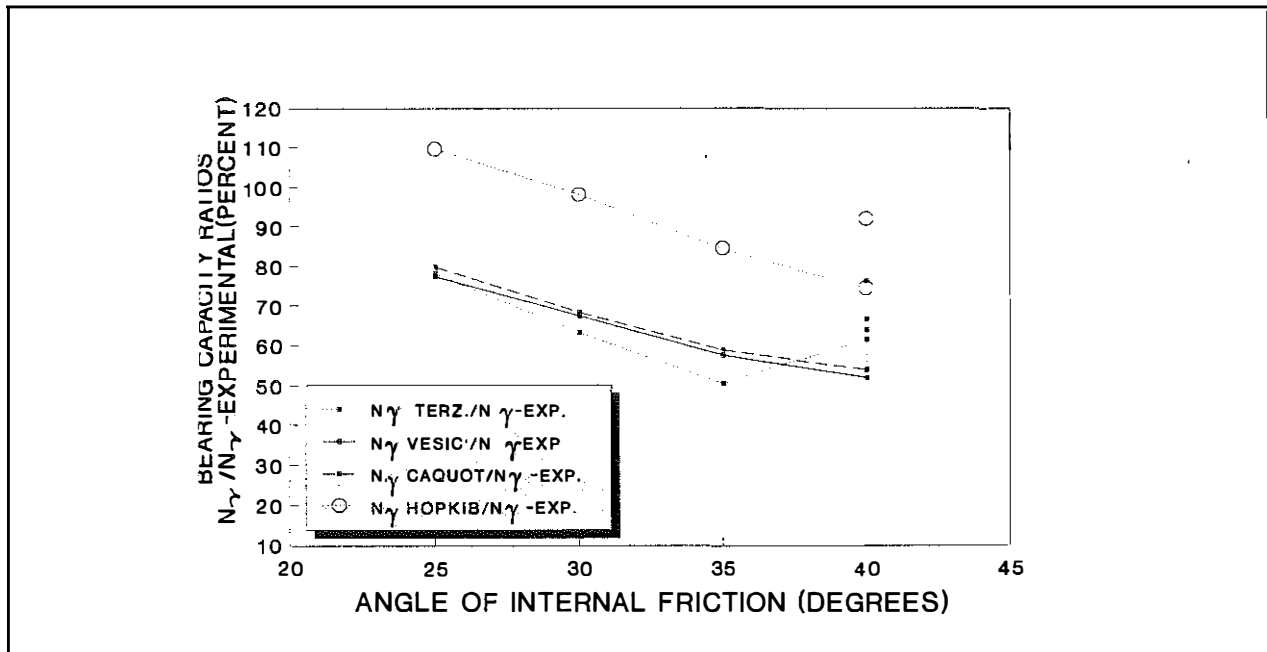


Figure 47. Variations of the Ratios of N_γ Bearing Capacity Factors Proposed By Terzaghi (1943); Vesic' (c.f. 1975 Winterhorn and Fang); Caquot and Kerisel (1961); and the HOPKIB Model to Experimental N_γ Bearing Capacity Factors Obtained By DeBeer and Ladanyi (1961); as a Function of ϕ , the Angle of Internal Friction.

Other experimental values of N_γ have been published by Vesic' (1969, cf. Lambe and Whitman) for circular and rectangular model footings. Test values of N_γ given by Vesic' for rectangular model footings are shown in Figure 49. Width and length of the rectangular footings were 2 inches and 12 inches, respectively, and in this series of experiments, ϕ values of the bearing medium ranged from about 35.7 to 41.3 degrees. Two modes of failure were designated by Vesic'. One mode was labeled as "first failure" while the second mode was called "second failure" or "general failure." In Figure 49, regression lines were fitted to each set of Vesic's experimental N_γ values. The regression curve for the general failure mode may be defined as:

$$N_\gamma = 0.000124e^{(0.302\phi)} \quad (35.7^\circ < \phi < 41.3^\circ). \quad (174)$$

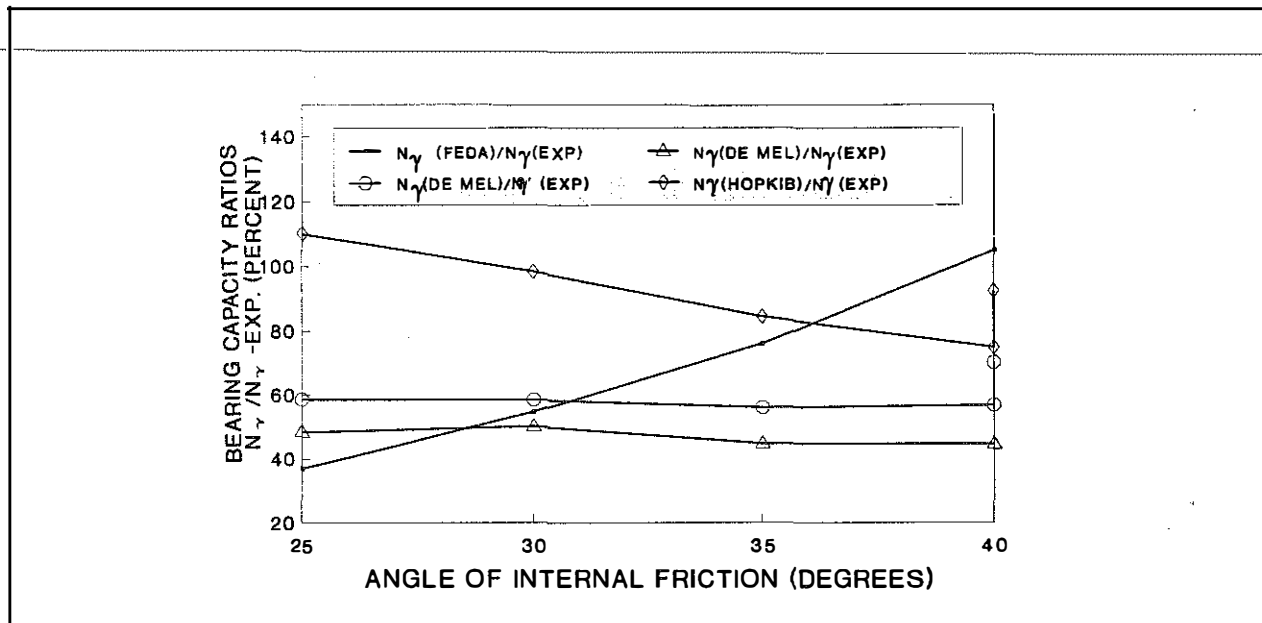


Figure 48. Variations of the Ratios of N_γ -Bearing Capacity Factors Proposed by Feda (1961); deMello (1969); and the HOPKIB Model to Experimental Values Obtained by DeBeer and Ladanyi (1961) as a Function of ϕ .

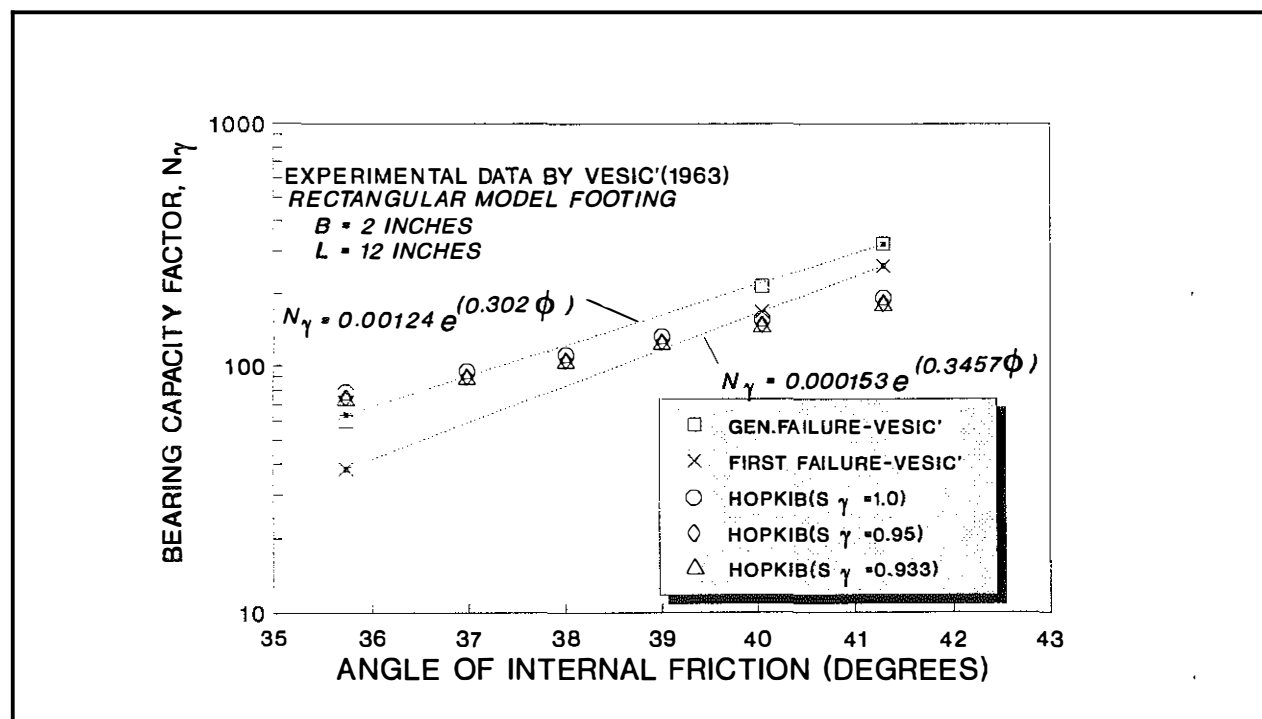


Figure 49. Comparison of N_γ Values from the HOPKIB Model and Experimental N_γ Values Obtained by Vesic' Using Rectangular Model Footings.

The "first failure" (when the start of failure was first observed) may be expressed as

$$N_\gamma = 0.000153e^{(0.346\phi)} \quad (35.7^\circ < \phi < 41.3^\circ). \quad (175)$$

Since the ultimate bearing capacity of rectangular and circular footings depends on shape (Terzaghi 1943), then a correction factor, or shape factor, is normally used. For a rectangular footing, Terzaghi proposed the following expression:

$$S_\gamma = 1 - \frac{(0.3)B}{L}, \quad (176)$$

and

$$q_u = (0.5)S_\gamma N_\gamma B \gamma. \quad (177)$$

Substituting the values of the dimensions of the model footings into Equation 176, then

$$S_\gamma = 1 - 0.3 \left(\frac{2}{12} \right) = 0.933, \text{ and} \quad (178)$$

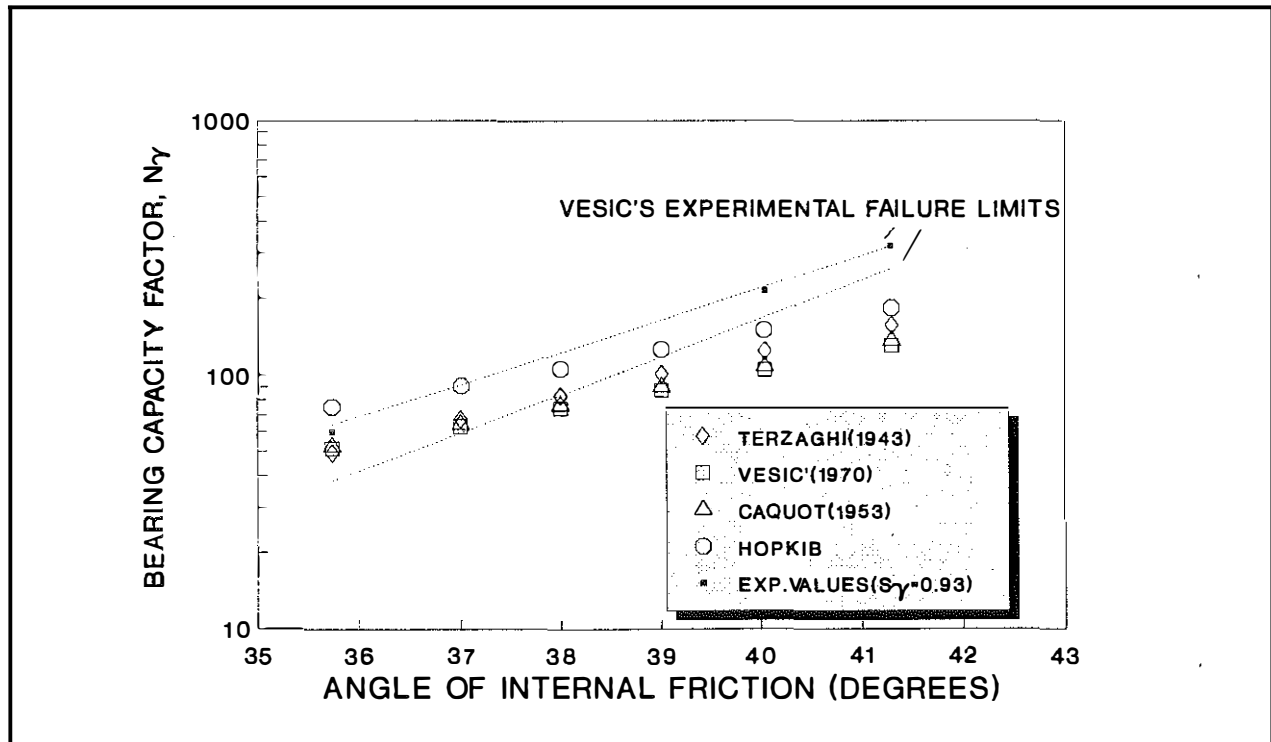


Figure 50. Comparison of N_γ Factors Proposed by Terzaghi, Vesic', Caquot and Kerisel, and the HOPKIB Model to N_γ Factors Determined Experimentally by Vesic' Using Rectangular Model Footings.

$$q_u = (0.5)(0.933)N_\gamma B\gamma. \quad (179)$$

N_γ values obtained from the HOPKIB model, which pertain to a strip, or infinitely long footing, were reduced by a factor of 0.933 before they were compared to the experimental values. The corrected N_γ values from the HOPKIB model are compared to Vesic's experimental N_γ values in Figure 49. The HOPKIB N_γ values generally fall within or close to the experimental values of N_γ . DeBeer (cf. Winterhorn and Fang 1975) proposed the following expression for S_γ :

$$S_\gamma = 1 - \frac{0.4B}{L}. \quad (180)$$

Based on this expression, the shape factor, S_γ , for Vesic's experimental footing is equal to 0.95 -- a value slightly higher than the value proposed by Terzaghi. HOPKIB values of N_γ corrected according to this factor are shown also in Figure 49. Except for slight differences near the ends of the experimental data, the N_γ values from the HOPKIB model fall within the limits of the experimental values. In Figure 50, N_γ values proposed by Terzaghi, Vesic', and Caquot and Kerisel are compared to Vesic's experimental N_γ values. Each of the theoretical values was corrected by Terzaghi's shape factor (0.933) before being compared. Above 38.5 degrees, the N_γ values proposed by Terzaghi, Vesic', and Caquot and Kerisel are below the limit curve described by Vesic' as "first failure." Below 38.5 degrees, all theoretical values fall within the two limits of failure. The HOPKIB N_γ values compare as well, or better, to the experimental values as the theoretical values proposed by Terzaghi, Vesic', and Caquot and Kerisel.

Vesic' also published (cf. 1975 Lambe and Whitman) experimental N_γ values determined from small, model circular footings. Diameters of the model footings ranged from two to 8 inches. The experimental values of N_γ are shown in Figure 51 as a function of ϕ . In these tests, the ϕ values ranged from about 35 degrees to 43 degrees. Theoretical values of N_γ obtained from the HOPKIB model are compared in Figure 51 to Vesic's experimental values. However, since the N_γ values obtained from the model are for a strip loading and considering that the N_γ values are dependent on footing shape, the HOPKIB N_γ values were corrected by a shape factor, S_γ , given by DeBeer and Vesic' (cf. 1975 Winterhorn and Fang). A shape factor of 0.6 was used to reduce values obtained from the HOPKIB model before comparisons were made with the experimental values. Vesic' represents two failure modes -- "first failure" and "general failure" -- for the round model footings. The trend of the "first failure" mode (lower curve) may be characterized as:

$$N_\gamma = (0.000185)e^{(0.3273\phi)}, \quad (181)$$

while the "general failure" mode (upper curve) may be characterized as

$$N_\gamma = (0.002668)e^{(0.2706\phi)}. \quad (182)$$

As shown in Figure 51, N_γ values from the HOPKIB model (corrected according to shape) generally fall within these two experimental failure limits. Moreover, the HOPKIB values are generally in closer agreement with the experimental values than those proposed by Caquot and Kerisel, Vesic', or Terzaghi. Figure 52 represents an attempt to combine the experimental results presented by DeBeer and Ladanyi (strip footings) and Vesic' (round and rectangular footings). The experimental N_γ values obtained by Vesic' were corrected as follows:

$$N_\gamma = \frac{2q_{u(obs)}}{S_\gamma} B\gamma \quad (183)$$

$$N_\gamma = \frac{2q_{u(obs)}}{S_\gamma B\gamma} \quad (\text{Vesic's rectangular footings}), \quad (184)$$

and

$$N_\gamma = \frac{2q_{u(obs)}}{0.6B\gamma} \quad (\text{Vesic's round footings}). \quad (185)$$

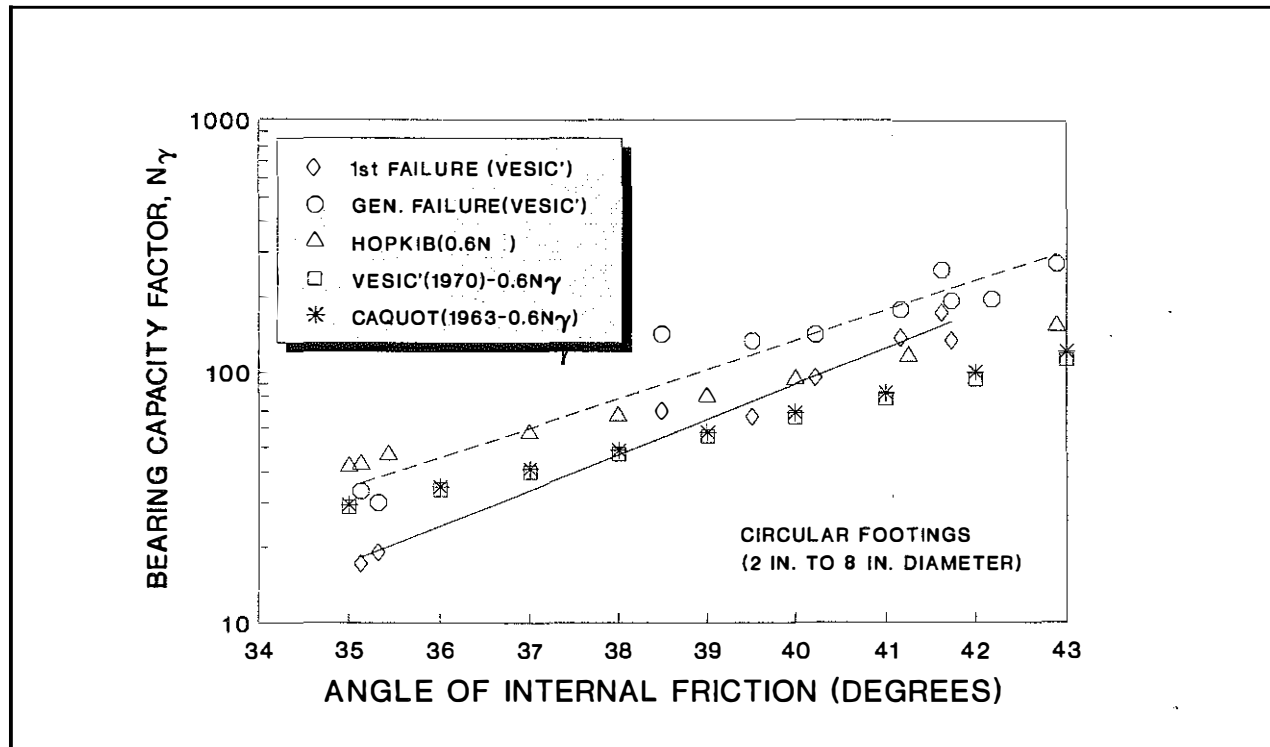


Figure 51. Comparison of the N_γ Factors Obtained from the HOPKIB Model, Terzaghi's, Vesic's, and Caquot and Kerisel's Methods to Experimental N_γ Factors Determined by Vesic's Circular, Model Footing Tests.

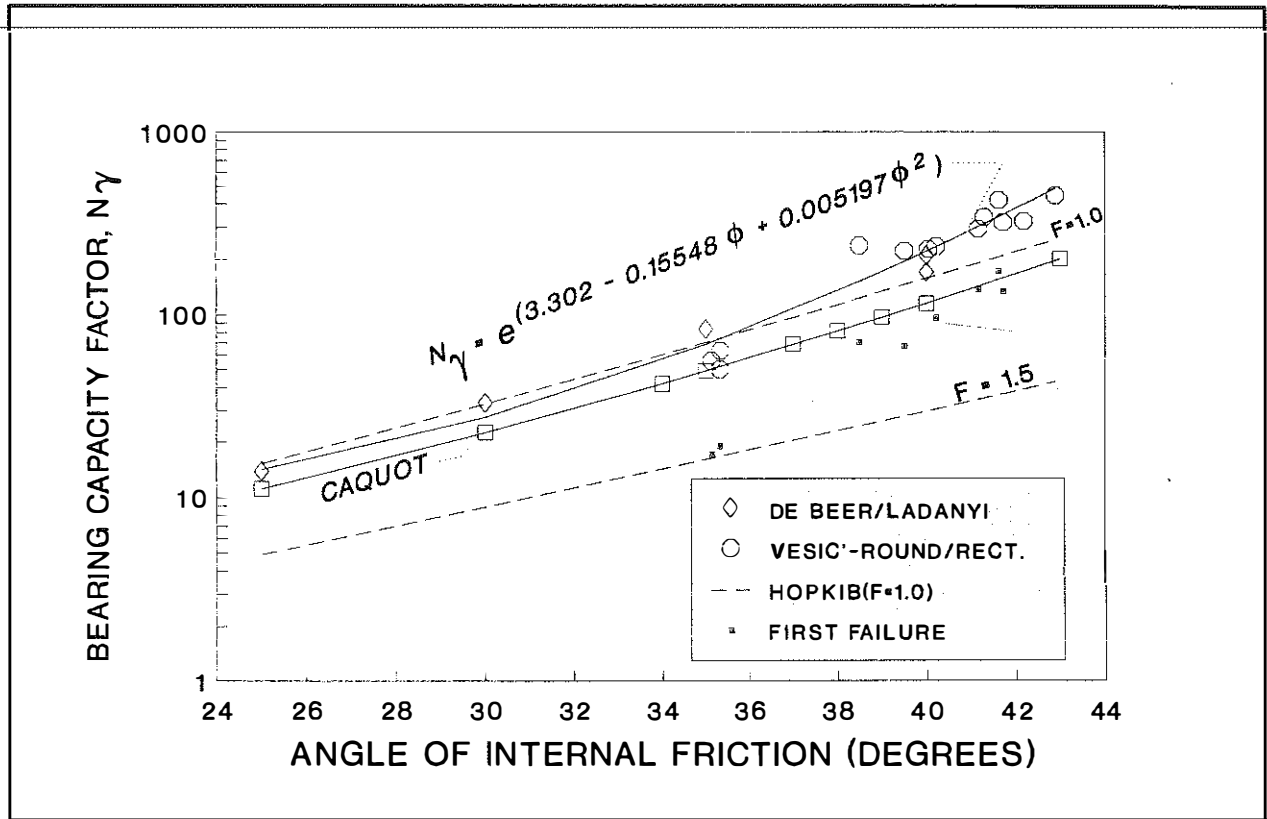


Figure 52. Comparisons of N_γ Factors (Corrected According to Shape of Footing) Obtained by DeBeer and Ladanyi (1961) and Vesic' (c.f. Lambe and Whitman (1969)) from Model Footing Tests and N_γ Factors Proposed by Caquot and Kerisel (1953) and N_γ Factors from the HOPKIB Model.

The dashed-line curve represents N_γ values from the HOPKIB model at a factor of safety of 1.0. The lower dashed-line curve represents N_γ values obtained from the proposed model at a factor of safety of 1.5. Variation of the ratio of the HOPKIB N_γ values to the (combined) experimental N_γ values are shown in Figure 53. The HOPKIB are some 148 to 64 percent of the experimental values. Caquot's N_γ values are about 108 to 49 percent of the experimental values. When the experimental N_γ values are used in the HOPKIB model, the factors of safety range (Figure 54) from 1.20 to 0.89 for ϕ values ranging from 25 to 42.9 degrees. Using Caquot's N_γ values in the HOPKIB model, factors of safety obtained from the model range from 1.15 to 1.09.

Scenario 4 -- Combined Bearing Capacity Factors ($N_c + N_\gamma$)

In the bearing capacity of subgrades subjected to wheel loads, the overburden depth is zero. Equation 152 reduces to

$$q_u = S_c c N_c + S_\gamma (0.5) \gamma B N_\gamma \quad (186)$$

When ϕ is not zero, then the ultimate bearing capacity depends on the bearing capacity factors N_c and N_γ .

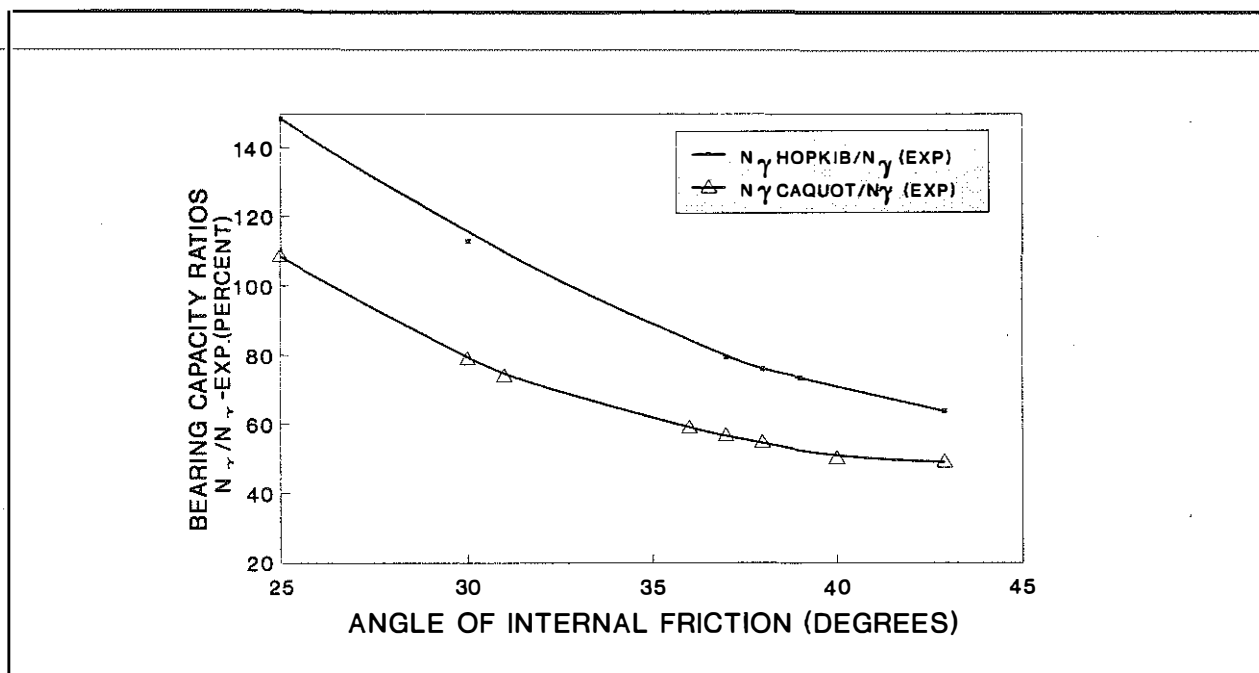


Figure 53. Ratios of N_{γ} Factors Obtained from the HOPKIB Model and Caquot and Kerisel's Method to Experimental N_{γ} Factors from Model Footing Tests.

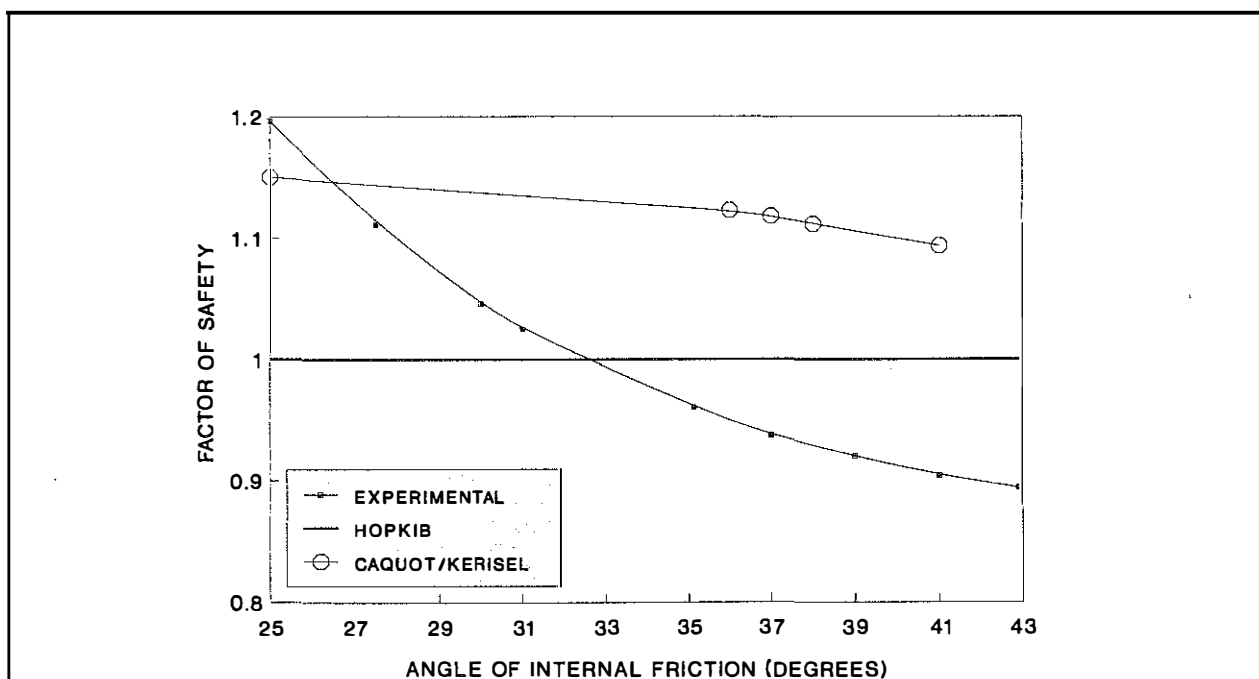


Figure 54. Factors of Safety Obtained from the HOPKIB Model When Experimental Values of N_{γ} --Corrected According to Shape--Reported by DeBeer and Ladanyi, and Vesic' and Theoretical N_{γ} Values Reported by Caquot and Kerisel are Inserted into the HOPKIB Model.

This situation may be analyzed using the HOPKIB model. Let

$$\begin{aligned} S_c &= S_\gamma = 1, \\ c &= 1, \\ B &= 2, \text{ and} \\ \gamma &= 1, \end{aligned}$$

then

$$q_u = (1)(1)N_c + (0.5)(1)(2)N_\gamma \quad (187)$$

$$q_u = N_c + N_\gamma = N_{c\gamma}. \quad (188)$$

If the above values are inserted into the HOPKIB model, and ranging ϕ from zero to 50 degrees (N_γ equals zero when ϕ equals 0), values of $N_{c\gamma}$ obtained from the HOPKIB model are compared in Figure 55 to $N_{c\gamma}$ values proposed by Terzaghi, Prandtl and Vesic'. The $N_{c\gamma}$ -factors from the proposed model are about 96 to 119 percent of $N_{c\gamma}$ values from Prandtl and Vesic's equations (see Figure 56). Values from Terzaghi's theory are some 110 to 147 percent of values obtained from Prandtl and Vesic's equations.

Scenario 5 -- Combined Bearing Capacity Factors ($N_q + N_\gamma$)

In this scenario, the two bearing capacity factors, N_q and N_γ , are considered. Let

$$\begin{aligned} S_q &= S_\gamma = 1 \\ c &= 0, \\ B &= 2, \\ \gamma &= 1, \text{ and} \\ q &= 1, \end{aligned}$$

then Equation 152 becomes:

$$q_u = (1)(0)N_c + (1)N_q + (0.5)(1)(2)N_\gamma, \quad (189)$$

and

$$q_u = N_q + N_\gamma = N_{q\gamma}. \quad (190)$$

Inserting the above values into the HOPKIB model, the sum of N_q and N_γ (defined as $N_{q\gamma}$ in Equation 190) may be calculated. Values of $N_{q\gamma}$ obtained from the HOPKIB model are compared to $N_{q\gamma}$ factors obtained from Prandtl's Equation 147 and Vesic's Equation 150 in Figure 57.

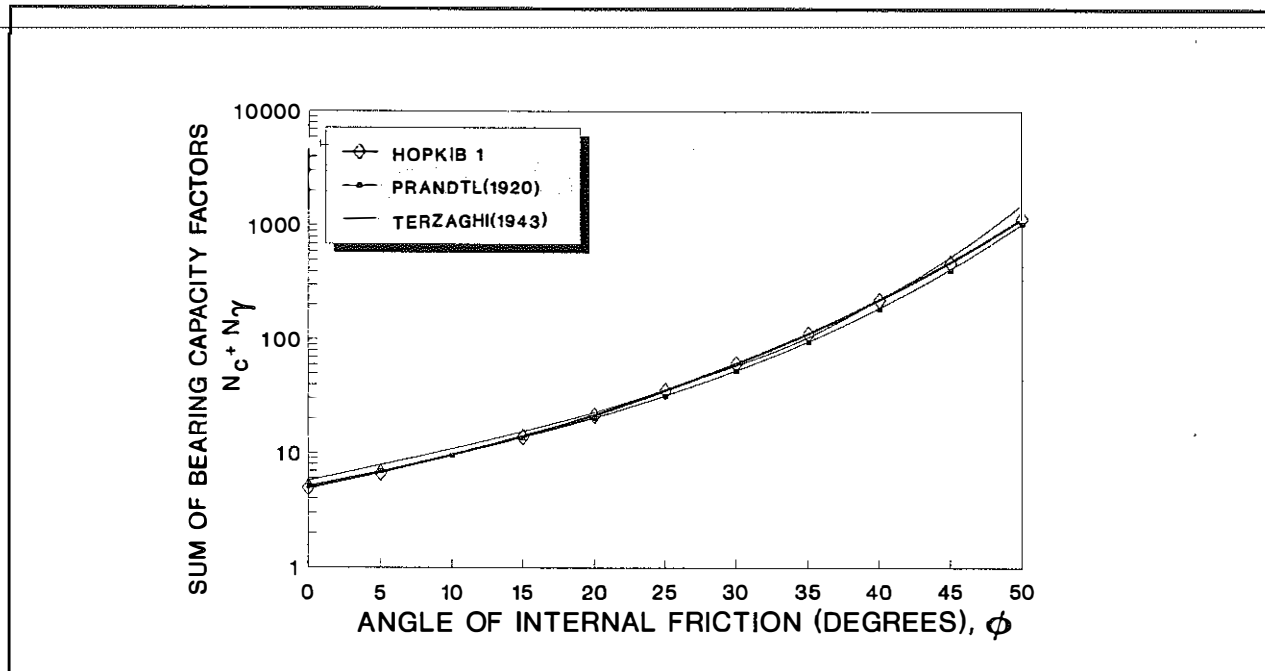


Figure 55. Comparisons of N_{cy} (Sum of $N_c + N_\gamma$) Values Proposed by Prandtl and Vesic' and Values Obtained from the HOPKIB Model.

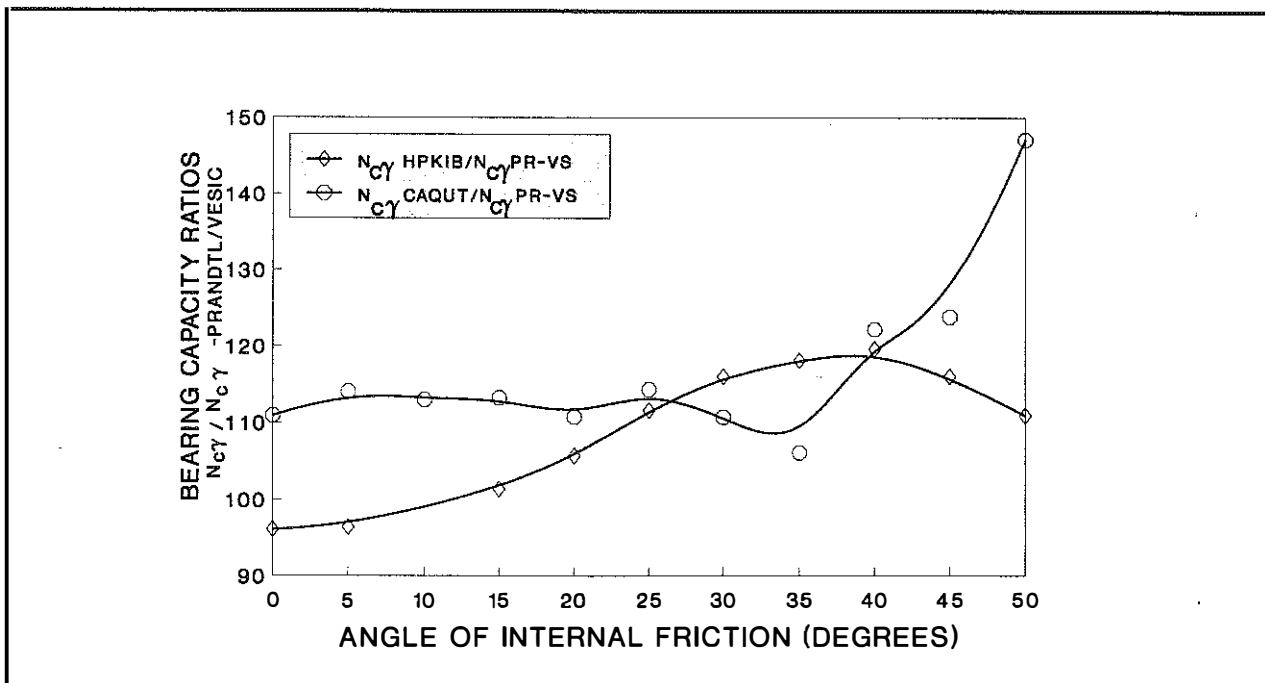


Figure 56. Ratios of N_{cy} Factors from the HOPKIB Model to N_{cy} Factors from Prandtl's and Vesic's Equations.

Ratios of $N_{q\gamma}$ obtained from the HOPKIB model to values obtained from Prandtl's and Vesic's equations are shown in Figure 58 as a function of ϕ . These results show that the $N_{q\gamma}$ factors obtained from the model analyses range from 96 to about 71 percent of $N_{q\gamma}$ factors from Prandtl's and Vesic's equations when ϕ ranges from zero to 47 degrees, respectively. When ϕ ranges from about zero to 43 degrees, the ratios in percent are about 96 to 82 percent, respectively.

Scenario 6 -- Combined Bearing Capacity Factors ($N_c + N_q + N_{q\gamma}$)

Let

$$S_c = S_q = S_{\gamma} = 1,$$

$$c = 1,$$

$$q = 1,$$

$$\gamma = 1, \text{ and}$$

$$B = 2,$$

then Equation 152 becomes:

$$q_u = (1)(1)(N_c) + (1)N_q + (0.5)(1)(2)N_{q\gamma} \quad (191)$$

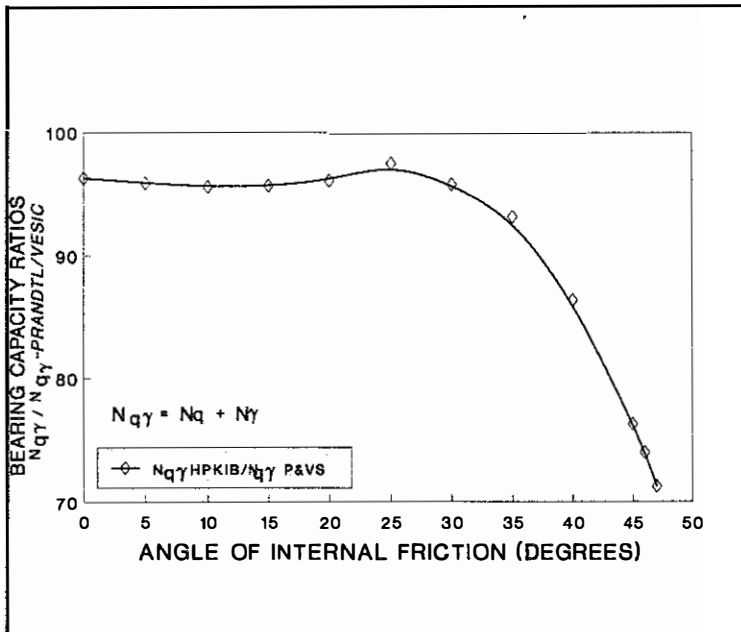


Figure 58. Ratios of $N_{q\gamma}$ Factors from the HOPKIB Model to $N_{q\gamma}$ Values Obtained from Prandtl's and Vesic's Equations.

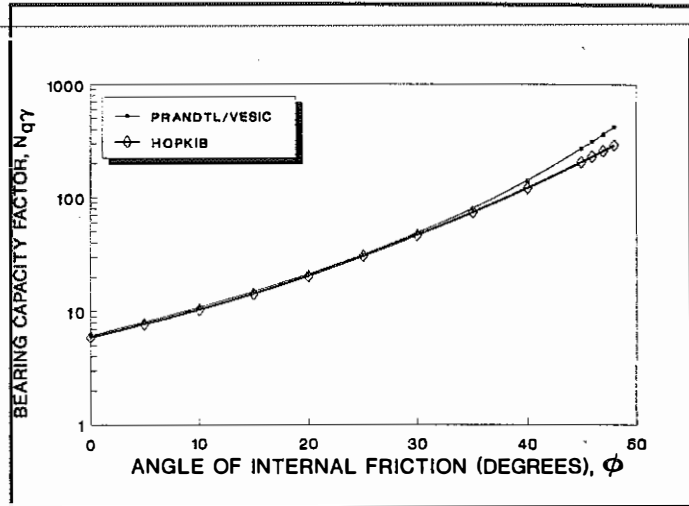


Figure 57. Comparison of $N_{q\gamma}$ Factors ($N_q + N_{q\gamma}$) Obtained from the HOPKIB Model and $N_{q\gamma}$ Factors from Prandtl's and Vesic's Equations.

and,

$$q_u = (N_c + N_q + N_{q\gamma}) = 5N_{cq\gamma} \quad (192)$$

Inserting the above values into the HOPKIB model, the sum, or $N_{cq\gamma}$ values, may be computed. The results obtained from the model analyses are compared to values obtained from Prandtl's equations and Vesic's equation in Figure 59. Ratios of $N_{cq\gamma}$ factors from the model analysis to those obtained from Prandtl's equations and Vesic's equations are shown in Figure 60. The sum of $N_{cq\gamma}$ factors is approximately 85 to 113 percent of the Prandtl and Vesic' $N_{cq\gamma}$ factors. Terzaghi's values range from 109 to 143 percent of Prandtl's and Vesic's factors.

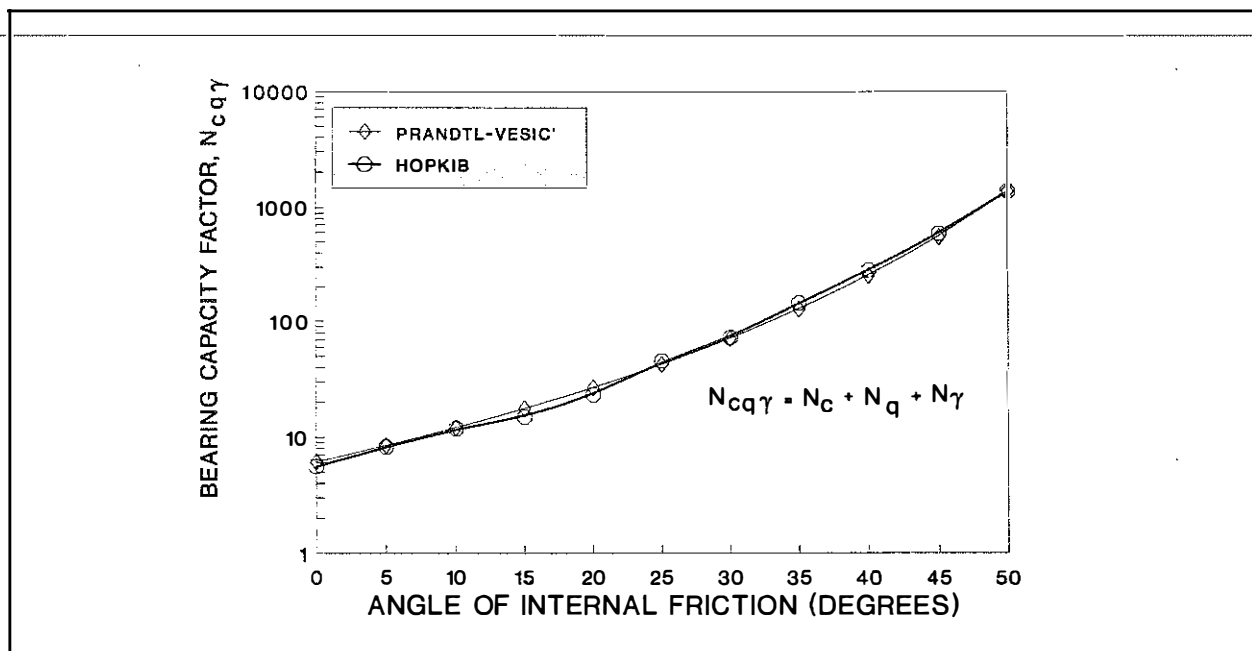


Figure 59. Comparison of $N_{cq\gamma}$ -Factors (Sum of N_c , N_q and N_γ) Obtained from the HOPKIB Model and $N_{cq\gamma}$ Values from Prandtl's and Vesic's Equations.

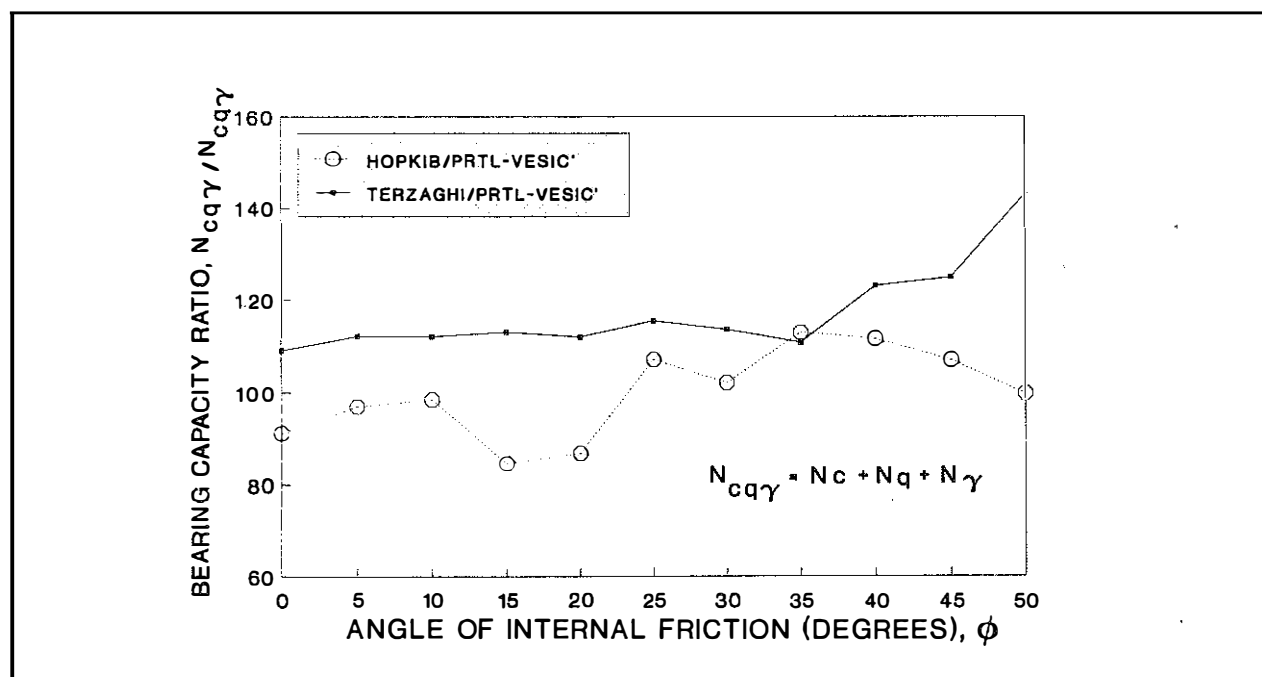


Figure 60. Ratios of the $N_{cq\gamma}$ Factors Obtained from the HOPKIB Model to $N_{cq\gamma}$ Factors Obtained from Prandtl's and Vesic's Equations.

Minimum Subgrade Strength

In the scenarios described, the values of bearing capacity factors, N_c , N_q , and N_γ , derived from the HOPKIB bearing capacity model were shown to be very close to values obtained from Prandtl's equations (numbers 147 and 148 and Vesic's semi-empirical equation, number 150), although slight differences exist among the two sets of values when ϕ is approximately greater than 43 degrees. The HOPKIB model may be used to develop some practical aspects concerning pavement subgrades during construction. For example, the model may be used to determine the minimum strength required to avoid failure of the subgrade subjected to construction traffic. The minimum CBR strength of the subgrade necessary to avoid failure under construction traffic and the minimum bearing strength to control a pavement may be found. These minimum values may be stated in terms of minimum values of the dynamic modulus of elasticity and dynamic cone penetrometer values. These aspects are discussed as follows.

Undrained Shear Strength

The minimum undrained shear strength, c , or S_u , of the subgrade required to withstand failure may be determined from the HOPKIB bearing capacity model. The assumed failure pattern of the subgrade when subjected to an assumed dual-wheel loading is shown in Figure 23. The relationship between undrained shear strength of the subgrade and tire contact stress, T_c , of the dual-wheel loading is shown in Figure 61. This relationship may be expressed in the form:

$$S_u = 0.171T_c \text{ (psi).} \quad (193)$$

At a factor of safety of 1.0 and a contact stress of 67.5 psi (AASHO Road Test 1972), the minimum undrained shear strength is 1,662 pounds per square foot (psf)(11.542 psi). At a contact stress of 80 psi, Equation 193 yields a minimum strength of 1,970 psf (13.68 psi). Assuming a factor of safety of 1.5, the relationship between undrained shear strength and tire contact stress may be expressed as (see Figure 62):

$$S_u = 0.26T_c \text{ (psi).} \quad (194)$$

At tire contact stresses of 67.5 and 80 psi, the undrained shear strengths are 2,527 psf(17.55 psi) and 2,995 psf(20.80 psi), respectively. Hence, Equations 193 and 194 may be used to approximate the minimum subgrade strengths required to avoid failure when the anticipated tire contact stress is known.

CBR Bearing Strength - Theoretical

Considering that many agencies have used and some continue to use the CBR as a means of expressing the bearing strength of subgrades and as a design parameter in pavement design schemes and considering that the HOPKIB model uses undrained shear strength in total stress analysis as a design parameter, development of a relationship between CBR and undrained shear strength is desirable so that minimum CBR values of the subgrade may be determined from the HOPKIB model. An approximate relationship may be developed by analyzing the conditions of the CBR test, as shown in Figure 63. The assumed failure pattern of the CBR penetrating piston is shown in this figure. The theoretical failure surface

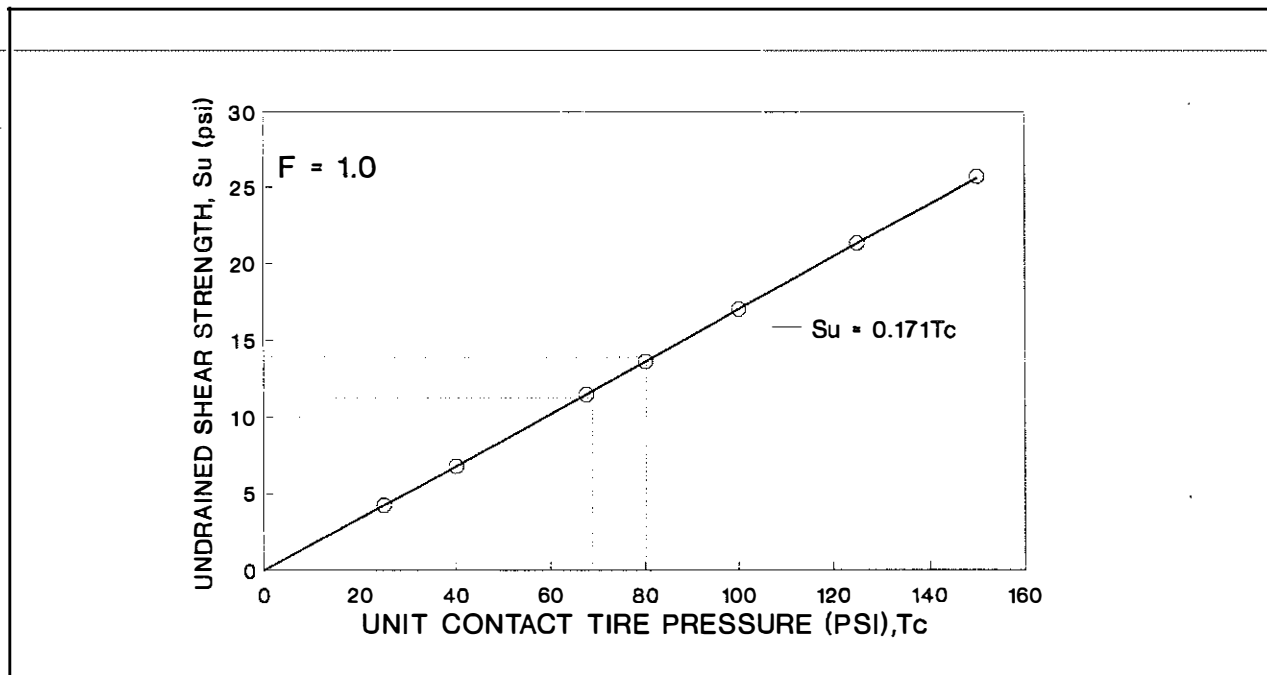


Figure 61. Relationship Between Subgrade Undrained Shear Strength and Contact Tire Stress Obtained from the HOPKIB Model for a Factor of Safety Equal to 1.0.

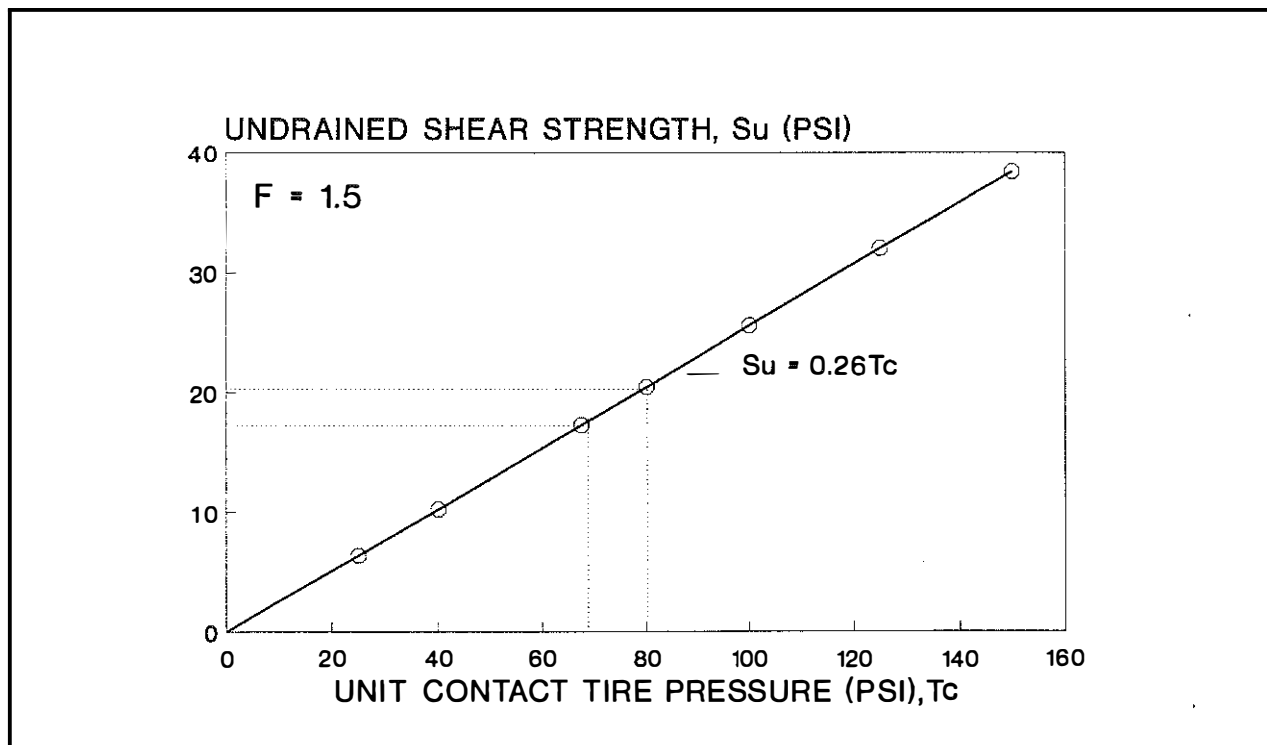


Figure 62. Relationship Between Subgrade Undrained Shear Strength and Contact Tire Stress Obtained from the HOPKIB Model for a Factor of Safety Equal to 1.5.

consists of an active wedge, central wedge, and passive wedge, respectively. These wedges are identified in Figure 63 as 1, 2, 3. The angle, θ_a , between the shear surface and a horizontal line (active wedge), and the angle, θ_p , between the shear surface and a horizontal line of the passive wedge are, respectively,

$$\theta_a = 45 + \frac{\phi}{2} \quad (195)$$

$$\theta_p = 45 - \frac{\phi}{2} \quad (196)$$

The two wedges, or shear surfaces, are connected by a logarithmic spiral, which may be expressed as:

$$r = r_o e^{\omega \tan \phi} \quad (197)$$

where

- r = radius vector of the logarithmic spiral,
- r_o = initial radius vector of the logarithmic spiral,
- ω = angle between two radius vectors, r_o and r , measured in radians.

Since a CBR specimen is normally soaked before penetration to saturate it, and considering that loading of the specimen during testing is very rapid, undrained conditions for clayey and silty clayey specimens are assumed to prevail. The value of ϕ is zero, and Equations 195, 196, and 197 become:

$$\theta_a = \theta_p = 45^\circ \quad (198)$$

and

$$r = r_o \quad (199)$$

Since ϕ equals zero, the logarithmic spiral becomes a circular arc, as shown in Figure 63. Geometrically, for a CBR mold with a six-inch diameter, the theoretical shear surface of the passive wedge (number 3) intercepts the specimen surface at the inside surface of the mold -- point *d* in Figure 63. From classical bearing capacity theory (Prandtl 1921), the ultimate stress that the soil specimen may sustain is

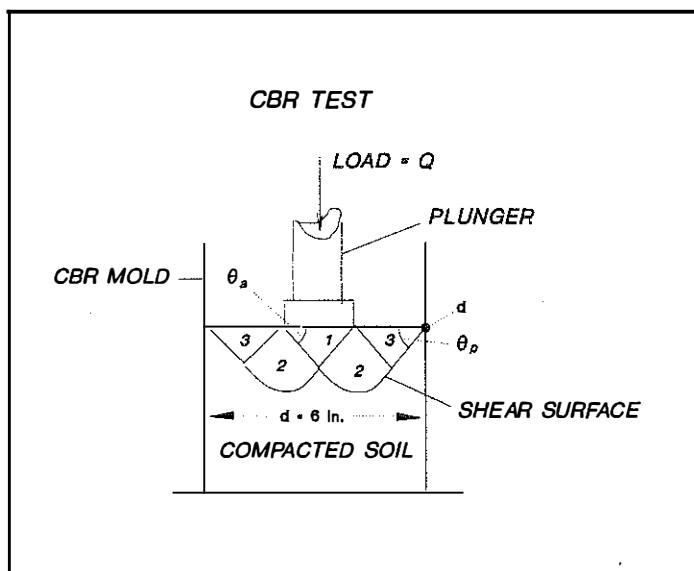


Figure 63. Theoretical Failure Pattern in the CBR Test.

$$q_u = S_c c N_c + S_q q N_q, \quad (200)$$

and,

$$q_u = \frac{Q_u}{a_p} = S_c c N_c + S_q q N_q, \quad (201)$$

and (after DeBeer 1967 and as modified by Vesic', 1975, cf. Winterhorn and Fang)

$$S_c = 1 + \frac{N_q}{N_c}, \text{ and} \quad (202)$$

$$S_q = 1 + \tan \theta, \quad (203)$$

where a_p is equal to the area of the CBR piston used to penetrate the specimen.

Since ϕ equals zero, S_c is equal to 1.195 and S_q is equal to 1.00. According to ASTM specifications, the diameter of the piston is 1.954 inches. Hence, a_p is equal to three square inches. Since loading is considered rapid, ϕ is equal to zero, N_c is equal to 5.14, and N_q is equal to one. Equation 201 becomes (rearranging terms):

$$Q_u = a_p (1.195) [5.14c + q], \quad (204)$$

$$Q_u = 3 (1.1945) (5.14c + q), \text{ and} \quad (205)$$

$$Q_u = 18.42c + \gamma d. \quad (206)$$

($q = \gamma d$; γ is the unit weight of overburden and d is the height of the overburden -- now, q is the stress of any surcharge loads placed on the specimen.)

Rearranging terms and solving for c ,

$$c \approx \frac{Q_u - \gamma d}{18.42} \quad (\text{psi}). \quad (207)$$

If the shape factor S_c is ignored, then ($S_c = 1$)

$$c \approx \frac{Q_u - \gamma d}{15.42} \quad (\text{psi}) \quad (208)$$

If the failure load, Q_u , is known during the CBR test, then the undrained shear strength, c , may be approximated from the CBR test. Several CBR tests were performed to obtain the necessary test data for correlating CBR and undrained shear strength. Specimens used in the tests included clayey and silty clay specimens and also specimens treated with hydrated lime, cement, and a waste by-product referred to as AFBC (Atmospheric Fluidized Bed Combustion) waste. The failure load, Q_u , observed in the CBR tests was assumed to occur at a penetration value of 0.1 inch. This assumption was based partly on observing the shapes of the load-penetration curves obtained during the CBR tests and partly on procedures outlined in ASTM D 1883-87, entitled "Bearing Ratio Test"; that is, the CBR value is defined at a penetration value

of 0.1 inches. Based on data from the CBR tests and Equation 208, the relationship between the undrained shear strength and CBR is shown in Figure 64. Additionally, data published by Thompson (1988) are shown in this figure. An expression (based on the two sets of data and regression analyses) relating the undrained shear strength, S_u , or c , and CBR is (for $S_c = 1$):

$$CBR = 0.465 S_u^{(1.05)} (\text{percent}). \quad (209)$$

Treating CBR as the independent variable,

$$S_u = 2.172 CBR^{(0.939)} (\text{psi}). \quad (210)$$

If DeBeer's shape factor (cf. Winterhorn and Fang) is ignored ($S_c = 1$), then

$$CBR = 0.46 S_u^{(1.014)} \text{ and} \quad (211)$$

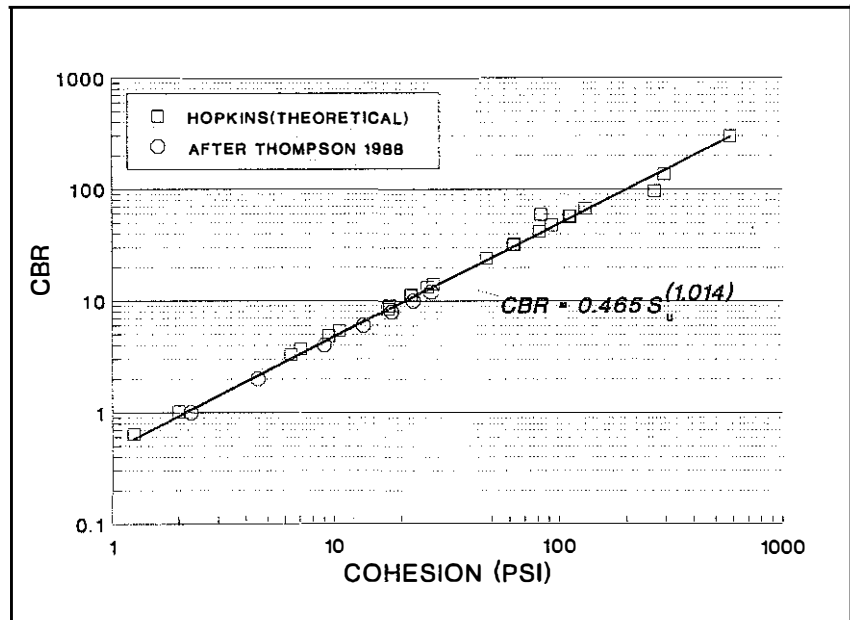


Figure 64. Relationship Between CBR and Cohesion Based on S_c Equal to 1.

$$S_u = 2.173 CBR^{(0.979)} \quad (212)$$

where S_u has units of psi.

As a check on the approximate relationship given by Equation 211 and to illustrate the influence of placement water content on the unconfined compressive strength (and CBR strength) of compacted clayey soils, a series of unconfined compressive tests was performed on remolded specimens of a typical clayey soil obtained from Fayette County, Kentucky. Specimens were remolded to various combinations of dry density and moisture content obtained from the moisture content-dry density relationship (ASTM D 698) shown in the upper portion of Figure 65. The undrained shear strength obtained from unconfined compression tests as a function of molding water content is shown in the lower portion of Figure 65. The trend line of the undrained shear strength-molding water content data may be characterized as:

$$S_u = 2530.86e^{(-0.22W_m)} \quad \text{psi}, \quad (213)$$

where w_m equals the molding water content of the silty clay.

Variations of CBR values and molding water contents are shown in Figure 66. One series of soaked CBR tests was done following ASTM standard specifications (ASTM D 1883-87) while another series of soaked CBR tests was performed following the Kentucky procedure (KM 64-501). In the Kentucky series of tests, the CBR values at 0.1 inch penetration were used instead of the minimum CBR value as specified in the Kentucky standard test method. A third series of CBR tests was done on unsoaked, compacted specimens. In these tests, the molding water contents were varied. The relationship between CBR and water content for the silty clay is shown in the lower portion of Figure 66. This relationship for the silty clay may be expressed approximately as:

$$CBR = 18355.1e^{(-0.323W_m)} \quad (214)$$

Assuming a moisture content ranging from 22 to 31 percent, using increments of moisture contents of 1 percent, and inserting the assumed water contents into Equations 213 and 214, values of undrained shear strength and CBR may be computed. These values are shown in Figure 67 and compared to the relationship given by Equation 211. The comparison of the relationship between S_u and CBR values obtained for the silty clay and the relationship between S_u and CBR values given by Equation 211 is reasonable. Based on the silty clay series of tests and data published by Thompson (1988), the approximate relationships expressed by Equations 211 and 212 seem valid.

Using the relationship given by Equation 212 and the HOPKIB bearing capacity model, minimum CBR values of soil subgrades may be established as a function of tire contact stress. In these analyses, a dual-wheel loading was assumed. The relationship between CBR and tire contact stress for a factor of safety

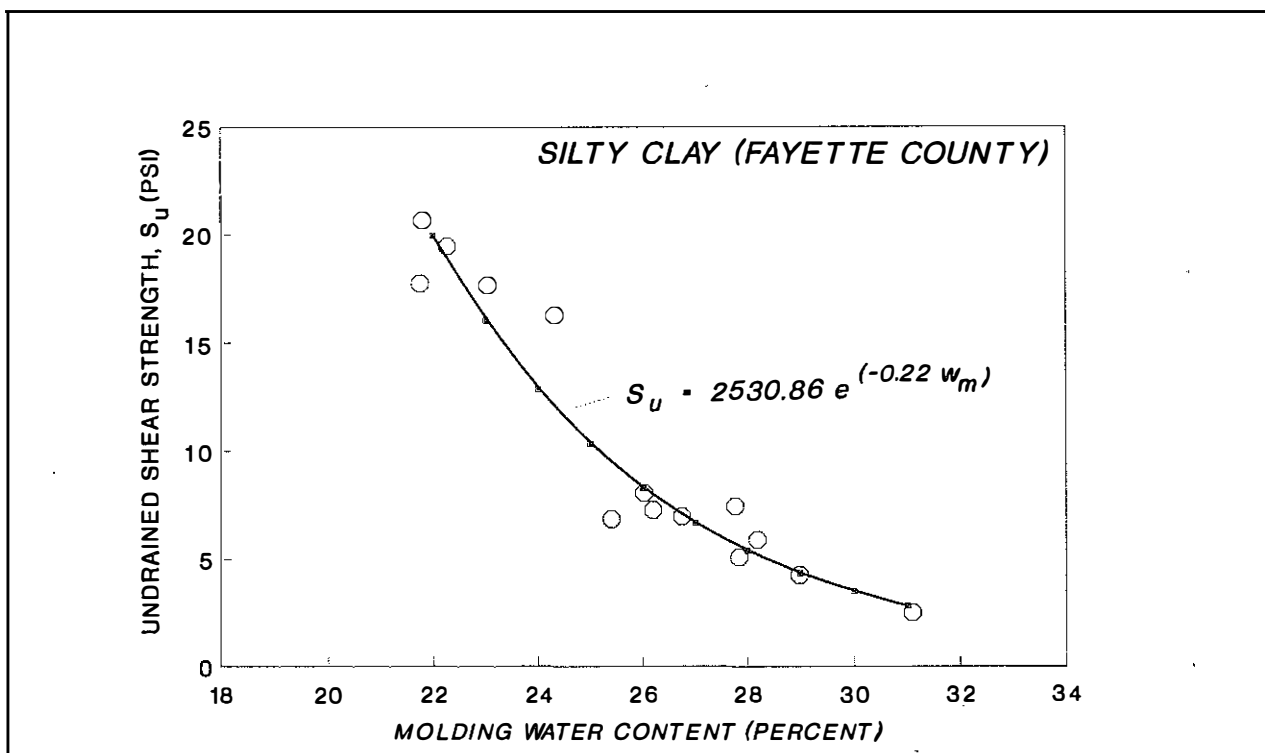
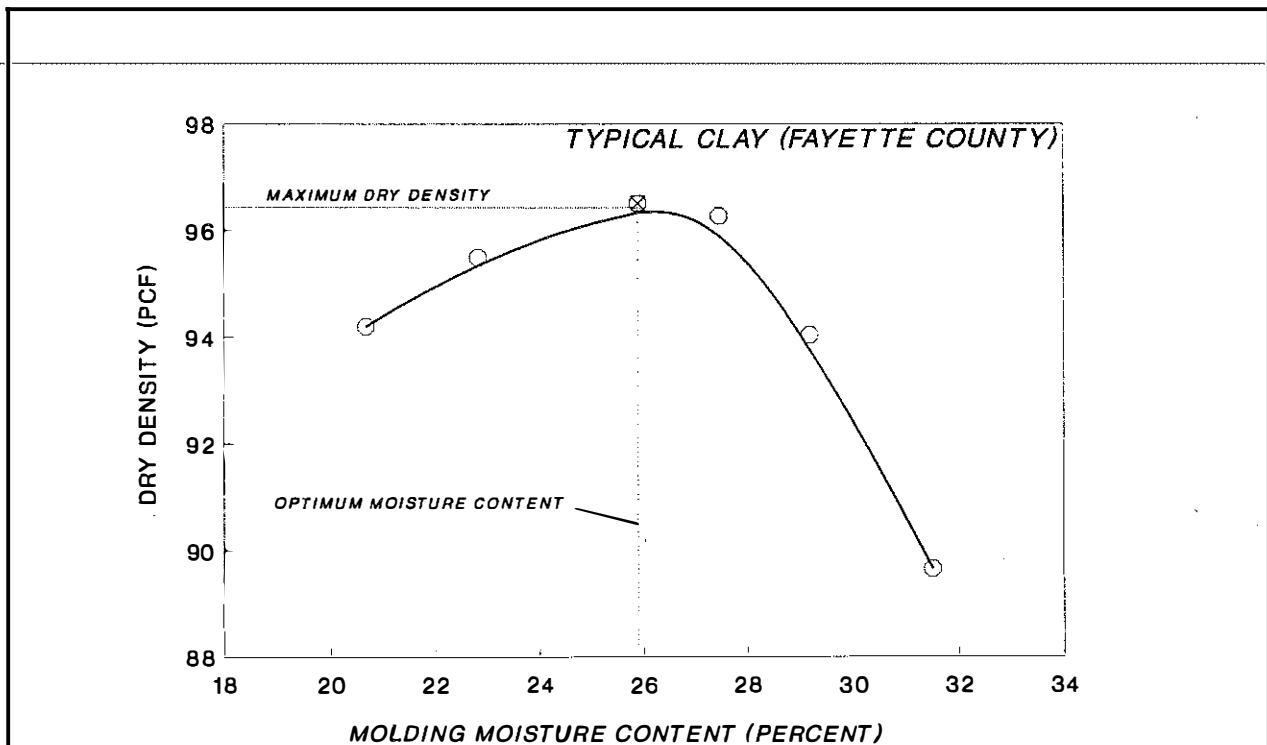


Figure 65. Variations of Dry Density and Undrained Shear Strength With Molding Water Content.

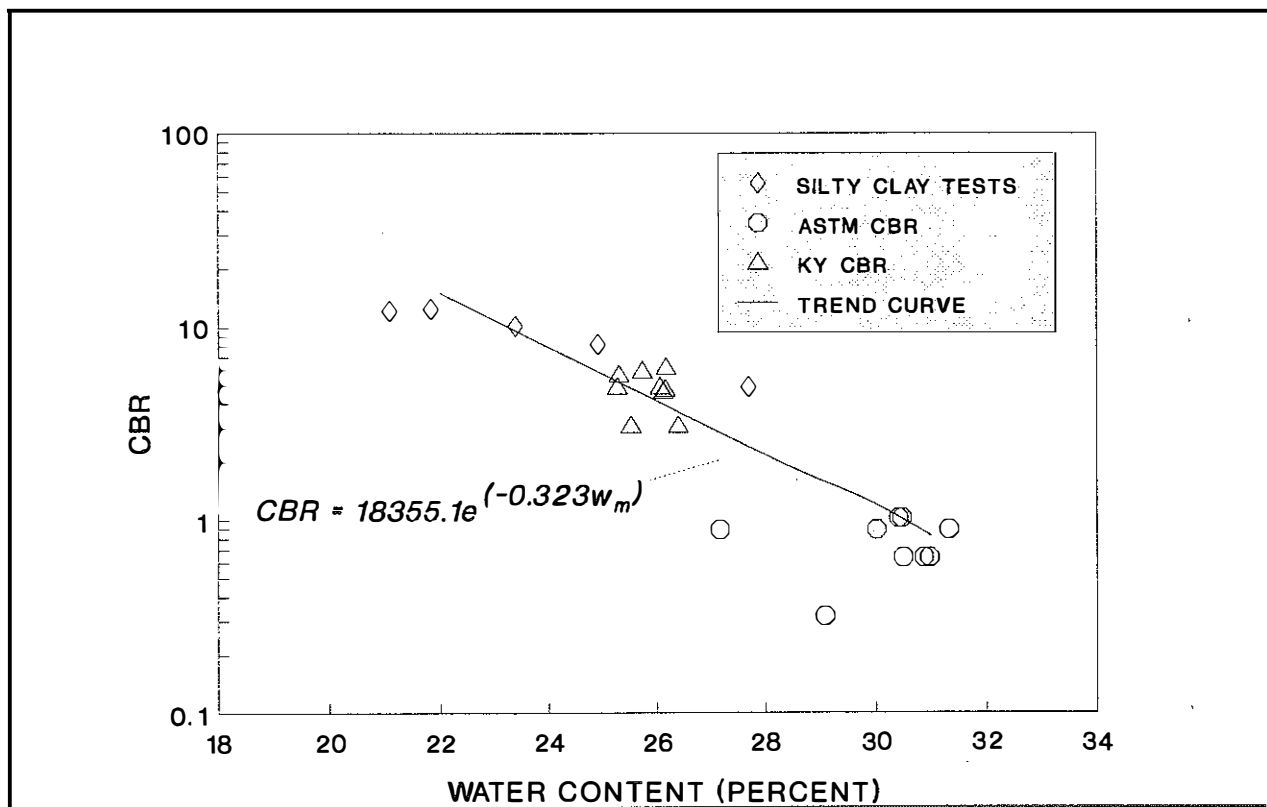
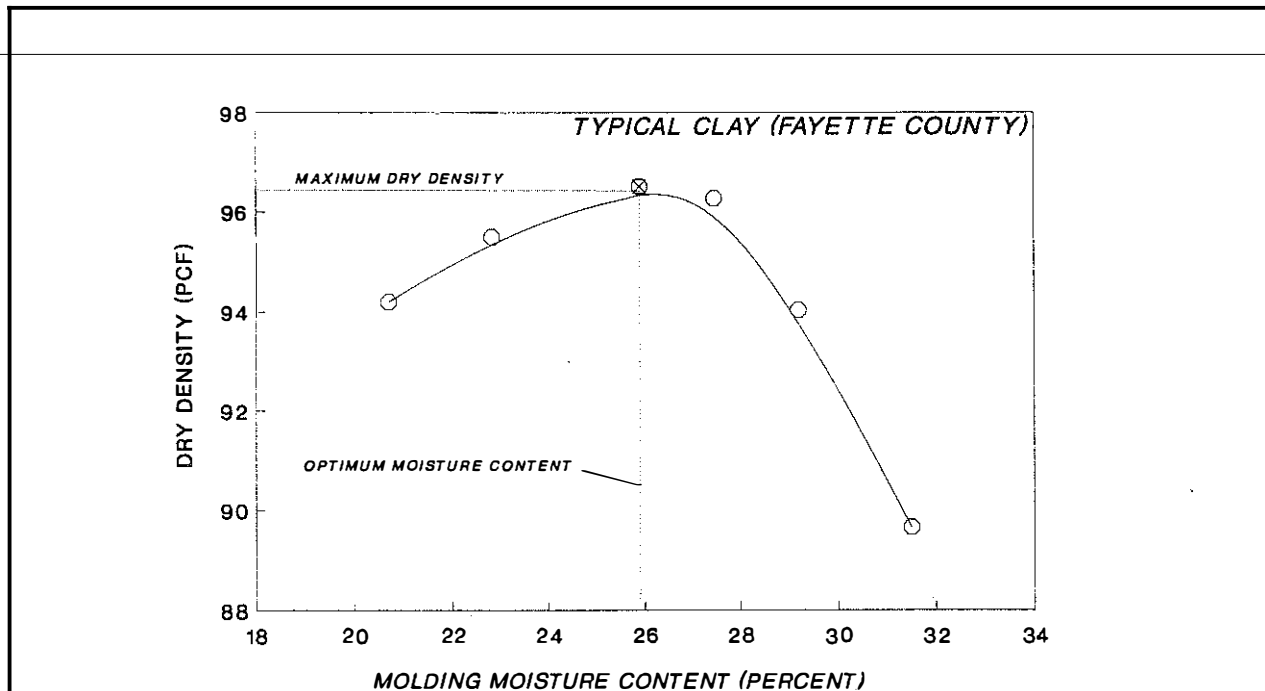


Figure 66. Variations of Dry Density and CBR With Molding Water Content.

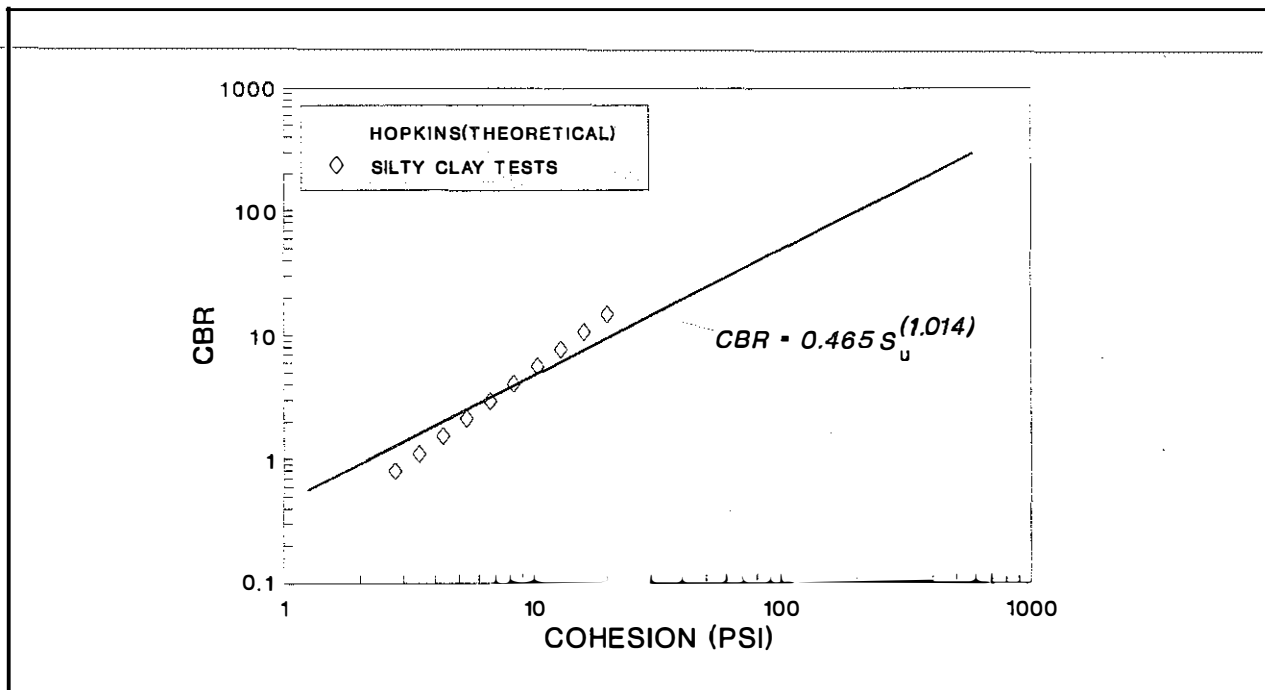


Figure 67. Comparison of the Results of Silty Clay Tests and the CBR-Cohesion Relationships.

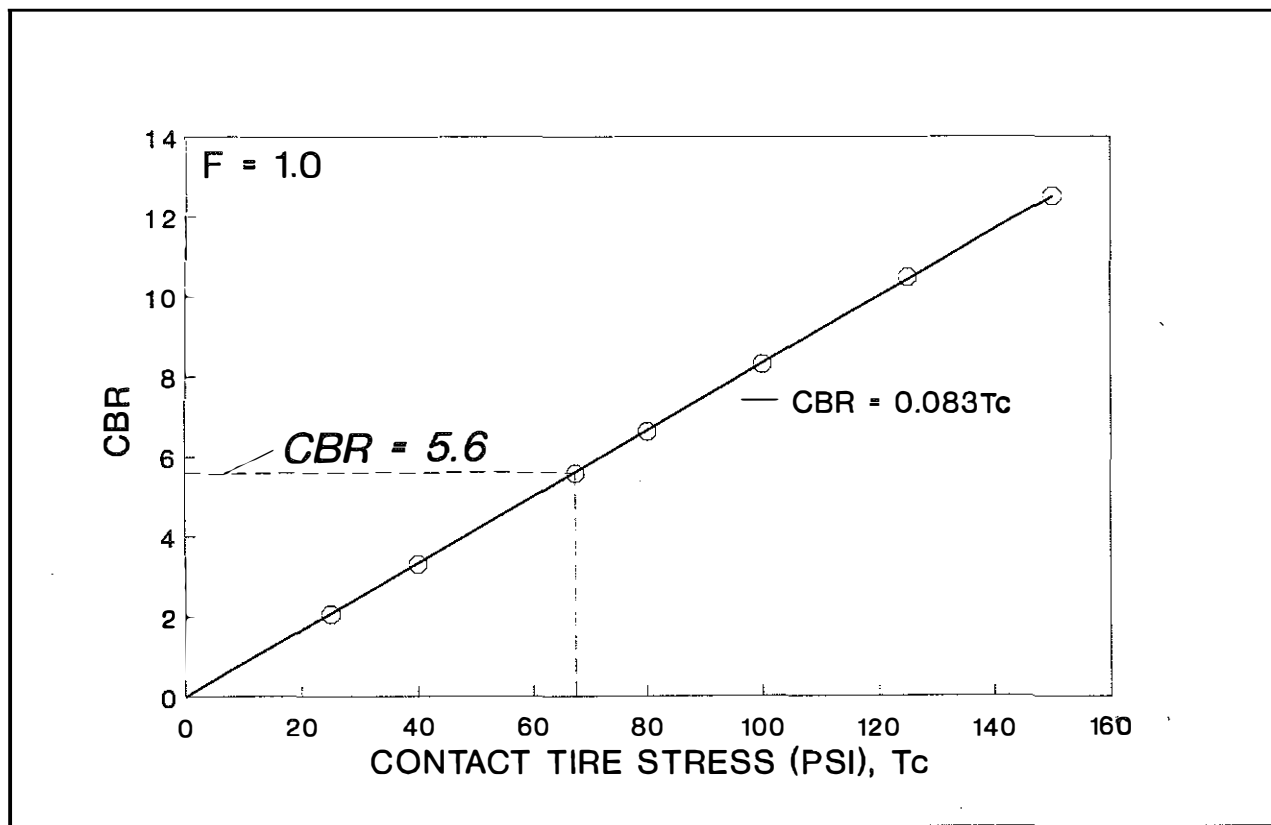


Figure 68. Relationship Between Subgrade CBR Strength and Tire Contact Stress Obtained from the HOPKIB Model at a Factor of Safety Equal to 1.0.

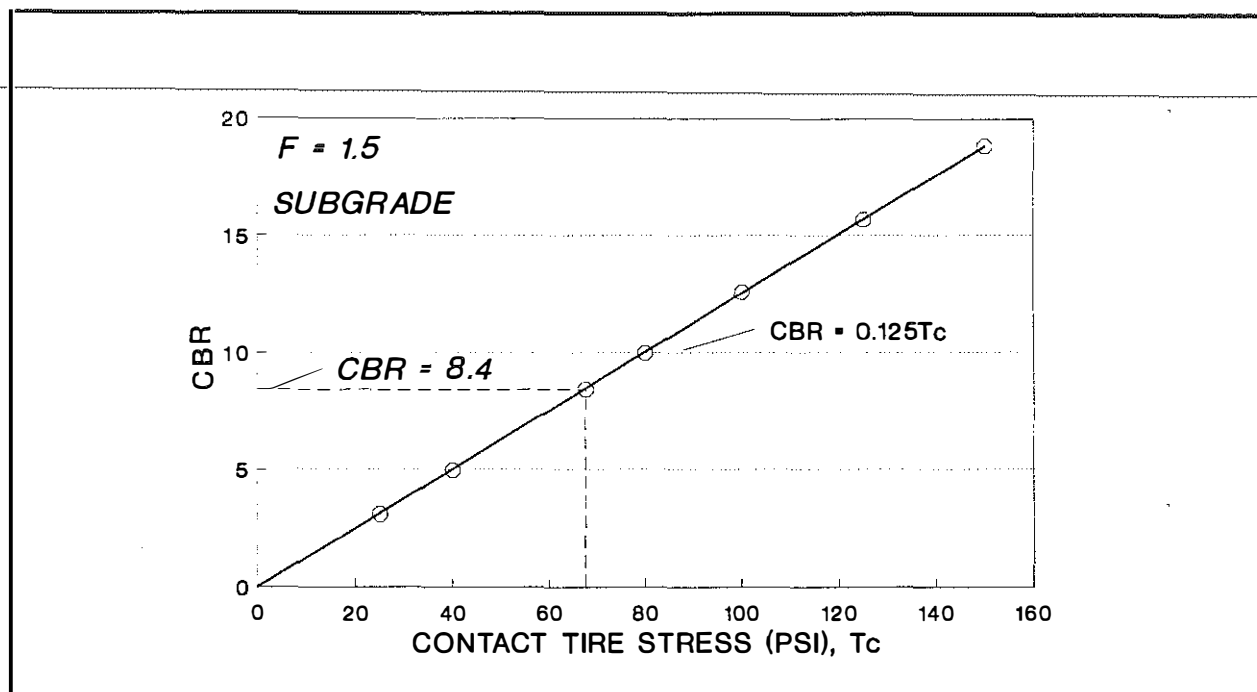


Figure 69. Relationship Between Subgrade CBR Strength and Contact Tire Stress Obtained from the HOPKIB Model at a Factor of Safety Equal to 1.5.

of one is shown in Figure 68. At a factor of safety of one and tire contact stress of 67.5 psi, the minimum CBR value of the subgrade is about 5.6. At a safety factor of 1.5, the minimum CBR-value is 8.4 as shown in Figure 69. To withstand a tire stress of 67.5 psi, the minimum CBR-strength of the subgrade must be approximately 5.6 to 8.4, or greater. When the tire contact stress increases, the CBR values must increase to prevent failure.

CBR Bearing Strength--Field Studies

Thompson (1988) cited two field subgrade studies that show the relationships among tire contact stresses, field CBR values, and tire sinkage (or rutting). Relationships between tire pressures and sinkage values for tire inflation pressures ranging from 50 to 80 psi are shown in Figure 70. For this range in tire pressures, the minimum CBR strength of the subgrade required to limit tire sinkage to 0.25 inches, or less, must be between about 5.3 and 8.5, respectively. Data labeled as "Kraft" in Thompson's paper (1988) were re-analyzed to obtain an equation which relates tire pressure (T_c), CBR, and tire sinkage(s). Graphical results of these re-analyses are shown in Figure 71 and may be expressed in the approximate form as:

$$CBR = \frac{1}{\frac{6.04}{T_c}(1+S) + 0.2S - 0.034} \quad (215)$$

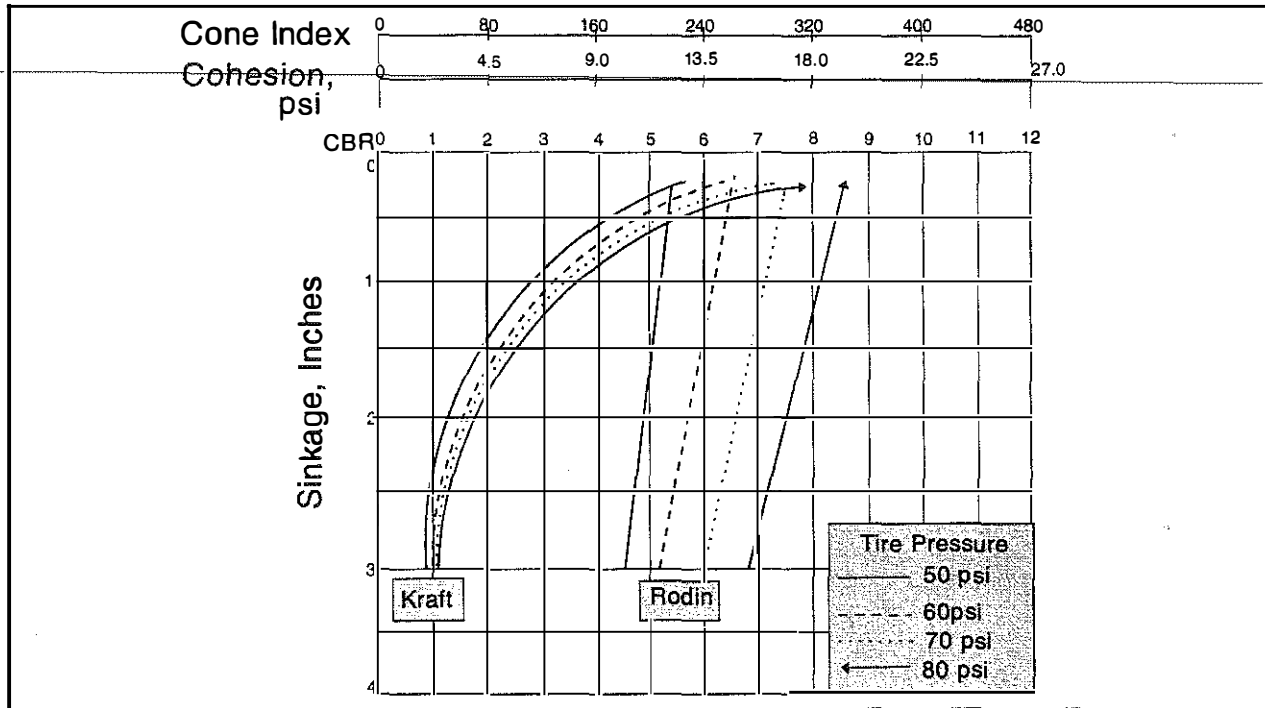


Figure 70. Soil Strength - Sinkage Relations for a 9-Kip Wheel Load (after Thompson 1988).

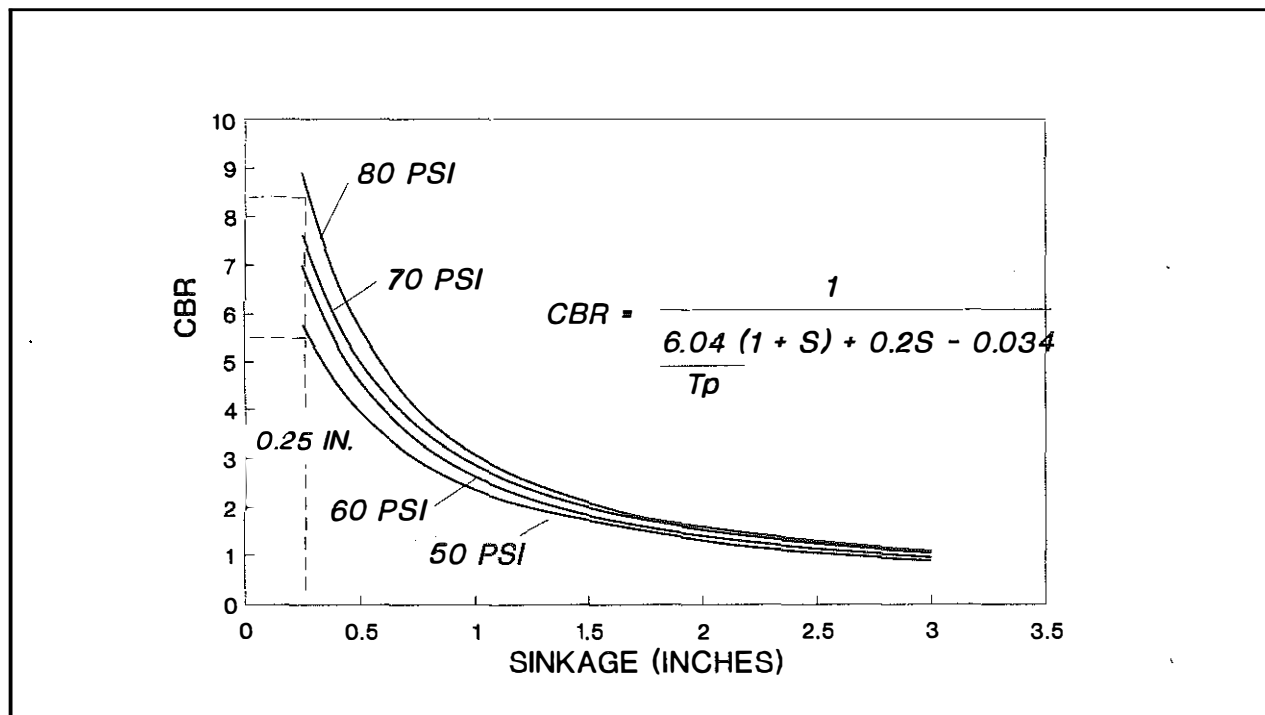


Figure 71. Relationship Between Subgrade CBR Strengths and Tire Sinkage for Tire Inflation Pressures Ranging from 50 to 80 psi (Data from Thompson 1988).

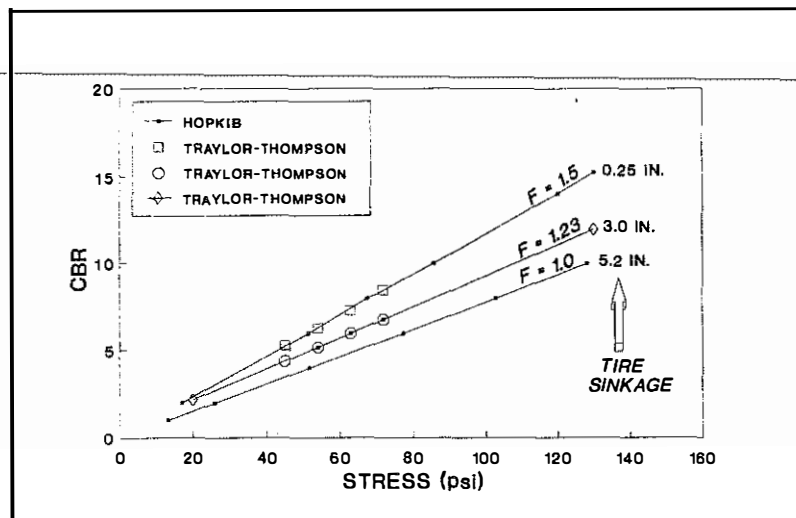


Figure 72. *Tire Sinkage Compared to Factor of Safety.*

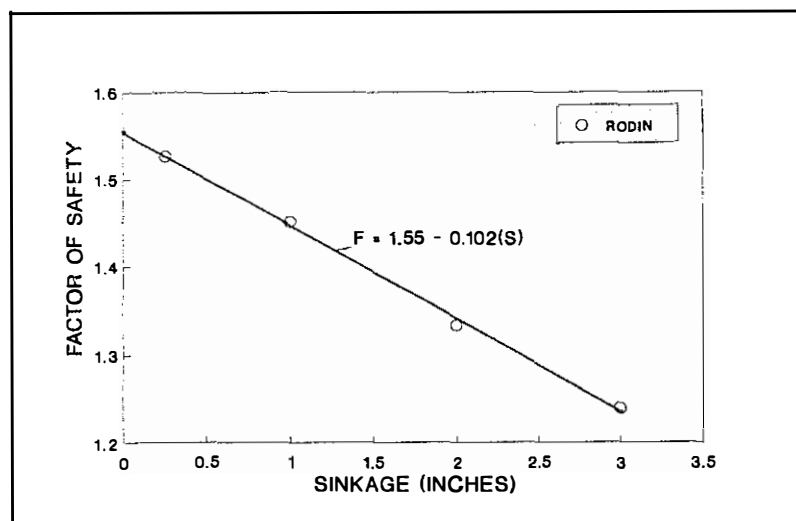


Figure 73. *Factor of Safety Obtained from the HOPKIB Model as a Function of Tire Sinkage.*

Thompson and labeled "Rodin" also confirm these analyses as shown in Figure 73. In this figure, factors of safety obtained from the HOPKIB model are shown as a function of tire sinkage. These data were obtained by using values of tire sinkage and corresponding values of tire pressures and CBR in the HOPKIB model. The factor of safety as a function of tire sinkage may be approximated as:

$$F = 1.55 - 0.102(S). \quad (216)$$

At a tire sinkage of 0.25 inches, the factor of safety is about 1.5. For a sinkage value of 3.0 inches, the factor of safety is about 1.24. At a sinkage value of 5.2 inches, the factor of safety is 1.02.

For example, for a tire inflation pressure of 80 psi, the CBR value of the subgrade required to limit tire sinkage to 0.25 inch is 9.1.

As shown in Figure 70, or in Figure 71, and for tire pressures ranging from 50 psi to 80 psi, the CBR values required to limit sinkage to 0.25 inch ranges from 5.3 to 8.5, respectively. Using these tire pressures and corresponding CBR values--which correspond to a tire sinkage of 0.25 inches--and converting the CBR values to undrained shear strength (Equation 212), the factor of safety obtained from the HOPKIB bearing capacity model for each combination of tire pressure and CBR value is 1.5 as shown in Figure 72. Performing a similar analysis using a tire sinkage of 3.0 inches and the corresponding relationships shown in Figures 70 and 71, a factor of safety of 1.23 is obtained. A similar analysis, based on extrapolation, shows that for a factor of safety 1.0, the tire sinkage is 5.2 inches--a failure condition. As the model analyses and actual field studies show, the factor of safety required to withstand failure and to limit the tire sinkage to 0.25 inch or less should be about 1.5, or larger. Field data shown by

Dynamic Modulus of Elasticity

Heukelom and Foster (1960), in a series of dynamic tests performed on a variety of subgrade types, established a relationship between the dynamic modulus of elasticity, E_s , of the subgrade and the CBR. This relationship (Figure 74), as shown by Heukelom and Foster, in equation form is:

$$E_s \approx 1564.5 \text{ CBR} \quad (217)$$

where E_s is in pounds per square inch (psi).

Later, Heukelom and Klomp (1962) represent the relationship as:

$$E_s \approx 1500 \text{ CBR (psi)} \quad (218)$$

Equation 218 is frequently used by pavement researchers and designers to estimate the dynamic modulus of the subgrade in performing "back-analyses." Using regression analysis (it is not clear in Heukelom and Foster's paper that regression analysis was done), their data were re-analyzed. The "best-fit" trend line in equation form may be expressed as:

$$E_s \approx 2596.25 \text{ CBR}^{(0.874)}, \text{ (psi)} \quad (219)$$

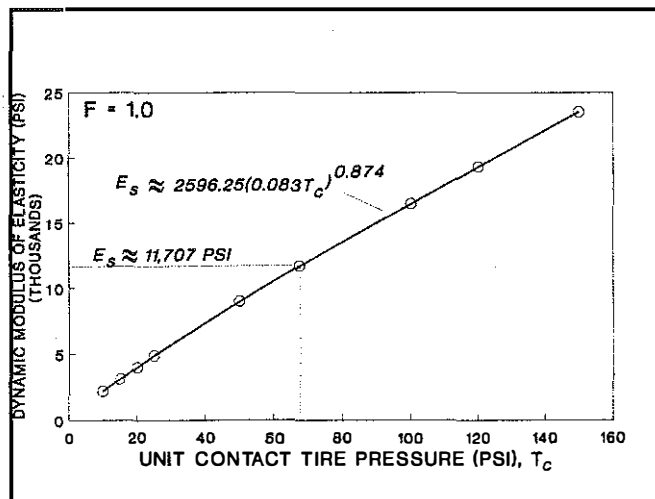


Figure 75. Relationship Between Dynamic Modulus of Elasticity and Contact Tire Stress Obtained from the HOPKIB Model at a Factor of Safety Equal to 1.0.

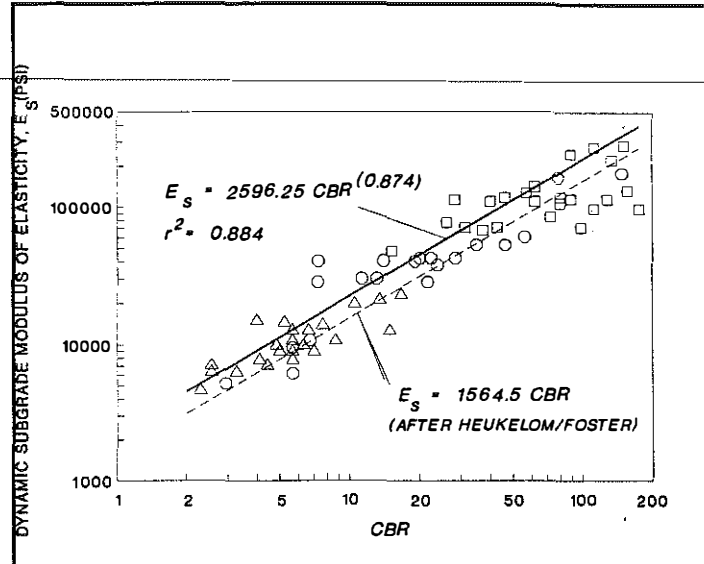


Figure 74. Variation of the Dynamic Modulus of Elasticity and Contact Tire Stress Obtained from the HOPKIB Model at a Factor of Safety Equal to 1.5.

By inserting the equation shown in Figure 68 into Equation 219, or

$$E_s \approx 2596.25(0.083T_c)^{(0.874)}, \quad (220)$$

an expression relating the dynamic modulus of elasticity and tire pressure may be obtained which corresponds to a factor of safety of 1.0. For a tire contact pressure of 67.5 psi, the dynamic modulus of elasticity is 11,707 psi. The minimum value of modulus, required to prevent failure of the subgrade, which corresponds to a factor of safety of 1.0 and a contact stress of 67.5 psi, is 11,707 psi. If Equation 218 given by Heukelom or Foster and

Heukelom and Klomp is used, then dynamic moduli values of elasticity of 8,761 and 8,400 psi, respectively, are obtained. For a factor of safety of 1.5, an expression for the dynamic modulus of elasticity may be obtained by inserting the expression shown in Figure 69 into Equation 219. For a contact tire stress of 67.5 psi, the modulus is 16,679 psi. To maintain stability and to avoid excessive sinkage, the dynamic modulus of elasticity of the subgrade must be approximately 11,707 to 16,679 (or greater) psi when the anticipated maximum tire stresses are 67.5 psi. The relationships between dynamic modulus of elasticity and contact tire stresses corresponding to factors of safety of 1.0 and 1.5, respectively, are shown in Figures 75 and 76. For any selected value of safety factor and anticipated tire contact stress, the dynamic modulus of elasticity may be computed from the following expression:

$$E_s \approx 2596.25(0.084FT_c)^{0.874} \quad (221)$$

Dynamic Cone Penetrometer Strengths

Several devices are available for use during construction to characterize the bearing strength of subgrades. The dynamic cone penetrometer (Thompson 1988) device is a rapid and economical hand-operated, portable apparatus for evaluating the strength of subgrades. A correlation between CBR and dynamic cone penetration values has been described by Thompson (1988). This relationship is shown in Figure 77. The relationship may be expressed as follows:

$$CBR = 10^{(2.20 - 0.71(\log DCP)^{1.5})} \quad (222)$$

where DCP is the dynamic cone penetration value in mm per blow. Inserting the equation given in Figure 68 into Equation 220, a relationship between DCP values and tire contact stress may be established for a factor of safety equal to one, or

$$10^{(2.20 - 0.71(\log DCP)^{1.5})} = 0.083T_c \quad (223)$$

and solving for DCP,

$$DCP \approx 10^{[3.099 - 1.408(0.083T_c)]^{2/3}} \text{ (mm/Blow).} \quad (224)$$

Values of DCP as a function of contact tire stress ($F=1.0$) are shown in Figure 78. At a contact stress of

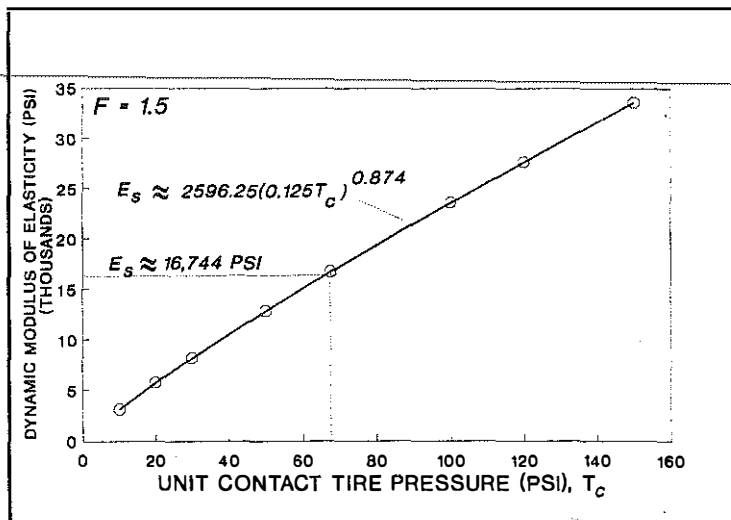


Figure 76. Relationship Between the Dynamic Modulus of Elasticity and Contact Tire Stress Obtained from the HOPKIB Model at a Factor of Safety Equal to 1.5.

67.5 psi, the maximum DCP value is about 41. If the DCP value is greater than about 41, failure of the subgrade would occur under a contact tire stress of 67.5 psi. To insure that failure does not occur under the tire stress of 67.5 psi, the DCP value must be lower. Variation of the DCP value as a function of contact tire stress for a factor of safety of 1.5 is shown in Figure 79. To insure a factor of safety of 1.5 for a contact stress of 67.5 psi, the value of DCP must be 29, or lower.

Although the dynamic cone penetrometer may be used to characterize the strength of the subgrade during construction and show that the first construction lifts of pavement may be placed without failure, problems may develop much later after construction when clayey subgrades become wet. When this occurs, the clays may swell and lose strength. The subgrade may be shown to have sufficient strength during construction due to dry weather but may lose this strength after soaking. The pavement design should consider the potential loss of subgrade strength after construction.

Two-Layered Problems

Typical Construction Situations and Analytical Approaches

Application of classical bearing capacity theory to problems involving nonhomogeneous soil conditions has been limited. A common type of soil nonhomogeneity that is often encountered consists of two distinctive soil layers of different strengths and about constant thicknesses. Solutions to this problem have been proposed by Button (1953) and Vesic' (cf. Winterhorn and Fang). The problem may be characterized, as noted by Vesic', in two ways:

- the bearing stratum is softer than the underlying stratum, or
- the bearing stratum is stiffer than the underlying stratum.

Button's (1953) analyses of these two situations apply only to situations where the clays are saturated, and undrained conditions prevail ($\phi = 0$). According to Brown and Meyerhof (1969), the assumed failure

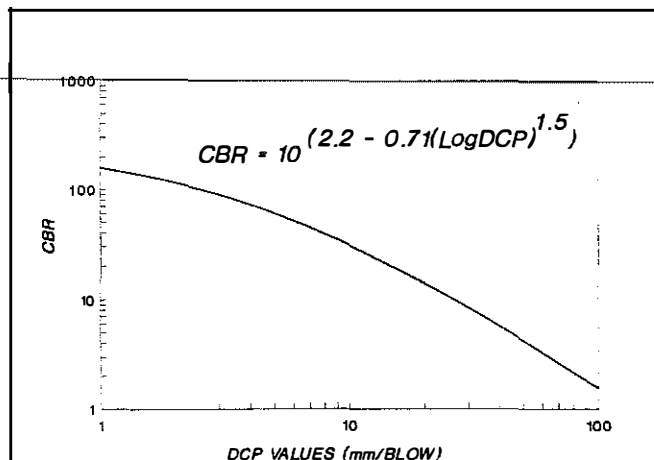


Figure 77. CBR as a Function of Dynamic Cone Penetrometer Values (DCP--After Thompson 1988 and Techion-Israel).

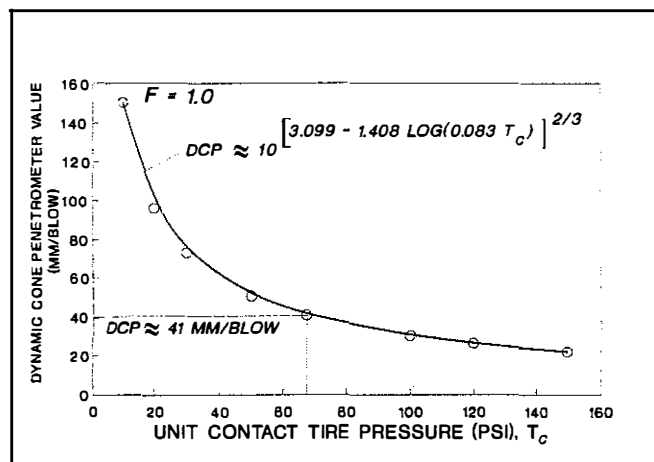


Figure 78. Relationship Between Dynamic Cone Penetrometer (DCP) Value and Contact Tire Stress, T_c , Established from the HOPKIB Model for a Factor of Safety of 1.0.

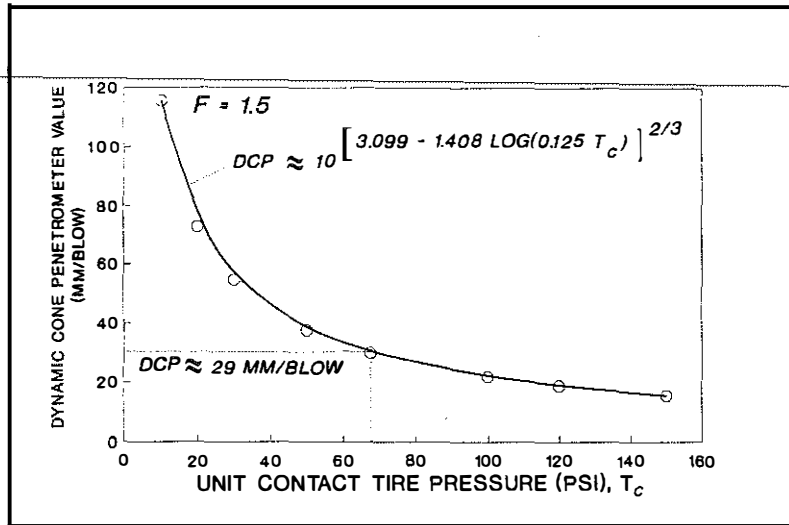


Figure 79. Relationship Between Dynamic Cone Penetrometer (DCP) Value and Contact Stress, T_c , Established from the HOPKIB Model for a Factor of Safety of 1.5.

modes in Button's analyses were not realistic and the bearing capacity factors obtained by Button were on the unsafe side. In Button's analyses, the shear surface was assumed to be circular.

Vesic' (cf. Winterhorn and Fang, 1975) proposed a general analysis of the two-layered problem where the upper layer is stiffer than the lower layer. In this analysis, Vesic' assumed that the slip surfaces are vertical. For the second situation, Vesic' proposed the following expression for the ultimate bearing capacity:

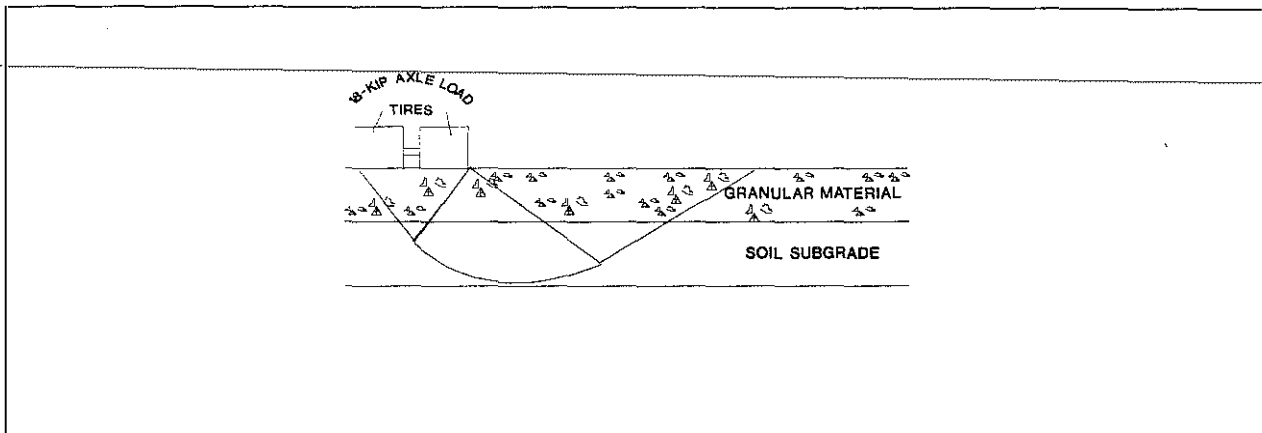
$$q_u = \left[q_o + \frac{c_1 \cot \phi_1}{K} \right] e^{\left[2 \left(1 + \frac{B}{L} \right) K \tan \phi_1 \frac{H}{B} \right]} - \frac{c_1 \cot \phi_1}{K}, \quad (225)$$

where

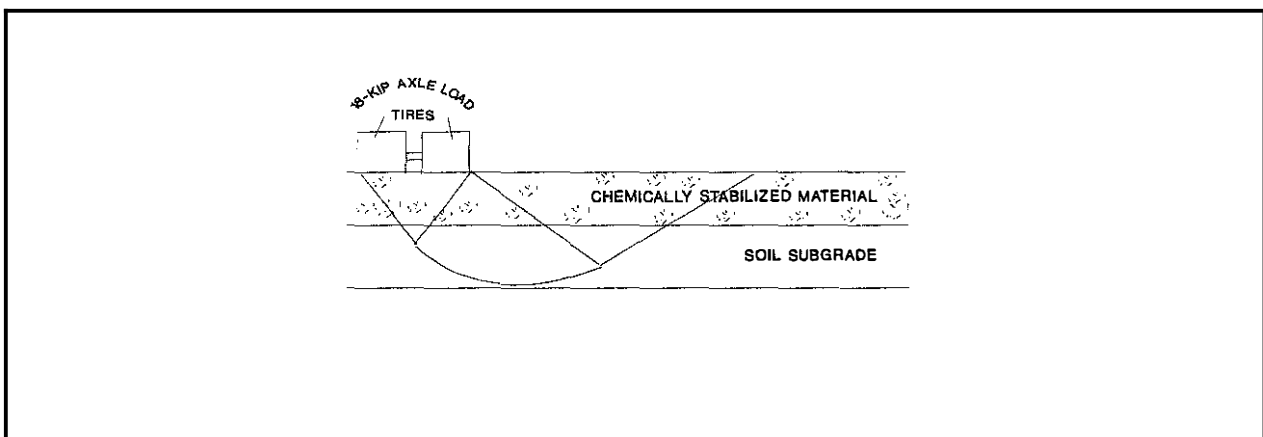
- q_o = the bearing capacity of a fictitious footing of the same size and shape as the actual footing, but the footing is assumed to be resting on the second layer -- the value is determined by using c_2 , ϕ_2 , and geometrical characteristics of layer 2,
- H = the distance between the bottom of the footing and the top of layer two,
- B = width of footing, and

$$K = \frac{1 - \sin^2 \phi_1}{1 + \sin^2 \phi_1}. \quad (226)$$

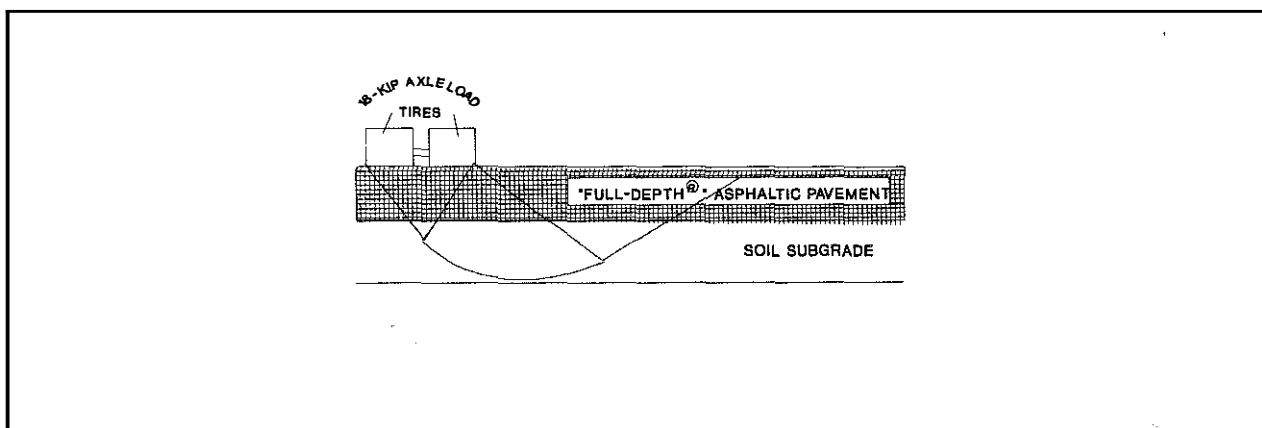
In the construction of pavements, the two-layered bearing capacity problem occurs typically in different forms. At least three scenarios may be envisioned. One two-layered situation occurs when a granular base is placed on a soil subgrade. Another two-layered situation occurs when the top portion of the subgrade is treated with chemical admixtures. A third two-layered situation may occur when "full-depth[®]" asphalt concrete is placed directly on the subgrade. The three situations are illustrated in Figure 80. In each situation, the top layer is usually stiffer than the underlying layer; the thickness of the top layer is essentially constant in the cross section. Each of these scenarios may be analyzed by the HOPKIB bearing capacity model and program. In certain situations, Vesic's solutions to these problems may be compared to solutions obtained from the HOPKIB model. These scenarios are described and analyzed below.



a) Granular Layer Resting on a Subgrade



b) Chemically Treated Layer Resting on a Subgrade.



c) "Full-Depth®" Asphalt Bearing Directly on the Subgrade.

Figure 80. Three Pavement Situations Involving Two Layers of Different Materials.

Construction of Granular Bases

The situation depicted in Figure 80a involves the placement of granular base material on the subgrade. Normally, the granular material (either bounded or unbounded) is constructed in lifts of selected thicknesses -- for example, the granular material may be placed in four-inch lifts. Placement of the granular base -- especially the initial lifts -- is a particularly critical phase during construction when the subgrade consists of clayey soils. The two-layered system may be very susceptible to shoving and pushing of the clayey subgrade when loaded with construction equipment, such as stone-laden vehicles, concrete trucks, or compaction equipment. Shoving and pushing of the subgrade, or the formation of deep ruts in the granular material, suggest that shear surfaces are being formed in the subgrade. Although construction oftentimes proceeds when deep rutting occurs by simply backfilling the ruts with material of a subsequent lift, a situation is created which may affect the future performance of the pavement after construction.

Two problems arise when bearing capacity shear failures are formed in the subgrade by construction traffic. First, if bearing capacity shear surfaces occur during construction -- as evidenced by deep rutting of the granular base -- then failure zones are built into the pavement subgrade. When a shear failure occurs in the subgrade due to construction traffic, the strength along the failure plane is reduced from some peak shear strength to a residual shear strength (Skempton 1964). When clayey subgrades are involved, the residual shear strength may be substantially lower than the original, peak shear strength

of the clayey subgrade that existed before failure. The built-in failure zones offer much less resistance to traffic loadings after the pavement is constructed. The situation is created where the subgrade contains weakened subgrade areas and may cause future cracking of the pavement. Secondly, pushing and shoving -- bearing capacity failures -- of the subgrade may create zones in the pavement that are thinner than the original design thickness, as illustrated in Figure 81. The thinner design thicknesses may lead to future cracking of the pavement because of insufficient pavement thickness. Performance of the subgrade during and after construction is vital to the future performance

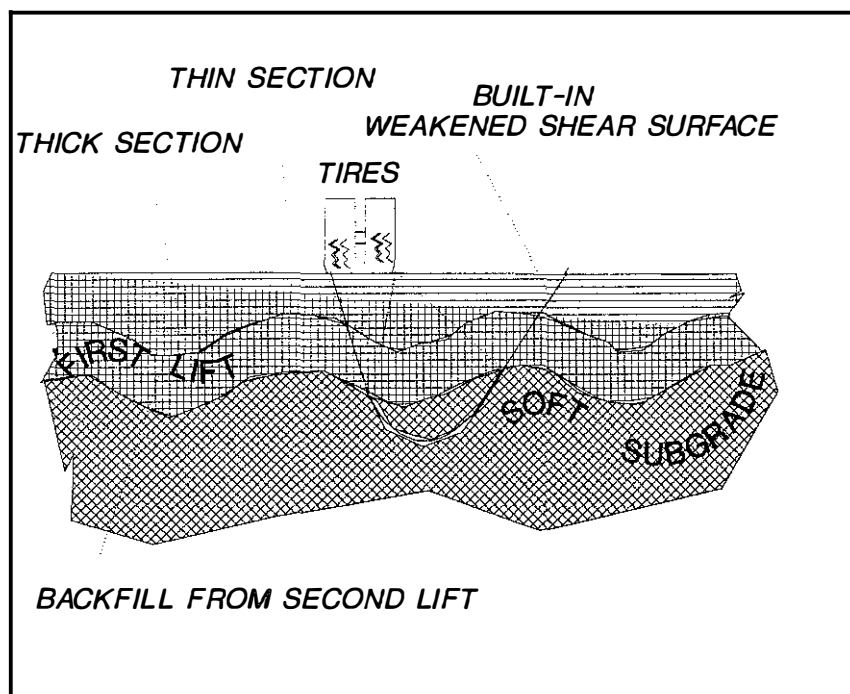


Figure 81. Problems That May Occur During the Construction of Pavements on Weak, Soft Subgrades.

of the pavement. Design of the subgrade during construction should receive strong consideration.

To obtain an approximate relationship between the thickness of granular base material required to

withstand failure and the undrained shear strength of the subgrade, a typical situation was analyzed using the HOPKIB bearing capacity computer program. In these analyses, the granular base material was

assumed to be unbound, that is, the cohesive component, c , of the granular material was assumed to be zero. The ϕ value of the stone was assumed to be 43° . A dual-wheel loading arrangement, a contact stress of 67.5 psi, and factors of safety of 1.0 and 1.5 were assumed in the analyses. Results obtained from the HOPKIB model are shown on the previous page in Figure 82. The upper curve in the figure represents a safety factor of 1.5. For an undrained shear strength of the subgrade equal to 313 psf, or a CBR value of one, the required thickness of the granular base must be some 40 to 61 inches (or greater) to avoid failure. At a CBR of three, the required thickness ranges from 17 to 31 inches. Variation of the thicknesses of the granular material with CBR is shown in Figure 83. This variation is based on the relationship given by Equation 211.

To determine the reasonableness of the results obtained from the HOPKIB, as shown in Figure 82, the problem was analyzed using Vesic's semi-empirical model, as expressed by Equation 225. In performing these analyses, the loading scheme shown in Figure 80, cannot be used in Vesic's analysis -- the spacing between tires cannot conveniently be considered.

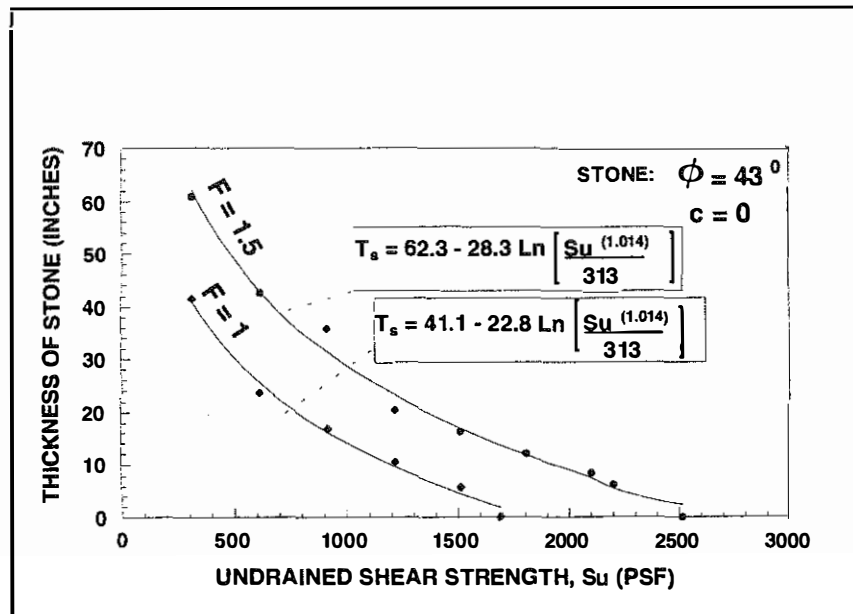


Figure 82. Variation of the Thickness of a Granular Layer With Undrained Shear Strength of a Clayey Subgrade for Factors of Safety Equal to 1.0 and 1.5.

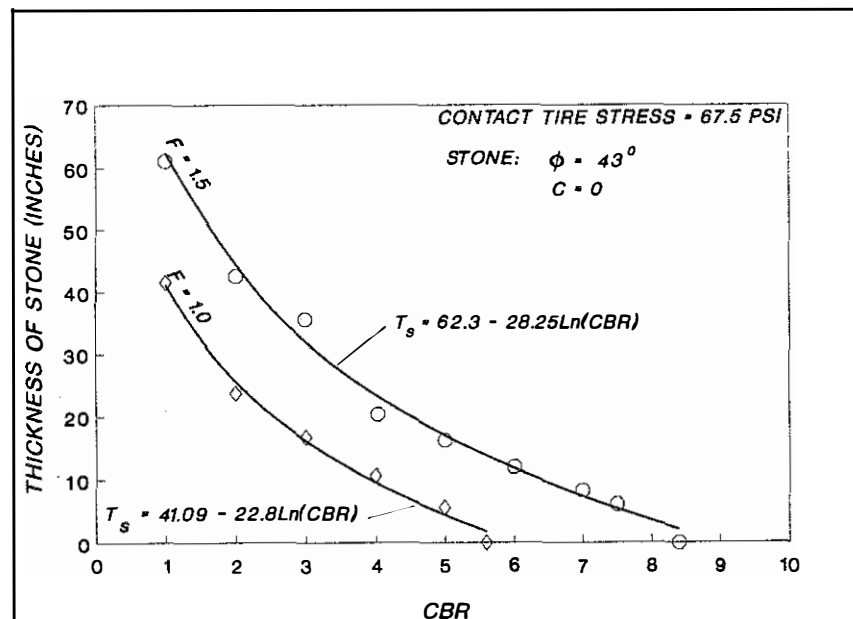


Figure 83. Relationship Between Thickness of Granular Base and CBR for Factors of Safety Equal to 1.0 and 1.5.

The loading scheme shown in the right portion of Figure 84 was used in Vesic's analyses; the HOPKIB

analyses were performed using the same loading scheme so that a direct comparison could be made. Based on using the same loading scheme in both analysis and assuming a factor of safety of 1.5, the relationships between thickness of granular material required to withstand failure and the undrained shear strength (and CBR) were calculated. The results are compared in Figure 84. When c_1 equals zero for layer one (granular base) in the Vesic's analysis, Equation 225 is reduced to:

$$q_u = q_0 e^{[2(1 + \frac{B}{L})K \tan \phi_1 (\frac{H}{B})]} \quad (227)$$

For an infinite strip loading,

$$\frac{B}{L} \rightarrow 0, \quad (228)$$

and

$$q_u = q_0 e^{(\frac{2H}{B} K \tan \phi_1)} \quad (229)$$

For a given value of H , the ultimate bearing stress may be computed from Equation 229. By definition:

$$F = \frac{q_u}{q_a} \quad (230)$$

and, in this case,

$$q_a = 67.5 \text{ psi}, \quad (231)$$

then it follows that

$$F = \frac{q_u}{67.5} = q_0 e^{(\frac{2H}{B} K \tan \phi_1)} \quad (232)$$

Equation 232 may readily be solved by trial and error using a spreadsheet type of computer program. A value of H is selected and the factor of safety is computed. If the factor of safety is not equal to 1.5 (the target value), a new value of H is selected. The iteration is continued until the factor of safety is equal to 1.5. For CBR values ranging from one to 6, as shown in Figure 84, the percentage differences in values of granular thicknesses obtained from Vesic's equation and the HOPKIB analyses (Curve A) range from about seven to 33. For CBR values greater than six, the thicknesses obtained from the

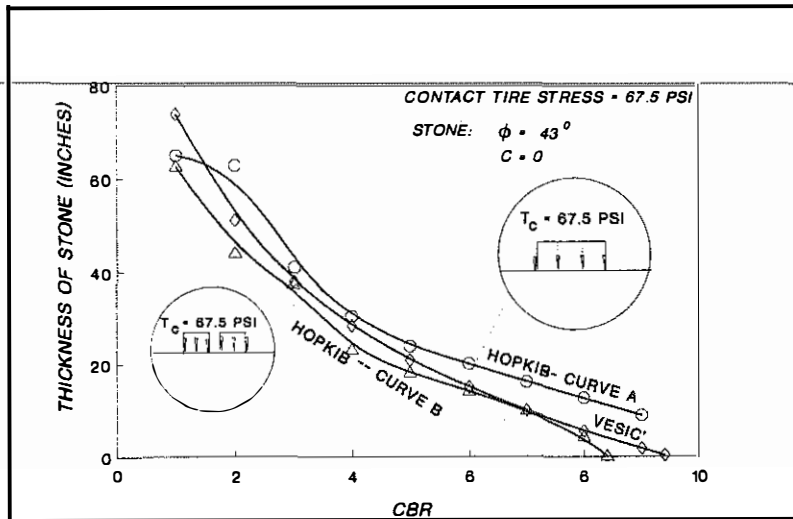


Figure 84. Comparisons of Thicknesses Obtained from Vesic's Method and the HOPKIB for a Factor of Safety of 1.5.

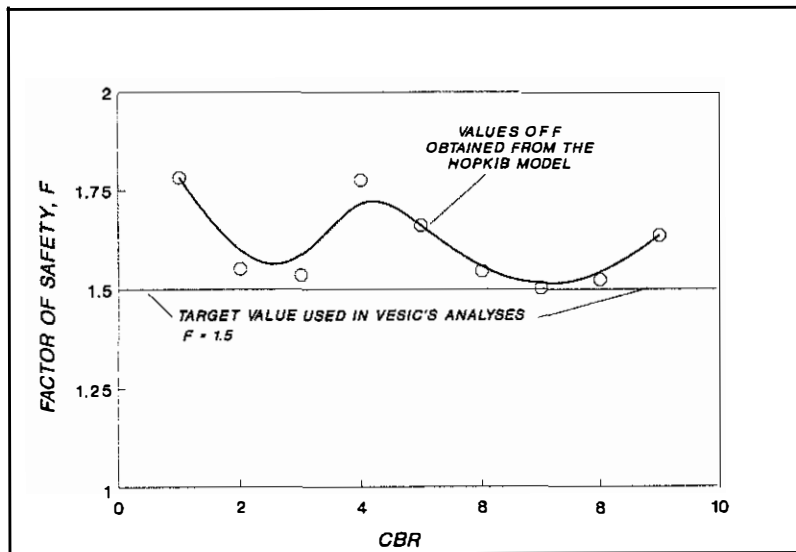


Figure 85. Comparison of Factors of Safety Obtained from the HOPKIB Model and Vesic's Approach for a Range of Values of CBR.

HOPKIB analyses are larger than those obtained from the Vesic' analysis. In both cases, the required thicknesses to withstand failure are relatively small when the CBR value is equal to or greater than about six. When the CBR value is below six, both the HOPKIB analyses and Vesic's analyses show that required thicknesses of the granular base must be relatively large to withstand large deformations, or failure. For example, at a CBR-value of three, the required thickness is about 35 to 40 inches. Viewing the Vesic's analysis in another manner, thicknesses obtained from Equation 232 (using a factor of safety of 1.5 and CBR values ranging from one to 9) were inserted into the HOPKIB computer program. Factors of safety obtained from the HOPKIB model ranged from 1.5 to 1.78 and averaged 1.61 as shown in Figure 85. The factors of safety from the HOPKIB model were generally only slightly larger than the target value of 1.50 used in the Vesic' analysis.

When the loading scheme shown in the left portion of Figure 84 is used in the HOPKIB model, the thicknesses required for a factor of safety of 1.5 are smaller than those obtained from the loading scheme shown in the right portion of Figure 84. These thicknesses were slightly

less than those obtained from Vesic's equation. Thicknesses obtained from this loading scheme (Curve b) are shown in Figure 84 and compared to those obtained from Vesic's equation. Percentage differences between the thicknesses obtained from the HOPKIB model (Curve B) and Vesic's equation for CBR values ranging from one to seven was about zero to 22. The thickness-CBR curve obtained from Vesic's equation lies between Curves A and B obtained from the HOPKIB analysis using the two different loading schemes. Considering that the theoretical basis of the Vesic' model equation (punching shear failure) and the HOPKIB model (general shear failure) are different, the thicknesses obtained from the two models are similar.

Subgrades Treated with Chemical Admixtures

Chemical admixtures, such as hydrated lime and cement, are used to improve the shear (or bearing) strength of weak subgrade soils. Normally, the chemical admixtures are added to the scarified subgrade soils, mixed in place, and compacted. When soil subgrades are improved in this manner, a two-layered system is formed and consist of a stiff top layer of treated material overlying a softer clayey layer of the originally-constructed subgrade of untreated soils as shown in Figure 80. Since loading of the subgrade by construction traffic is usually rapid and the two layers generally consist of clayey-type soils (permeabilities of the two clayey layers are usually low), total stress analysis may be used. In this simple approach, the ϕ values of the two layers are assumed to be zero. The shear strengths of the two layers are defined by c_1 (upper layer) and c_2 (lower layer). The problem becomes one of determining the required thickness of the treated subgrade layer to withstand failure for a given design factor of safety and for a given tire contact stress. The problem may be analyzed using approaches proposed by Vesic', 1970 (and modifications by Brown and Myerhoff, 1969) and by Thompson (1988). The problem may also be analyzed using the HOPKIB bearing capacity computer program. These approaches are described as follows.

Vesic's Method

For the case where a bearing clayey stratum is stiffer than the underlying clayey soil, Vesic' (1975, cf. Winterhorn and Fang) proposed that the bearing capacity may be represented as:

$$q_u = c_1 N_m + q \quad (233)$$

where

- c_1 = the undrained strength of the upper layer (in this case, the treated layer),
- N_m = a modified bearing capacity factor that depends on the ratio of the shear strengths of the two layers, $K = c_2/c_1$, the relative thickness of the upper two layers, H/B , and the shape of the foundation, and
- q = overburden stress (this value is assumed to be zero for the highway case).

For a stiff layer of clayey material resting on a layer of softer clayey material, Brown and Meyerhof (1969) proposed the following expression for evaluating the modified bearing capacity factor, or

$$N_m = \frac{1}{\beta} + K S_c N_c (\leq S_c N_c), \quad (234)$$

where β (Vesic' 1970) is defined as the punching index of the footing. In developing this expression, Brown and Meyerhof assumed simple shear punching around the footing perimeter. For long rectangular footings, Vesic' (cf. Winterhorn 1975) defines the punching index as:

$$\beta = \frac{B}{2H}, \quad (235)$$

and

$$N_c = 5.14. \quad (236)$$

Therefore, Equation 234 becomes ($S_c = 1$):

$$N_m = \frac{1}{\beta} + 5.14K, \quad (237)$$

and

$$N_m = \frac{2H}{B} + 5.14K. \quad (238)$$

Equations 233 and 238 may be used to approximate the ultimate bearing capacity of the two-layered system shown in Figure 80 c if it is assumed that the moving dual-wheel loading of the stiff upper layer acts, in effect, as a long rectangular footing.

To illustrate the use of Equations 233 and 238, the following example may be solved. Let

- H = 12 inches = distance measured from the top of layer 1 (or the contact point of the tires and top of layer 1) to the bottom of layer 1,
 B = 24.5 inches = two tires, 11 inches in width,

Equations 233 and 238 may be re-arranged so that the thickness of layer 1 (in this case, the chemically treated layer), H, may be solved for directly, or

$$N_m = \frac{2H}{B} + 5.14K, \text{ and} \quad (239)$$

$$q_u = c_1 N_m = c_1 \left(\frac{2H}{B} + 5.14K \right). \quad (240)$$

Solving for H,

$$H = (0.5)B \left(\frac{q_u}{c_1} - 5.14K \right) \quad (241)$$

since, by definition,

$$F = \frac{q_u}{q_a}, \quad (242)$$

then $q_u = Fq_a$, and

$$H = (0.5)B \left(\frac{q_a F}{c_1} - 5.14K \right) \quad (243)$$

The thickness of the modified layer (number 1) may be determined directly if values of the anticipated tire stress (q_a), the width of the dual tires (B), the strengths of layers 1 and 2 (c_1 and c_2), and the design factor of safety is known, or assumed. For example, assume the following values are known:

$B = 24.5$ inches

$q_a = 67.5$ psi

$c_1 =$ cohesion or undrained shear strength of layer 1 = 50 psi

$c_2 =$ cohesion or undrained shear strength of layer 2 = 6.37 psi

$K = c_2/c_1 = \frac{6.37 \text{ psi}}{50 \text{ psi}} = 0.1274$

$F = 1.0 =$ assumed factor of safety.

Inserting these values into Equation 243, then

$$H = (0.5)(24.5) \left(\frac{(67.5 \text{ lb/in.}^2)(1.0)}{50 \text{ lb/in.}^2} - (0.1274)(5.14) \right) \quad (244)$$

$$H = 12.25(1.35 - 0.655) \quad (245)$$

and

$$H = (12.25)(0.695) \quad (246)$$

$$H = 8.5 \text{ in.} \quad (247)$$

The performance of the two-layered system would be very marginal based on a factor of safety of 1.0 -- that is, serious rutting would probably occur. To increase stability, assume a factor of safety against failure of 1.5. Inserting this value into Equation 243:

$$H = (0.5)(24.5) \left(\frac{(67.5)(1.5)}{50} - (0.1274)(5.14) \right) \quad (248)$$

$$H = (12.25)((2.025) - (0.1274)(5.14)) \quad (249)$$

$$H = (12.25)(1.37) \quad (250)$$

and

$$H = 16.7 \text{ in.} \quad (251)$$

The factor of safety of 1.50 would be sufficient to prevent subgrade rutting based on tire sinkage data given by Thompson (1988) and the analysis previously described -- that is, a factor of safety of about 1.5 is needed to minimize rutting, or tire sinkage.

Thompson's Approach (1988)

In an effort to develop a guideline for approximating the thickness of a chemically treated subgrade, Thompson analyzed the two-layered problem, as shown in Figure 80b, using elastic-layered methods. Thompson assumed that the CBR value of the treated layer was 10-12

percent; the subgrade strength was varied in the analysis. Five hundred coverages and 32 kip tandem dual-wheel loading were assumed. Based on these assumptions, the relationship obtained by Thompson between thickness of subgrade to withstand the assumed loading and CBR value is shown in Figure 86. This relationship may be approximated by the expression (based on a regression analysis of his data):

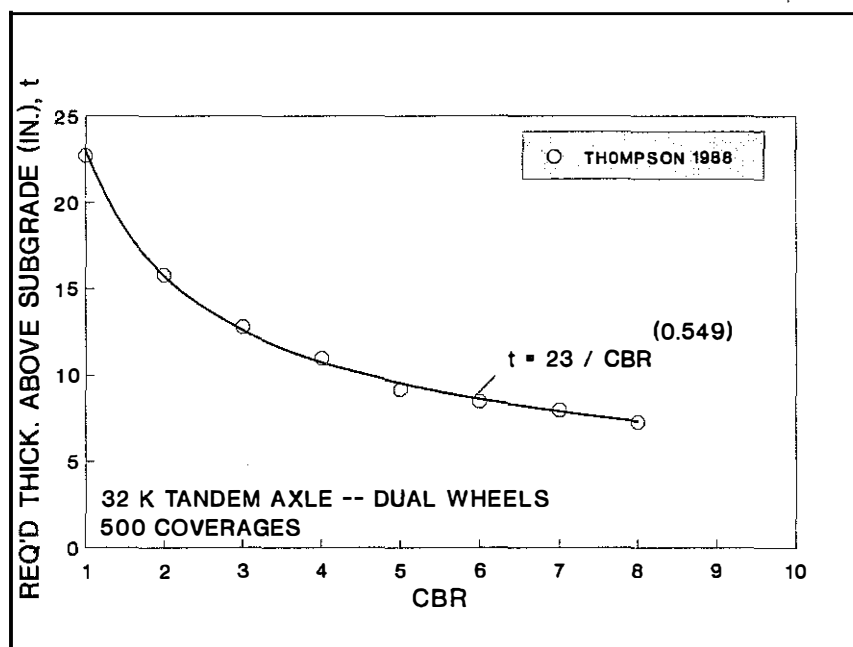


Figure 86. Required Thickness of Chemically Treated Subgrade and Granular Layer as a Function of Subgrade CBR (data from Thompson 1988).

$$t = \frac{23}{CBR^{(0.549)}} \quad (252)$$

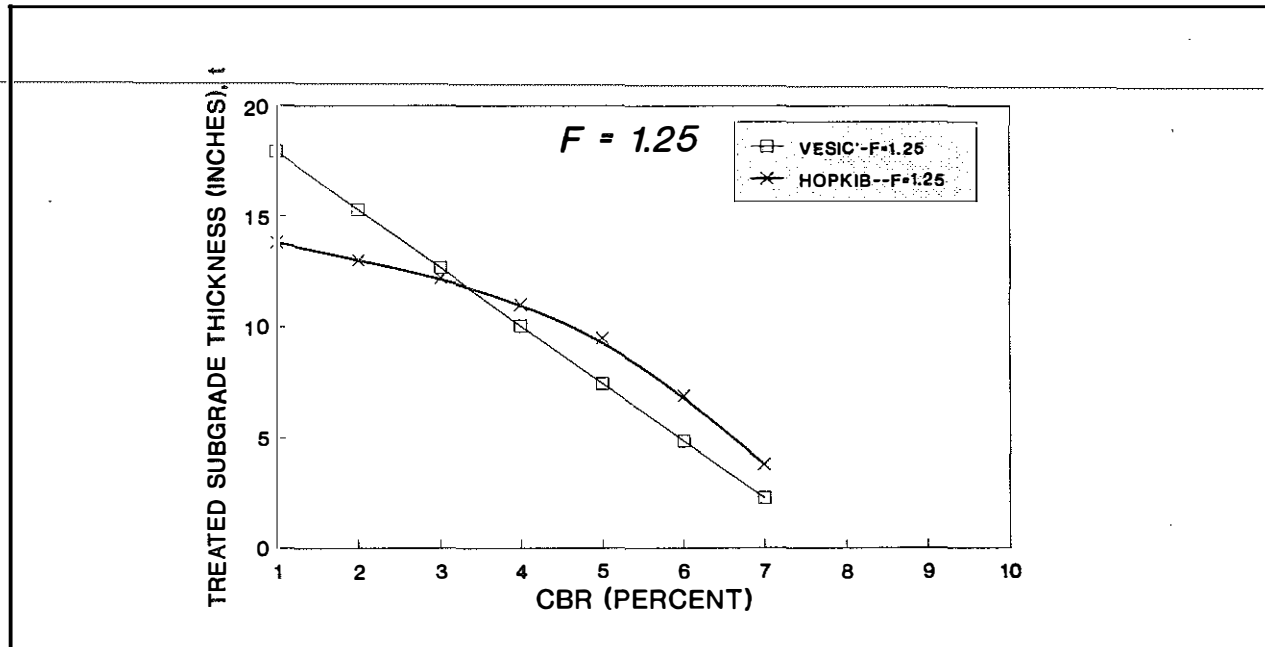
Assuming factors of safety of 1.25 and 1.50, respectively, the maximum, anticipated tire contact stresses of 68 psi, and width of the dual wheels of 24.5 inches, thickness as a function of CBR may be computed from Equation 243. Curves representing factors of safety of 1.25 and 1.50 obtained from Vesic's equation are compared to Thompson's relationship in Figure 87a and 87b, respectively. Results obtained from the HOPKIB program ($F = 1.5$ and 1.25) are also shown in Figure 87a and 87b. Ratios of thicknesses obtained from the HOPKIB model to thicknesses obtained from Vesic's (and Brown and Meyerhof, 1969) Equation 243 ranged from 77 to 139 percent for CBR values ranging from one to six. Ratios of thicknesses obtained from Equation 252 (Thompson) to thicknesses obtained from Equation 243 (Vesic) ranged from 75 to 104 percent. These comparisons show that similar thicknesses are obtained from the three different approaches.

It should be emphasized that in Vesic's approach, punching, or vertical shear failure around the perimeter of the loaded area is assumed while in the HOPKIB analysis, the entry and exit angles of 45 degrees are assumed in the analysis since ϕ is equal to zero in both layers of material. In the later case, the theoretical failure pattern in the HOPKIB analysis occurs at a shallower depth than the pattern assumed in Vesic's approach. The approach used by Thompson (1988) was based on elastic analysis. Data (Hopkins and Hunsucker 1991) collected on chemically treated subgrades indicate that the strength may be much higher than the values used in these analyses. Thicknesses obtained from any of the methods would be smaller and discrepancies among the methods would decrease. Regardless of these differences, any of the approaches may be used, provided adequate factors of safety are assumed in the analyses.

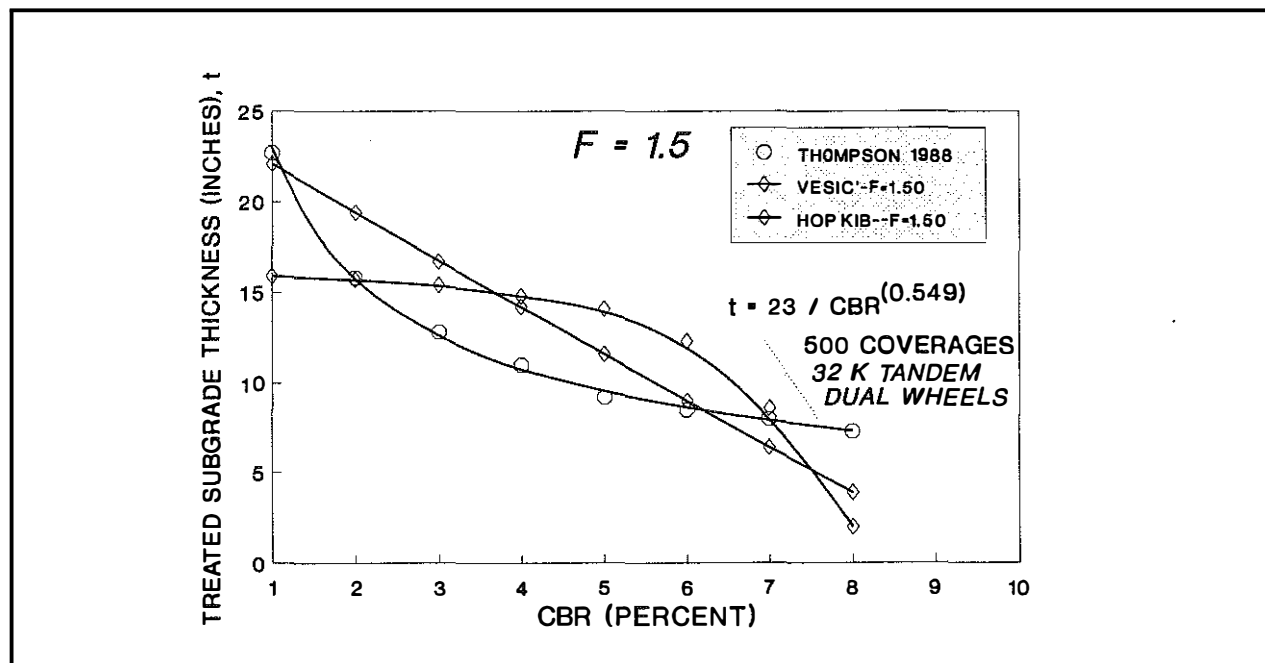
"Full-Depth®" Asphaltic Pavements

Construction of "full-depth®" asphaltic pavements essentially creates a two-layered problem, as visualized in Figure 80c. Use of this technique on soft, weak subgrades can lead to potential construction problems and to problems after construction. Difficulties have been encountered in the past when attempts have been made to use this technique on soft, weak subgrades. This two-layered problem may be analyzed using the HOPKIB bearing capacity computer program. The most critical period during construction occurs when the first lift of asphaltic pavement is placed and compacted. If the subgrade soils are too weak, then cracking of the first lift and pushing and shoving of the subgrade may occur. Partially completed layers of the asphaltic pavement are particularly vulnerable to failure. (This critical construction occurs also when the first lift of stone is placed when the pavement structure contains a granular base.)

In the development of an approach to perform the analysis of this two-layered problem using the HOPKIB program, changes in shear strength occurring in the asphaltic pavement with depth must be considered. Since the shear strength of asphaltic materials vary with temperature and temperatures within the asphaltic materials vary with depth, the shear strength varies with pavement depth. To examine the variation of shear strength and temperature and to observe the general pattern of this variation, a series of unconsolidated-undrained triaxial compression tests was performed on asphaltic core specimens obtained from an asphaltic pavement site (KY 94). As a means of varying the temperature of the asphaltic specimens, coiled, copper tubing was fitted around each specimen in the triaxial chamber, as shown in Figure 88. The copper tubing was connected to a temperature-controlled, water bath. Water was circulated from the water bath through the copper coils and back to the water bath. The testing arrangement and equipment are shown in Figure 89.



a) Factor of Safety Equals 1.25



b) Factor of Safety Equals 1.50.

Figure 87. Comparisons of Treated Subgrade Thicknesses Obtained from the HOPKIB Model, Vesic's Approach, and Thompson's Method.

Before placement of the asphaltic specimen in the triaxial chamber, a testing temperature was selected. The temperature of the water bath was set, and the water in the copper coils was circulated for approximately two hours, or until the temperature in the triaxial chamber reached the desired temperature (the temperature of chamber water was checked with a thermometer). After the temperature of the chamber water reached the desired value, the asphaltic specimen was placed in the chamber and sufficient time -- about two hours -- was allowed to elapse before testing. The temperature of the asphaltic specimen was allowed sufficient time to equalize with the temperature of the water. The specimen was then tested.

A minimum of three specimens were tested at a selected temperature. Selected temperatures ranged from 77 to 140° Fahrenheit. Typical, unconsolidated-undrained triaxial test results obtained from asphaltic specimens performed at 100° F are shown in Figure 90. Variation of the total stress parameter, cohesion, or c , with temperature is shown in Figure 91. For this asphaltic material, this variation may be expressed as:

$$c = 679e^{(-0.03227T)} \quad (253)$$

Variation of the total stress parameter, ϕ , with temperature is shown in Figure 92 and may be expressed in the form:

$$\phi = 20.7 + \frac{6791.7}{T} - \frac{494486}{T^2} \quad (254)$$

Although data scatter occurs in the graphs shown in Figures 91 and 92, the trend of the variations of cohesion c and the internal angle of friction, ϕ , with temperature is evident. That is, as the temperature of the

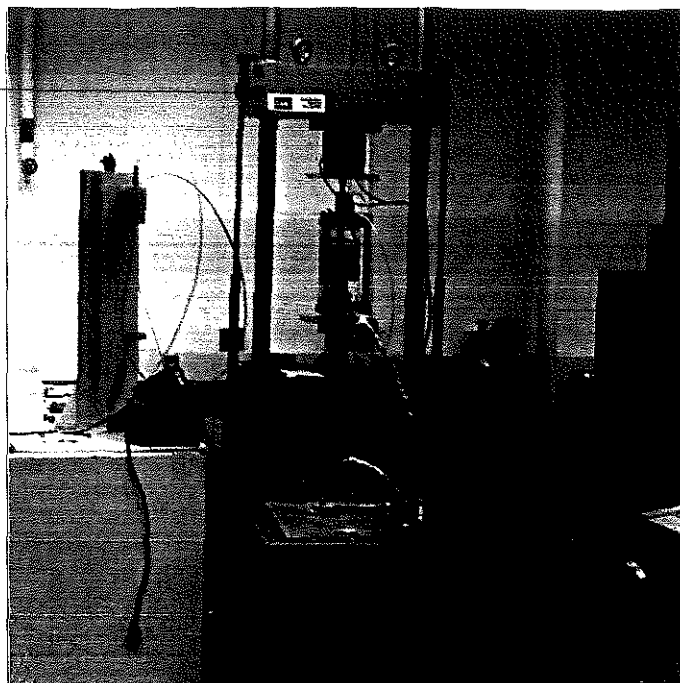


Figure 88. Arrangement of Triaxial Equipment Used to Test Asphalt Core Samples.

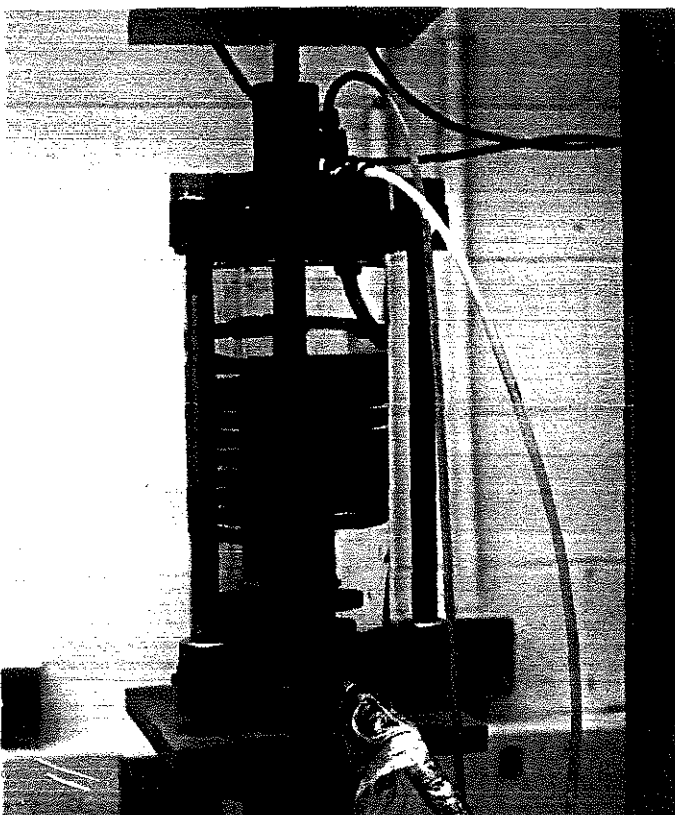


Figure 89. Close-Up View of Triaxial Chamber and Coiled Copper Tubing Used to Control Temperature of Asphalt Core.

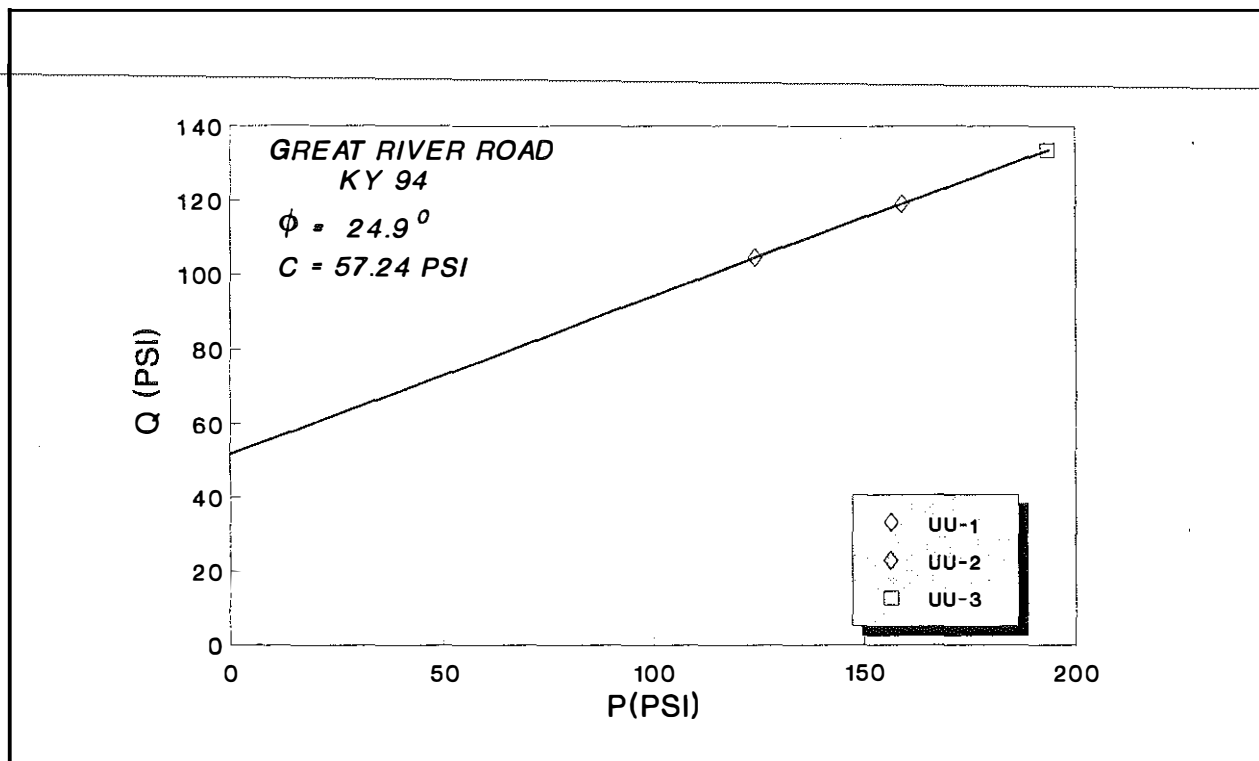


Figure 90. Typical Results Obtained from Unconsolidated-Undrained Triaxial Compression Tests of Asphalt Core Specimen.

asphaltic material increases, the cohesive component of strength decreases while the ϕ value increases. Hence, at relatively normal temperatures (for example, 77 ° F), the asphaltic pavement exists in a strength state where the c value (≈ 56 psi) is very high and the angle of internal friction is relatively low ($\approx 25.5^\circ$ F). At elevated temperatures (for example, 140 ° F) the cohesive component, c , is relatively low (≈ 7.40 psi) and the ϕ value is somewhat high ($\approx 44^\circ$ F).

The mechanism controlling the two strength component states at the two extreme temperatures is visualized in Figure 93. When the temperature is low, or near 77 ° F, failure or shearing, is mainly controlled by the asphalt because the asphalt at normal or average temperatures is very stiff and strong. The asphalt behaves more like a solid than a fluid. The contact along the shearing plane of the upper and lower parts of the specimen consists mainly of asphalt sliding against asphalt. Because of the large stiffness of the asphalt at relative low temperatures, the cohesive strength component is large. Shearing at low temperatures is mainly controlled by the asphaltic stiffness, which produces high cohesive strengths. The relatively low angles of internal friction are largely a result of asphalt shearing against asphalt at low temperatures. At large temperatures, the asphalt becomes more viscous and assumes properties that are more characteristic of a fluid than a solid. During loading, the individual granular particles have more freedom to reposition in the granular-asphalt matrix at elevated temperatures than at lower temperatures because the asphalt behaves more like a fluid than a solid. More particle-to-particle contacts develop at elevated temperatures than at lower temperatures and the shearing strength of the granular-asphaltic matrix is controlled more by frictional characteristics of the particle-to-particle contacts in the matrix than the asphalt. Angles of internal friction of the granular-asphaltic matrix at elevated temperatures tend to be higher than those at lower temperatures where the asphalt behaves more

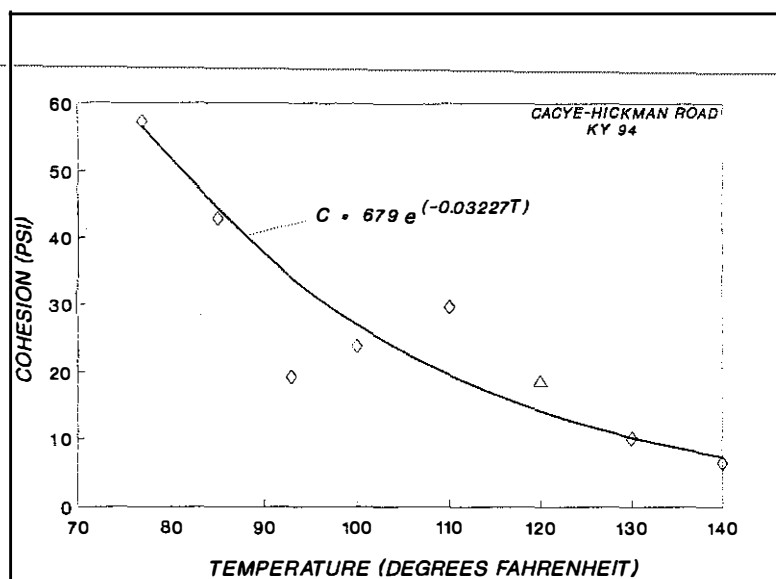


Figure 91. Cohesion of Asphalt Cores as a Function of Temperature.

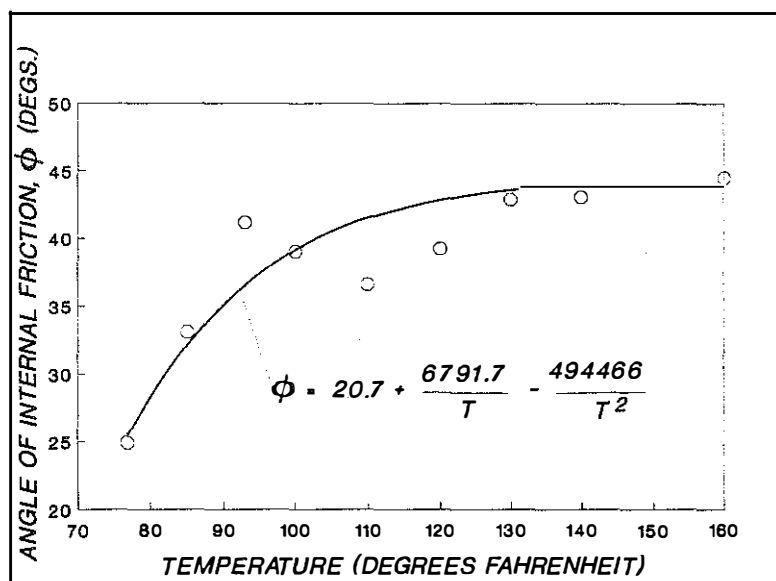


Figure 92. Angle of Internal Friction, ϕ , of Asphalt Cores as a Function of Temperature.

like a solid than a liquid. Since fluid-like materials cannot sustain large shearing stresses, the cohesive strength of the matrix will be lower at elevated temperatures than at lower temperatures.

During construction of asphaltic pavements, a critical stage of construction occurs when the first lift of asphaltic pavement is placed. In "full-depth" construction, the first lift is particularly vulnerable to failure under construction traffic. Factors that must be considered during this stage of construction to avoid failure include the thickness of the lift, the shear strength, or bearing strength, of the subgrade, anticipated maximum tire contact stresses, and the temperature of the asphalt. Temperature of the asphalt may be due to placement temperatures at the time of construction or/and to the time when the asphaltic pavement reaches equilibrium with the air temperature and subgrade temperature. To study the relationships among these factors, a typical construction scenario was analyzed using the HOPKIB bearing capacity computer program. Typically, lift thickness of asphaltic base courses is 2.5 inches. A tire contact stress of 80 psi and dual-wheels was assumed for construction traffic. For a given value of asphaltic temperature, the ϕ and c values were computed from Equations 253 and 254 (see Figures 91 and 92).

Variations of the factor of safety against failure and temperature of the asphaltic lift for a selected CBR value of subgrade are shown in Figure 94 (This scenario assumes that the first lift is loaded during the construction of the second base-course lift). When the CBR of the subgrade is equal to six, the factor of safety ranges from 1.33 at an asphaltic temperature of 77° Fahrenheit to 0.99 at a temperature of 140° F. As these data show, the placement of the lift could be completed successfully provided the asphaltic temperature did not exceed a value of about 120°. However, some rutting may occur at any temperature

when the subgrade CBR value is equal to or less than six since the factors of safety are below 1.5.

When the subgrade CBR value is below six, the factors of safety are smaller than 1.0. As shown in Figure 94, the CBR of the subgrade should be at least equal to a value of 9.3 or greater to obtain a factor of safety of about 1.5 or greater for temperatures ranging from 77 ° (or lower) to 140 ° F. This is more evident in Figure 95 where the variation of factor of safety with CBR value is shown for assumed asphaltic pavement temperatures of 77 ° and 140 ° F. Preferably, however, the CBR of the subgrade should be nine or greater, to insure that the factor of safety is equal to about 1.5 or greater. These analyses strongly indicate that "full-depth®" asphaltic pavement should not be considered unless the CBR of the subgrade is about 9 or greater. Alternately, the clay subgrade should be treated with a chemical admixture to increase the value of CBR to 12 or greater. These analyses emphasize the need to analyze placement temperatures and CBR values of the subgrade at the time of construction of the first lift of "full-depth®" asphalt pavements to insure safe construction.

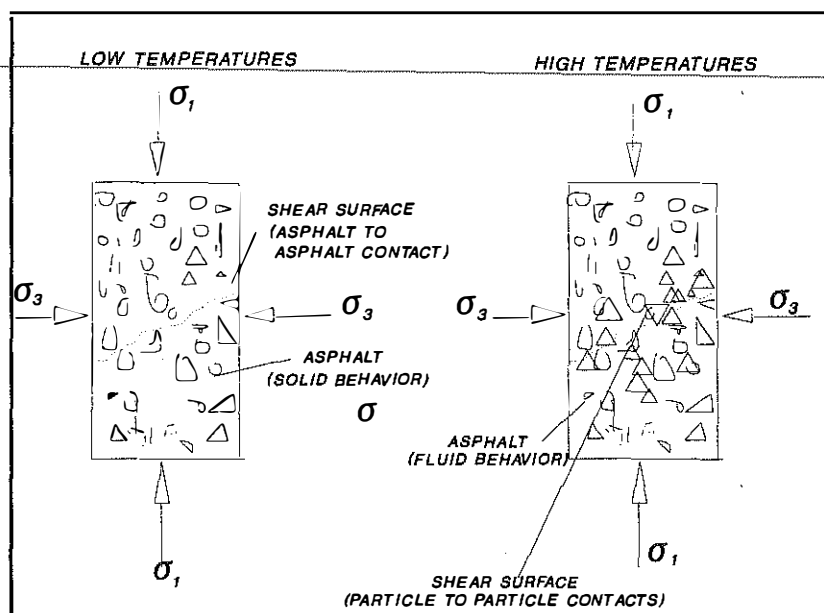


Figure 93. Mechanical Behavior of Asphaltic-Granular Matrix at Low and High Temperatures.

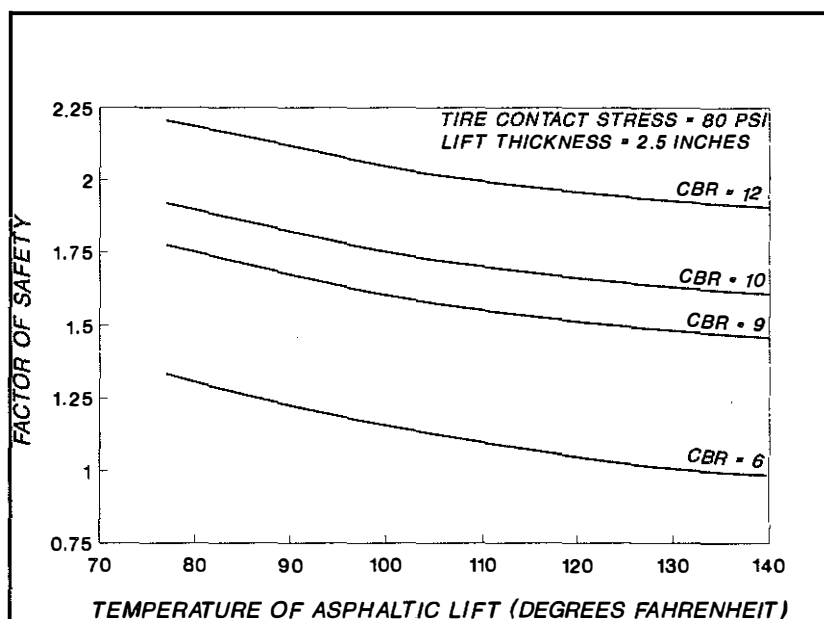


Figure 94. Factor of Safety Obtained from the HOPKIB Model as a Function of the Temperature of an Asphalt Lift for Different CBR Values of the Subgrade.

Stable construction of "full-depth®" asphalt pavements without excessive deformations or bearing capacity failures depends on the condition of the subgrade at the time of construction. A common assumption among many engineers is that if fine-grained soils (clays and silts) are compacted to 95 percent of standard maximum dry density (AASHTO T 99 or ASTM D 698) and a value (± 2 percent) near optimum moisture content, then pavement problems during or after construction will not develop.

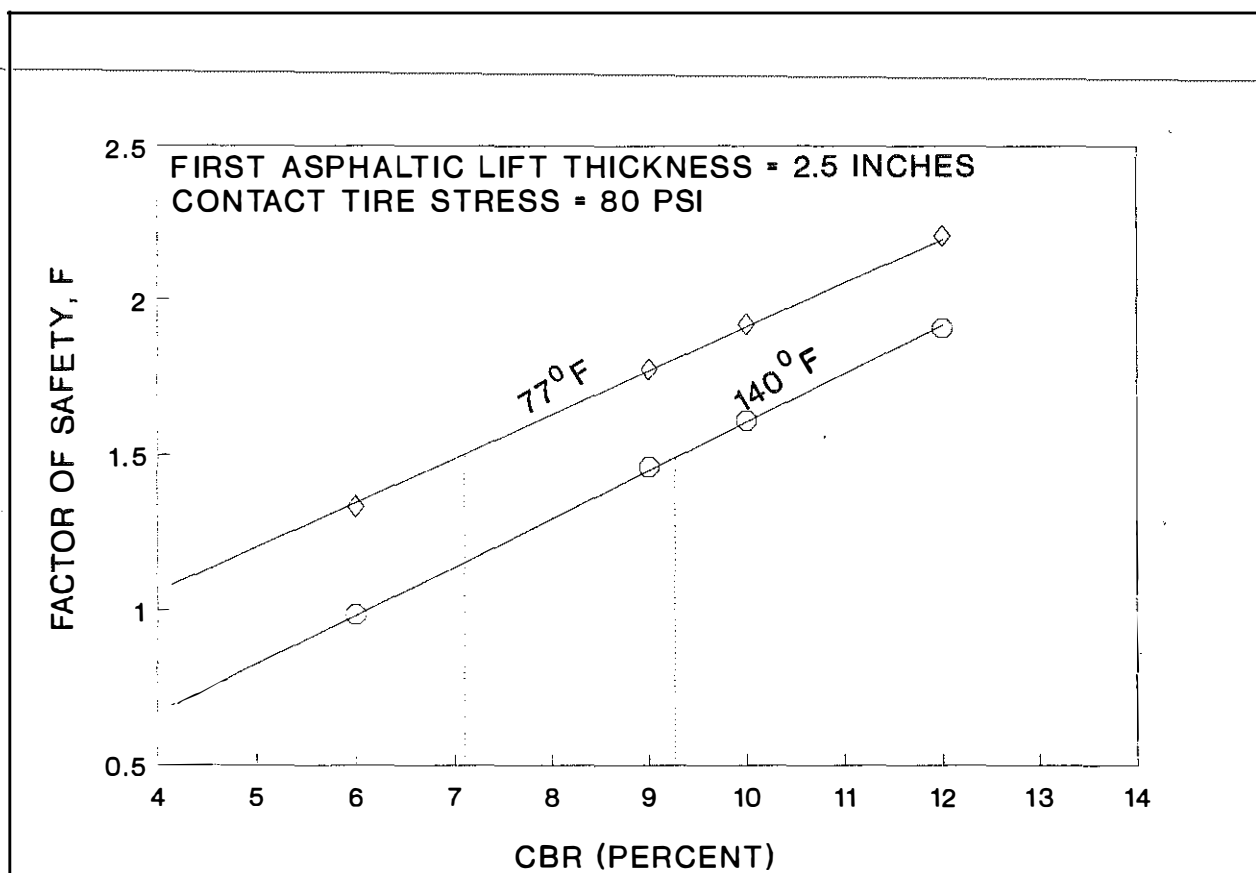


Figure 95. Factor of Safety as a Function of Subgrade CBR for Asphalt Temperatures of 77°F and 140°F.

This assumption is generally valid at the time of construction of the subgrade. However, the assumption is conditional and depends on the time of exposure of the clayey subgrades to weather conditions before paving and on the exposure of the subgrade to infiltration of surface and subsurface waters during or after construction. Fine-grained soils when initially compacted have a degree of saturation -- the portion of the void spaces in the compacted mass, which are filled with water -- of about 80 to 85 percent. Since the degree of saturation is normally below 100 percent, large negative pore pressures exist in the compacted clayey soil. Most clayey soils have high bearing, or shearing strength when first compacted.

These high strengths are not static. For example, 89 percent of Kentucky soils have unsoaked KYCBR values greater than 9.3 as shown in the left portion of Figure 10. In these tests, the Kentucky CBR tests were penetrated immediately after compaction of the specimen. Eight percent of the 727 specimens had unsoaked KYCBR values greater than six and less than or equal to 9.3. Only 3 percent of the specimens had KYCBR values less than six. Based on these statistics, "full-depth[®]" asphalt pavement could be constructed on compacted clayey soils if it was placed immediately after compaction of the soils and if the soils were compacted according to standard specifications. However, the unsoaked value of KYCBR depends on the placement water content. If the initial compactive state of the fine-grained soils could be maintained throughout and after construction, then most Kentucky soils would generally have sufficient bearing capacity to withstand construction traffic and post-construction traffic loadings. This conclusion must be viewed cautiously. Unfortunately, the KYCBR remolding procedure generally

produces compacted specimens that have dry densities and moisture contents that are not commensurable with dry densities and moisture contents referred to in standard compaction specifications. There is a tendency for the KYCBR to be larger than the CBR value obtained from specimens remolded to 95 percent of maximum dry density and optimum moisture content. For example, compaction specifications normally require that fine-grained soils be compacted to 95 percent of standard maximum dry density (AASHTO T 99 or ASTM D 698) and ± 2 percent of optimum moisture content. The Kentucky Laboratory procedure produces specimens that usually have dry densities that are much higher than the dry densities referred to in the standard compaction specifications (see Figure 96 and 97). Moisture contents of specimens compacted according to the KYCBR procedure are generally lower (even after soaking) than the optimum moisture contents obtained from AASHTO T 99. For example, the average dry densities of the specimens (mentioned above) before soaking averaged some 112 percent of maximum dry densities (AASHTO T 99) of these same specimens. Even after soaking, the average dry densities of these specimens were 107 percent of the maximum dry densities. Moisture contents of the specimens generally averaged some 2 percent lower than optimum moisture contents. Therefore, the KYCBR laboratory specimens are not characteristic of the field compacted soils. CBR values of the laboratory

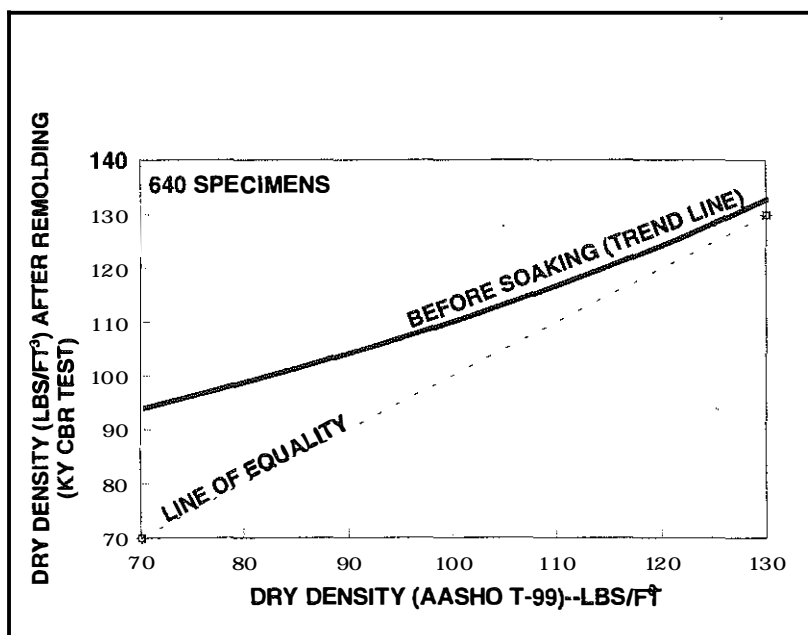


Figure 96. Dry Densities of Remolded Specimens Obtained from the KYCBR Testing Procedure as a Function of Maximum Dry Densities Obtained From AASHTO T-99.

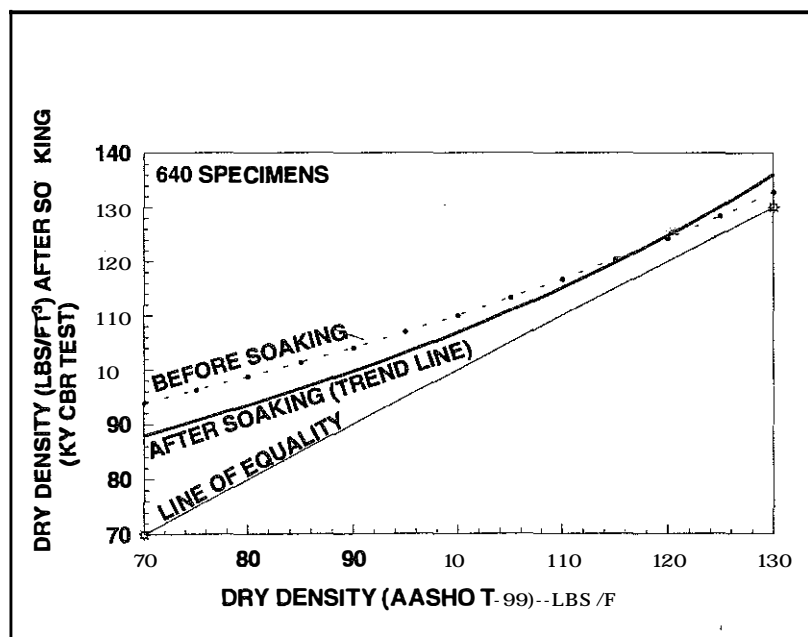


Figure 97. Dry Densities of Soaked Specimens Obtained from the KYCBR Testing Procedure as a Function of Maximum Dry Densities Obtained From AASHTO T-99.

specimens compacted according to the KYCBR procedure are usually larger than specimens compacted according to AASHTO T 99 (Hopkins 1972; Hopkins 1986; and Beckham and Allen 1989). For example, tests on a specimen of the AASHTO Road Test (1962) subgrade soils yielded a CBR value of 3.3 while the Kentucky procedure produced a value of 5.2.

The problem (Hopkins 1972) may be traced to the errant compactive nature of the Kentucky procedure. For example, the method specifies that the maximum dry density and optimum moisture content be used to calculate quantities for remolding the CBR specimen. Apparently, the intent was to remold a specimen having a diameter of 6 inches, a height of 5.0 inches, and the ability to conform to maximum dry density and optimum moisture content of AASHTO T 99. The procedure specifies that a static compaction pressure of 2000 psi be used to compact the specimen. A specimen cannot be remolded to standard dry density and optimum moisture content when a static pressure of 2,000 psi is specified because the height of the specimen cannot be controlled. To obtain standard compaction, the 2,000 psi pressure would have to be ignored and the specimen would have to be compacted statically so that a specimen measuring 5 inches in height would be obtained. Standard compaction would be achieved. The KYCBR testing procedure specifies using a 2,000 psi static pressure. Generally, specimens measuring about 4 inches in height are obtained.

Data in Figures 10 and 11 show that when compacted clayey soils and shales are exposed to water, the bearing strengths may be completely altered and lowered. The overall stability of the "full-depth[®]"

pavement is not constant throughout the life of the pavement because the bearing strength of the clayey subgrade is subject to change if surface and subsurface waters infiltrate into the subgrade. Although the "full-depth[®]" asphalt pavement (or other different structural asphalt designs) may perform very well during and after construction because of the high bearing strength of the unsaturated (unsoaked) clayey subgrade, the pavement may perform very poorly or fail at some time in the life of the pavement if surface and subsurface waters eventually infiltrate into the subgrade. For example, consider the

potential consequences of constructing a "full-depth[®]" asphalt pavement on a typical brown clay from Fayette County (Kentucky). As shown in Figure 66, the unsoaked (unsaturated) CBR value of this compacted clay is about 12 when the clay is compacted to 95 percent of maximum dry density and optimum moisture content (AASHTO T 99). After soaking, the CBR value of this same compacted clay

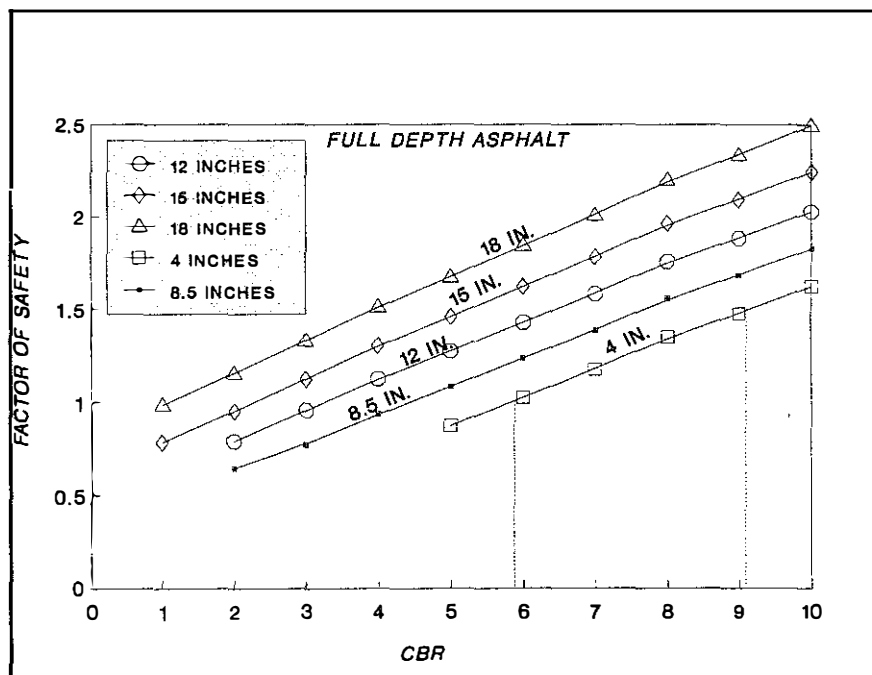


Figure 98. Factors of Safety of Different Thicknesses of "Full-Depth[®]" Asphalt Pavement as a Function of CBR.

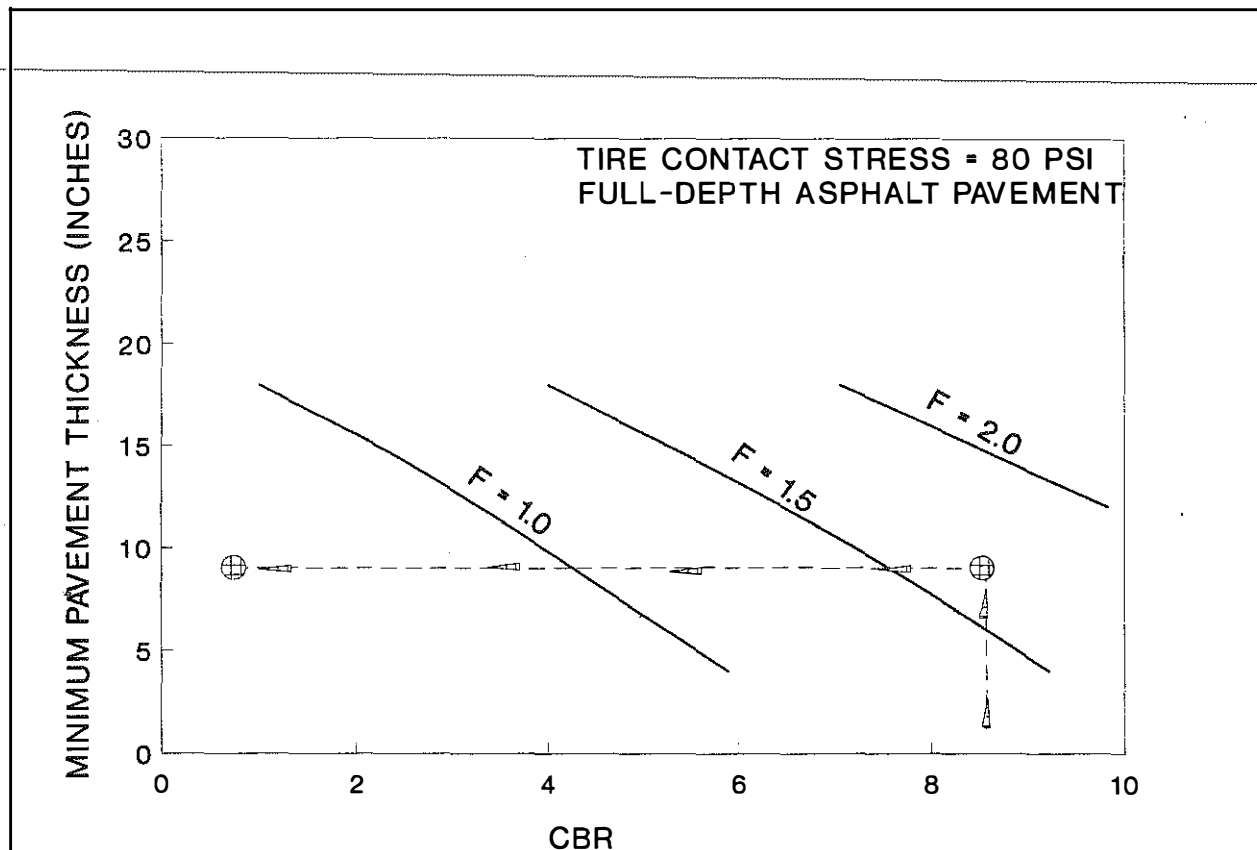


Figure 99. Minimum Thickness of "Full-Depth" Asphalt Pavement as a Function of CBR and Factor of Safety.

is about four according to the KYCBR method and about 0.8 according to the ASTM testing procedure. For a 15-inch "full-depth" pavement, as shown in Figures 98 and 99, the factor of safety against failure is greater than 2 for a CBR value of 12. If the subgrade is exposed to waters due to infiltration of surface and subsurface seepage for a sustained period of time, the factor of safety of the pavement gradually decreases to a value near one or lower since the CBR value of the clay approaches a value of about one to four. Similar arguments can be made for the group of 727 specimens represented in Figure 10. Initially, 89 percent of these specimens had CBR values greater than 9.3. As shown by the curves in Figures 98 and 99 obtained from the HOPKIB computer model, no problems would be encountered in constructing the first asphaltic lift measuring 2.5 inches in thickness since the factor of safety is equal to 1.5 (or greater). Thicknesses greater than the first lift would yield higher factors of safety. If subgrades were constructed of soils represented by the 727 specimens and were exposed to water, then the factors of safety of many of these soils would approach a value of one and a significant number of these soils would cause poor pavement performance (this result can be inferred by studying Figure 99). The stability of pavements on clayey subgrades is highly dependent on the moisture state of the subgrade materials since the bearing strength is very dependent on the moisture content of the clayey subgrade. This concept indicates that fatigue -- the tendency of the structural components to break under repeated traffic wheel loadings -- may be as much related to the moisture condition of the subgrade than to the condition of simply wearing down.

In many instances, the pavement may fail somewhat abruptly if the moisture content of the clayey

subgrade increases to some level greater than optimum moisture content. With an increase in moisture content, there is a decrease in the bearing strength and a decrease in the factor of safety as shown in Figures 66 and 99. Observations of pavement failures during the AASHO Road Test (1962) partially support this idea. According to Peattie (1984), the "incidence of failures at the AASHO Road Test was not regular throughout the duration of the test. Most of the failures in the flexible (pavement) sections occurred during the spring periods (periods where moisture contents of the silty clay subgrades at the AASHO were most likely to increase) of 1959 and 1960, although the number of axle load applications increased smoothly throughout the test. There was no smooth relationship between axle applications and damage to the subgrade."

MULTILAYERED PAVEMENT ANALYSES -- CASE STUDIES

During this study, published information specifically discussing and applying the principles of limit plastic equilibrium theory to the analysis of pavements involving multiple layers was not found. Comparisons of results obtained from the HOPKIB bearing capacity model and involving the analyses of multi-layered pavements to results from other models could not be made. However, another approach was used to test the validity and reasonableness of the results obtained from the HOPKIB model. This approach consisted of analyzing many pavement failures that occurred in the past few years in Kentucky. It may be reasoned that if a pavement failed, then the factor of safety is 1.0, or near 1.0. The HOPKIB model was used to analyze several pavement failures involving multiple layers and to compute factors of safety against failure. Results could be viewed as reasonable if the HOPKIB model predicted factors of safety of 1.0, or near 1.0. A description of these case studies is given as follows.

Alexandria-Ashland Highway -- Sections 13 and 14

Site Conditions

During construction of Sections 13 and 14 of the Alexandria-Ashland Highway in Northern Kentucky, gross failures occurred throughout the partially completed pavements. Thicknesses of the partially completed pavements at the time of failure ranged from about three to 9.3 inches. The failures occurred under wheel-axle loadings of gravel trucks. At the time of the failures, trucks were hauling gravel across Sections 13 and 14 to other sections of the Alexandria-Ashland Highway. Gross weights of the gravel trucks ranged from about 44,560 pounds to 83,580 pounds and averaged 61,360 pounds. The pavement failures occurred in June 1988. Surface temperatures of the partially completed pavement was about 140 ° Fahrenheit.

Soils and Geology

According to results tabulated on the soil profile sheets, the soils in this region classify typically as A-7-6 (10-35) and A-6 (6-33) based on the AASHTO Soil Classification System and CL and CH according to the Unified Soil Classification System. These materials are residual soils derived from the Kope Geological Formation. Typically, the Kope Formation consists mainly of shale. This firm shale breaks down rapidly into a soil-like material when exposed to water. Liquid limits of the soils range from 34 to 61 percent and average 42 percent. Plasticity indices range from 13 percent to 38 percent and average 20 percent. The clay content, or the percent finer than 0.002 mm, ranges from 17 to 54 percent and averages about 32 percent. Soaked KYCBR values of the residual soils obtained at sampling sites along

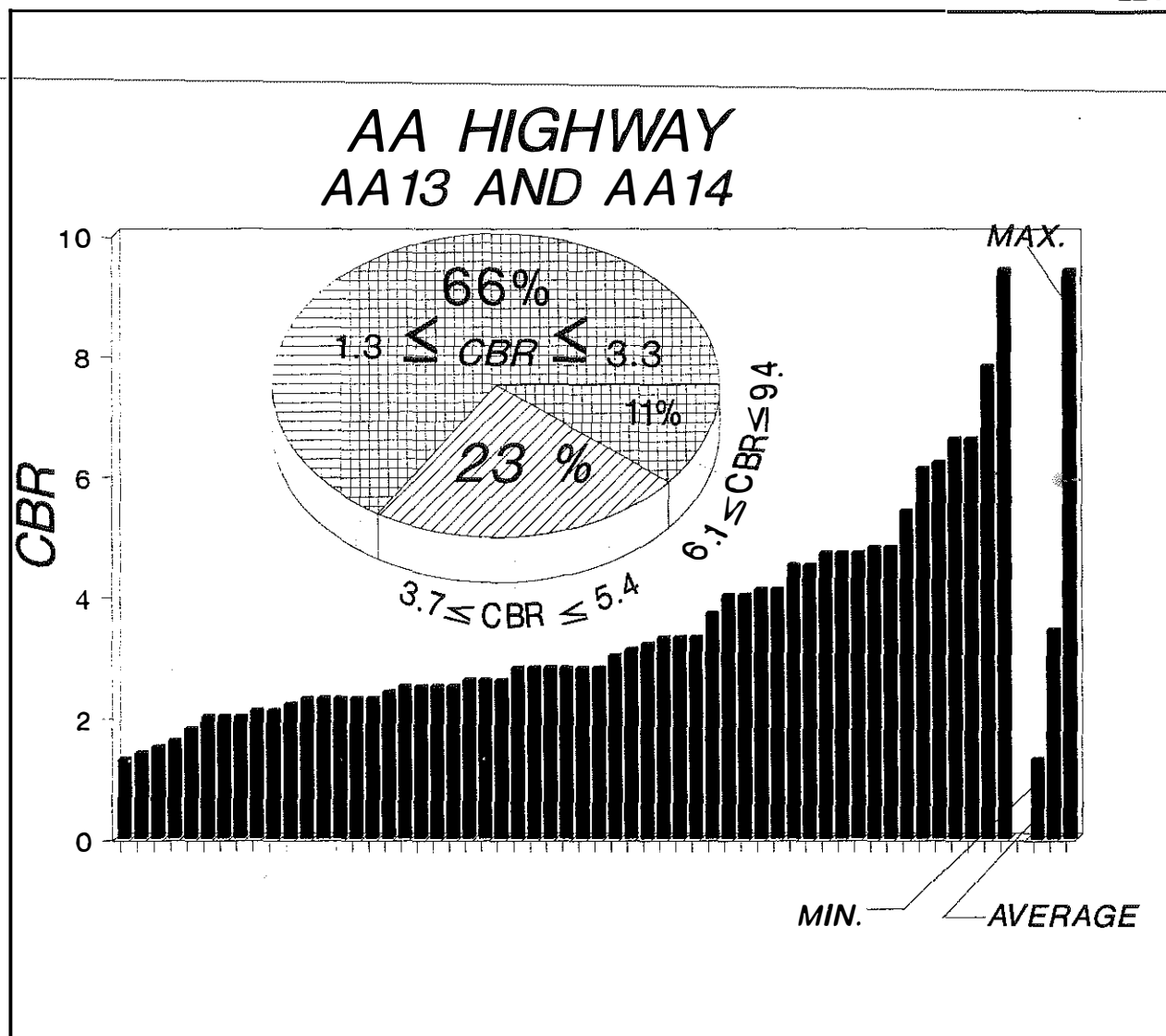


Figure 100. Values of CBR of Soils Located Along the Highway Corridor of Sections AA-13 and AA-14.

the highway corridor before construction are shown in Figure 100. About 66 percent of the soils (statistically) have soaked KYCBR values that lie between 1.3 and 3.3; soaked KYCBR values of about 23 percent of the laboratory specimens lie between 3.7 and 5.4. Approximately 89 percent of the test values fall below a soaked KYCBR value of 6.

The pavement subgrades of Sections 13 and 14 were mainly constructed using the residual soils of the Kope Geologic Formation. The subgrade matrix contained shale particles from the Kope Geologic Formation. Unsoaked KYCBR tests of the residual soils and shale of the Kope Formation generally exhibit large values of KYCBR values (Hopkins 1985). For example, typical unsoaked KYCBR values of remolded specimens of these residual soils and shale range from 18 to 32 percent. When the remolded specimens are soaked and allowed to swell, the soaked KYCBR is typically two. In one KYCBR test, the specimen was soaked and allowed to swell (Hopkins 1985) for 2.5 years. The soaked KYCBR value of this test specimen was 0.5. The variation of KYCBR value with increasing time of soaking is shown

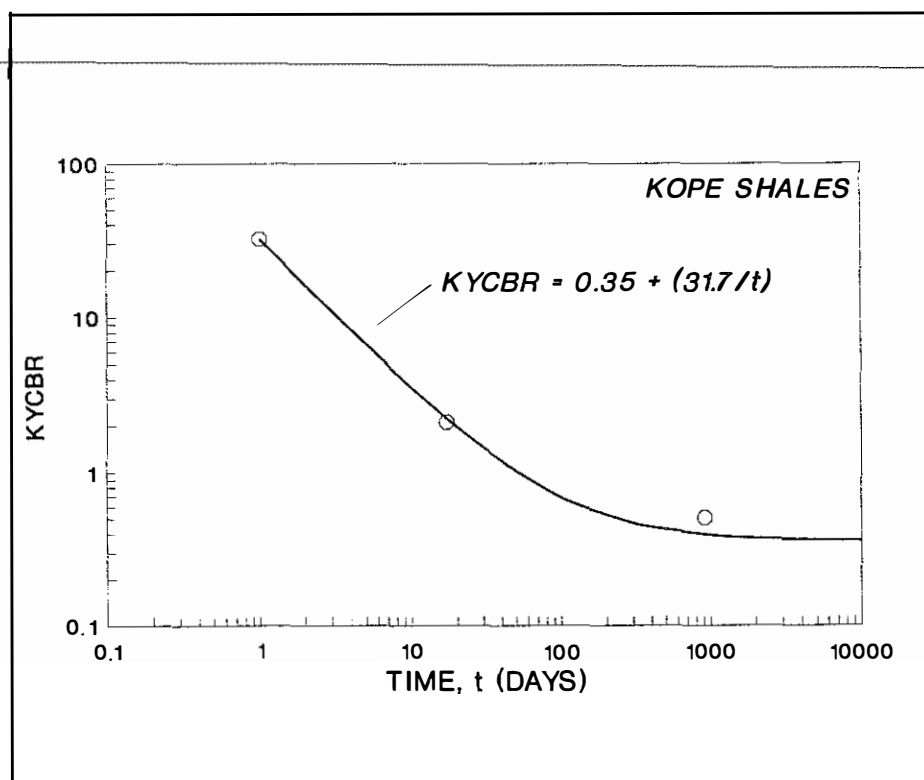


Figure 101. Relationship Between KYCBR and Time for Compacted Shales from the Kope Geological Formation.

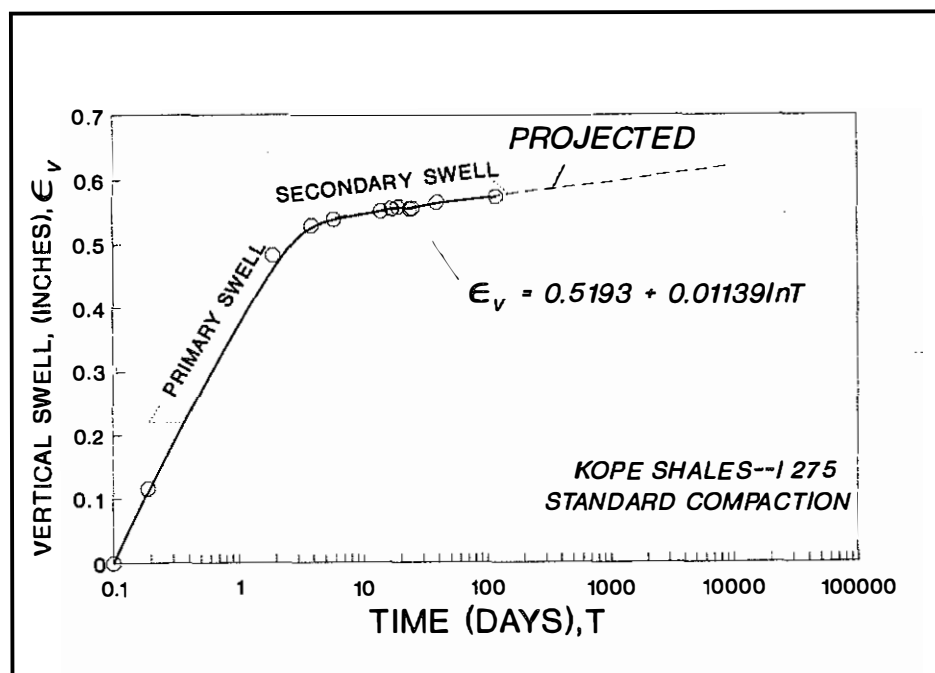


Figure 102. Vertical Swell of Compacted Shales from the Kope Geological Formation as a Function of Time.

in Figure 101. The pattern of swell (in percent) as a function of increasing soaking time for the specimen soaked for 2.5 years is shown in Figure 102. Based on this relationship, a significant portion (primary swell) of the total swell occurs quite rapidly. The pattern of swell shows that significant secondary swell will occur in these compacted residual soils and shales over a period of several years. When compacted subgrades of these materials are exposed to water for a sustained period, there is a dramatic decrease in bearing strength. As the moisture content increases, the bearing strength and pavement stability decreases.

Field Testing

The original or planned pavement design thickness included 4 inches of dense graded aggregate (DGA); three asphaltic base courses measuring 2, 2.5, and 3.5 inches in thicknesses; a binder course measuring 1.5 inches in thickness; and a 1-inch thick surface course.

The design section is shown in Figure 103. Total thickness of the original design section was 14.5 inches. At the time of failure during construction, thicknesses of the partially completed pavement ranged from about 3.2 to 9.3 inches as shown in Table 2. The failures occurred abruptly -- that is, there was not a smooth relationship between wheel-axle load applications and pavement damage.

In-situ CBR values of the subgrade conducted (Sharpe 1988) shortly after failure ranged from two to 11 and averaged 4.5. Moisture contents of the subgrades ranged from 15.8 to 26.3 percent. Laboratory KYCBR

values of tests performed on the residual soils and Kope shales are shown in Figure 104 as a function of moisture content. This relationship may be approximated as:

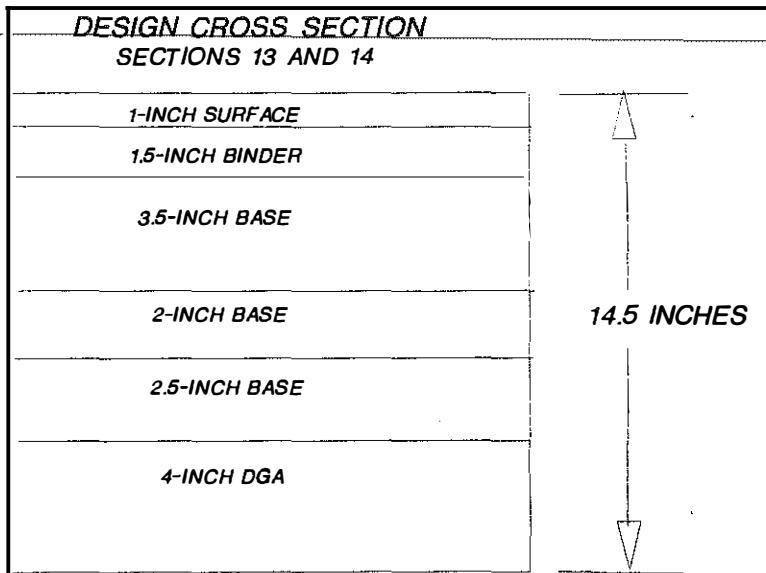


Figure 103. Design (and As-Built) Pavement Cross Section of Section AA-13 and AA-14.

$$KYCBR = \frac{1}{0.122W_m - 1.56} \quad (255)$$

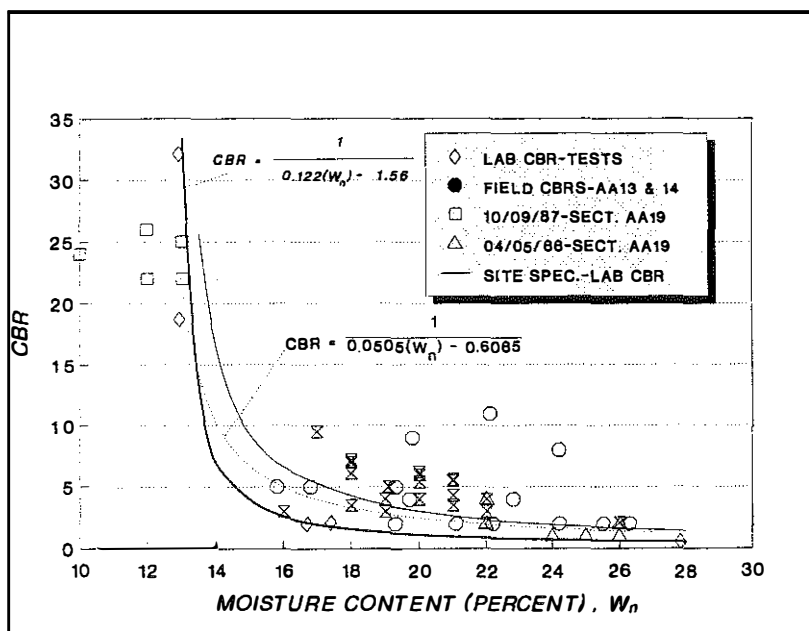


Figure 104. CBR as a Function of Moisture Content.

where W_m is the molding water content. Based on this relationship, the KYCBR value is about five, or smaller, when the moisture content is equal to or greater than about 14.5. To test the validity of this relationship, in-situ, or field, CBR values and corresponding in-situ moisture contents of the subgrades of Section 13 and 14 were compared to the trend of the laboratory CBR-moisture content relationship as shown in Figure 104. Generally, this comparison shows that when the moisture content is greater than about 16.0 percent, the field CBR value is below five in approximately 80 percent of the cases.

Soils (residual soils of the Crab Orchard Geologic Formation) used to construct the subgrades of Section 19 of the Alexandria-Ashland Highway are similar to the soils used in the construction of the subgrades of Sections 13 and 14. Soaked KYCBR values obtained from soil and profile sheets are shown in graphical form in Figure 105. Seventy-four percent of the test specimens had laboratory KYCBR values that ranged from 1.3 to 4.1 while 26 percent of the specimens had KYCBR values that ranged from 4.8 to 7.8. These values are very similar to KYCBR values of the subgrade soils of Sections 13 and 14. At Section 19, two series of field CBR tests were conducted. The first series of in-place CBR tests were done in the Fall (October 9) 1987 almost immediately after compaction of the subgrade soils. The in-place CBR values of the subgrade shortly after compaction ranged from 22 to 26. Moisture contents of the subgrade soils during these field tests ranged from about 10 to 14 percent. In-place CBR tests performed on the subgrade soils in the following spring (April 4) 1988 -- some six months after construction -- showed that CBR values of the subgrade

soils decreased and ranged from one to four. Moisture contents of the exposed subgrade had increased from about 10 to 14 percent to values ranging from about 22 to 26 percent. Exposure of the unpaved subgrade to winter and spring weather (rainfall and snow melt) caused increases in the moisture content and decreases in the bearing strengths. Moisture content and field CBR values of the two series of tests are compared in Figure 104 to values obtained at Sections 13 and 14 and to laboratory CBR tests. The trend of all field data lies close to the trend of the laboratory data. The trend of the field data may be approximated by the expression:

$$CBR_{field} = \frac{1}{0.0505 W_n - 0.6065} \quad (256)$$

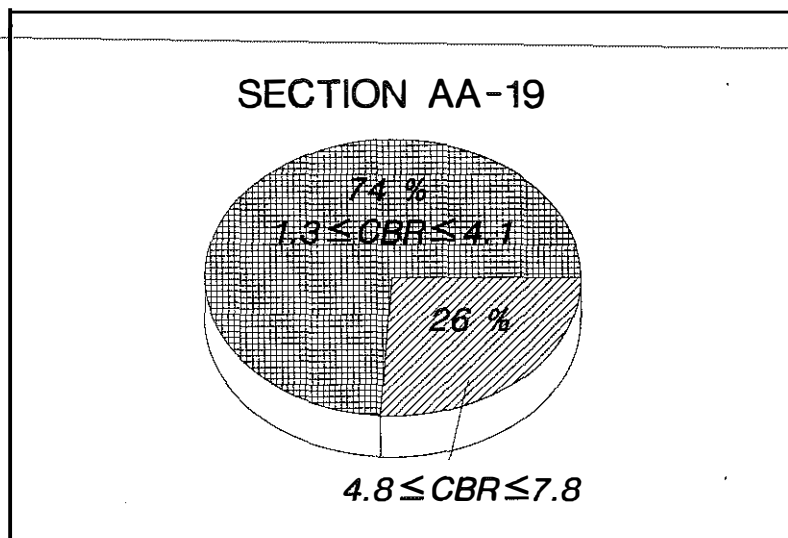


Figure 105. Values of Laboratory KYCBR.

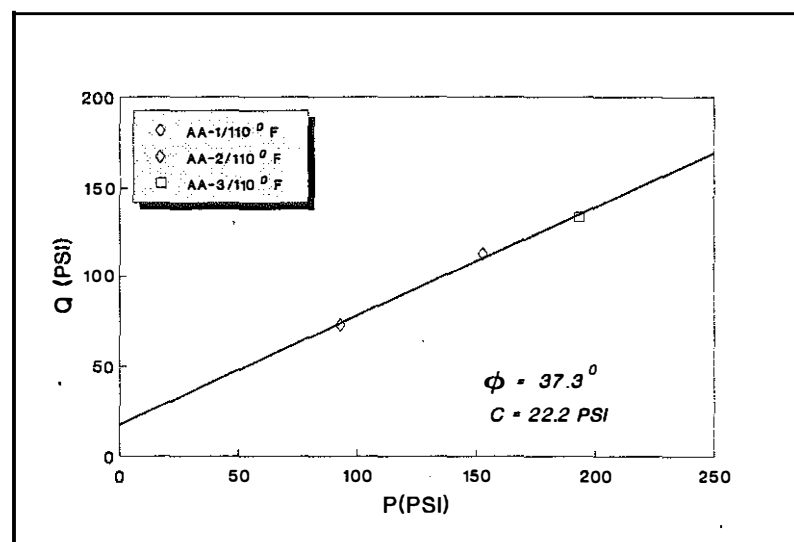


Figure 106. Typical Triaxial Tests Results Obtained at a Temperature of 100°F.

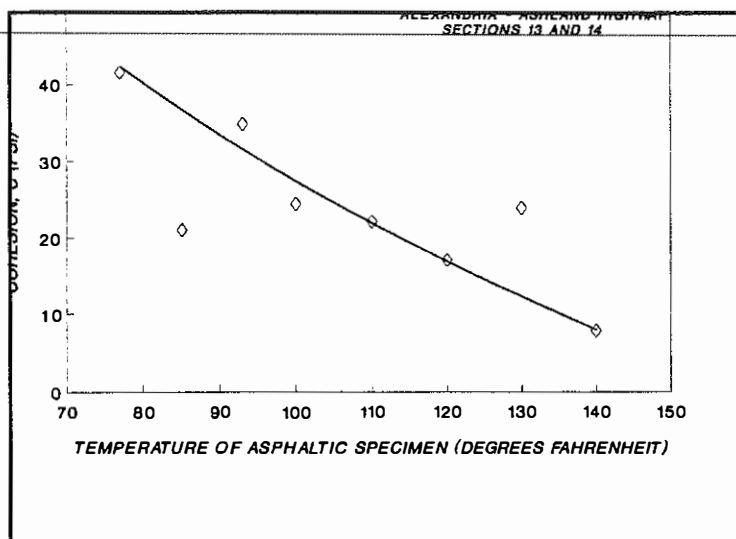


Figure 107. Variation of the Total Stress Parameter, c , With Temperature of Asphalt Pavement Core Specimens.

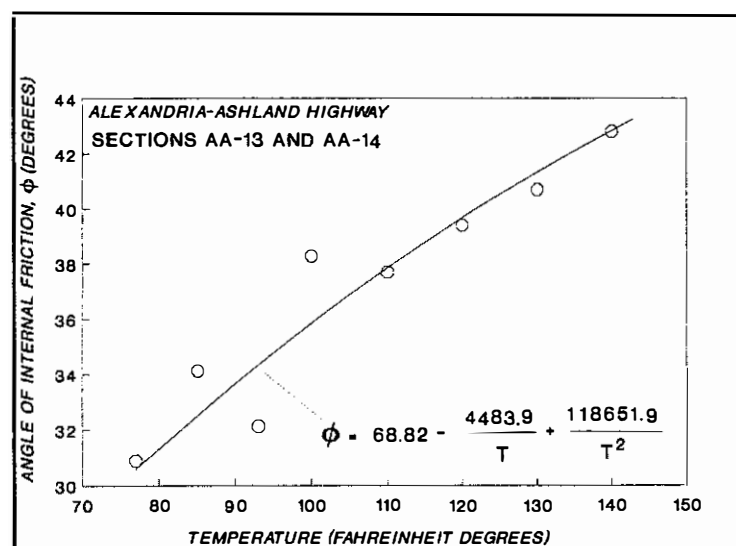


Figure 108. Variation of the Total Stress Parameter, ϕ , With Temperature of Asphalt Pavement Cores.

Laboratory Shear Strengths

To determine the variation of shear strength of the asphaltic pavement of Sections 13 and 14 with temperature, core specimens were obtained and unconsolidated-undrained (UU), triaxial compression tests were done at selected temperatures ranging from 77 ° to 140 ° F. A minimum of three tests were performed at a given temperature. A typical "p-q" diagram of the triaxial results obtained at 100 ° F is shown in Figure 106. Variation of the cohesive component of strength, c , obtained from the UU-tests with temperature is shown in Figure 107. The relationship between c and temperature may be expressed as:

$$c = 292.34 - 57.54 \ln(T). \quad (257)$$

The relationship between the total stress parameter, ϕ , and temperature is shown in Figure 108 and may be expressed in the form:

$$\phi = 68.8 - \frac{4484}{T} + \frac{118652}{T^2} \quad (258)$$

The investigation conducted shortly after failure of the two sections indicated that surface temperatures of the asphaltic pavements were near 140 ° F. To account for temperature variation (and variation of shear strength) in the HOPKIB model with depth in the asphaltic pavement,

relationships given by Southgate (1969) were used. Based on an assumed surface temperature of 140 ° F and an average air temperature of 81 ° F, the temperature for any given depth may be determined from the relationships given by Southgate. The relationship, as shown in Figure 109, between temperature, T , and depth, D , for the assumed temperatures may be expressed as:

$$T = 139.6 - 8.34D + 0.388D^2. \quad (259)$$

The total stress parameter, ϕ , of the dense graded aggregate was assumed to be 43° . The total stress parameter, c , was assumed equal to zero since this material contained less than 5 percent fine material passing the number 200 sieve. Undrained shear strengths of the soil subgrades were based on in-situ CBR test values. The CBR values were converted to undrained shear strengths, S_u or c , using the relationship shown in Figure 64.

Analyses and Results

In performing the analyses of sections 13 and 14 of the Alexandria-Ashland Highway, three situations were considered and included:

- partially completed pavement sections at the time of failure at each testing location and in-situ subgrade strengths,
- the design cross section and in-situ subgrade strengths, and
- the remedial cross section and in-situ subgrade strengths.

In the analyses of each situation, the asphalt pavement was divided into one-inch layers. The temperature at the mid-point of each one-inch layer was calculated from Equation 259. Using Equations 257 and 258 and the temperature of each asphalt layer, ϕ and c values were computed for each 1-inch layer.

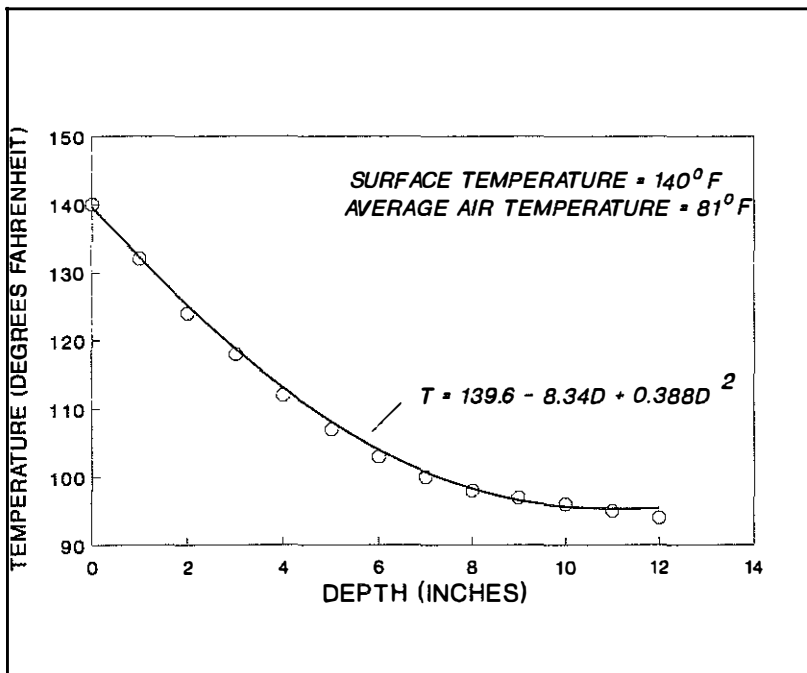


Figure 109. Variation of Temperature of Asphalt Pavement and Depth of Asphalt Pavement.

Table 4 summarizes the factors of safety obtained from the HOPKIB Program for the partially completed pavement as it existed at several testing locations (or stations) when the failures occurred. Tire contact stress used in the analyses was 80 psi. A typical setup of the shear strength parameters for analyses of a partially completed pavement section is illustrated in Figure 110 (site 3 in Table 4). Thicknesses of asphaltic pavement at the time of failure at each testing location and

the in-situ CBR value of the subgrade during the failure investigation at each location are also summarized in this table. Factors of safety obtained from the HOPKIB model for the partially completed pavement ranged from 0.36 to 2.1.

TABLE 4. SUMMARY OF FACTORS OF SAFETY FOR ACTUAL PAVEMENT THICKNESS AT TIME OF FAILURE AND ORIGINAL PAVEMENT SECTIONS--AA-13 and AA-14

SITE NO.	STATION NO.	ASPHALTIC PAVEMENT THICKNESS AT FAILURE (inches)	INSITU CBR VALUE OF SUBGRADE (percent)	UNDRAINED SHEAR STRENGTH, S_u^1 (or c) (psi)	MOISTURE CONTENT OF SUBGRADE (percent)	FACTOR OF SAFETY (Tire Stress = 80 psi)	
						ACTUAL SECTION THICKNESS AT FAILURE ² (F)	ORIGINAL DESIGN SECTION ³ (F)
1	2051	3.15	2	4.28	24.2	0.36	1.07
2	2114+50	5.30	11	22.73	22.1	2.02	2.51
3	2140	4.67	8	16.64	24.1	1.53	2.06
4	2194+50	4.06	4	8.44	22.8	0.78	1.42
5	2203+25	8.25	2	4.28	21.1	0.86	1.07
6	2232	8.10	2	4.28	-	0.85	1.07
7	2260	8.50	2	4.28	25.5	0.87	1.07
8	2278+72	7.55	4	8.44	19.7	1.15	1.42
9	2288+79	7.55	2	4.28	19.3	0.71	1.07
10	2288+87	7.75	2	4.28	26.3	0.73	1.07
11	2292	8.25	2	4.28	22.2	0.86	1.07
12	2298+33	9.25	5	10.50	15.8	1.45	1.59
13	2319+97	7.55	5	10.50	-	1.31	1.59
14	2349+28	7.80	5	10.50	19.3	1.33	1.59
15	2382+78	7.80	9	18.68	19.8	1.95	2.21
16	2446+20	5.25	5	10.50	16.8	1.12	1.59

1. Estimated from the relationship: $S_u = 2.173 \text{ CBR}^{(0.979)}$.

2. Actual pavement thicknesses at the time of failure used in the analyses.

3. The original pavement design consisted of 10.5 inches of asphaltic pavement and 4 inches of dense graded aggregate.

At 10 of the 16 locations (see Figure 111), the factors of safety ranged from 0.36 to 1.15 -- essentially failure. At 13 of the 16 sites, the factor of safety was less than 1.5. Hence, the HOPKIB model would have predicted the failures. Factors of safety for the design or planned pavement section are also summarized in Table 4. The original planned pavement cross section is shown in Figure 103 and consisted of 10.5 inches of asphaltic pavement resting on 4 inches of dense graded aggregate. Factors of safety for the original planned section using in-situ CBR values shown in Table 4 ranged from 1.07 to 2.51 (also see Figure 112). At seven of the 16 locations, the factor of safety

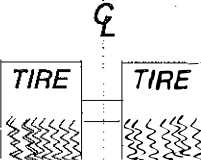
		$T_s = 140^\circ\text{F}$			
		ϕ			
ASPHALT PAVEMENT	$T_1 = 135.5^\circ\text{F}$	$\phi_1 = 42.2^\circ$	$c = 8.568 \text{ PSI}$	$D = 1.0 \text{ IN.}$	
	$T_2 = 128.0^\circ\text{F}$	$\phi_2 = 41.0^\circ$	$c = 10.928 \text{ PSI}$	$D = 1.0 \text{ IN.}$	
	$T_3 = 121.2^\circ\text{F}$	$\phi_3 = 39.9^\circ$	$c = 13.592 \text{ PSI}$	$D = 1.0 \text{ IN.}$	
	$T_4 = 115.2^\circ\text{F}$	$\phi_4 = 38.8^\circ$	$c = 16.496 \text{ PSI}$	$D = 1.0 \text{ IN.}$	
	$T_5 = 113.2^\circ\text{F}$	$\phi_5 = 38.5^\circ$	$c = 17.596 \text{ PSI}$	$D = 0.7 \text{ IN.}$	
DGA		$\phi_5 = 43^\circ$	$c = 0$	$D = 4.0 \text{ IN.}$	
CLAYEY SUBGRADE		$\phi_7 = 0$	$c = 3.232 \text{ PSI}$		

Figure 110. Parameters Used to Analyze Site Number 3, Station 2140, of Sections AA-13 and AA-14.

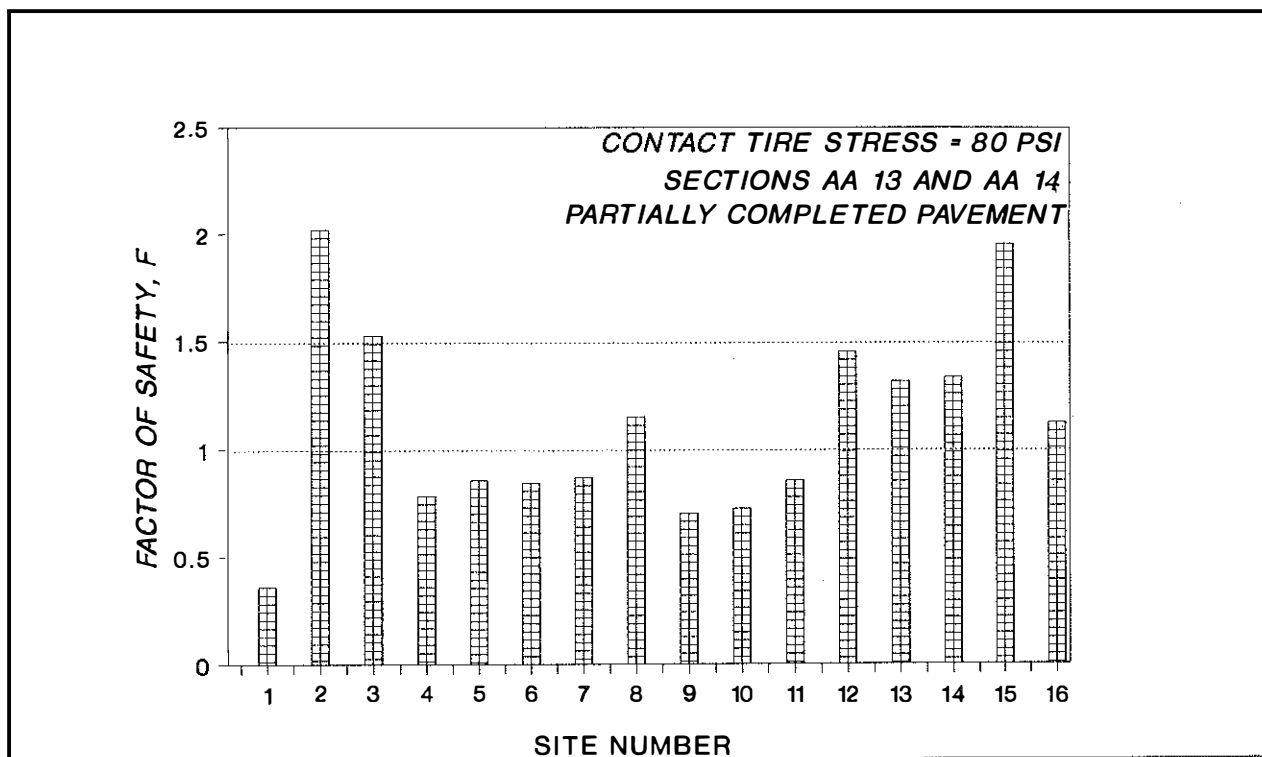


Figure 111. Factors of Safety of the Partially Completed Pavement Sections of Sections AA-13 and AA-14.

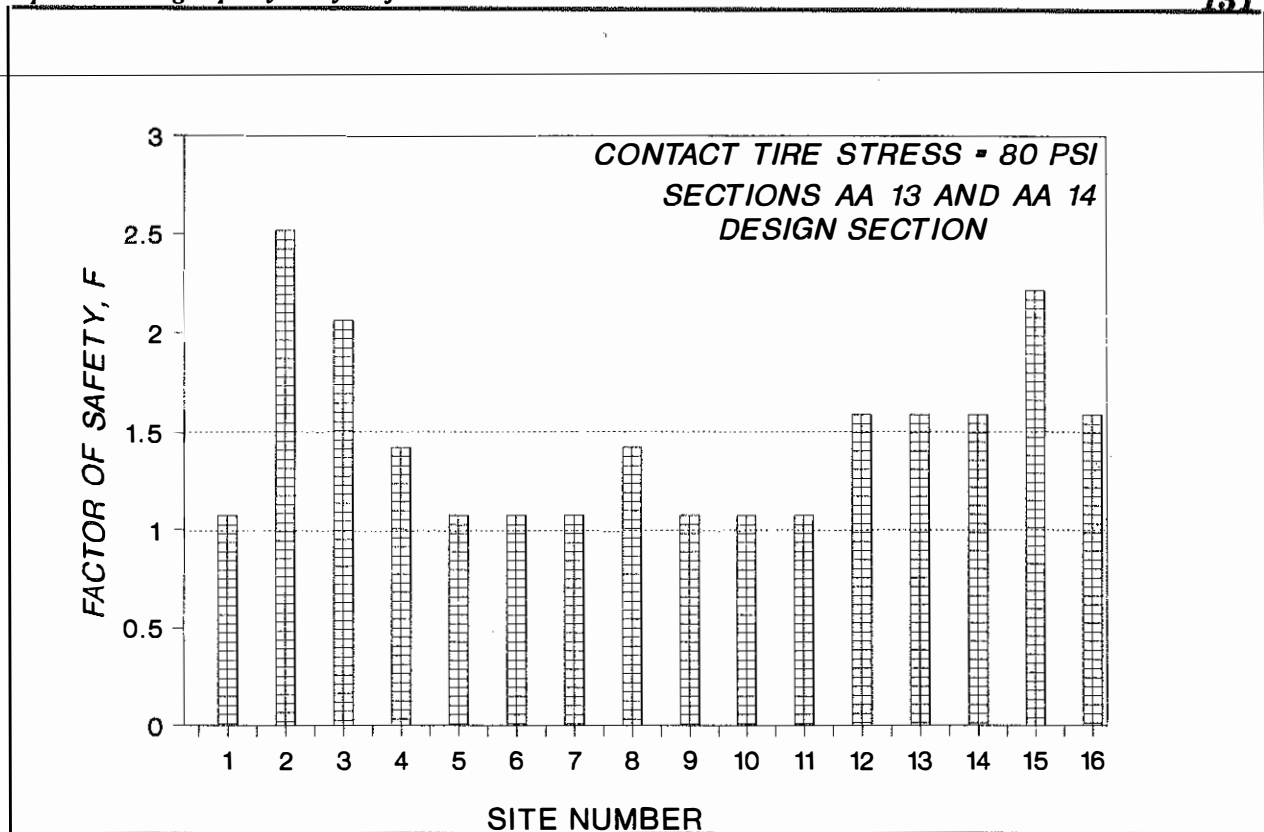


Figure 112. Factors of Safety of the Pavement Cross Sections of Sections AA-13 and AA-14.

was 1.11 -- near failure. At 12 locations, the factor of safety was less than about 1.6. The small values of factors of safety show that serious pavement problems would have developed in the future -- this assumes that the pavement as planned could have been constructed.

Remedial analyses by Sharpe (1989) proposed overlaying the failed sections with asphaltic pavement. Final pavement cross sections throughout the length of sections 13 and 14 are shown and compared to the original planned section in Figures 113 and 114. Thicknesses of the final (remedial) sections (Sharpe 1991) ranged from 15.5 to 18.75 inches -- some 0.5 to 4.25 inches thicker than the original planned section. Results obtained from the HOPKIB model for the sections as built are summarized in Table 5 and shown in graphical form in Figure 115. Factors of safety ranged from 1.14 to 2.52. The stability of the reconstructed pavement appears adequate in most areas.

Great River Road -- State Route KY 94

Site Conditions

During construction of the Great River Road in Fulton County, Kentucky (State Route KY 94), extensive failures occurred in the partially completed pavement. Certain areas contained deep ruts and alligator-type cracking. The original (planned) pavement section, as shown in Figure 116 consisted of 7.5 inches of asphaltic concrete and 6 inches of bank gravel (base course). When failure occurred, approximately 5 inches of the bituminous pavement had been placed.

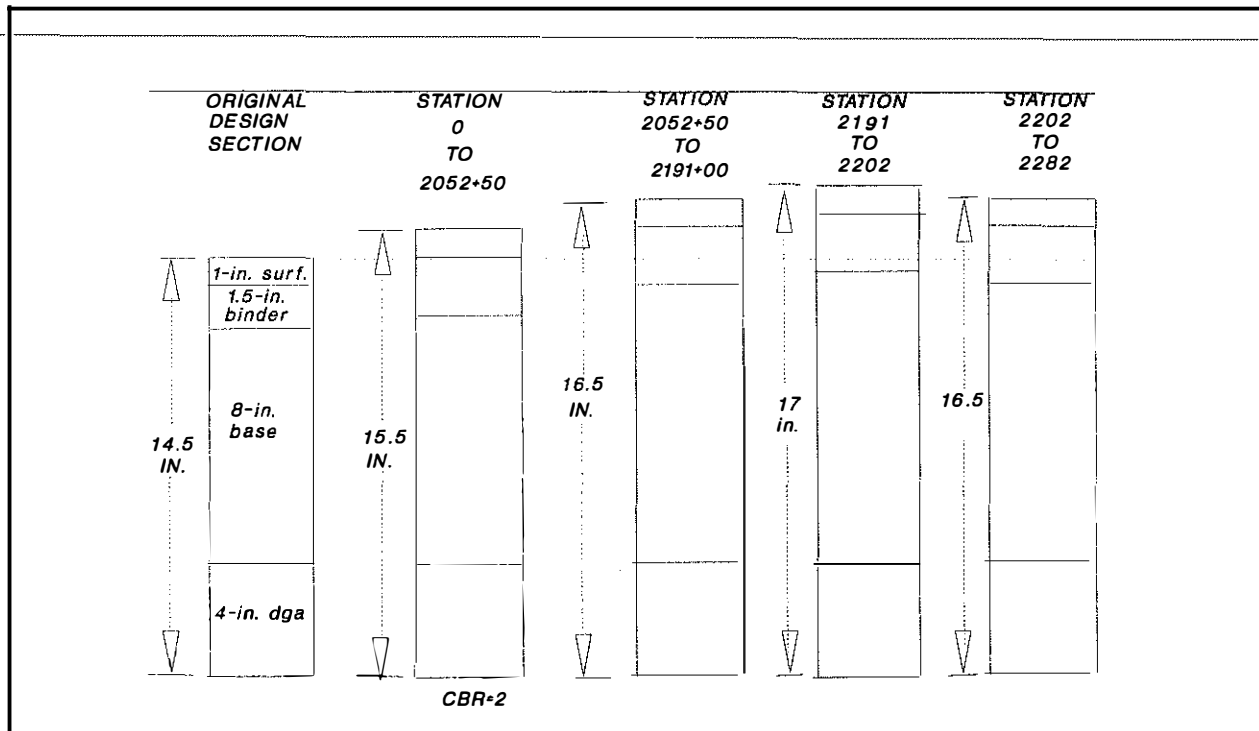


Figure 113. Remedial Overlay Pavement Sections of Sections AA-13 and AA-14.

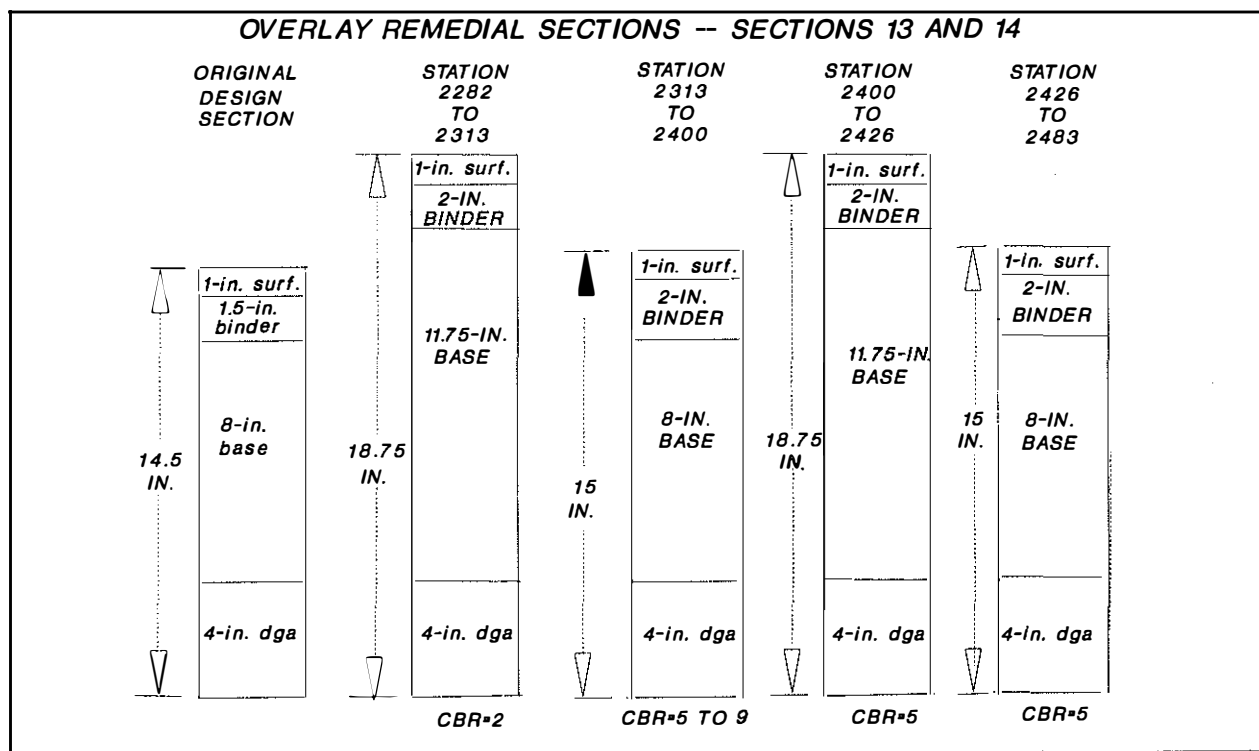


Figure 114. Remedial Overlay Pavement Sections.

TABLE 5. SUMMARY OF FACTORS OF SAFETY FOR REMEDIAL PAVEMENT DESIGN SECTIONS USED AT SECTIONS 13 AND 14 OF THE ALEXANDRIA-ASHLAND HIGHWAY

STATIONS	ASPHALTIC PAVEMENT THICKNESS (inches)	INCREASED ASPHALTIC PAVEMENT THICKNESS* (inches)	In-situ CBR value OF SUBGRADE (percent)	FACTOR OF SAFETY
0 +00 to 2052+50	11.5	1.0	2	1.14
2052+50 to 2191+00	12.5	2.0	9.5	2.52
2191+00 to 2202+00	13.0	2.5	3	1.46
2202+00 to 2282+00	12.5	2.0	2	1.23
2282+00 to 2313+00	14.75	4.25	2	1.40
2313+00 to 2400+00	11.00	0.50	7.0	1.63
2400+00 to 2426+00	14.75	4.25	5	1.95
2426+00 to 2483+00	15.0	0.50	5	1.63

Soils and Geology

The highway is in a geologic region known as the Mississippian Embayment. Soils in this area consist of wind-blown silts (loess), alluvial silts, and clays. Groundwater levels in the area (swampy) are close to the ground surface and generally are two to 5 feet below the natural ground surface. Silts and clays have low plasticity. Plasticity indices range from about four to 12 percent. Liquid limits range from about 25 to 35 percent finer than the number 200 sieve ranges from about six to 26 percent. Generally, the soils used to construct the pavement subgrade classify as ML, CL, or ML-CL. Optimum, moisture content of the soils ranged from 16.4 to 17.8 percent and

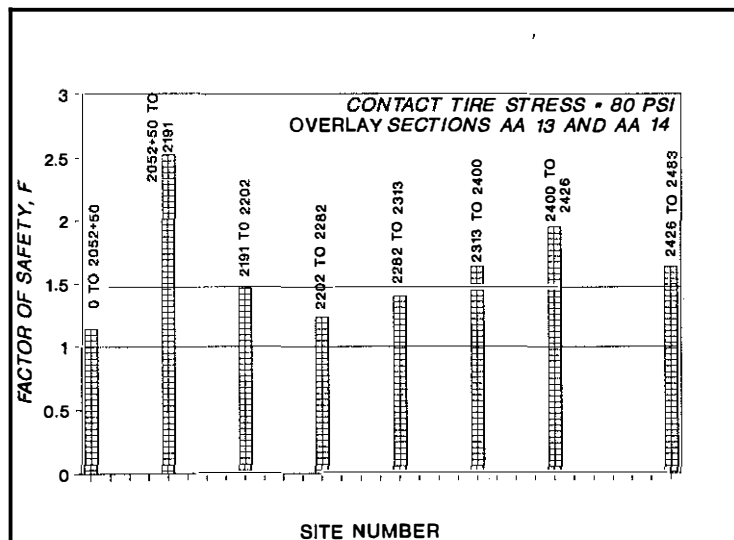


Figure 115. Factors of Safety of Overlay Sections Obtained from the HOPKIB Computer Program for Sections AA-13 and AA-14.

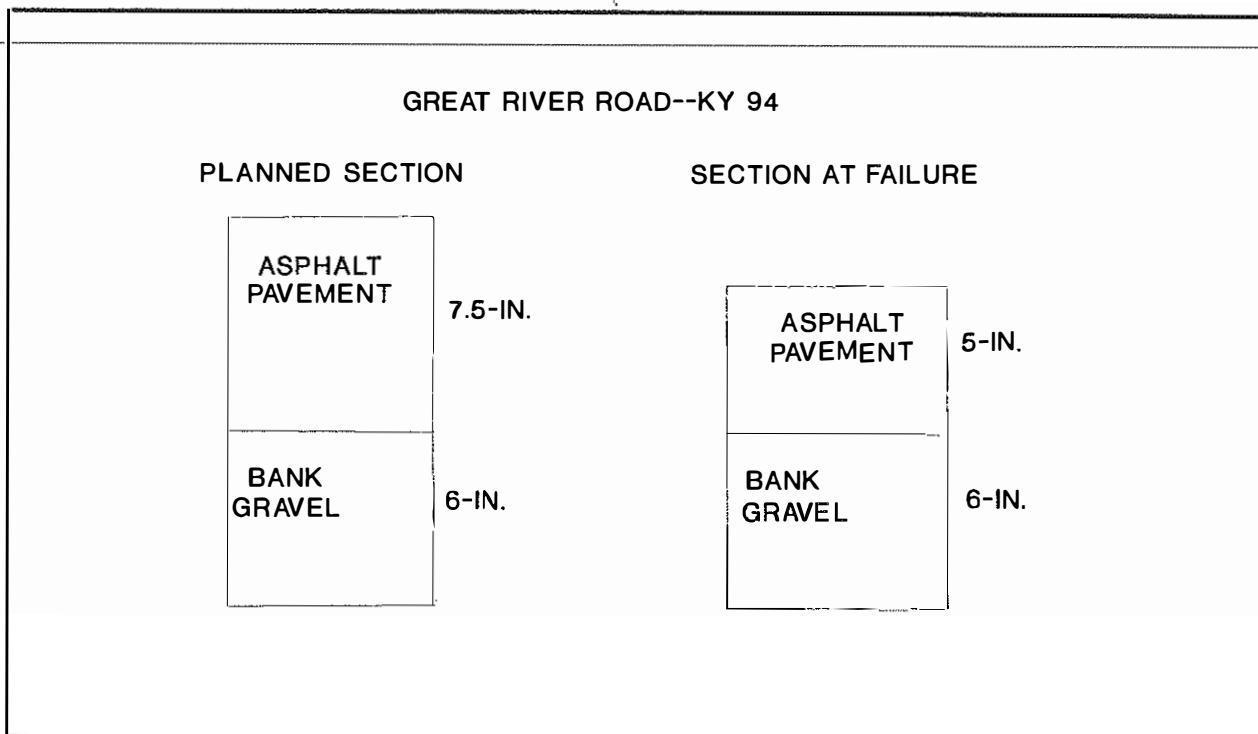


Figure 116. Design Pavement Section of the Great River Road (KY 94) and the Pavement Section at the Time of Failure.

averaged 17.4 percent. Maximum dry density ranged from 104.4 to 106.3 pounds per cubic foot and averaged 105.3 pounds per cubic foot.

Optimum moisture content of the bank gravel ranged from 124.2 to 127.8 pounds per cubic foot and averaged 126.1 pounds per cubic foot. The optimum moisture content ranged from 9.7 to 10.7 and averaged 10.4 percent. Compaction tests were performed in accordance with ASTM D 698 (or AASHTO T-99).

Field Study and Sampling

Core specimens of the partially completed pavement were obtained as well as bag samples of the bank gravel. Thin-walled tube samples of the clayey and silty subgrade were also obtained. Road Rater tests were done (Sharpe 1988) on the partially completed pavement; in-situ CBR tests were performed on the subgrade through cored holes. These data were used by Sharpe (1986) to develop a remedial plan.

Laboratory Shear Strengths

Unconfined compression tests were performed on the thin-walled tube specimens by the Geotechnical Branch of the Kentucky Department of Highways. Those data and factors of safety are summarized in Tables 6 and 7. The factors of safety shown in Table 7 represent tests on specimens of the subgrade obtained from areas within the project that were described visually as "failed."

**TABLE 6. SUMMARY OF UNDRAINED SHEAR STRENGTHS OF SUBGRADE OF KY 94
AND FACTORS OF SAFETY**

Site No.	Station Number	Unconfined Compressive Strength	Undrained Shear Strength	Dry Density (Pounds/Foot ³)	Moisture Content (%)	Factor of Safety	
		(psi)	(psi)			Partially Completed Pavement	3.25-inch Overlay
0	386+50	37.32	18.66	106.7	16.5	1.741	2.049
		12.92	6.46	94.0	25.0	0.696	1.067
		(specimen depth = 3'-5')	8.19	88.9	26.7	0.422	0.765
		6.81	3.40	87.1	27.2	0.329	0.694
1	376+50	22.06	11.53	103.1	19.8	1.208	1.489
		12.90	6.45	106.7	15.7	0.695	1.066
2	366+50	22.06	11.03	102.51	17.8	1.169	1.449
3	356+50	11.38	5.69	101.5	21.0	0.613	0.996
		11.20	5.60	101.1	22.2	0.603	0.987
4	346+50	48.09	24.05	108.2	17.8	2.131	2.457
5	336+50	63.79	31.90	106.1	19.0	2.688	3.041
6	316+50	24.25	12.13	111.5	19.0	1.252	1.537
7	306+50	33.34	16.67	105.8	19.4	1.593	1.895
8	296+50	32.14	16.07	107.6	16.5	1.549	1.849
		45.67	22.84	109.8	17.1	2.044	2.366
9	284+50	61.88	30.94	110.6	17.0	2.620	2.970
		42.18	21.09	108.2	17.3	1.918	2.234
10	274+50	20.99	10.49	105.4	21.1	1.126	1.405
11	264+50	52.36	26.18	107.4	19.9	2.284	2.617
12	254+50				20.7		
13	244+50	17.92	8.96	106.4	16.7	1.995	1.276
14	234+50				18.4		
15	224+50	40.99	20.50	108.9	17.2	1.875	2.189
		12.74	6.37	103.4	19.0	0.686	1.060
16	218+50				12.2		
17	208+50				12.9		
18	198+50				24.8		
19	188+50	27.84	13.92	101.8	19.4	1.389	1.680
20	186+50	17.33	8.67	95.9	23.8	0.982	1.255
21	166+50	24.98	12.49	99.0	24.2	1.280	1.566
		27.81	13.91	98.1	24.2	1.388	1.679
22							
23	146+50	33.66	16.83	94.9	22.5	1.605	1.907

TABLE 7. FACTORS OF SAFETY FOR AREAS ON KY 94 DESCRIBED AS VISUALLY FAILED

Site Number	Station Number	Moisture Content	Dry Density	Factor of Safety
24	192 + 73	19.5	109.7	0.41
25	249 + 22	22.8	102.2	0.92
		16.6	113.9	2.12
		21.1	101.9	1.53
		16.5	111.0	2.67
26	255 + 98	24.8	97.9	1.10
		21.6	101.2	1.14
27	299 + 30	20.7	105.8	0.689
28	306 + 18	20.7	104.7	0.93
29	315 + 00	23.1	101.1	0.92
30	315 + 00	22.6	-	-
31	375 + 41	18.6	106.6	1.30
		18.8	108.5	2.63
32	377 + 72	17.8	107.0	2.59
		25.9	98.0	1.48

According to data supplied by the resident's office of the Kentucky Department of Highways (Paducah, Kentucky), the maximum dry density (AASHTO T 99) of the compacted bank gravel was 127.8 pounds per cubic foot and optimum moisture content was 9.7 percent. Consolidated-undrained triaxial compression tests with pore pressure measurements were performed on specimens remolded or compacted to conform to these conditions. Results of these tests are shown in Figure 117. The ϕ' and c' values of the bank gravel were 39.6° and 0.0, respectively.

Unconsolidated-undrained triaxial compression tests were performed on core specimens using the special arrangement shown in Figure 88. These tests were performed at temperatures ranging from 77° to 140° F. The testing procedure has been described previously in the section referred to as "Full-Depth® Asphalt Pavements." Variations of the total stress parameter, c , and temperature, T , are shown in Figure 91. The relationship between the total stress parameter, ϕ , and temperature is shown in Figure 92.

Analyses and Results

The failed pavement at the KY 94 site was analyzed using the HOPKIB bearing capacity computer model. Factors of safety were computed for each location where unconfined compression test data had

been obtained. Two series of analyses were performed. The first series consisted of analyzing the pavement section at the time of failure. In the second series, the pavement section with the proposed overlay was analyzed. At the time of failure, surface temperature of the partially completed pavement was reported to be 140 F. To account for variation of temperature with depth within the partially

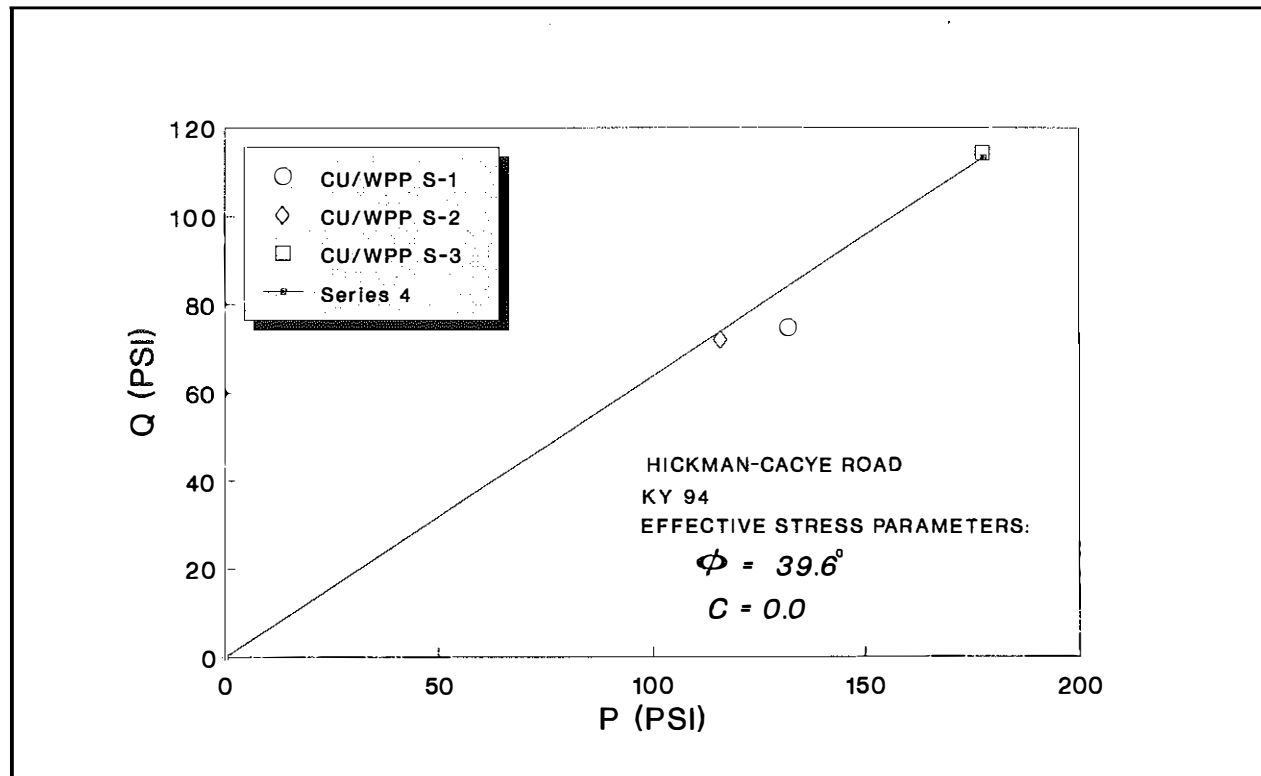


Figure 117. *Effective Stress Parameters of Bank Gravel Used to Construct the Base Course of KY 94.*

completed asphaltic layer, the relationship given in Figure 109 was used. Both the partially completed asphaltic pavement and the asphaltic pavement with the asphaltic overlay were divided into 1-inch layers. Values of c and ϕ were computed using the temperature of each 1-inch layer obtained from the equation in Figure 109 and equations shown in Figures 91 and 92, respectively. Contact tire stresses used in all analyses were assumed to be 80 psi. Factors of safety obtained for the partially completed pavement and the pavement with the overlay section are summarized in Tables 6 and 7, respectively. As shown in the left large portion of Figure 118, the factors of safety at 37 percent of the testing locations were less than or equal to 1.10 -- a condition that may be defined as failure. At 24 percent of the locations, the factors of safety ranged from 1.10 to 1.48. The stability of the pavement at these testing locations may be defined as marginal. At 39 percent of the sites, the factors of safety were greater than 1.53. In this case, the pavement had high stability. Factors of safety (Table 6) at the testing locations are shown in a bar chart in Figure 119.

Factors of safety at all testing locations shown in Table 7 for the pavement sections with the overlay are shown in Figure 120. As shown in Figure 118, the factors of safety at 54 percent of the test

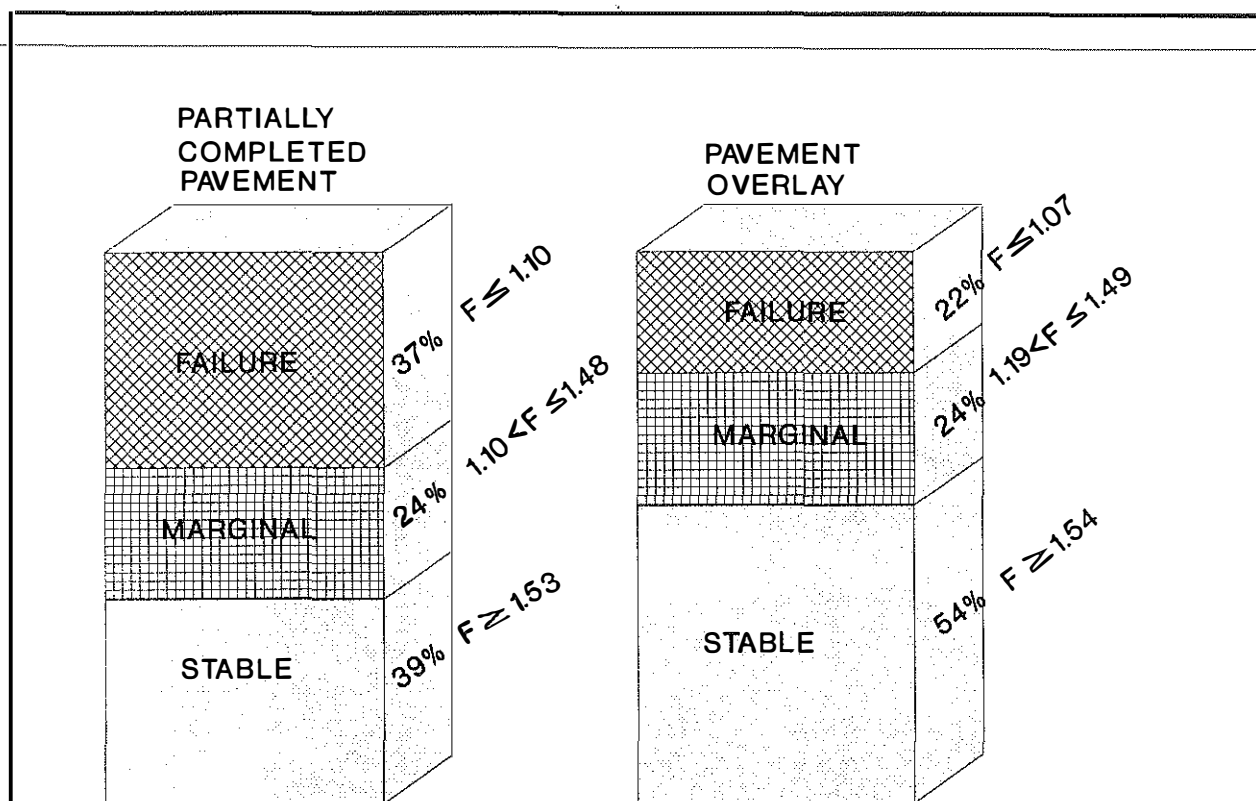


Figure 118. Percentages of Stable and Unstable Areas of the Great River Road (KY 94) Obtained from the HOPKIB Model.

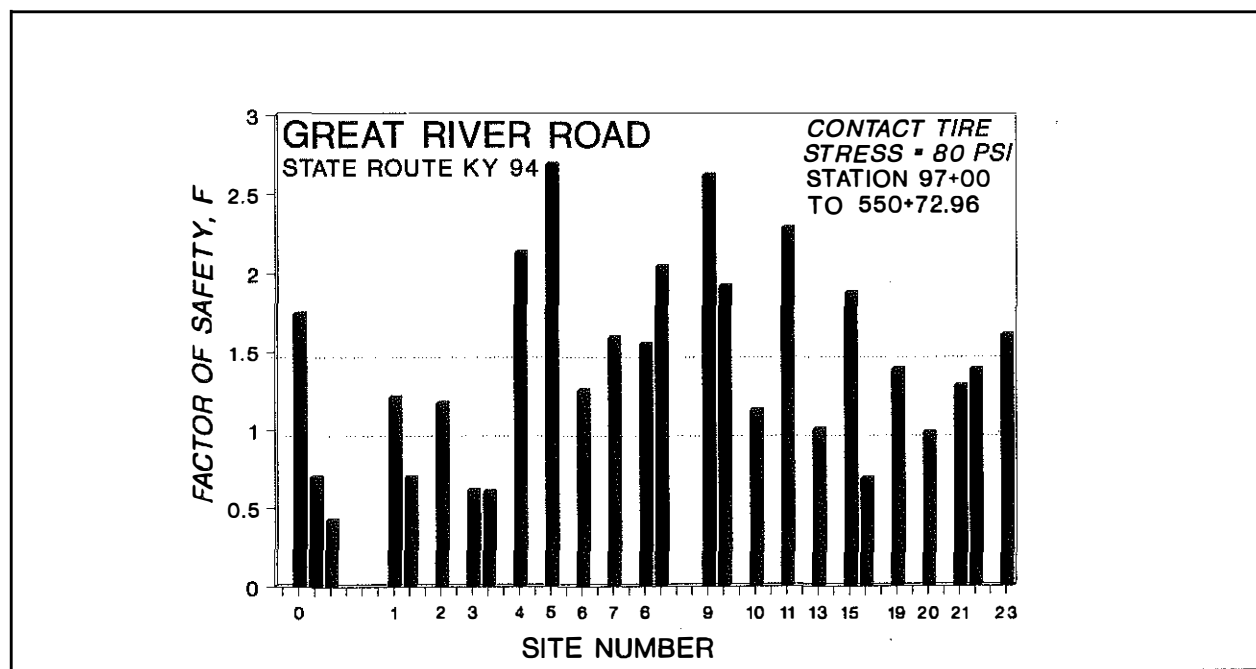


Figure 119. Factors of Safety of the Partially Completed Pavement Sections of the Great River Road (KY 94)

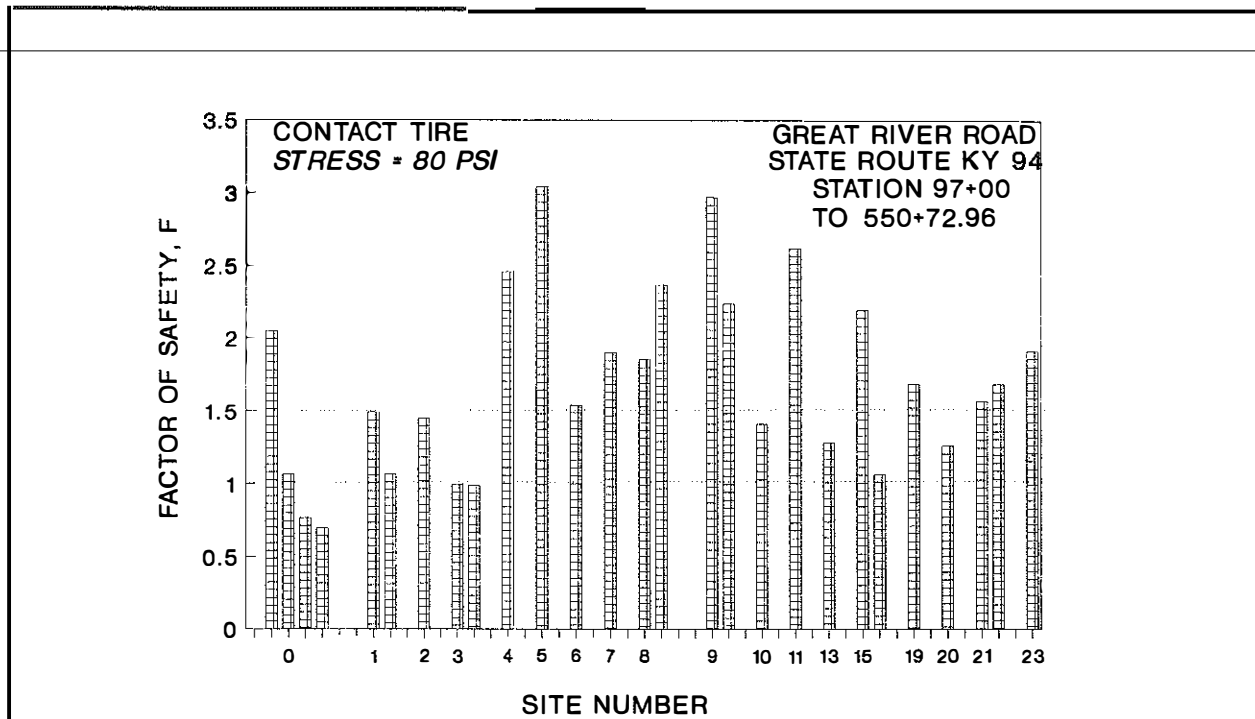


Figure 120. Factors of Safety of the Pavement Overlay Sections of the Great River Road (KY 94).

locations were equal to or greater than 1.54. The overlay (including the surface course) increased the stable areas some 15 percent. Areas considered having marginal stability ($1.19 < F \leq 1.48$) essentially remained the same -- 24 percent. The unstable areas ($F \leq 1.07$) decreased from 37 percent for the partially completed pavement to 22 percent for the pavement section with the overlay.

The relationship between dry density (or dry unit weight) of the soil subgrade and moisture content is shown in Figure 122. These data were obtained from measurements of the unconfined compression test specimens. These data show that at 35 percent of the test locations, the measured values of dry density of the soil subgrade were less than 95 percent of maximum dry density obtained from the standard compaction test (AASHTO T 99).

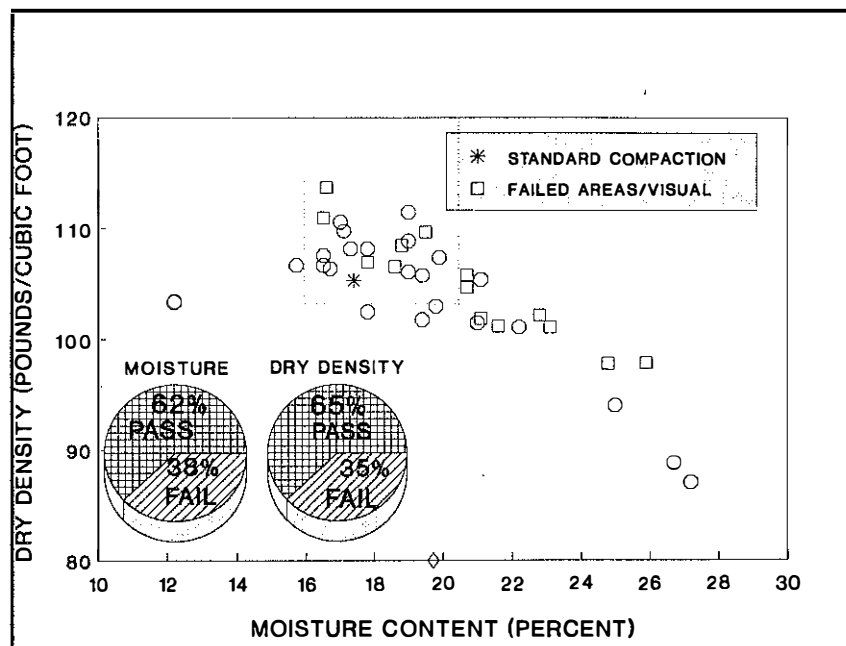


Figure 121. In-Situ Dry Density as a Function of Moisture Content--KY 94.

Moreover, the moisture contents of the subgrade at 38 percent of the locations exceeded the value of optimum moisture content plus 2 percent. Hence, compaction of the subgrade generally did not meet state specifications at the time of failure (although compaction specifications were apparently met at the time of construction of the subgrade). Apparently, the subgrade soils swelled with increasing time and there was a decrease in dry density. There was a decrease in shear strength. The analyses indicate that the overlay should have been thicker to avoid future pavement problems. Factors of safety for the partially completed pavement that occurred at locations that were described as "visually-failed" are shown in Figure 122. A steady decrease of strength of the subgrade occurs with increasing time after compaction of the subgrade. The relationship between undrained shear strength of the subgrade and moisture content is shown in Figure 123. Although there is considerable scatter in these data, there is a trend in the data; that is, as the moisture content increases, the undrained shear strength decreases. The stability of the partially completed pavement decreases as shown in Figure 124. At many locations, the factor of safety is near or smaller than 1.0. Results obtained from the HOPKIB bearing capacity analyses show that the pavement failures at this site were mainly caused by low bearing strengths of the soil subgrade.

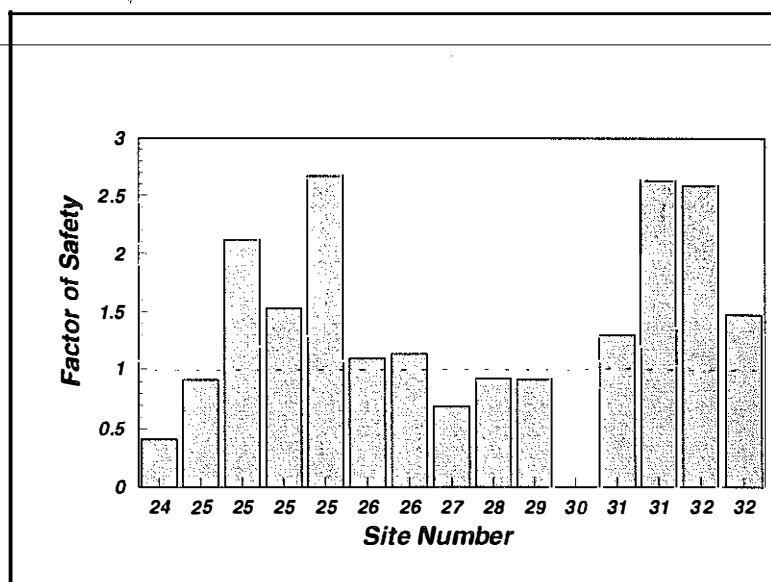


Figure 122. Factors of Safety at Locations on KY 94 During Construction That Were Described as "Visually Failed."

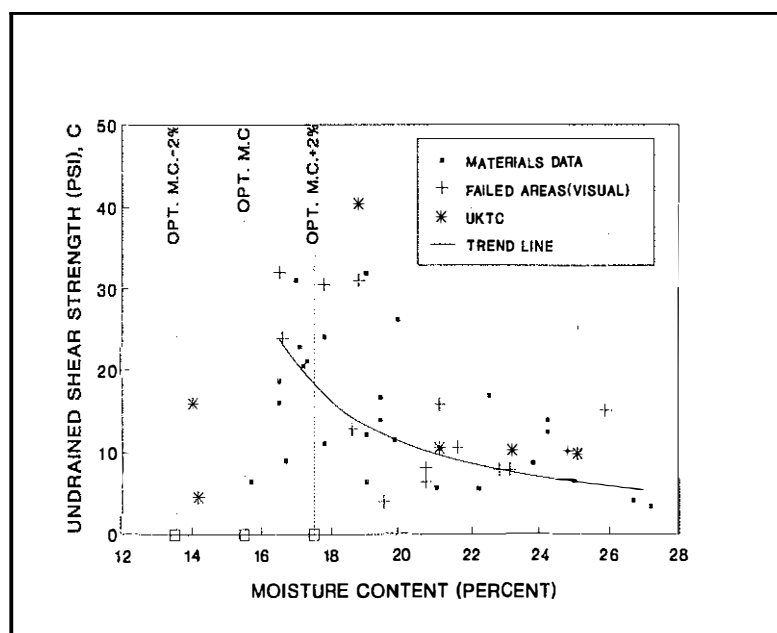


Figure 123. Undrained Shear Strength as a Function of Moisture Content--KY 94.

Metropolitan City Streets

Metropolitan city streets are typically designed for low values of 18-kip equivalent single-axle load

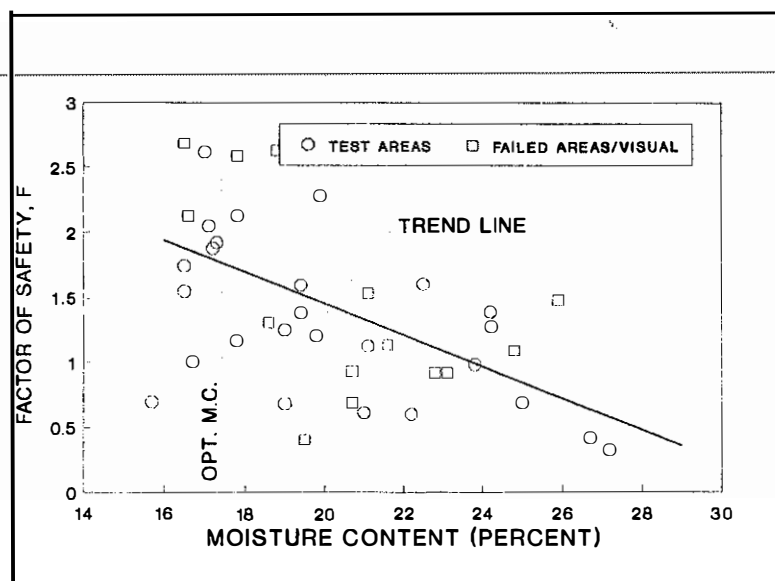


Figure 124. Factors of Safety as a Function of Moisture Content--KY 94.

divided into 1-inch layers and the temperature at the midpoint of each 1-inch layer was computed using the relationship given in Figure 109.

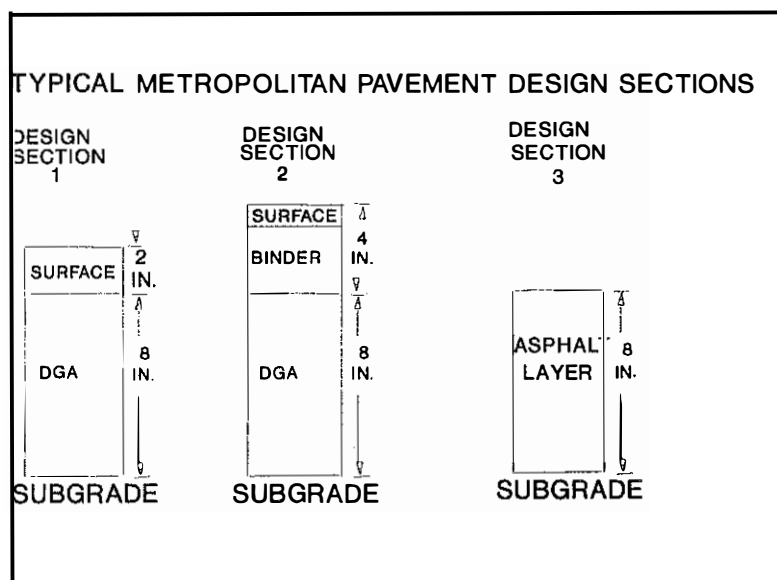


Figure 125. Typical Pavement Sections of Metropolitan City Streets for Low-Volume Traffic.

assumption that the subgrade was untreated. Values of the CBR of the subgrade were ranged from one to seven. Factors of safety of the three pavement sections are shown in Figures 126, 127, and 128, respectively, as a function of subgrade CBR. Critical subgrade CBR values (those with a factor of safety equal to about 1.15) for these sections are 6, 5, and four, respectively. In those cases where the CBR values are equal to or less than these critical CBR values the pavement sections would fail or deform under heavy-laden vehicles. Difficulties may be encountered in constructing the first lifts of the base

applications (ESAL). Since some current design methods assume a smooth relationship between load applications and damage, low values of ESAL are often used, and relatively thin pavement sections are frequently obtained. For example, three typical pavement sections were analyzed using the HOPKIB mathematical model and computer program. The three typical pavement sections are shown on the previous page in Figure 125. In performing the analyses, the surface temperature of the asphalt pavement was assumed to be 140 ° F and the average air temperature was assumed to be 81 ° F. Each asphalt layer of each typical section was divided into 1-inch layers and the temperature at the midpoint of each 1-inch layer was computed using the relationship given in Figure 109. The assumption was also made that ϕ and c values were computed from the relationships given in Figures 107 and 108. The contact tire stress was assumed to be 80 psi. Although low values of ESAL may be applied to the finished pavement after construction of the pavement (and the city development), vehicles laden with construction materials (gravel, concrete, and etc.) will load the pavement during construction; i.e., hauling materials to different portions of the development.

Two scenarios were analyzed using the HOPKIB computer program. In the first scenario, analyses of the three sections were based on the

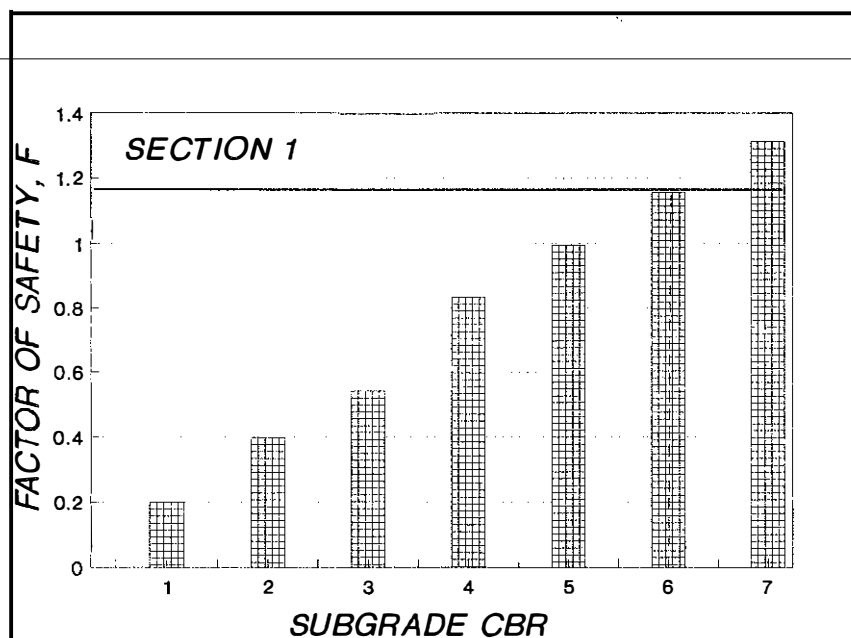


Figure 126. Factors of Safety of Section 1 Constructed on an Untreated Subgrade.

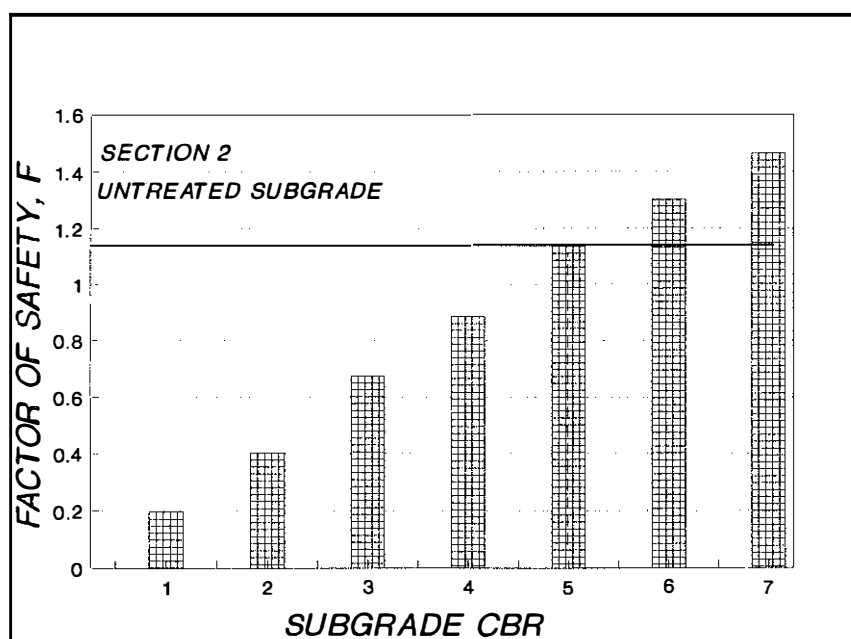


Figure 127. Factors of Safety of Section 2 Constructed on an Untreated Subgrade.

courses. In situations where subgrade CBR strengths approach, or fall below these values, other alternatives need to be explored. Options might include the following:

- Limit the loads (and tire contact stresses) of trucks hauling materials
- Increase the thickness of the pavement section, or
- Modify or stabilize the subgrade.

For example, the subgrade could be stabilized using an 8-inch layer of stabilized, or chemically-treated layer of subgrade. Analyses of the three sections using an 8-inch layer of treated subgrade, based on the assumption that c equals 50 pounds per square inch ($\phi = 0$), are shown in Figures 129, 130, and 131. Critical CBR values of the untreated subgrade ($F \leq 1.15$) become about 4, 3.5, and three, respectively. For CBR values below three, the sections having an 8-inch layer would still be inadequate. The thickness of the pavement sections would probably need to be increased, or the strength of the treated layer would need to be increased to obtain a factor of safety larger than about 1.10.

Pavement sections that would meet certain standards, that is, factors of safety equal to 1.3 or greater could be devised using the HOPKIB model. It is suggested that design practices and standards in metropolitan areas be reviewed.

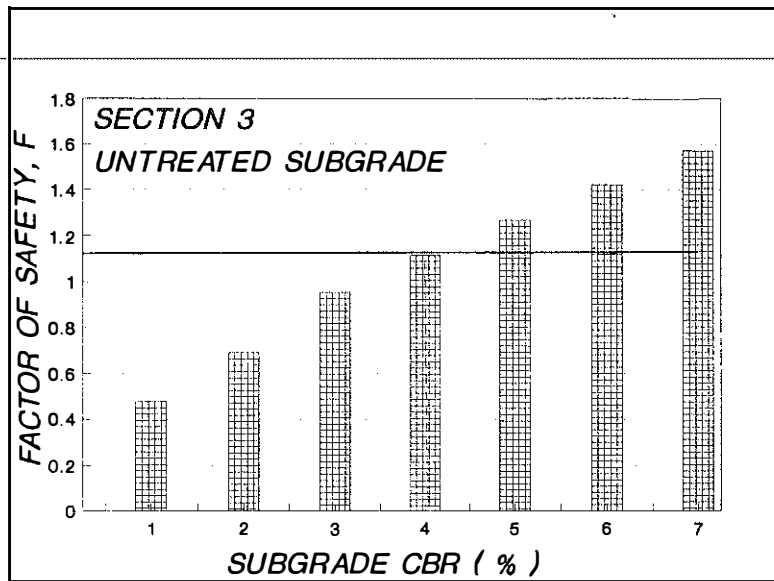


Figure 128. Factors of Safety of Section 3 Constructed on an Untreated Subgrade.

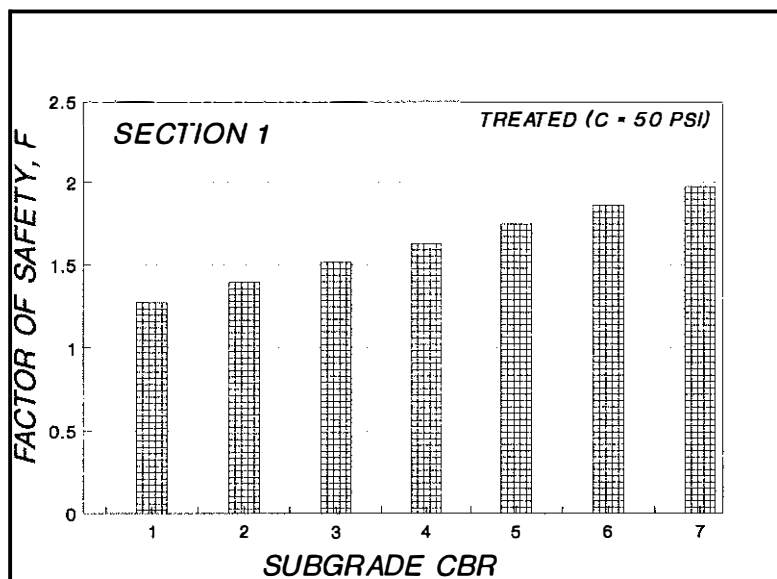


Figure 129. Factors of Safety of Section 1 and an Eight-Inch, Chemically-Treated Subgrade Layer.

concrete to 25 percent crushed stone; and 100 percent bituminous concrete -- "full-depth® asphalt" -- (only CBR curves ranging from 1 to nine are shown in this figure - other curves are shown elsewhere - Havens, et al, 1981).

The pavement design curves shown in Figure 132 were analyzed using the HOPKIB bearing capacity computer model. In the analyses, tire contact stresses were assumed to equal 80 psi. Total width of the

Analyses of Two Flexible Pavement Design Systems

1981 Kentucky Pavement Design Curves

To determine flexible pavement thickness, the method (Havens, et al, 1981) currently used in Kentucky (1991) makes use of design charts that relate equivalent axle loads (EAL's), the CBR value of the subgrade, and the modulus of elasticity of the bituminous concrete. The charts were formulated so that pavement structures could be selected based on alternative proportions of bituminous concrete and crushed stone base. A portion of a typical design chart currently in use in Kentucky is shown in Figure 132. This chart was formulated on the basis that one third of the total pavement thickness is bituminous concrete and two-thirds is crushed stone base. For example, if the EAL value is 10^7 repetitions and the CBR is equal to three, then the total pavement thickness is 30 inches. According to the chart in Figure 132, one third of the total thickness would be 10 inches of asphaltic concrete and two-thirds would be crushed stone base. Other charts shown in the 1981 design guide proportion the two components based on 50 percent bituminous concrete to 50 percent crushed stone; 75 percent bituminous

dual tires was assumed to be 25.5 inches. For a selected CBR value of the subgrade, values of EAL were selected from the range of EAL's (10^3 repetitions to 10^8 repetitions) represented by the x-axis of this design chart. For each selected value of EAL, and for a given CBR curve, an associated total pavement thickness was obtained from the y-axis in Figure 132. For example, using a selected value of EAL equal to 10^6 repetitions and a CBR value equal to two, the total pavement thickness is equal to 24.8 inches. Since these curves were developed on the basis that one third of the total pavement structure consists of bituminous concrete, the asphaltic concrete is about 8.3 inches. The crushed base is equal to 16.5 inches. To account for variation of shear strength with depth in the bituminous layer, the ϕ , c , and temperature relationships shown in Figures 91 and 92 were assumed. Additionally, a surface temperature of 140°F was assumed in the analyses. Distribution of the temperature with depth in the bituminous layer was computed according to the equation in Figure 109. Analyses were performed using CBR curves (and values) ranging from two to 12.

Factors of safety as a function of thicknesses obtained from the 1981 design chart for selected values of

EAL's and selected CBR values are shown in Figure 133. For small values of CBR (two through 6), the analyses show that certain thicknesses obtained from the 1981 design curves yield factors of safety that are equal to 1.0 or less -- that is, the pavements would fail under a dual-wheel tire stress of 80 psi. For example, an analysis of the CBR curve for two shown in Figure 132 yields factors of safety that range from about 0.3 to 1.07 for thicknesses ranging from about 6.0 inches to 23 inches and values of EAL ranging from 10^3 to 5×10^5 . For the CBR curve represented by the value of three, the factor of safety

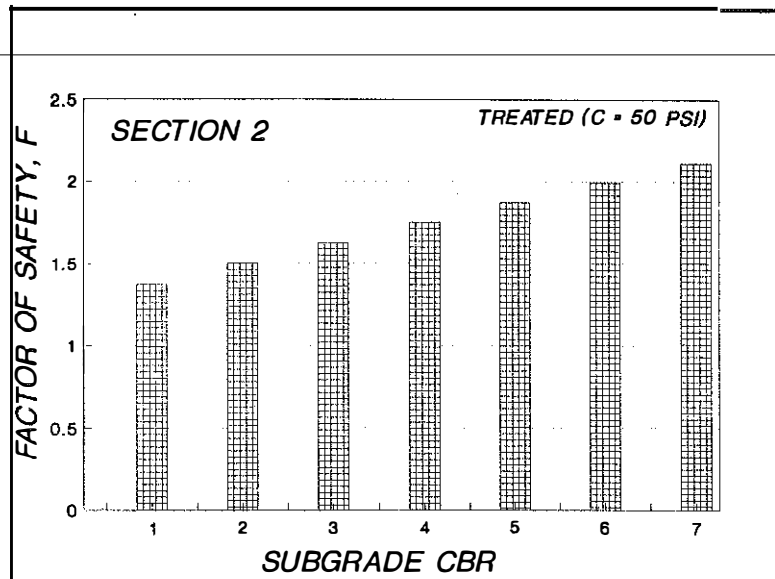


Figure 130. Factors of Safety of Section 2 and an Eight-Inch, Chemically Treated Subgrade Layer.

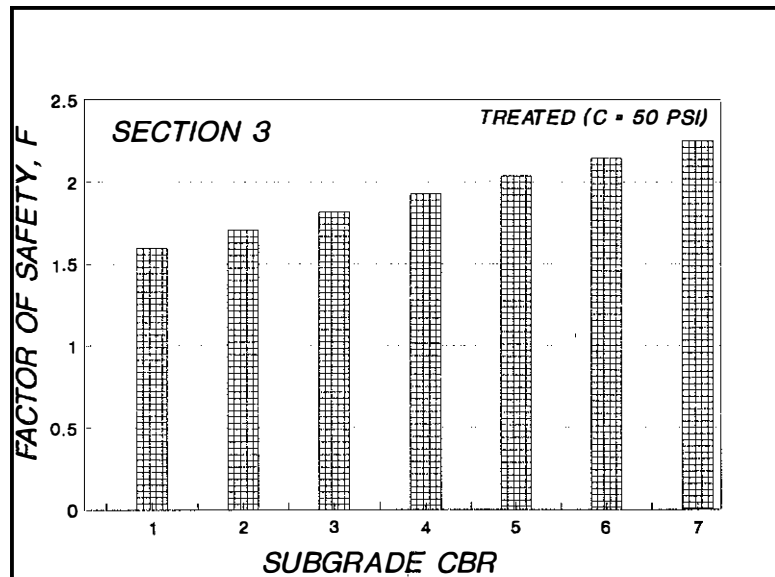


Figure 131. Factors of Safety of Section 3 and an Eight-Inch, Chemically Treated Subgrade Layer.

is equal to one or less for thicknesses ranging from about six to 17 inches. For thicknesses ranging from about 17 to 34, the factors of safety are only in a range of 1.0 to 1.6. As the tire contact stress increases, the situation becomes more critical. For example, the factor of safety for the CBR curve represented

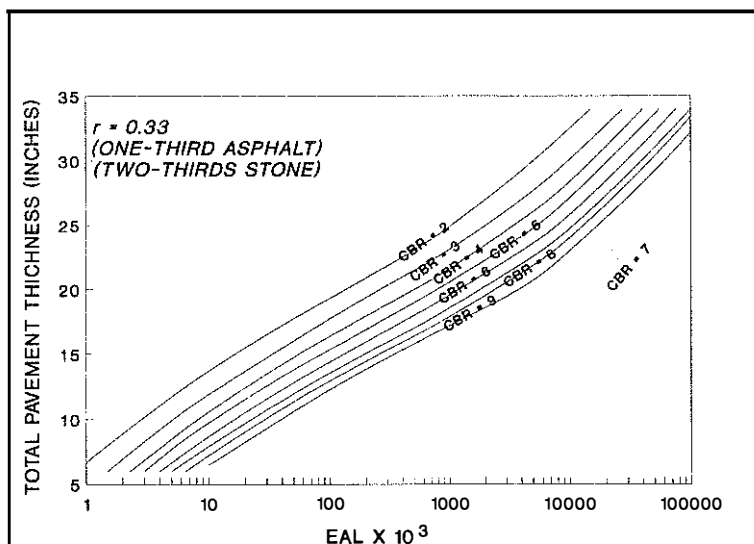


Figure 132. Examples of the 1981 KYCBR Curves Used in the Design of Flexible Pavements in Kentucky.

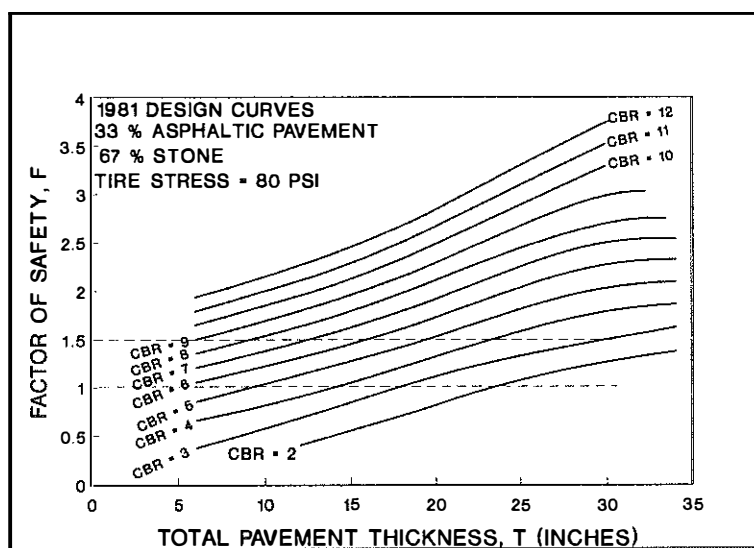


Figure 133. Factors of Safety Obtained from the HOPKIB Model as a Function of Total Pavement Thickness for CBR Values Ranging from 2 to 12.

Geologic Formation. Soaked CBR values of many of these materials have been shown to be less than or equal to three. These low-bearing materials are prevalent in northern Kentucky. There are many other

by the value of two is below 1.1, as shown on the previous page in Figure 134. In these analyses, a tire contact stress of 105 psi was used. Thicknesses range from six to about 34 inches. For thicknesses ranging from six to 23 inches, the factor of safety of the CBR curve represented by a value of three is equal to or less than 1.0. When the factor of safety is less than about 1.4 to 1.5, then serious pavement deflections, tire sinkage, or punching shear may occur. Normally, engineering structures are not built using design factors of safety less than about 1.5. Typically, factors of safety of 1.5 to 2.5 are used. Only when the CBR value of the subgrade is greater than nine is the factor of safety greater than 1.5 (Figure 133). As shown in Figure 10, some 40 percent (statistically) of Kentucky soils have soaked CBR values equal to or less than six. Based on an analysis of the Kentucky soils data bank, some 20 percent of Kentucky soils (statically) have soaked CBR values equal to or less than three as shown in Figure 135. If the design curves were used for very low-bearing soils (less than about three to 4), serious pavement problems may occur according to the results of analyses obtained from the HOPKIB bearing capacity model. This design situation is not trivial. Hundreds of miles of pavement have been constructed in northern Kentucky on subgrades of low-bearing residual soils and clayey shales of the Kope

large areas in Kentucky where hundreds of miles of pavement have been constructed on residual soils and clayey shales that have soaked CBR values of less than three to four, and, oftentimes these values are two and three. For example, residual soils and clayey shales of the Crab Orchard, Tradewater, Nada, New Providence, Nancy, Clayton-McNairy, Lower Caseyville, and Osgood Geologic Formations have soaked CBR values of six or less, (Hopkins 1985; Hopkins 1984; Hopkins 1983). Typically, the soaked CBR values are less than three. These geological formations cover vast areas of Kentucky.

Essentially, the 1981 design curves assume that there is a smooth relationship between the number of EAL repetitions and damage to the pavement. As shown in Figure 132 the total pavement thicknesses increase as the number of EAL repetitions increase. The concept on which these curves were developed recognizes that the pavement must be thicker as the repetitions increase in order to minimize damage (or accumulate damage). This concept may be valid. The results of analyses using the HOPKIB show that the magnitude of the applied wheel load is critical in

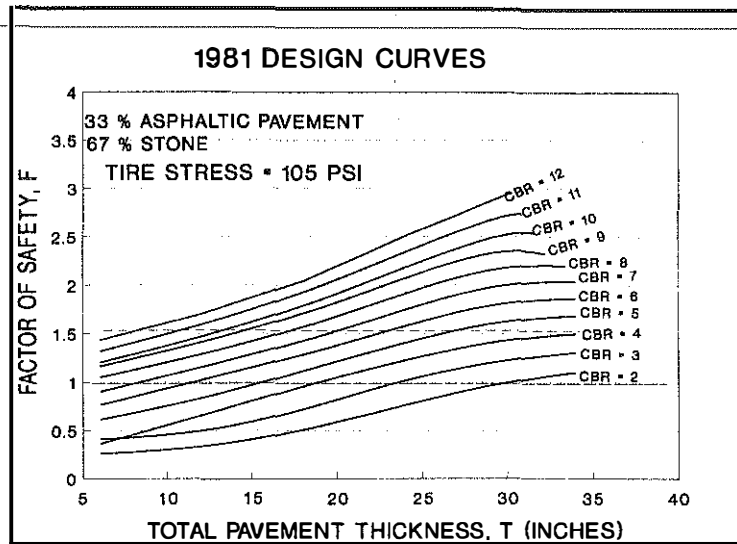


Figure 134. *Factor of Safety Obtained from the HOPKIB Model as a Function of Total Pavement Thickness for CBR Values Ranges from 2 to 12 and a Tire Contact Stress of 105 psi.*

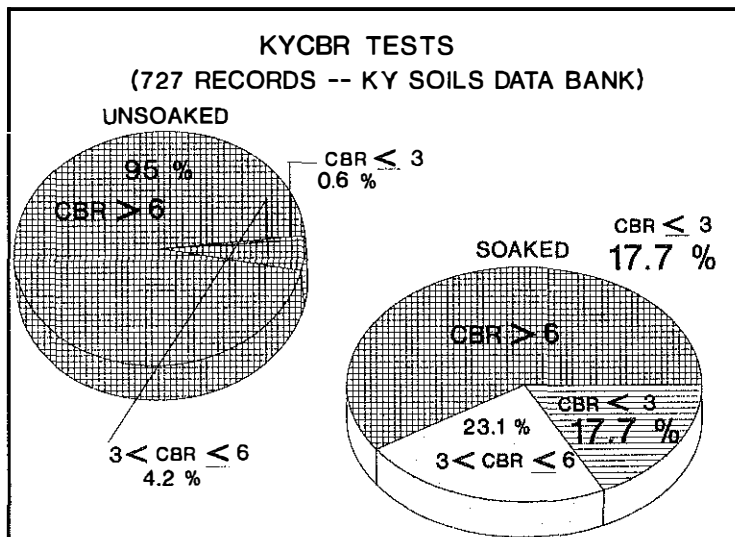


Figure 135. *Comparison of Unsoaked and Soaked Values of KYCBR and the Percentage of Soaked Values of KYCBR Equal to or Lower Than 3.*

pavements constructed on low-bearing subgrades. A threshold pavement thickness must exist to avoid complete failure of the pavement or to limit serious deformations. Theoretically, for a given subgrade value of CBR, only one wheel load of a given magnitude would be sufficient to crack, or cause collapse of the pavement when the pavement thickness is less than some threshold value. In this situation, the number of wheel-load repetitions is not important, but the amount of stress becomes a more important consideration. Threshold thicknesses may be obtained from the results of the analyses shown in Figure 133. These minimum (required) thicknesses for a selected factor of safety may be obtained from Figure 133 as a function

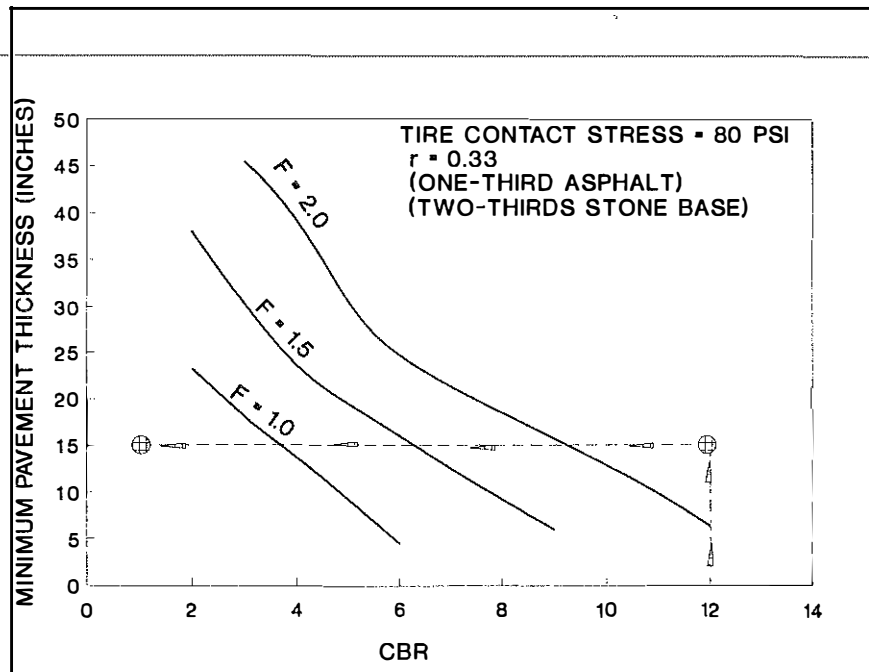


Figure 136. Minimum Pavement Thickness (One-Third Asphalt; Two-Thirds Granular Base) as a Function of CBR.

of subgrade CBR. Minimum (or threshold) pavement thicknesses as a function of subgrade CBR strength for selected safety factors of 1.0, 1.5, and 2.0 are shown in Figure 136. Any flexible pavement thickness design obtained from the 1981 Kentucky design curves should receive a critical review when the factor of safety is less than or equal to about 1.3, or the value of CBR is less than about six. It is recommended that a re-analysis of the proposed design be made using the HOPKIB bearing capacity computer program.

AASHTO Road Test -- Factors of Safety

In 1962, the American Association of State Highway Officials (AASHTO -- currently identified as AASHTO, or the American Association of Highway Transportation Officials) published the results of an extensive road test conducted at Urbana, Illinois during 1959 and 1960. Many trucks having various axle configurations and loads were driven continuously for several months over pavement sections of various thicknesses. Several pavement loops were constructed. Several loops contained sections of various combinations and thicknesses of asphaltic concrete, base material (crushed stone), and a subbase material (a sand-gravel mixture). Some 237 pavement sections occurring on loops 3, 4, 5, and six (lanes 1 and 2) were analyzed using the HOPKIB bearing capacity computer model.

The performances of the roadway sections at any given time were judged in terms of a present serviceability index. This index, defined as a measure of the pavement condition, depends on the surface roughness, cracking, and patching. The index ranges on an arbitrarily selected scale from zero to five. Asphaltic pavements generally had an initial index of about 4.2. When a pavement section reached a value of 1.5, the section was considered to be in a failure condition. Most often when the index decreased to 2.0, it decreased immediately to 1.5; the section was either taken out of the test, or an overlay pavement was constructed, and the testing of the section continued. The purposes of the HOPKIB model analyses were to gain an overview of the magnitudes of the factors of safety obtained for the various pavement sections and to determine the reasonableness of results obtained from the analyses. Most of the pavement sections essentially failed; that is, the serviceability index reached a value of 1.5. The exact nature of the failures was not described. About 89 percent of the sections analyzed reached a serviceability index of 1.5.

*Subgrade soils**Index properties*

Soils used to construct the subgrades at the AASHO Road Test (1962) site classified as A-6 or A-7-6 (group index ranged from nine to 13). Liquid limits and plasticity indices ranged from 27 to 32 percent and 11 to 15 percent, respectively. Particle-size analyses showed that about 80 to 85 percent of the soil was finer than the 200-mesh sieve. About 34 to 40 percent of the particles was finer than 0.005 mm. Maximum dry density of the soil ranged from 114 to 118 pounds per cubic foot, and optimum moisture content ranged from 14 to 16 percent. These values were determined from the standard compaction test -- AASHTO T-99.

Bearing strengths

During the spring and summer of 1960, in-situ CBR tests were conducted by the AASHO officials (Woods 1962). The tests were part of a trenching program performed at selected sites on loops 3, 4, 5, and 6. Woods noted that "a great deal of structural deterioration (of the pavements) took place in the spring months than during the summer months . . . the decrease in the indicated strength of the embankment soil during the spring months was not attributed to a decrease in its density, nor to an increase in its moisture content." According to Woods (Table 2 in TRB Special Report 73), the average CBR values of the subgrade soils of loops 3 through 6 was about 3.6 percent during the spring months of 1960 and 5.7 percent during the summer months of 1960. The CBR values for the spring months and those of the summer months of 1960 are compared in Figure 137. Although the differences in the two different seasonal groups of CBR values appear slight (Table 2 of TRB Report 73 -- Woods 1962), the differences, when viewed as shown in Figure 136, are significant. As shown in Figure 138, there is a significant relationship between moisture content and the CBR strength of the subgrade. As the moisture content of the subgrade increases, the CBR strength decreases. The relationship between CBR (spring months) and moisture content of the AASHO roadbed soils may be expressed as:

$$CBR = 74701.4 W_n^{(-3.662)} \quad (260)$$

The moisture contents of the soil subgrades as measured during the summer and spring months are compared in Figure 139. The moisture contents of the subgrade in the spring months were slightly higher than those measured in the summer months. Additionally, there was a significant relationship between values of CBR measured in the spring months and dry density as shown in Figure 140. This relationship may be expressed in the form

$$CBR = 545 - 9.946\gamma_d + 0.0456(\gamma_d)^2 \quad (261)$$

With a decrease in dry density of the subgrade, there is a significant decrease in bearing strength, or the value of CBR. Sufficient data were not found to determine if the soils swelled during the testing period. When soils swell, there is an increase in moisture content and a decrease in dry density and bearing strength. In-situ dry densities as a function of in-situ moisture content obtained from the trenching program are shown in Figure 141. Data in this figure show that at the time of the sampling program, the in-situ values generally would meet standard specifications used by most states.

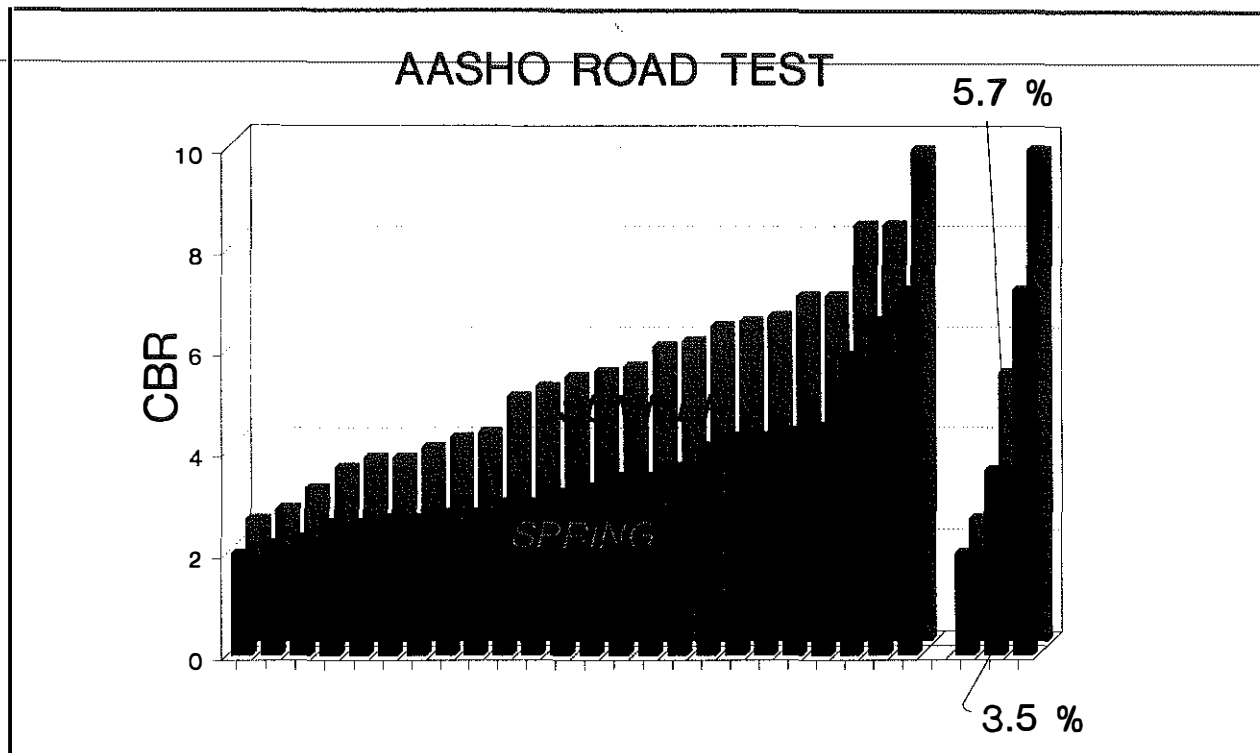


Figure 137. Comparison of Subgrade CBR Values Observed In the Summer of 1959 and the Spring of 1960 at the AASHO Road Test.

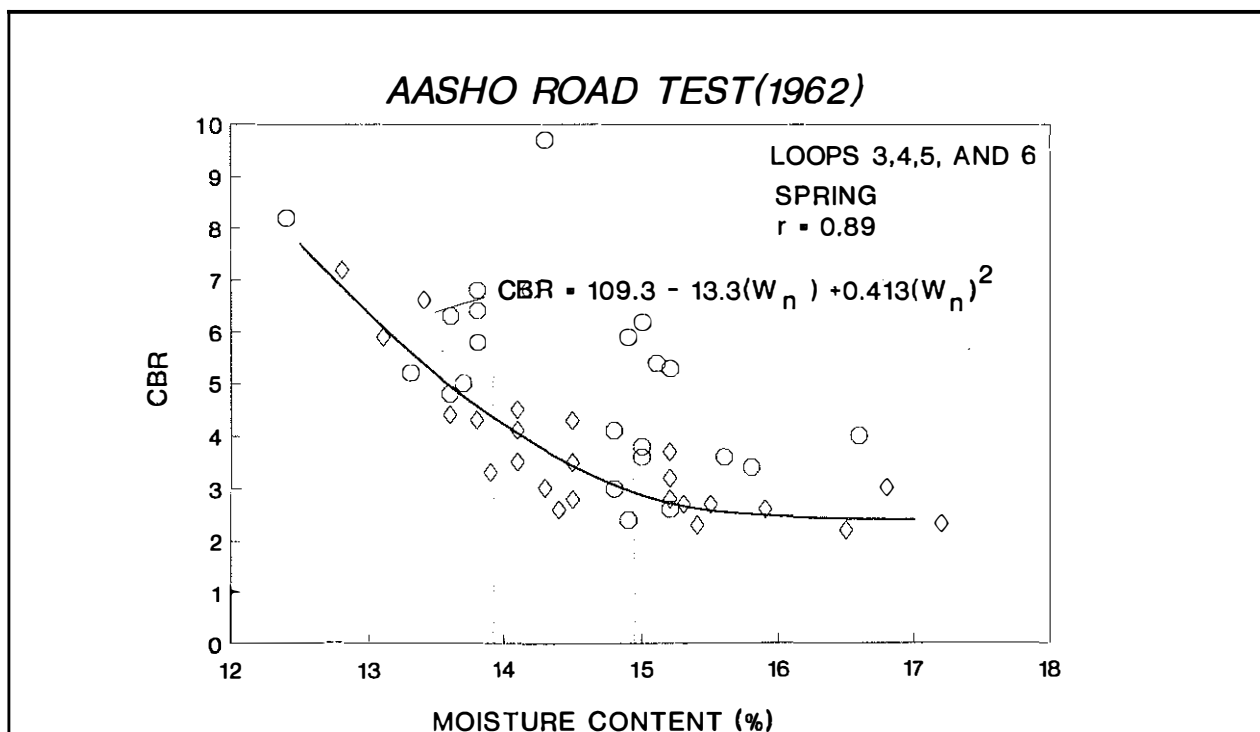


Figure 138. In-Situ CBR Values (Spring Months) of the AASHO Roadbed Soils as a Function of Moisture Contents.

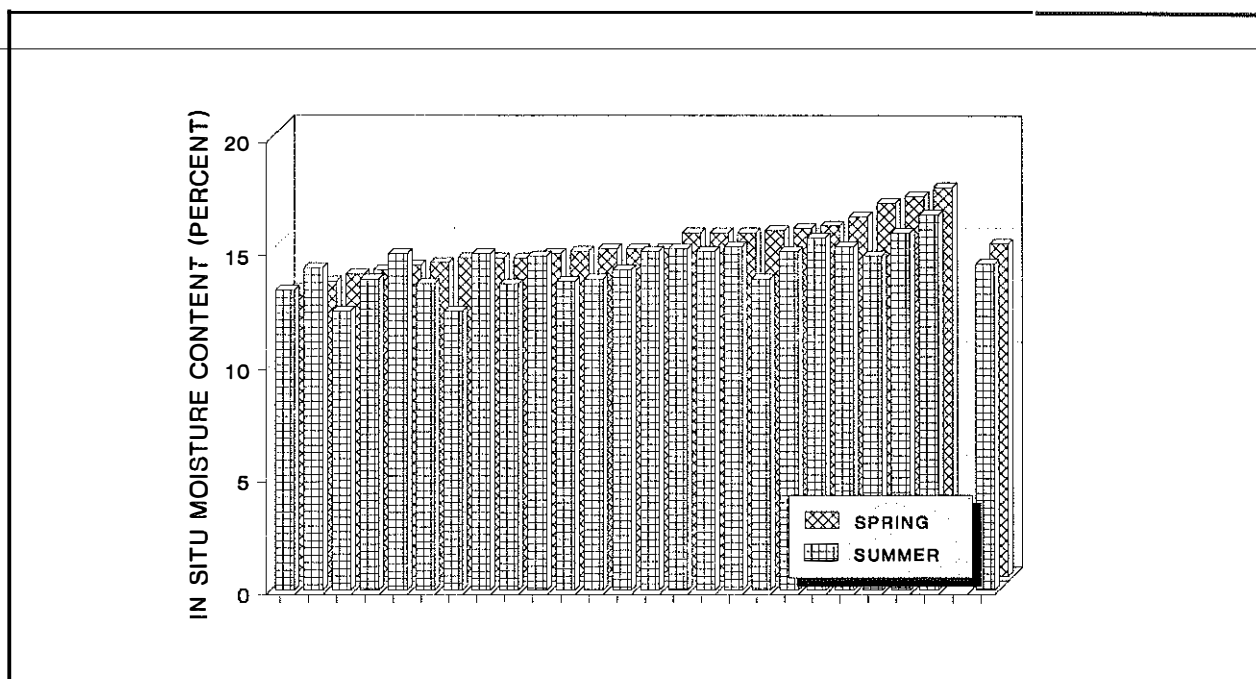


Figure 139. Comparison of In-Situ Moisture Contents Observed in the Summer of 1959 and the Spring of 1960.

Analyses and Results

Factors of safety

Pavement sections of loops 3, 4, 5, and 6 of the AASHO Road Test (1962) were analyzed using the HOPKIB bearing capacity computer program. Both lanes 1 and 2 of the loops were analyzed. In making the analyses, certain assumptions were required. First, the shear strengths of the asphaltic pavements of the sections were not available. An assumption was made that the shear strength behavior could be represented by the data given in Figures 91 and 92 and the relationships given by Equations 257 and 258. Although this assumption is not strictly correct, the effects on the results were considered small. Secondly, the ϕ and c values of the crushed stone base and the gravel-sand subbase were assumed to be 43°F and zero, respectively. Based on the nature and description of these materials, this appeared to be a reasonable assumption since these materials were compacted. The shear strengths of the soil subgrades were

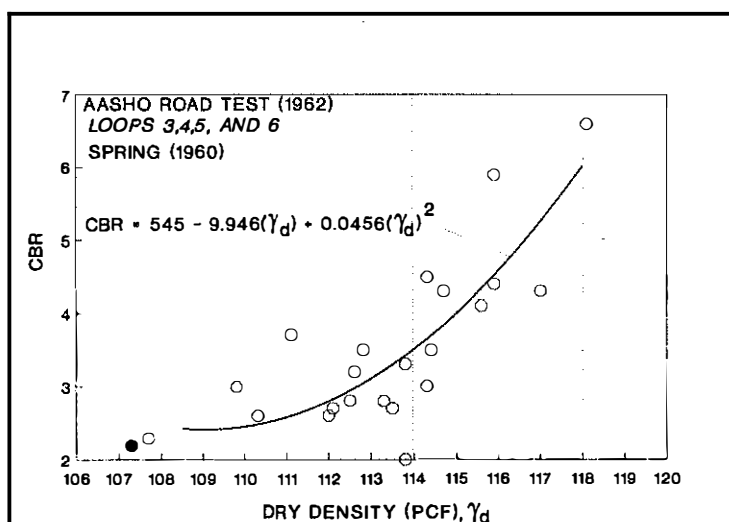


Figure 140. In-Situ CBR Values (Spring Months) of the AASHO Roadbed Soils as a Function of Dry Density.

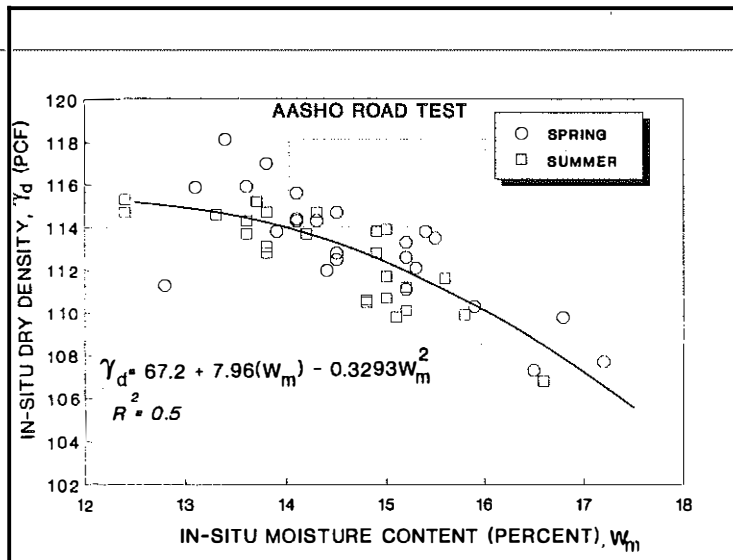


Figure 141. *In-Situ Dry Density of the AASHO Roadbed Soils as a Function of In-Situ Moisture Content.*

based on the CBR values (spring) reported by Woods (1962--Table 2 in his report). Using the lowest CBR values reported by Woods for each loop, the CBR values were converted to undrained shear strengths using the relationship shown in Figure 64.

The analyses were also performed using two different assumptions of pavement temperatures. In the first analysis, the surface temperature and the average air temperature were assumed to be 140 ° and 81 ° F, respectively. The distribution of temperatures with depth in these analyses were determined according to curves given by Southgate (1973). A second set of analyses of the loops was performed using a surface temperature

of 77 ° F. In these analyses, the temperatures were assumed to be 77 ° F throughout the full depths of asphalt pavements of the various sections of the loops. Representation of a typical problem (pavement section 599, loop 4, lane 1) for analysis is shown in Figure 142.

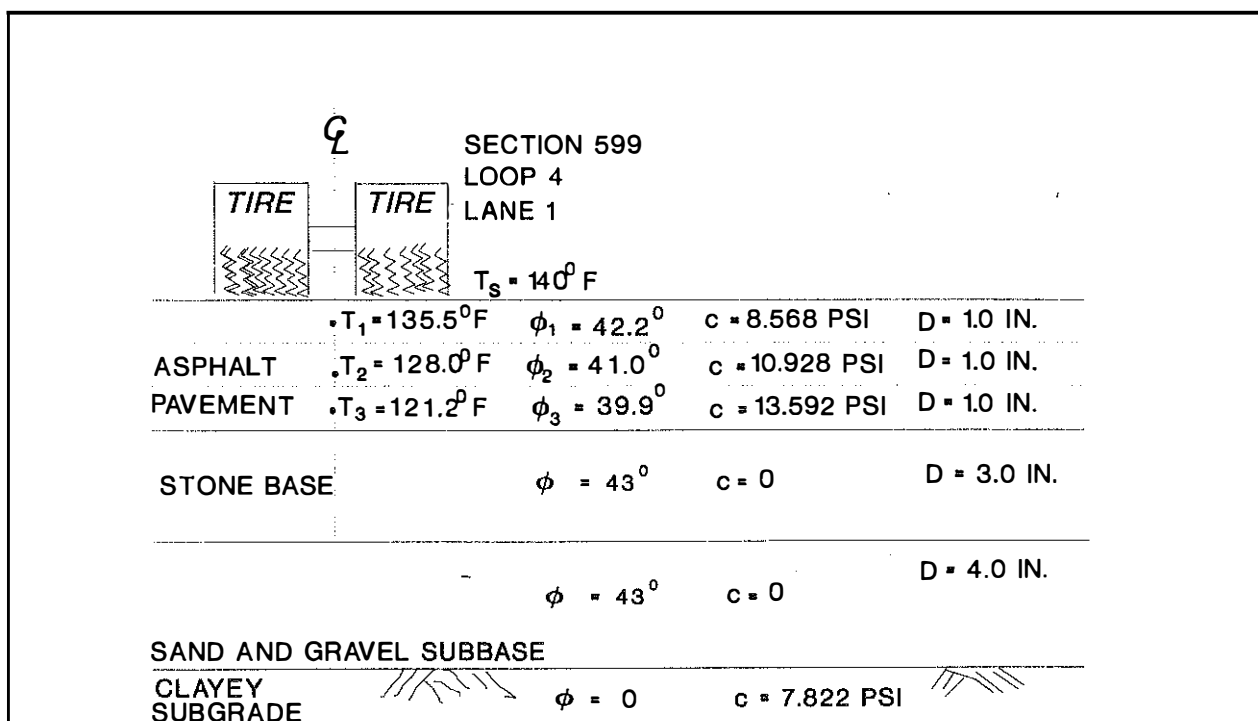


Figure 142. *Typical AASHO Road Test Pavement Section Illustrating the Setup of Parameters for Analysis.*

Factors of safety obtained for pavement sections of loops 3, 4, 5, and 6 are summarized in Tables 1 A through 8 A in APPENDIX A. Both lanes 1 and 2 of each loop were analyzed. These tables also show the loop number, section number, axle load, ground contact stress of the tires, CBR value of the soil subgrade, the number of load applications of a given load, total thickness of each pavement section as well as individual thicknesses of each layer of the pavement structure, two values of factors of safety for each pavement section, and weighted values (AASHO Road Test 1962, Report 61 E) of 18-kip equivalent single axle loads (ESAL). Sections subjected to axle loads of 12-kip (single axle), 24-kip (tandem axle), 18-kip (single axle), 32-kip (tandem), 22.4-kip (single axle), 40-kip (tandem), 30-kip (single), and 48-kip (tandem) were analyzed. The first set of values of the factors of safety shown in the tables for a given section is based on an assumed surface temperature of 140 ° F and an average air temperature of 81 ° F. The temperature at any given depth was determined from the graphs given by Southgate (1975). Shear strength parameters, ϕ and c , for a given depth and corresponding temperature were determined from Equations 257 and 258. The second set of values of the safety factors in the tables is based on the assumption that the temperature of the asphalt was 77 ° F for the full depth of each asphaltic pavement section. Factors of safety for all sections (based on a surface temperature of 140 ° F and an average air temperature of 81 ° F) ranged from 0.57 to 2.08. Some 237 pavement sections were analyzed.

In Figure 143, the factors of safety of the pavement sections are shown as a function of weighted 18-kip equivalent single-axle loads. The values of 18-kip equivalent single-axle loads correspond to a

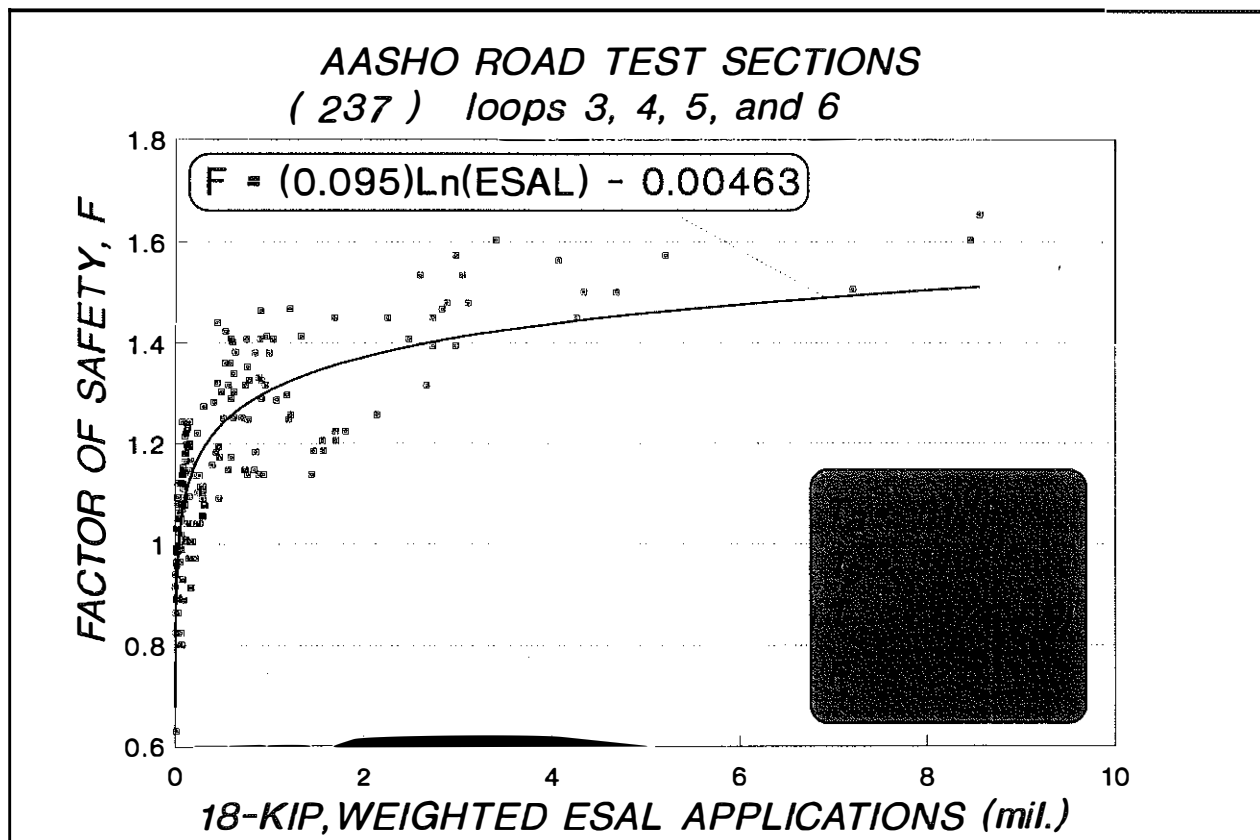


Figure 143. Factor of Safety as a Function of Weighted Equivalent Single-Axle Load Applications.

serviceability index, P_t , of 2.0. Factors of safety for some 26 pavement sections of a total of 237 sections are not shown in this figure because the serviceability index never reached a value of 2.0. The factors of safety of these 26 sections ranged from 1.19 to 2.00 and averaged 1.51. The ESAL values for those sections were greater than eight million. The relationship between the factor of safety and weighted, 18-kip equivalent single-axle load may be expressed as (for a surface temperature equal 140 ° F):

$$F = 0.095 \ln(ESAL) - 0.00463. \quad (262)$$

As shown in Figure 143, the slope of the factor of safety-ESAL curve rises sharply up to a factor of safety of about 1.3 and an ESAL value of one million. When the factor of safety is greater than 1.3, or the ESAL value is greater than about one million, the slope of the curve tends to flatten and approach a value of about 1.5 at an ESAL value of eight million. These data strongly imply that the minimum design factor of safety when the HOPKIB model is used should be about 1.3 for ESAL values up to one million. For ESAL values between about one million and eight million, the design factor of safety should be 1.3 to 1.5 or greater. When the factor of safety generally equaled or exceeded a value of 1.5, the pavement sections generally sustained an ESAL value greater than eight million; that is, the serviceability index did not drop to a value of 2.0 during the testing period at the AASHO Road Test. The use of a minimum design factor of safety 1.5 would appear to be adequate when using the HOPKIB model to design primary, parkway system, or interstate-type pavement structures where anticipated ESAL values may reach values larger than eight million. For pavement structures where anticipated values of ESAL's may range from one million to eight million, the minimum design values of factors of safety should be approximately 1.3 to 1.5. When the anticipated ESAL values are less than one million, the minimum factor of safety should be about 1.3 (intuitively, any type of engineering structure should not be designed for a factor of safety of less than about 1.3).

The curve shown in Figure 143 was based on a surface temperature of 140 ° F and an average air temperature of 81 ° F. As a means of examining the effect of temperature on the factor of safety, the analyses were repeated using a surface temperature of 77 ° F. However, this temperature was assumed to prevail throughout the depth of any given pavement section. Variation of the factor of safety and 18-kip equivalent single-axle load is shown in Figure 144. This relationship may be expressed as:

$$F = 0.464 + (0.0784) \ln(ESAL). \quad (263)$$

Decreasing the surface temperature of the asphalt pavement from a temperature of 140 ° F to 77 ° F causes a slight increase in the factor of safety. A factor of safety of 1.60 is obtained when an ESAL value of two million is inserted into Equation 263 (temperature throughout the depth of the asphalt pavement is assumed equal to 77 ° F). At a surface temperature of 140 ° F and average air temperature of 81 ° F (and if the temperature decreases with depth), a factor of safety of 1.33 is obtained from Equation 262. The difference in the factors of safety is about 0.27, or a difference of about 17 percent. Curves obtained from Equations 262 and 263 are compared in Figure 145. To determine the total pavement thickness required to sustain a given value of ESAL's and factor of safety, an analysis was

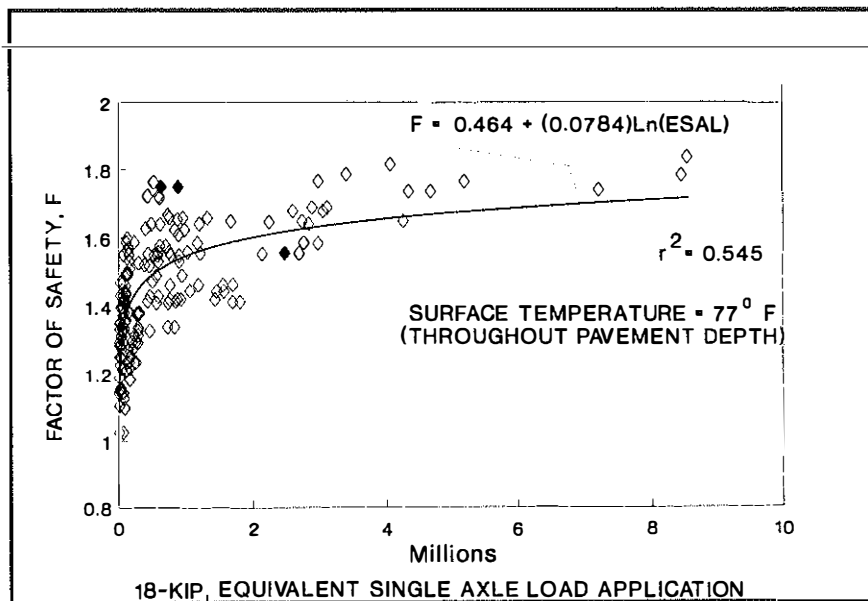


Figure 144. Factor of Safety Obtained from the HOPKIB Model as a Function of Weighted, ESAL Values Assuming the Temperature of the Pavement is 77°F Throughout.

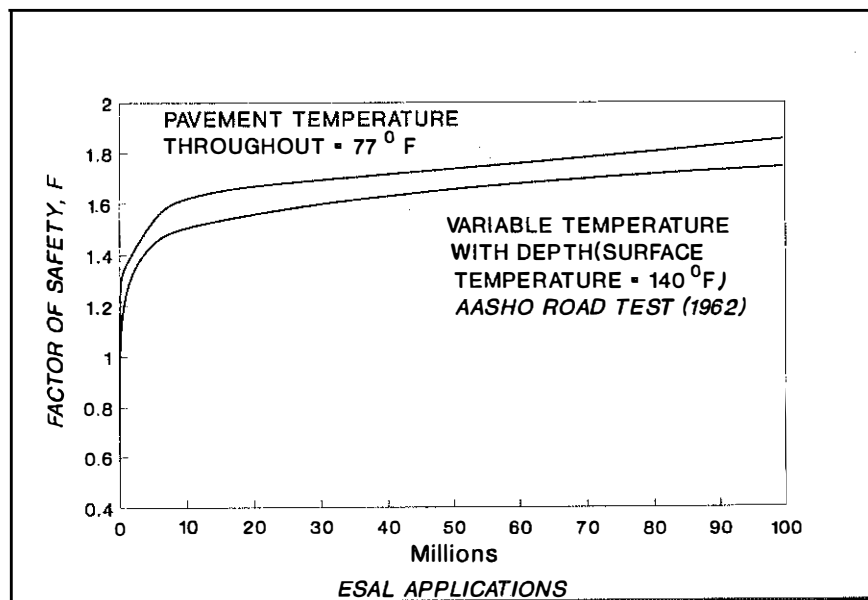


Figure 145. Comparison of Factor of Safety - ESAL Curves Assuming Two Different Temperatures.

$$T_p = 28.01(F) - 3.568(F)^2 - 12.737. \quad (264)$$

To obtain a factor of safety of 1.3, the total pavement thickness (based on the assumption that one third of the total pavement thickness is asphaltic concrete and two-thirds of the total thickness is a crushed stone base) must be about 17.7 inches for a CBR value of 3.6. There are many instances where

performed using an average CBR of 3.6, as determined from the spring trenching program at the road test site (loops 3 through 6), and a tire contact stress of 67.5 psi. For a given value of ESAL, the factor of safety was determined from Equation 262. Using the HOPKIB model, the factor of safety was computed for an assumed pavement thickness. In these analyses, the total pavement thickness was assumed to consist of one third of asphaltic concrete and two-thirds of crushed stone base. If the computed factor of safety did not equal the factor of safety computed from Equation 262 -- which corresponded to a selected value of ESAL -- a new pavement thickness was assumed, and the analysis was repeated. Iteration in this fashion was continued until the computed factor of safety was equal to the factor of safety obtained from Equation 262. Total pavement thickness, T_p , for the above cited conditions as a function of factor of safety is shown in Figure 146. This relationship may be expressed in the form:

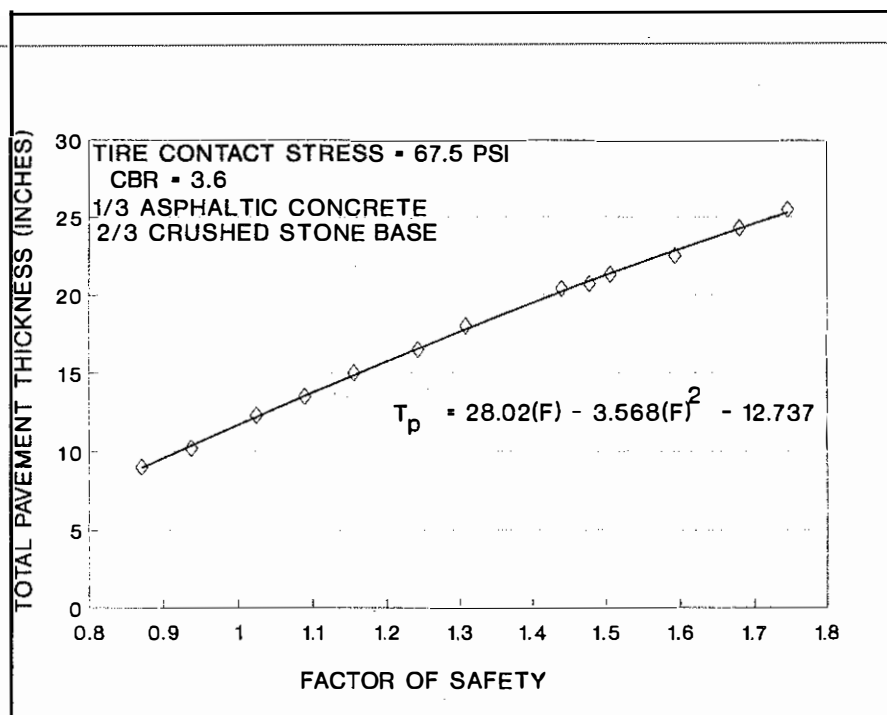


Figure 146. Pavement Thickness (One-Third Asphalt; Two-Thirds Granular Base) as a Function of the Factor of Safety.

residential roadways are much thinner than 18 inches and these roadways are constructed on soils having CBR strengths of 3.6 or less. For example, in some metropolitan areas of the state of Kentucky, pavement thicknesses of 11 or 12 inches are commonly constructed on low bearing soils -- CBR values equal to 3.6 or less. For such conditions, the factor of safety is near 1.0 or less as shown in Figure 146. Although the anticipated ESAL values of such roadways are less than about 100,000, the HOPKIB analyses show that pavement thicknesses of 11 or 12 inches are

inadequate and susceptible to failure (cracking and rutting) -- especially if the pavement is subjected to tire contact stresses greater than 67.5 psi.

The data (surface temperature equals 140 ° F) displayed in Tables 1A through 8 A in APPENDIX A may be illustrated in another form as shown in Figures 147 through 152. The ESAL values were sorted in an ascending order and grouped (arbitrarily) as shown in the upper graph of each figure. In the lower graph of each of these figures, the individual factor of safety of each pavement section corresponding to each value of ESAL of each group is shown in the lower graph. The average factor of safety of each ESAL group, as well as the range of ESAL values for each group, is shown in each figure.

The ESAL group and average factor of safety are as follows:

ESAL GROUP	AVERAGE FACTOR OF SAFETY
< 50,000	0.95
50,000 - 200,000	1.08
200,000 - 500,000	1.14
500,000 - 1 million	1.30
1 million - 8 million	1.40
> 8 million	1.51

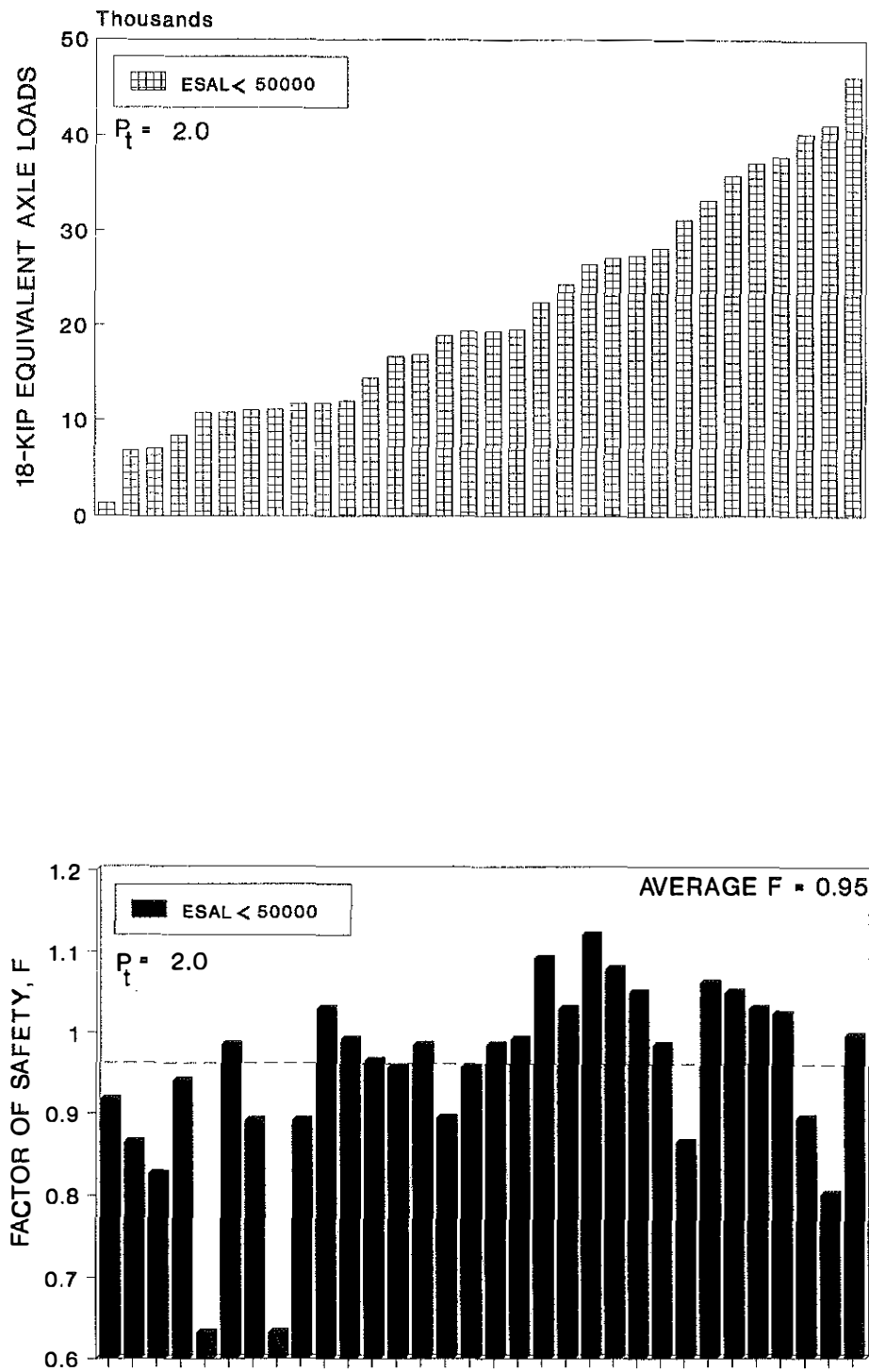


Figure 147. Factors of Safety for Values of ESAL Less Than 50,000.

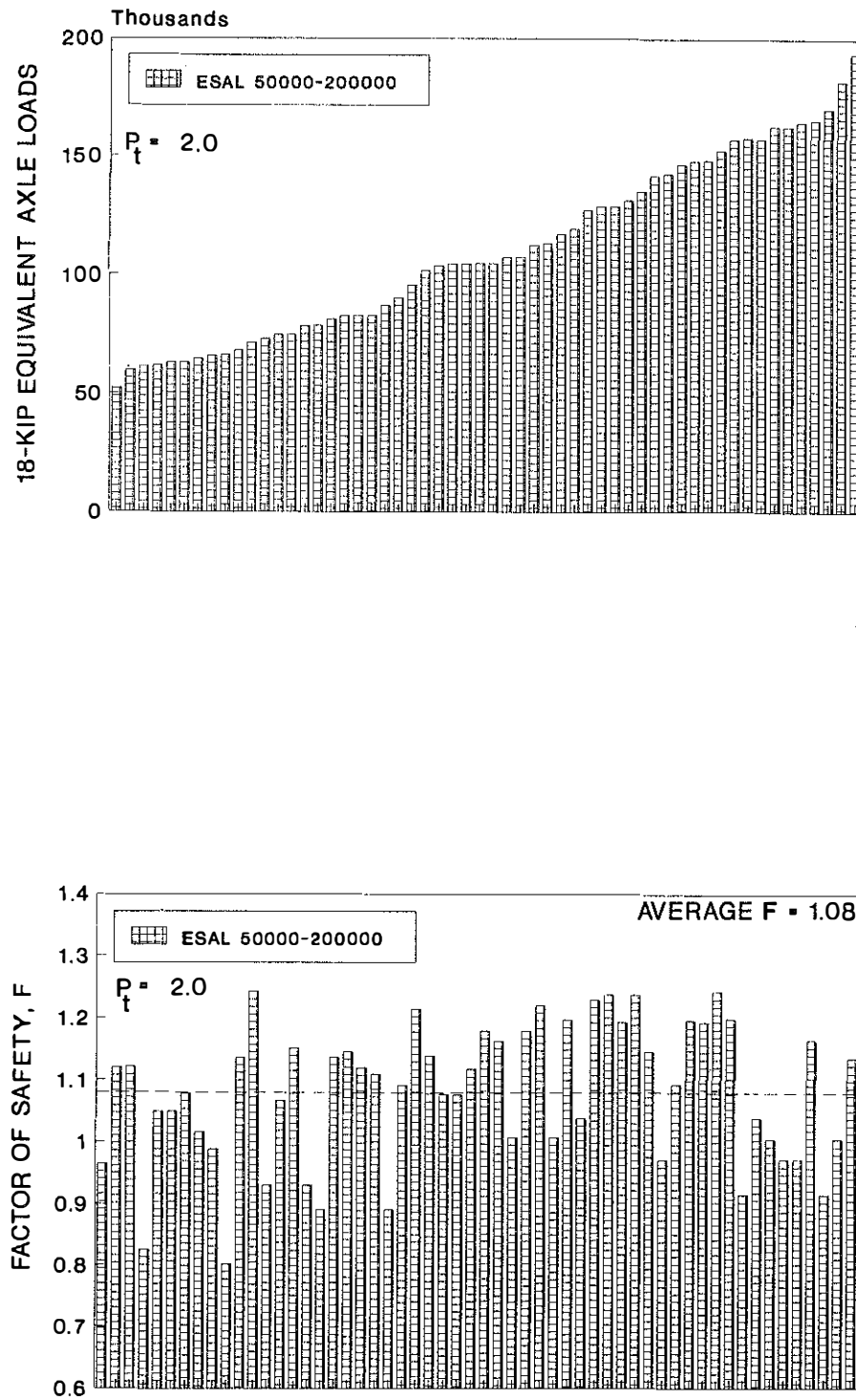


Figure 148. Factors of Safety for Values of ESAL Between 50,000 and 200,000.

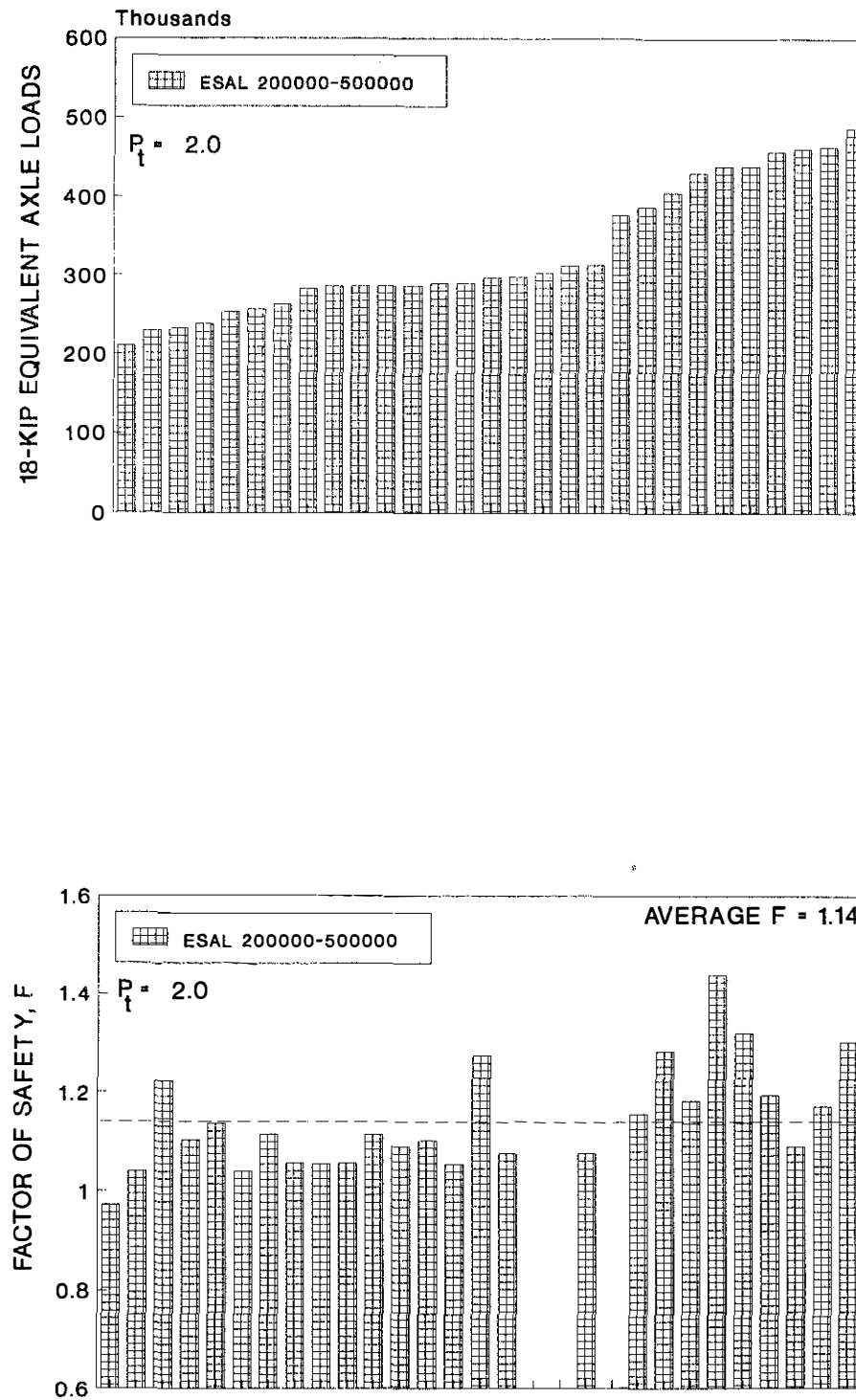


Figure 149. Factors of Safety for Values of ESAL Ranging from 200,000 to 500,000.

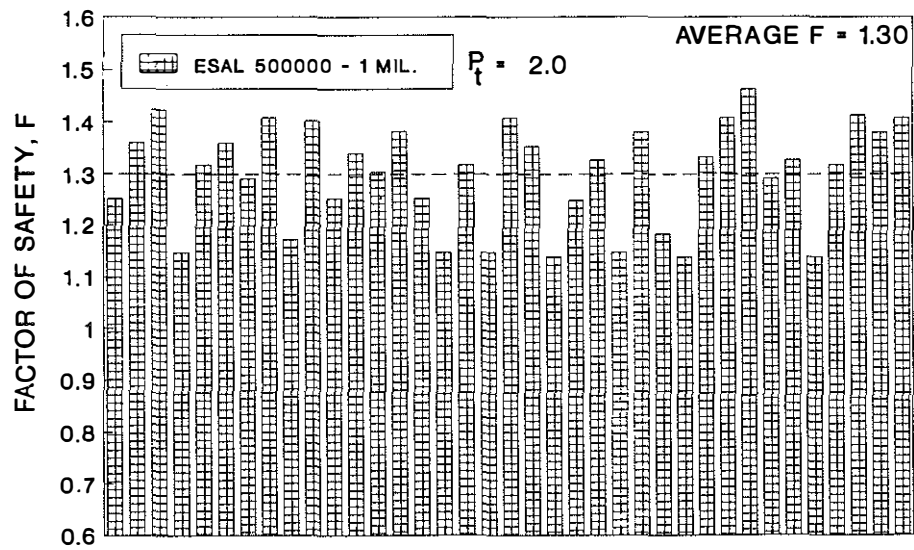
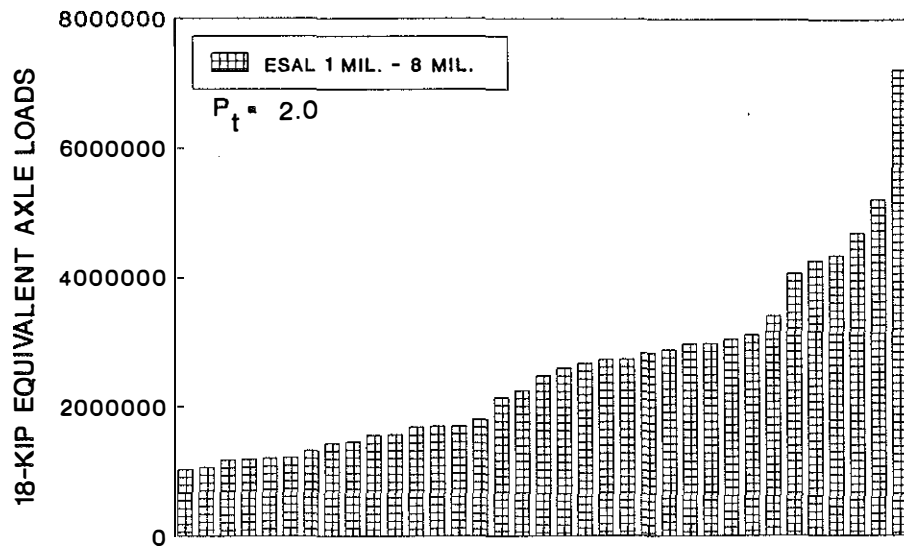


Figure 150. Factors of Safety for Values of ESAL Ranging from 500,000 to 1 Million.

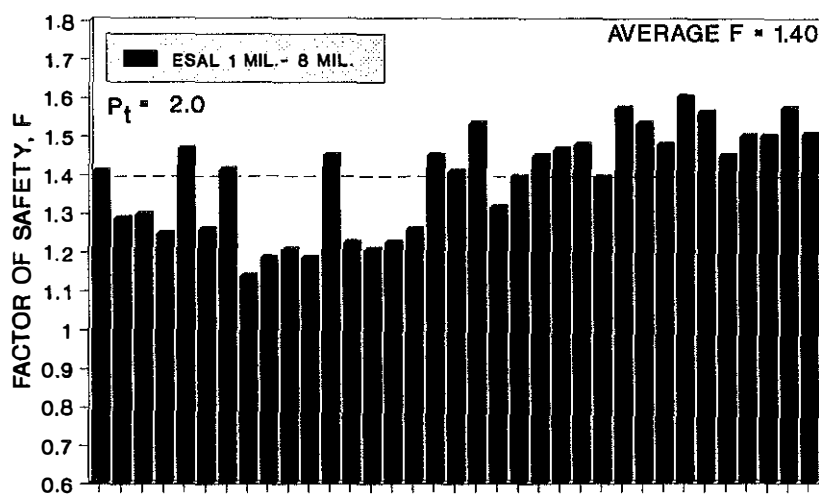
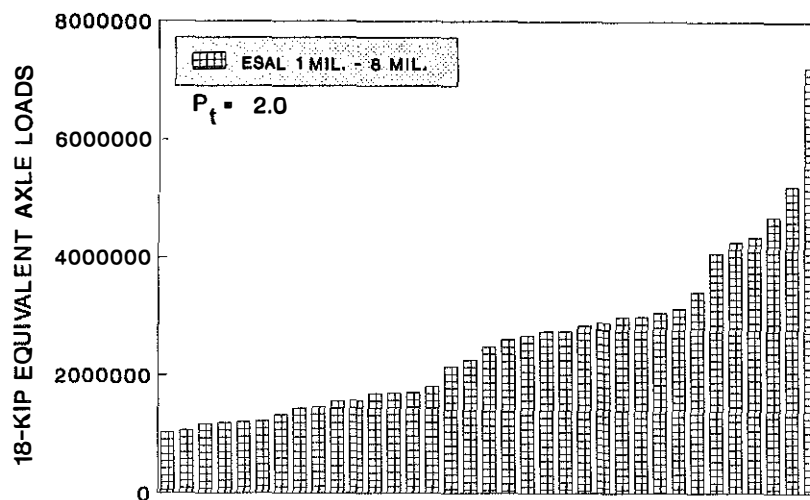


Figure 151. Factors of Safety for Values of ESAL Ranging from 1 Million to 8 Million.

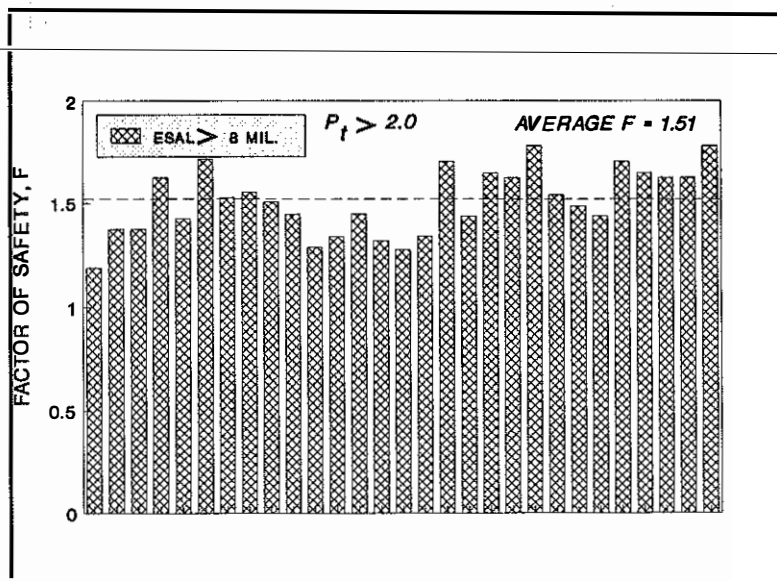


Figure 152. Factors of Safety for Sections that Remained for the Duration of the AASHO Road Test.

expressed in the form

$$ESAL = 11.218e^{(6.953F)} \quad (265)$$

For a temperature of 77 ° F, the relationship is

$$ESAL = 60.722e^{(7.0372F)} \quad (266)$$

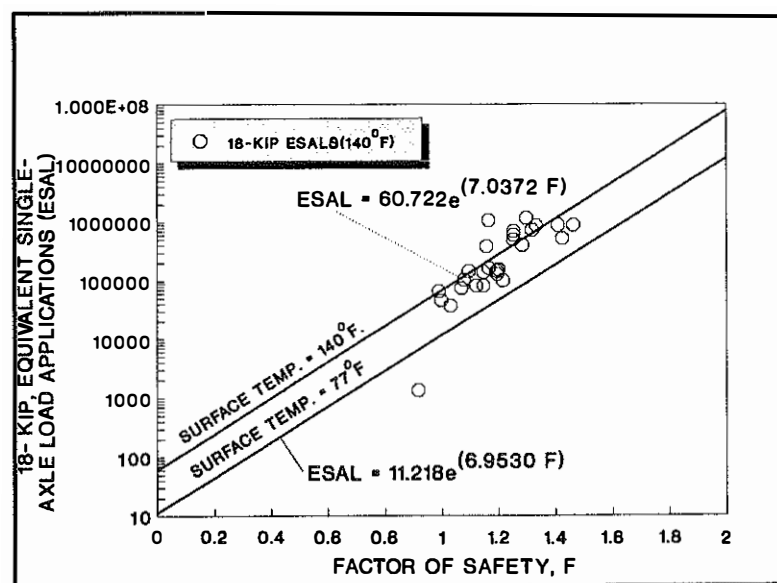


Figure 153. Relationships Between Values of Equivalent Single-Axle Load Applications and Factors of Safety for Two Different Pavement Temperatures.

Influence of the magnitude of contact tire stresses

Unit tire contact stress of all loads of loops 3 through 6 used in the AASHO Road Test (1962) was about 68 psi. Relationships between the factor of safety obtained from the HOPKIB computer program for all pavement sections and weighted values of equivalent single-axle loads (ESAL's) were shown in Figures 143 and 144. In Figure 153, the regression analysis is shown where the value of ESAL for loops 3 through 6 is treated as the dependent variable and the factor of safety is treated as the independent variable. This relationship (surface temperature equals 140 ° F) may be

The two curves are compared in Figure 153. To determine the effect and significance of changing the unit tire contact stress on the factor of safety and value of ESAL, analyses were performed using the pavement sections of lane 1 of loop 4. The axle load (single) used on these pavement sections was 18-kip. The unit contact stress was 67.5 psi. Factors of safety obtained from the HOPKIB model based on the 67.5 psi and surface temperature of 140 ° F are shown in Figure 154 as a function of (weighted) values of ESAL ($P_t = 2.0$) observed in the Road Test (since 18-kip loads were used on lane 1, loop 4, then the weighing

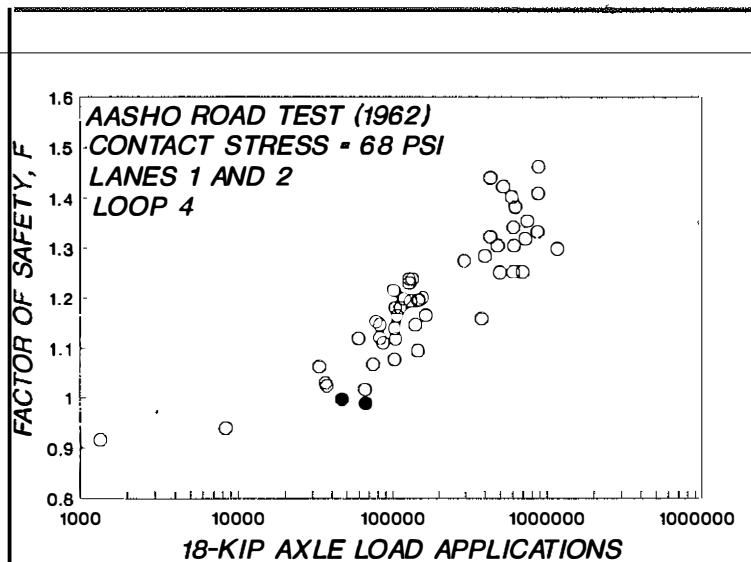


Figure 154. Values of ESAL from the AASHO Road Test as a Function of Factor of Safety.

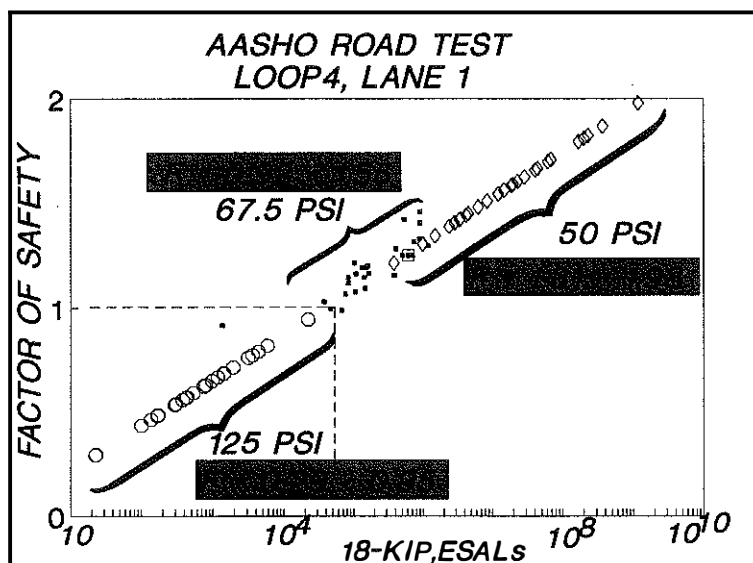


Figure 155. Effects of Unit Ground Contact Tire Stresses on the Values of ESAL.

factor is 1.0). These data points are identified in Figure 154. Pavement sections of lane 1 of loop 4 were also analyzed using unit tire contact stresses of 50 psi and 125 psi.

When the contact stress is reduced from 67.5 psi to 50 psi (about 25 percent), the factors of safety of the pavement sections of lane 1, loop 4, increase from a range of 0.92 - 1.55 to a range of 1.31 - 1.98, respectively. When the unit tire contact stress increases from 67.5 psi to 125 psi, the factors of safety decrease from a range of 0.92 - 1.55 to a range of 0.29 - 0.95. If the contact stress decreases from 67.5 psi to 50 psi (or lower values) the factor of safety increases and the values of ESAL increase. The pavement sections subjected to contact stresses of 50 psi would sustain larger values of ESAL (before reaching a serviceability index of 2.0) than values of ESAL corresponding to a unit contact stress of 67.5 psi. This appears logical since the factors of safety corresponding to 50 psi are larger than those obtained for the unit contact stress of 67.5 psi. Conversely, if the unit contact stress increases from 67.5 psi to 125 psi (or higher values), then the factors of safety decrease, and the value of ESAL could be expected to decrease. These two conditions are illustrated in Figure 155. By inserting factors of safety obtained from the analyses using 50

psi and 125 psi into Equation 265, new estimated values of ESAL may be obtained. As shown in Figure 155, when the contact stress is reduced from 67.5 psi to 50 psi the values of ESAL (diamond-shaped points) increase significantly and become much larger than ESAL values recorded for 67.5 psi. Consequentially, when the contact stress is increased from 67.5 to 125 psi, the values of ESAL (circle points) are decreased significantly and are much lower than values of ESAL recorded at the AASHO Road Test for 67.5 psi (lane 1, loop 4). For this case, the analyses show that all sections of lane 1, loop 4 would have failed rapidly. Decreasing the tire contact stress from 67.5 psi significantly increases the

life of a pavement, while increasing the tire contact stress above 67.5 psi significantly reduces the pavement life. The gross load, or weight of large vehicles, is not necessarily the most important factor when considering the effects of large vehicles on pavements, but rather the unit tire contact stress appears to be the most significant factor. Studies are needed to determine unit tire contact stresses of current vehicles since these tire stresses may have changed significantly from tire stresses that existed in 1962. Major increases in these stresses may cause major damage to existing highways.

AASHTO Road Test Equation -- Flexible Pavement

The general AASHTO Road Test equation (1962) has been published in the following form:

$$\log W' = 9.36 \log(SN+1) - 0.20 + \frac{G}{0.40 + \frac{1,094}{(SN+1)^{0.519}}}, \quad (267)$$

where

W' = weighted (the number of seasonal load applications multiplied by a seasonal weighing function) traffic factor, and

$$SN = \text{structural number} = a_1 D_1 + a_2 D_2 + a_3 D_3, \quad (268)$$

where

a_1, a_2, a_3 = coefficients determined in the AASHTO Road Test,
 D_1 = thickness of bituminous surface course (in inches),
 D_2 = thickness of base course (in inches),
 D_3 = thickness of subbase (in inches), and
 G = a function (the logarithm) of the ratio of loss in serviceability at any time (during the life of the pavement) to the total potential loss taken to a point where p equals 1.5.

The term G was defined mathematically as:

$$G + \log \left(\frac{c_o - P}{c_o - c_1} \right) = \beta (\log w - \log p), \quad (269)$$

where

β = a function of design and load variables that influences the shape of the p vs. W serviceability curve,

G = a function of design and load variables that denotes the expected number of axle-load applications to a serviceability index of 1.5,

c_o = initial serviceability value, and

P = serviceability at a given time.

Let

$$D_3 = 0, \quad (270)$$

$$D_2 = T - D_1, \text{ and} \quad (271)$$

$$D_1 = r T. \quad (272)$$

Substituting the latter two relationships into Equation 268, then

$$SN = a_1 r T + a_2 (T - D_1) \quad (273)$$

$$= a_1 r T + a_2 (T - r T) \quad (274)$$

$$= T(a_1 r + a_2 - a_2 r), \quad (275)$$

and solving for T :

$$T = \frac{SN}{r(a_1 - a_2) + a_2}. \quad (276)$$

For a selected value of r , the total pavement thickness may be determined. For example, let

$$a_1 = 0.44,$$

$$a_2 = 0.14, \text{ and}$$

$$r = 0.33 \text{ (selected arbitrarily)}$$

$$ESAL = W' = 75,000 \text{ (for a 20-year pavement life).}$$

Solving Equation 267 by iteration using a spreadsheet type of computer program, the calculated value of SN is about 2.524. Substituting this value into Equation 276,

$$T = \frac{2.524}{0.33(0.44 - 0.14) + 0.14} = 10.56 \text{ inches.} \quad (277)$$

From Equation 272,

$$D_1 = 0.33(10.56) = 3.52 \text{ inches, and} \quad (278)$$

$$D_2 = 10.56 - 3.52 = 7.04 \text{ inches.} \quad (279)$$

Using selected values of r equal to 0.33, 0.5, 0.75, and 1.00 and a wide range of ESAL values, pavement thicknesses were computed. Factors of safety of each of the computed thicknesses were determined from the HOPKIB model. The results are shown in Figure 156 where the variation of the factor of safety is shown as a function of total pavement thickness and the ratio, r . These data show that in cases where small values of ESAL ($< \approx 100,000$) are anticipated and where the CBR value of the subgrade is small (in this case the CBR value is equal to 3.5 – the same overall value of the AASHTO Roadbed soils), factors of safety are near a value of 1.0, or lower. That is, the stability of the pavement is marginal. For the example cited, the factor of safety is about 0.92 -- a failure condition. Most engineering structures would normally not be designed using a factor of less than one. Normally, the smallest, acceptable design factor of safety would be 1.25 or 1.30. The minimum total pavement thickness (for $r = 0.33$) corresponding to a minimum factor of safety for this case would be 17 inches -- about 5.5 inches of bituminous concrete resting on about 11.5 inches of crushed stone base. Based on Equation 262, this pavement design would accommodate an ESAL value of 540,000. Although this value of ESAL is larger than the estimated value of 75,000, the factor of safety of 1.25 is sufficiently larger than 0.92. Failure of the pavement should not occur. The analyses indicated that to provide good stability, the factor of safety must be greater than 1.0 regardless of the estimated value of ESAL. For a design factor of safety of 1.25, the pavement thicknesses corresponding to r values of 0.5, 0.75, and 1.0 ("full-depth" bituminous concrete) are 13.6 inches, 10.4, and 8 inches, respectively. In any of these cases, difficulties would be encountered in constructing the first layer lift of pavement on a subgrade with a CBR-strength of 3.5.

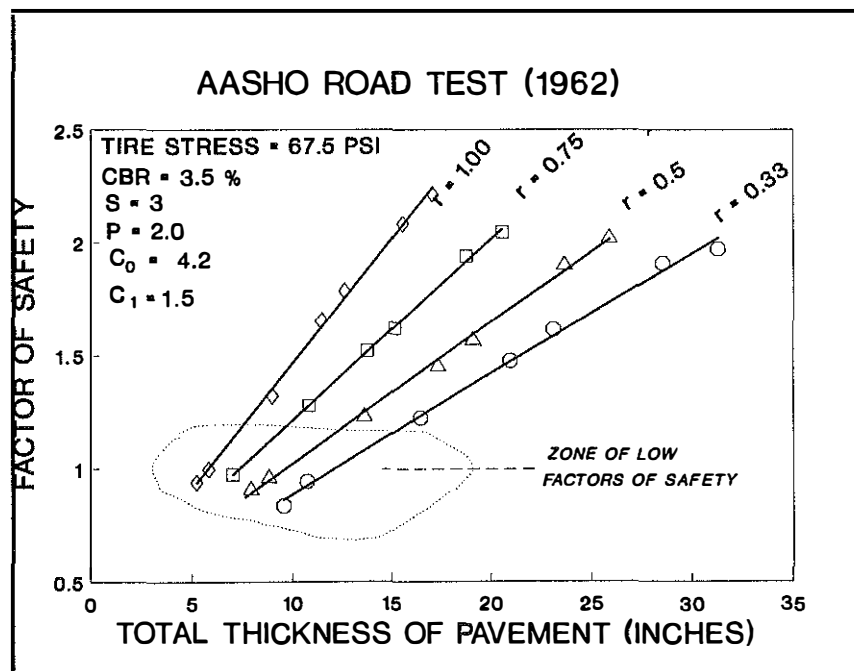


Figure 156. Factor of Safety as a Function of Total Pavement Thickness and Different Proportions of Asphalt and Granular Base.

Sensitivity of Stability to Changes in Subgrade Bearing Strength

As shown in Figure 137 and according to values published by Woods (1962), the CBR strengths of the AASHO Roadbed soils averaged about 3.6 during the spring months of 1960 and about 5.7 during the summer months. Factors of safety obtained for pavement sections of lane 1, loop 4 for a CBR value of 3.6 is compared in Figure 157 to factors of safety obtained from analyses of the same pavement sections using a CBR value of 5.7. Increasing the CBR value of the soil subgrade from 3.7 to 5.7 causes a significant increase in the factors of safety of the pavement sections of lane 1, loop 4. With an increase in the factors of safety, there is a significant increase in the values of ESAL that the pavement could sustain. By inserting the factors of safety obtained from an analysis of the pavement sections resting on a subgrade of a CBR strength of 5.7 into Equation 262, predicted values of ESAL may be obtained. Actual values of ESALs observed on lane 1, loop 4 (based on a CBR value of 3.6) are compared to estimated values of ESAL obtained from the analysis using a CBR value of 5.7 in Figure 158. If the subgrade soils had remained at a value of 5.7, the (estimated) ESAL values (shown as a function of factors of safety obtained when the subgrade averaged a CBR value of 5.7) ranged from one million to values over 100 million ($P_t = 2.0$). The actual values of ESAL ranged from 1,348 to 893,305 ($P_t = 2.0$). As shown in Figure 159, 73 percent of the pavement sections failed (that is, P equals 1.5) during the spring months (March, April, and May) when the CBR value averaged 3.6. One failure occurred in February (winter month). If two sections are excluded, then the total pavement thicknesses of the sections that failed during the spring months were generally equal to or less than about 17 inches. Generally, the thicknesses were less than 15 inches. As shown in Figure 159, six sections did not fail during the full duration of the testing period; that is, P_t was greater than 1.5. Total pavement thicknesses of those sections ranged from 18 to 23 inches.

Critical Design Choices

In the design of pavements and subgrades, certain questions or issues arise:

- How should the design strength, such as CBR or elastic moduli, of the subgrade be selected?
- What minimum strength of the subgrade is required to prevent failure of the subgrade during construction and to allow construction to proceed efficiently? When is subgrade stabilization or modification required?
- If subgrade modification is needed, then should the treated subgrade be considered merely as a working platform and given no structural credit in the composite pavement design, or should structural credit be given to the treated subgrade and be included in the design of the composite pavement?

These questions are discussed below.

Selection of Subgrade Strength

In a given highway corridor, different types of soils having different bearing strengths may exist. Different philosophies abound concerning the method of selecting the subgrade design CBR value (or other types of design strength parameters, such as resilient modulus, R values, shear strength, soil support, and modulus of subgrade reaction). Many correlations exist among these different parameters.

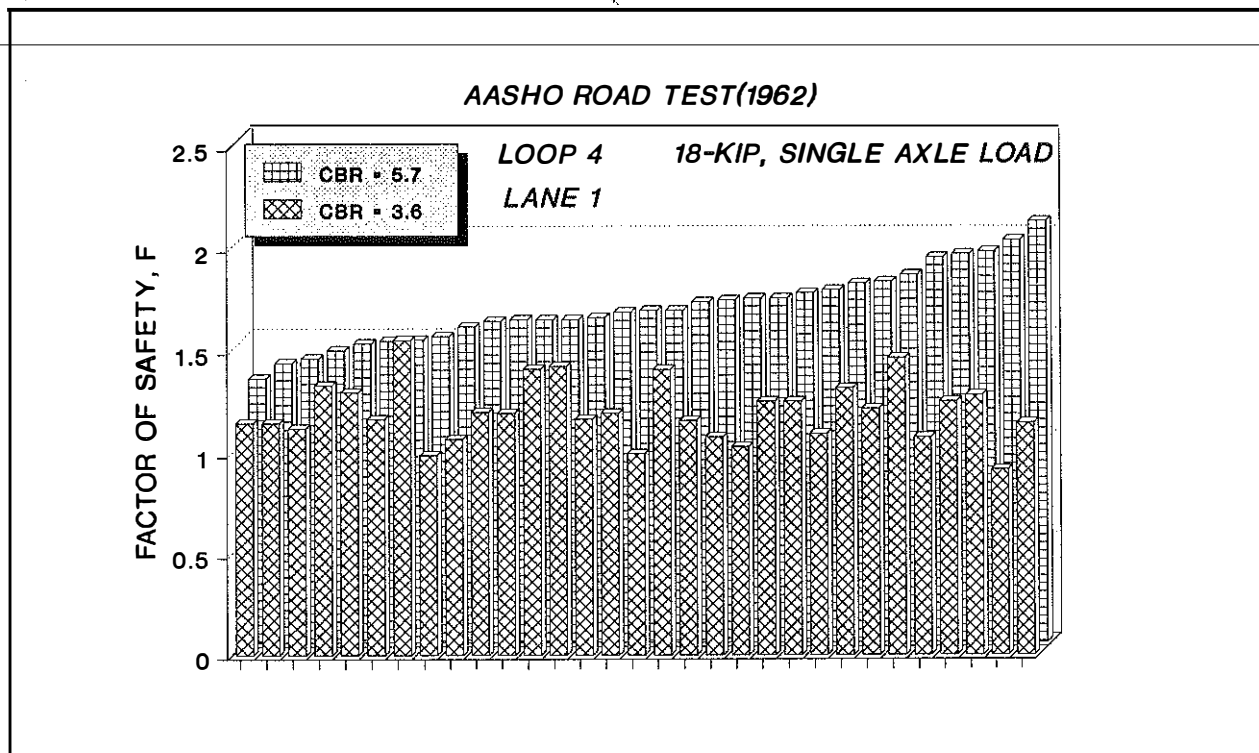


Figure 157. Comparison of Factors of Safety for Two Different Values of CBR.

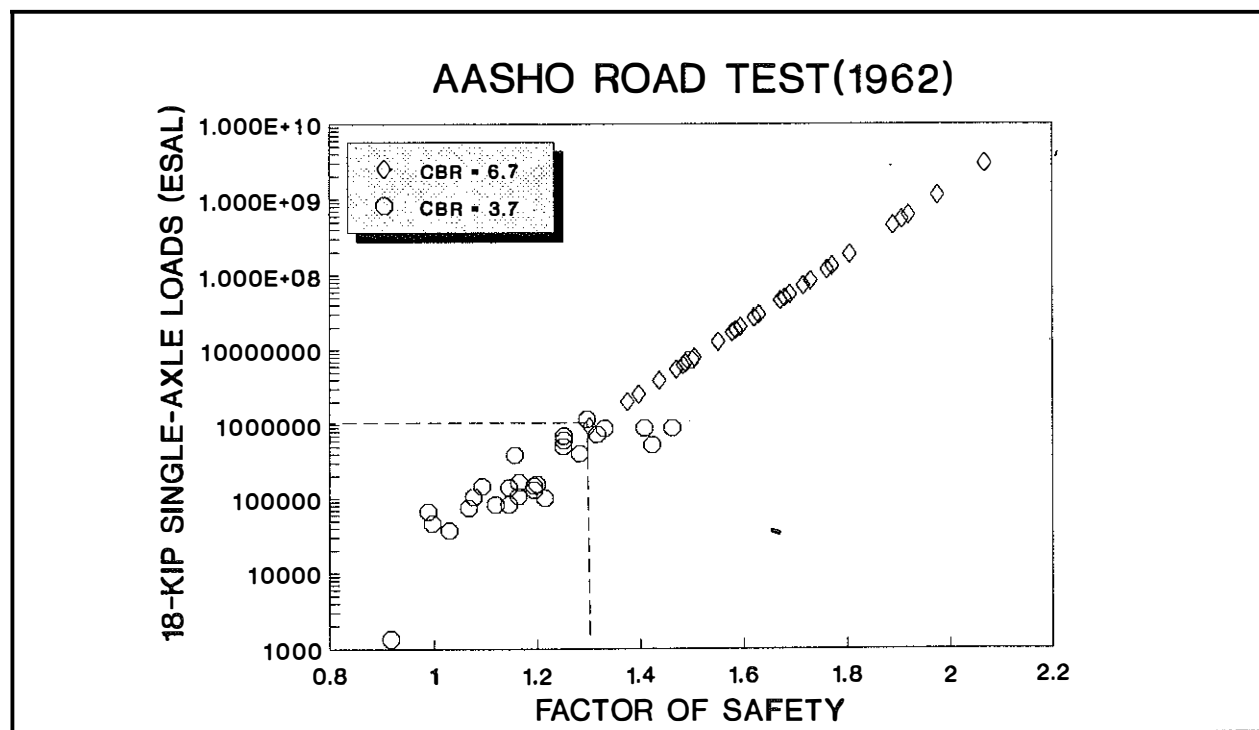


Figure 158. Comparison of Values of ESAL Based on Two Different Values of CBR.

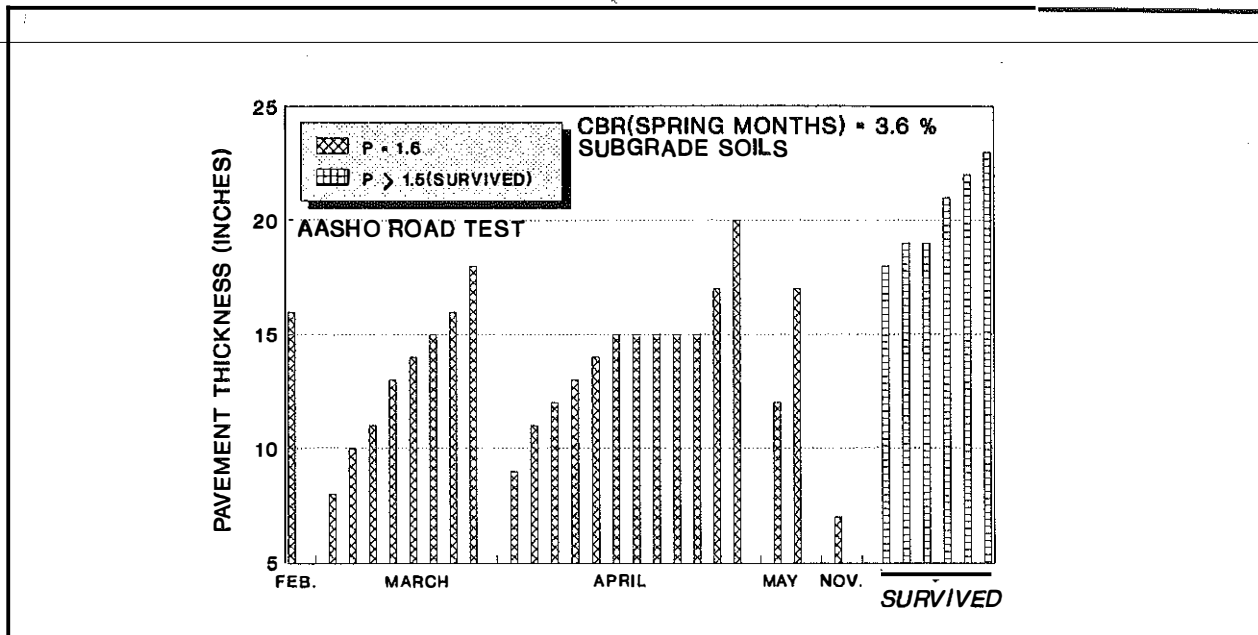


Figure 159. Failures of Pavement Sections of (AASHO Road Test 1962) Loop 4 (Lane 1) During the Spring Months of 1960.

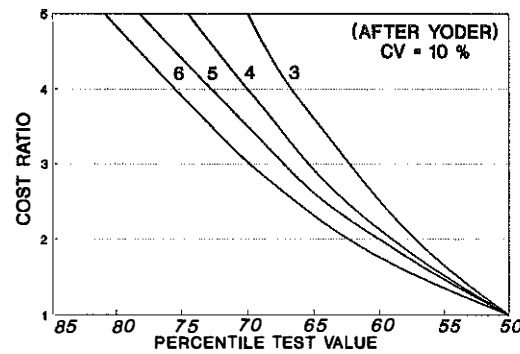
As noted by Yoder and Watzak (1975), the value of CBR (or other strength parameter) selected for design may lead to a pavement structure overdesigned or to one underdesigned. Some approaches used include the following:

- selecting the lowest CBR value,
- using an average CBR value,
- using probability or reliability theory to obtain a design CBR value, and
- using a CBR value based on a least-cost design.

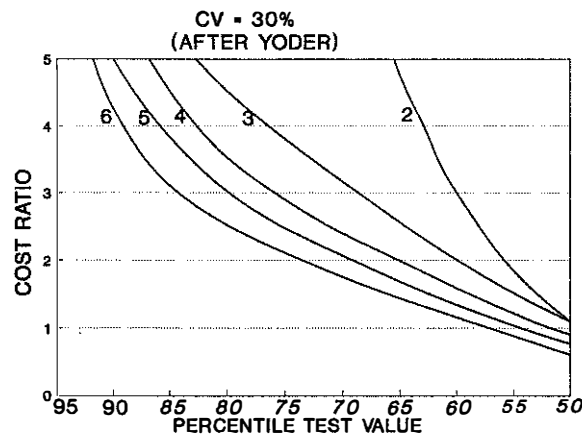
When the lowest value is selected, the pavement may be overdesigned. Using the lowest value runs the risk that the lowest value may be a spurious test value. If the average value of the data set is selected, approximately one-half of the pavement may be overdesigned while about one half may be under designed (Yoder and Watzak 1975). Another approach embraces the normal distribution curve and reliability concepts. Both high and low values of the data set must be considered since the normal distribution involves upper and lower limits for the selected confidence interval. However, this approach assumes the data set is normally distributed -- which may not always be the case.

Another approach, based on a least-cost design, has been proposed by Yoder (1969). According to Yoder, the optimum design, as indicated by a least-cost analysis, depends on two factors:

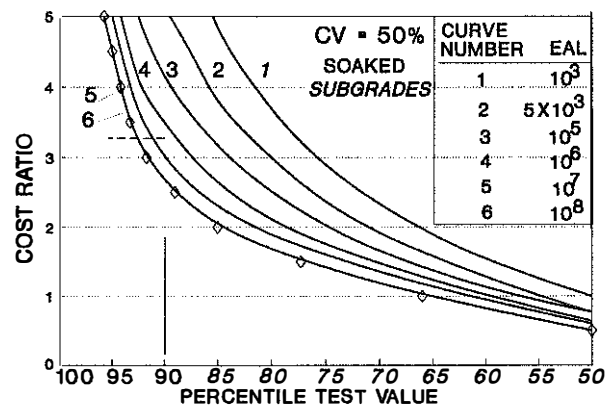
- The variability of the soils located in the highway corridor, and
- The estimated traffic conditions.



a) Coefficient of Variation Equals 10 Percent.



b) Coefficient of Variation Equals 30 Percent.



c) Coefficient of Variation Equals 50 Percent (Soaked Subgrades).

Figure 160. Relationships Between Cost Ratio and Percentile Test Values for Different Values of EAL (Equivalent Axle Load) and Coefficients of Variance (after Yoder 1965)

Yoder presents a series of curves (Figure 160) that relate percentile test values to soil variability (measured by the coefficient of variance of the test data set), traffic (EAL), and unit cost of the pavement. Unit cost of maintaining a highway is expressed in terms of a cost ratio (CR). The cost ratio is defined as the unit maintenance cost divided by the unit initial construction costs. Proposed or suggested values of cost ratio for different traffic conditions (Annual Daily Traffic -- ADT) and roadway location (readily, urban, and rural, or a remote location) are summarized by Yoder. When detailed information is lacking, according to Yoder, the 90th to 80th percentile may be used (coefficient of variation is approximately equal to 30 percent) to obtain the optimum design.

To test and compare the results of the different approaches, an analysis of the laboratory CBR values of Sections 13 and 14 of the Alexandria Highway were done. A detailed stability analysis of these two sites was presented previously in this report in a section entitled "Multi-layered Pavement Analysis -- Case Studies." The planned pavement structure at these locations consisted of 10.5 inches of asphalt concrete and 4 inches of dense graded aggregate (see Figure 103). The design CBR value originally selected for these sites was about five and a design value of four million equivalent single-axle load of (ESAL) was selected.

Laboratory CBR values of Sections 13 and 14 are shown graphically in Figure 100. The lowest CBR value for this data set is 1.3. Based on the assumption that the CBR data are normally distributed, lower and upper CBR values for a 95 percent confidence interval are 2.9 and 4.1, respectively. Based on the approach proposed by Yoder (1965), a percentile test value-CBR curve is developed as shown graphically in Figure 161. Cost ratio for Sections 13 and 14 were not available. In this case, as noted by Yoder, the 90th to 80th percentile test value may be used. At the 95th, 90th, and 85th percentile test values (see Figure 161), the CBR values are 1.4, 1.8, and 2.1, respectively. Since the coefficient of variance is about 50 percent for the data set, and the EAL value is four million, the cost ratio is approximately 3.5 (See Figure 160 c). Yoder's suggested values for rural areas is about three to five.

Therefore, the 90th percentile is a reasonable choice.

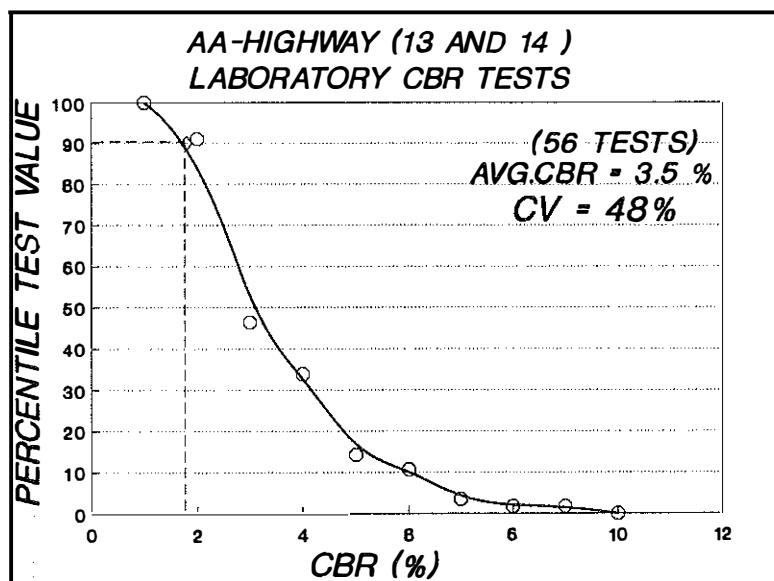


Figure 161. Variation of Percentile Test Value and Subgrade CBR--Sections 13 and 14 on the Alexandria-Ashland Highway.

To compare the different CBR selection approaches, factors of safety were computed using the HOPKIB model and the pavement design shown in Figure 100. For each approach, the subgrade was assumed to have a CBR strength corresponding to that method of the design CBR selection. The undrained shear strength of the subgrade was determined from the relationship given by Equation 2.12. As an example, when the CBR subgrade strength is assumed to be 1.3 (the lowest value of the data set), the computed factor of safety is 0.9. Factors of safety obtained from the

HOPKIB analyses when the different CBR design assumptions are made are compared in Figure 162. If an average CBR value of the data set is assumed to be the correct design CBR value (3.4), then a factor of safety of 1.33 is obtained. However, such a large value of factor of safety is not

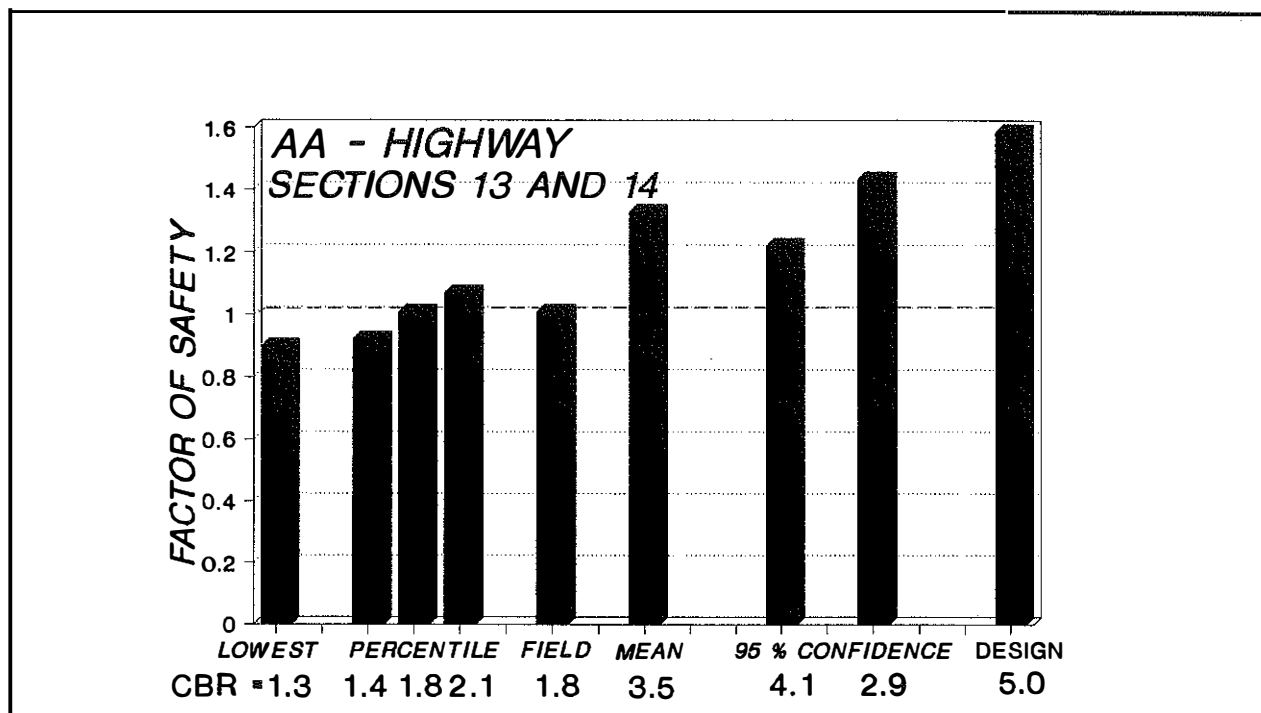


Figure 162. Factors of Safety Obtained When Different Design Values of CBR Are Assumed.

commensurable with the fact that the pavement sections failed during construction; that is, the factor of safety was equal to one. Using the average factor of safety yielded an unsafe condition. The actual factor of safety was much lower than 1.33. If it is assumed that the correct design CBR value is five, then a factor of safety of about 1.59 is obtained. Again, this factor of safety is not commensurable with the fact that the pavements at these two sites failed-- the factor of safety was actually near one. If the CBR values (2.9 and 4.1) obtained from reliability theory at a confidence interval of 95 percent are used, then factors of safety of 1.22 and 1.43 are obtained. This approach yields an unsafe design. This approach is not appropriate because the CBR data set is not normally distributed as shown Figure 163. Equations for normal distribution conditions do not apply.

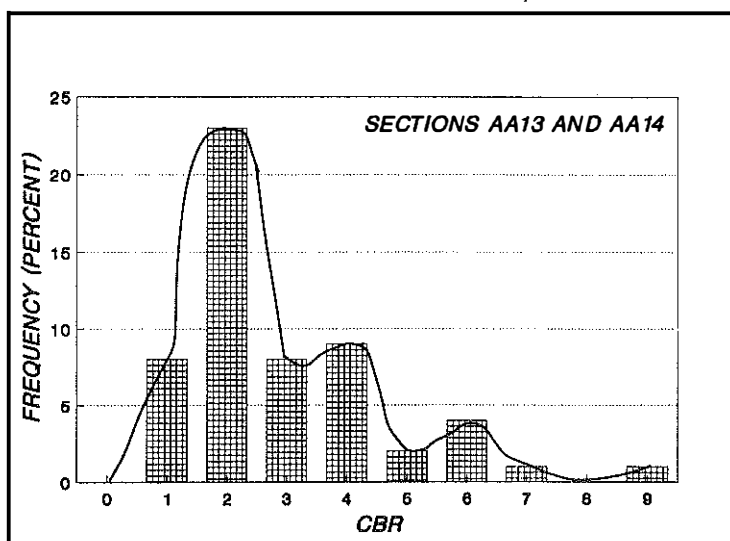


Figure 163. Frequency of Occurrence as a Function of CBR--Sections 13 and 14.

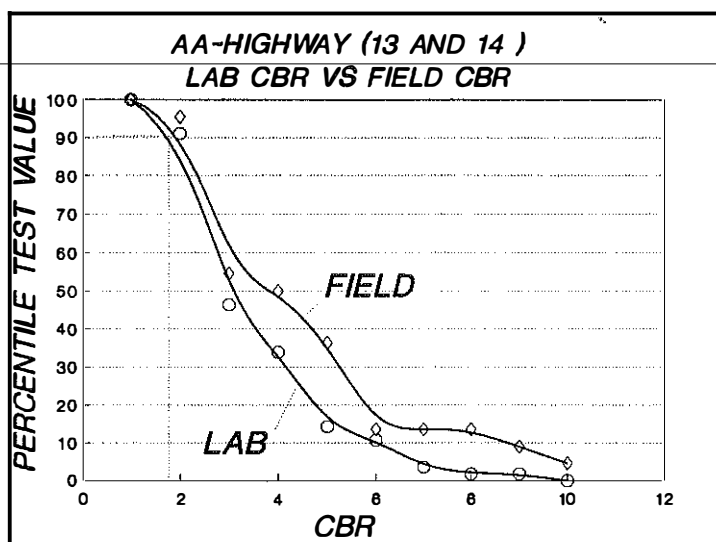


Figure 164. Variation of Field and Laboratory Percentile Test Values with Values of CBR—Sections 13 and 14.

types of soils used to construct subgrades of Sections 13 and 14. Percentile test value as a function of the field CBR value is shown in Figure 164. The field percentile test value - CBR curve is nearly identical to the laboratory percentile test value - CBR curve. The field CBR value at the 90th percentile is about 1.8 -- the same CBR value obtained from the laboratory percentile test value- CBR curve.

The problem of selecting a design CBR value may be illustrated in another manner using the HOPKIB bearing capacity model. In these analyses, the model was used to determine the required thickness for a given factor of safety. Since the estimated value of ESAL is four million, the design factor of safety may be estimated from Equation 262 (see Figure 143), or

$$F = (0.095) \ln (4,000,000) - 0.00463 = 1.44.$$

The total pavement thickness corresponding to a selected subgrade CBR value and design factor of safety may be determined from the HOPKIB bearing capacity model by iteration. The thickness of the pavement is varied until the factor of safety obtained from the model analyses is equal to the selected design factor of safety. These analyses were performed using the shear strength parameters, ϕ and c , given in Figures 107 and 108, and the temperature-depth relationship presented in Figure 109. A surface temperature of 140 ° F and an air temperature of 81 ° F was assumed. In these analyses, the thickness of the DGA (4 inches) is held constant so that the various thicknesses (based on different assumed CBR values of the subgrade) could be compared to the thickness of the pavement section as originally designed and to the thicknesses of the pavement sections after overlays were constructed.

Thicknesses obtained from the various analyses, based on different design CBR values and corresponding to a factor of safety of 1.44, are shown in Figure 165 and compared to the original design

Based on CBR values (1.4, 1.8, and 2.1) corresponding to the percentile test values of 95, 90, and 85 (Figure 161), factors of safety of 0.91, 1.00, and 1.07 are obtained respectively. The CBR value corresponding to the 90th percentile test value -- factor of safety equals to one -- appears to be an appropriate design choice since this condition is commensurable with the fact that the pavements failed at the two sites, and the computed factor of safety is near a value of one.

Some 22 field or in-situ CBR tests have been performed on the untreated subgrades of Sections 13 and 14 and an adjacent site, Section 12. Subgrade soils of Section 12 are essentially the same

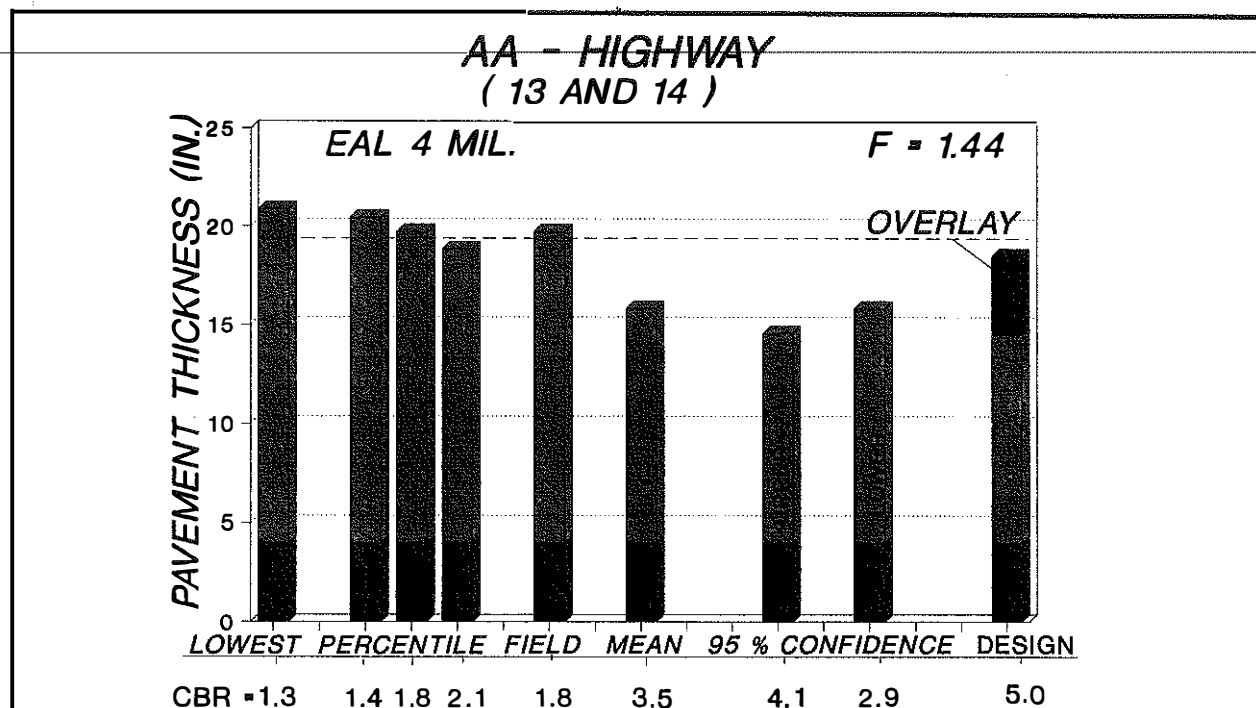


Figure 165. Pavement Thickness Obtained When Different Design Values of CBR are Assumed--Sections 13 and 14.

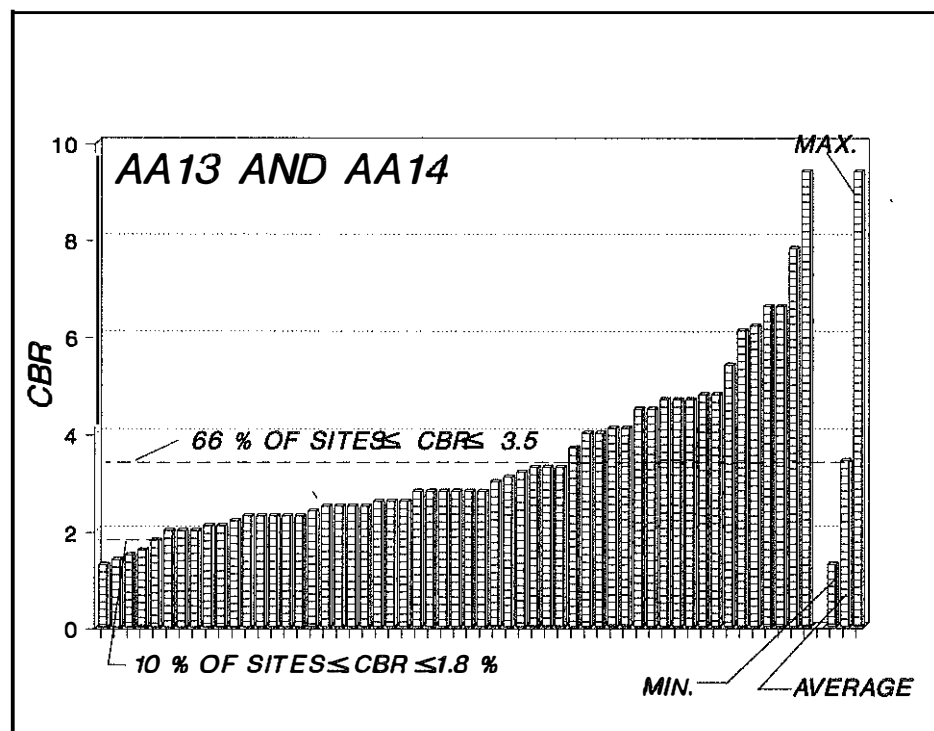


Figure 166. Percentages of Sites Where Values of CBR Are Less Than the Average Value of CBR and the Value of CBR at the 90th Percentile Test Value--Sections 13 and 14.

thickness and to thicknesses after asphalt overlays were constructed. For instance, if the lowest CBR value (1.3) is assumed to be the correct design value, then a total thickness of about 20.9 inches is required for a factor of safety of 1.44. This pavement structure is some 6.5 inches thicker than the structure as originally planned.

If it is assumed that the average CBR value (3.5) is the correct design value, then a total thickness of 15.8

inches is required for a factor of safety of 1.44. This value is only 1.3 inches thicker than the original design. Use of the average CBR value seems inappropriate since the original structure of 14.5 inches failed and the structure obtained when the average value is used is only slightly thicker. At 66 percent of the sampling locations, CBR values are lower than 3.5 percent as shown in Figure 166. If the average value was used, then a large portion of the pavement would be under designed. Additionally, the CBR value of 3.5 corresponds to a percentile test value of only about 40 to 50 percent as determined from the curves in Figure 164. Accordingly, numerous portions of the pavement would require future maintenance. Required thicknesses obtained when the upper and lower values of CBR are assumed to be the correct design values yields thicknesses that are only about 0.1 to 0.8 inches thicker than the original design section. This approach appears inappropriate. As shown in Figure 163, the CBR data set is not normally distributed; consequently, equations for normal distribution theory are not applicable. If the CBR value (1.8) at the 90th percentile is assumed to be the correct design value, then a thickness of 19.7 inches is obtained. This pavement structure is some 5.2 inches thicker than the original pavement design thickness. As shown in Figure 166, only about 10 percent of the sampling sites have CBR values lower than 1.8. The pavement would be underdesigned at only a few locations. Based on an analyses of the pavement sections after failure, Sharpe (July 1988) recommended that an asphalt overlay of a thickness ranging from approximately three to 5 inches be used to repair the pavement failures. Approximately 50 percent of the length of Sections 13 and 14 was repaired using an overlay thickness of about 5 inches. Total thickness of the pavement at those locations after overlaying was about 19.5 inches. This value is nearly identical to the thickness (19.7 inches) obtained when the CBR value corresponding to the 90th percentile test value is used. The method proposed by Yoder appears to be a reasonable approach to the problem of selecting the most appropriate design CBR value. At approximately half of the length of Sections 13 and 14, only about one inch of asphalt overlay was used. Analyses indicate that future problems may develop at those locations. Based on a CBR of two (1.8 is not shown in the design chart) and an EAL of four million, a total pavement thickness of 18-19 inches is indicated when these curves are used (see Havens, et al -- ratio of asphalt layer thickness to total thickness is 0.75) to select a design thickness. This thickness is near the value of thickness obtained from the HOPKIB model using the 90th percentile CBR value (although slightly less) and thickness of the pavement after placement of the overlay. If a design CBR value of five is used, the thickness is about 14.5 inches. If the average value of CBR is used, then the total pavement thickness is about 16 inches. However, as shown by the preceding analyses, pavements constructed on untreated residual soils of the Kope shales failed; the selection of a design CBR of five (or average CBR value) was too large. Proper selection of a design CBR is vital to pavement performance.

Subgrade Modification

The minimum strength of the subgrade required to prevent failure during construction was discussed in the section entitled "Minimum subgrade strength." The analyses showed that the CBR value of the subgrade should be about six to 8.5 to prevent failure and to provide a sound platform for pavement construction. When the CBR strength is below six, it was recommended that subgrade modification be performed.

Structural Credit of Modified Subgrades

When subgrade modification is successfully applied, the strength of the treated portion of the subgrade is usually several times greater than the strength of the untreated subgrade. The structural integrity of

the composite pavement is improved (provided the thickness is not decreased). The improved structural integrity of the composite design depends on the strength of the subgrade located below the treated layer and the strength of the treated layer. The choice of the design value of CBR of the untreated subgrade is vital to the future performance of the pavement as described previously. Failure to recognize that CBR values of untreated subgrades may change during the pavement life may lead to future pavement failure. With regard to subgrade modification using chemical admixtures, such as hydrated lime or cement, a question arises: if subgrade modification is needed, then should the treated subgrade be considered merely as a working platform and given no structural credit in the composite design, or should structural credit be given to the treated subgrade and be included in the design of the composite pavement? If structural credit is given to the improved subgrade, then there are at least three other questions that must be examined:

- What is the long-term strength of subgrades treated with hydrated lime or cement, and will the improved strength last throughout the pavement design life?
- What design strength should be assigned to the treated subgrade layer?
- Will cracking of the treated layer occur, and what effect will cracking (if it occurs) have on the future performance of the pavement?

These questions cannot be fully answered at this time (1991). Whether structural credit should be included in the composite design cannot be fully answered at this time. Much more research is needed to develop vital information concerning these important questions.

Recent research conducted by Hopkins and Hunsucker (1991) indicates that the improved strength obtained when cement or hydrated lime are used to treat subgrades is long-lasting. (An extensive literature search failed to reveal any study that purposely investigated the long-term strengths of subgrades treated with hydrated lime or cement. Indirect evidence cited in a few studies showed that the improved strengths were long lasting.) At one location in Kentucky, a 20-mile stretch of pavement was found to have been constructed on a 6-inch layer of a soil-cement mixture. The pavement consists of 8 inches of a bituminous layer resting on 6 inches of DGA. In-situ CBR tests conducted in 1990 at four locations on the soil-cement layer were about 10, 100, 123, and 153. This stretch of highway was constructed some 30 years ago (about 1961). After 30 years, the soil-cement has very high shear strengths. Overlay placement intervals have averaged about 12-15 years for this stretch of pavement. Cracking of this pavement is inconsequential. Other sites containing soil-cement are under study. In-situ CBR tests show that these old subgrades have very high strengths. Several sites containing hydrated lime-treated subgrades are under study. Results obtained since 1987 indicate that subgrades treated with hydrated lime are long lasting.

To illustrate how the structural integrity of a composite pavement may be improved when the soil subgrade is modified using a chemical admixture, 12 pavement sections (identified as B1, B2, B3, B4, C1, C2, C3, 6A, 6, 12, 17, and 18) of the Alexandria-Ashland Highway were analyzed using the HOPKIB model. In each case, the soil subgrade had been mixed with hydrated lime and compacted. Thickness of each treated layer was 6 inches. Additionally, Sections 13 and 14, which contained soil subgrades that were not treated, were analyzed. Except sections 17 and 18, the soil subgrades of all of the sections were constructed of the same materials. Materials used to construct the soil subgrades consisted of clays and clayey shales obtained from the Kope and Fairview Geological Formations. The subgrades consisted of the same materials. Sections 17 and 18 were constructed with residual clays and

clayey shales of the Bull Fork and Crab Orchard Geologic Formations. Engineering properties of these materials are very similar to the engineering properties of the materials from the Kope and Fairview formations. In the analysis, the actual pavement cross section (as built) of each highway section was used. The pavement thickness and the proportion of asphalt to stone base were almost identical for the 14 highway sections. Surface temperature was assumed to be 140° F. The asphalt pavement of each section was divided into one-inch layers. The temperature at the center of each one-inch layer was obtained from Equation 259. Parameters, ϕ and c , for each one-inch layer were calculated from Equations 257 and 258.

Three general cases were analyzed. In the first case, the average laboratory CBR of the untreated subgrade of each of the 14 highway sections of the AA-Highway selected for analyses was determined. In the second case, the value of CBR of each highway section occurring at the 90th percentile test value was determined. In these two cases, the improved strength gains obtained when hydrated lime used were not considered -- that is, it was assumed that the pavements of each highway section rested directly on the untreated subgrade. The purposes of these two case analyses were to examine the stability of the pavements when they rested directly on the untreated subgrade and to examine

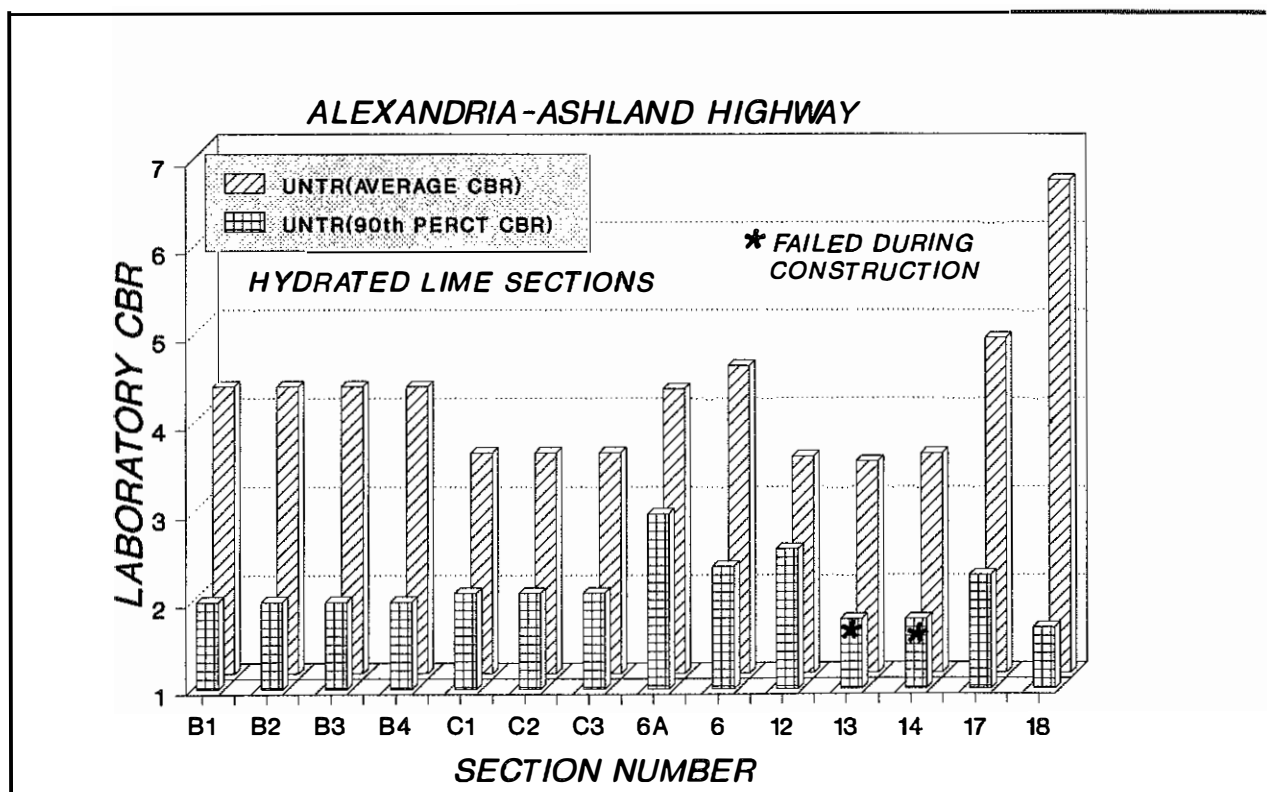


Figure 167. Comparison of the Average CBR Values of Selected Subgrades of the Alexandria-Ashland Highway and CBR Values Occurring at the 90th Percentile Test Value.

differences in the stability when different CBR design assumptions were used. The average CBR value of the untreated soils and the CBR value occurring at the 90th percentile test value of each highway section are compared in Figure 167. Factor of safety obtained from the HOPKIB model of each highway

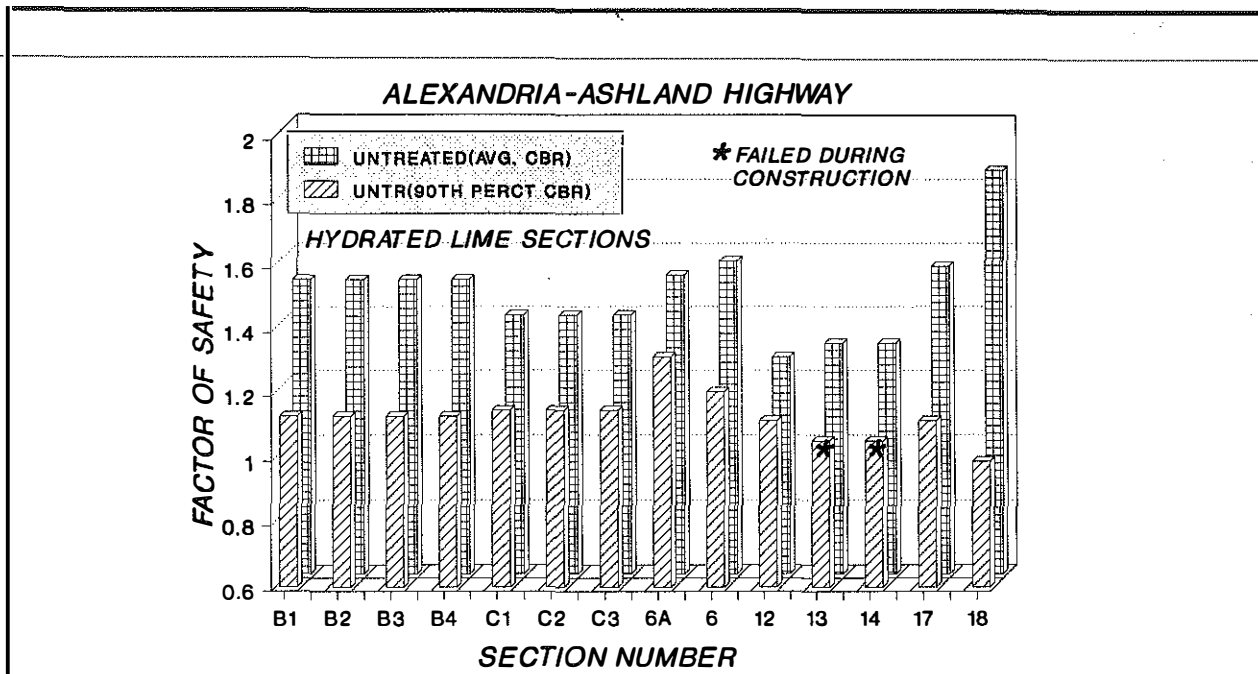


Figure 168. Comparison of Factors of Safety Obtained When the Average Subgrade CBR Values Are Assumed to Factors of Safety Obtained When CBR Values Occurring at the 90th Percentile Test Value Are Assumed.

pavement section using the two different CBR design assumptions are compared in Figure 168. When the average CBR was used, factors of safety ranged from 1.31 to 1.86. Hence, these analyses, based on the average CBR value, indicate that the stability of these highway sections should have been adequate. Pavement sections 13 and 14 -- factors of safety equal to 1.31 -- failed during construction, although the factors of safety based on the average CBR value indicated that failure should not have occurred. This indicates that the other 12 sections would have been unstable if the subgrades had not been treated -- the subgrade materials and pavement section thicknesses of all 14 highway sections were nearly identical. When the CBR values occurring at the 90th percentile test value are used, factors of safety of Sections 13 and 14 were 1.05 as shown in Figure 168 -- this factor of safety is commensurable with the fact that these sections failed during construction. Analyses of the other 12 highway sections based on the CBR value at the 90th percentile test value yield factors of safety ranging from 1.00 to 1.31. If Sections 6 and 6A are excluded, the factors of safety range from 1.00 to 1.15. These analyses indicate that the stability of these sections would have been very marginal and most likely would have failed prematurely if subgrade treatment had not been done -- an indication that is supported by the fact that Sections 13 and 14 (untreated subgrades) failed.

In the third case, analyses of the sections were performed to determine the effects of the 6-inch layer of hydrated-lime treated subgrade on pavement stability. All highway sections were analyzed using the 6-inch treated layer, except Sections 13 and 14. In the latter two cases, the subgrades had not been treated. In performing these analyses, field CBR strengths were used. The value of CBR used in the analyses was selected at the 90th percentile test value, as shown in Figure 169. This value is about 25. Based on Equation 211, the undrained shear strength is estimated to be about 50 psi. In each case, the

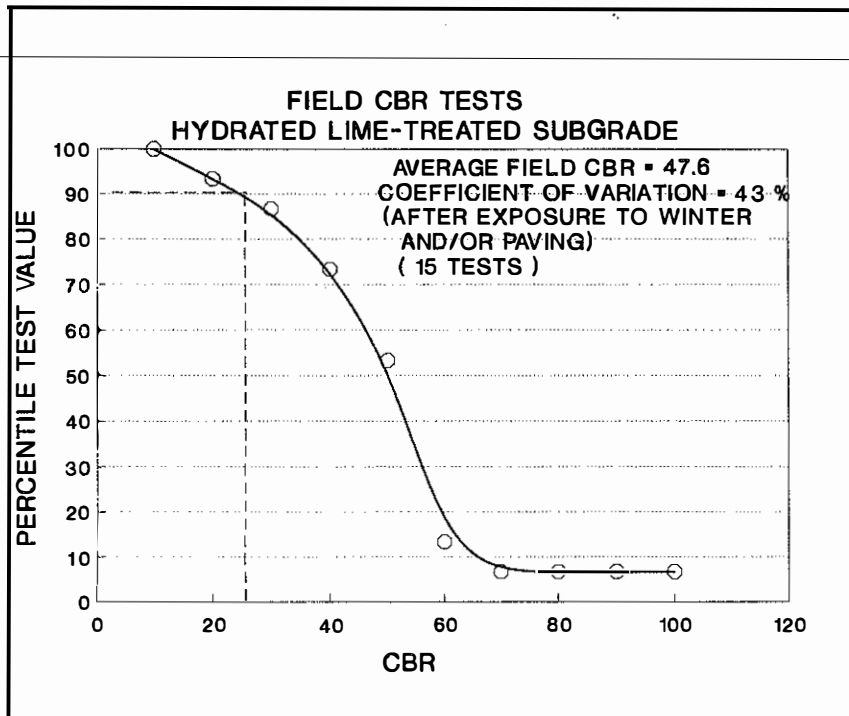


Figure 169. Percentile Test Value as a Function of Field Values of CBR for Subgrade Soils Treated With Hydrated Lime.

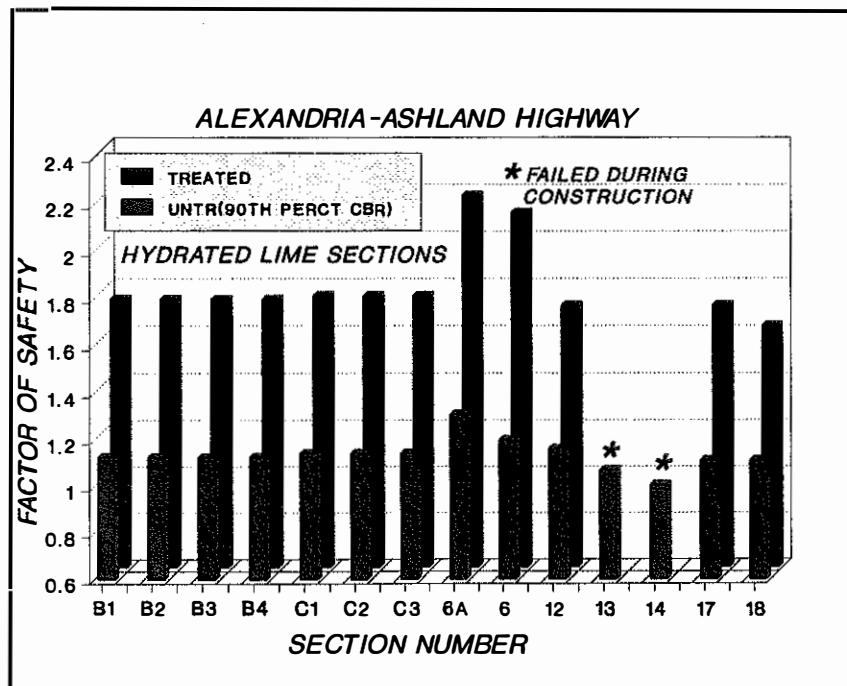


Figure 170. Comparison of Factors of Safety Obtained When the Average CBR Values of Selected Untreated Subgrades Are Assumed to Factors of Safety Obtained When CBR Values Occurring at the 90th Percentile Test Value Are Assumed.

CBR value of the untreated subgrade beneath the treated layer was taken at the 90th percentile test value. Factors of safety obtained when the treated layer is considered are shown in Figure 170 and compared to factors of safety obtained when no treated layer is considered. When the treated layer is considered, the factors of safety range from 1.63 to 2.19. If treatment had not been performed, then the factors of safety range from 1.1 to 1.3. The treated layer improved the stability significantly. To obtain an indication of the degree of improvement, values of ESAL were estimated for the two subgrade conditions using Equation 262 and the factors of safety obtained when the subgrades are assumed to be untreated. When the subgrade is assumed to be untreated, values of ESAL range from 60,000 to 620,000 as shown in Figure 171. Considering that the design value of ESAL was 4,000,000, the estimated pavement lives range from 0.3 to 3.1 years. This indicates premature failures of these sections would have occurred if the subgrades had not been treated. Estimated values of ESAL from Equation 262, when the 6-inch treated layer is considered, range from 13.4

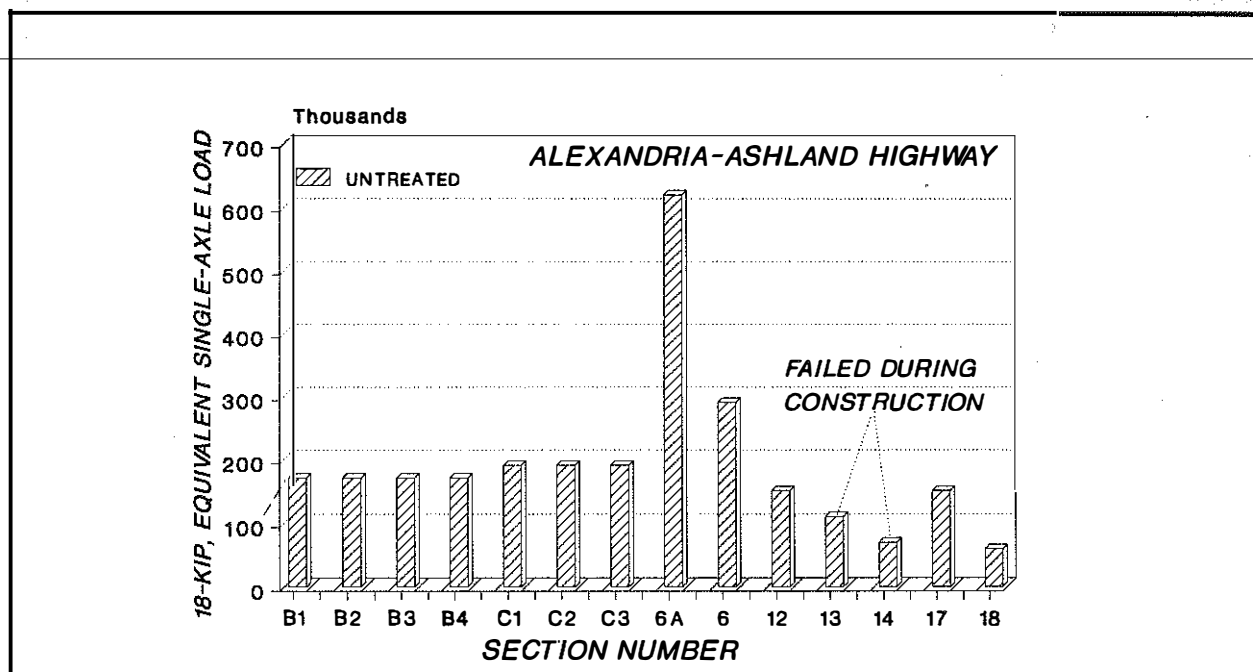


Figure 171. Predicted Values of ESAL for Selected Pavement Sections Resting on Untreated Subgrades of the Alexandria-Ashland Highway.

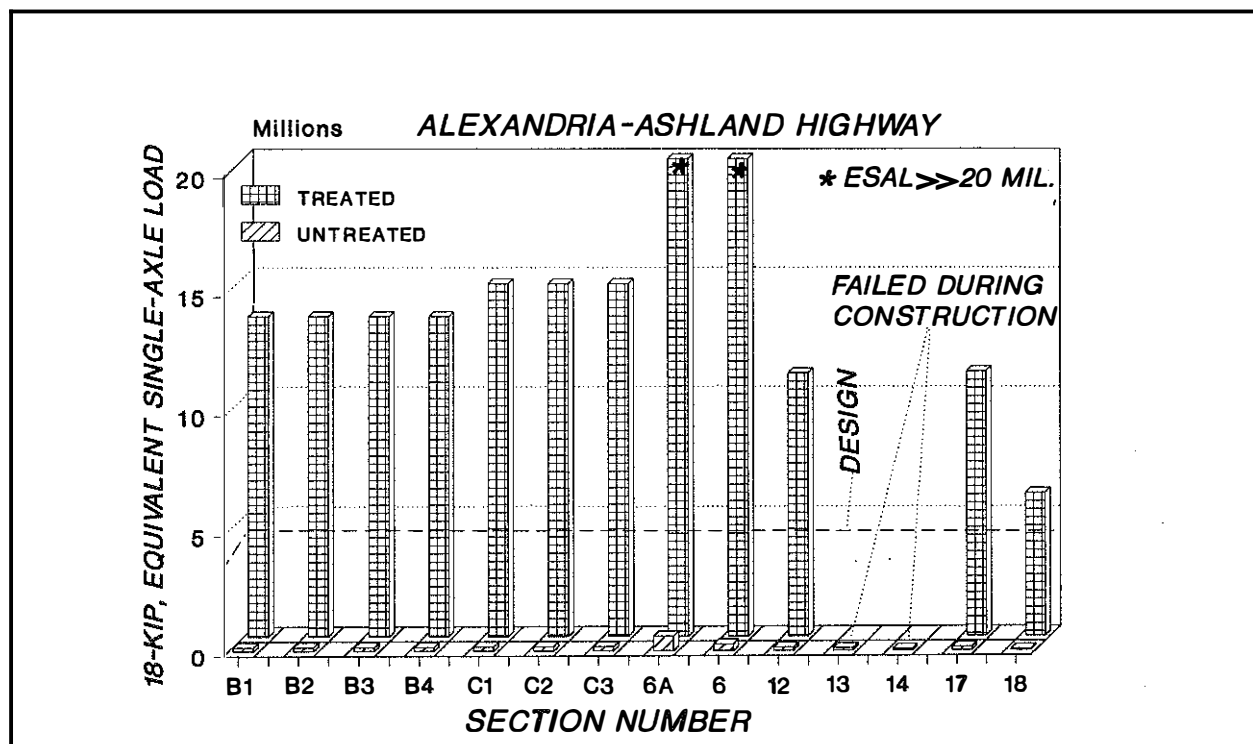


Figure 172. Predicted Values of 18-kip, ESAL Obtained for Selected Pavement of The Alexandria-Ashland Highway When the Strengths of Hydrated-Lime Treated Subgrades are Considered.

million to values over 20 million, as shown in Figure 172. In each case, the estimated ESAL values exceed the design value of four million. Therefore, the recommendation proposed by Hopkins and Allen (1986) that all subgrades on the AA-Highway be modified is justified as shown by the preceding analyses. In all of the preceding analyses, the unit tire contact stress was assumed to be 80 psi. If the tire contact stress exceeds 80 psi, estimated values of ESAL decrease significantly, and consequently, pavement life decreases. To examine the relationship between tire contact stress and ESAL values, analyses were performed using a selected

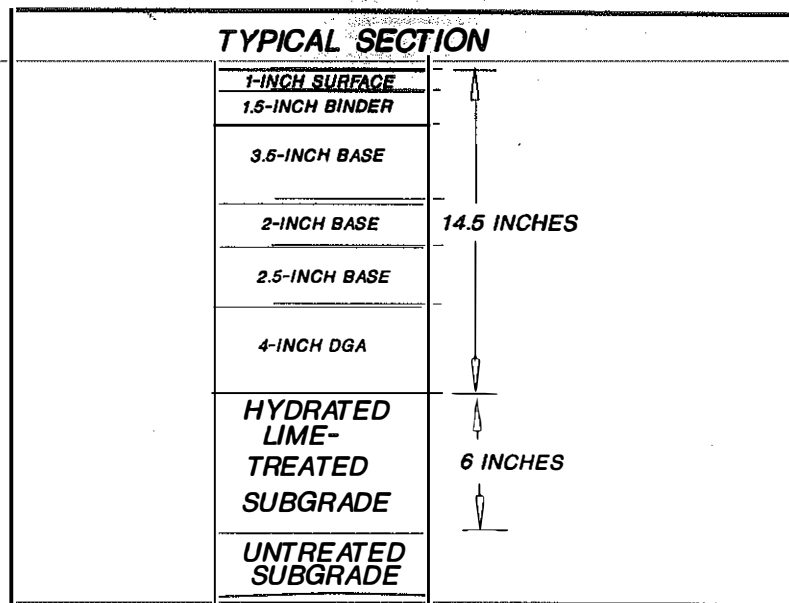


Figure 173. Typical Cross Section Used in the Analyses to Illustrate the Effects of the Variation of Tire Contact Stresses on Factor of Safety and Predicted Values of ESAL.

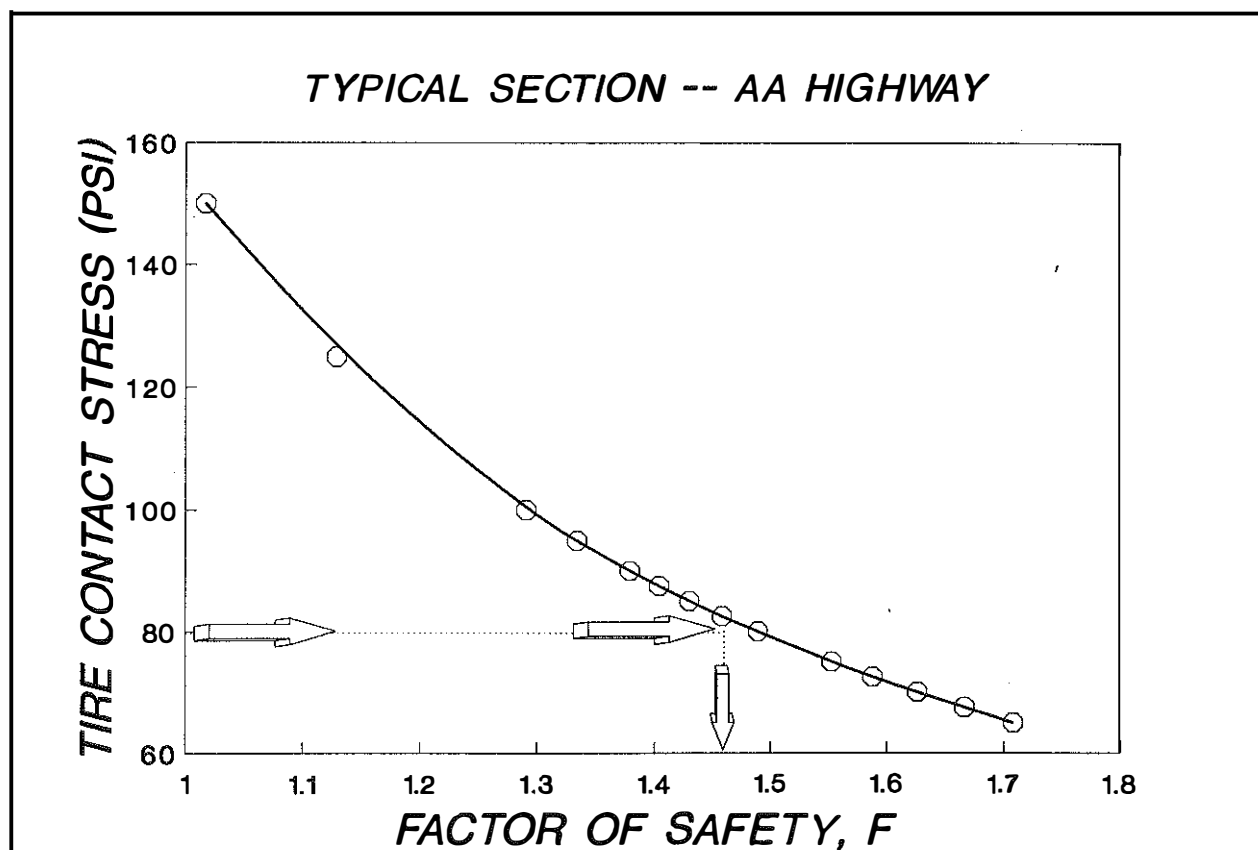


Figure 174. Factor of Safety as a Function of Tire Contact Stress.

typical pavement section of the sections cited previously. This typical section, as shown in Figure 175, consists of 10.5 inches of asphalt, 4 inches of crushed stone base, and 6 inches of a hydrated-lime treated subgrade. Undrained strength of the treated subgrade was 50 psi. The subgrade below the treated layer was assumed to have a CBR strength of 1.8 and an undrained shear strength of about 3.7 psi. The relationship between tire contact stress and factor of safety for the pavement section is shown in Figure 173. As the tire contact stress increases above 80 psi, the factor of safety decreases rapidly.

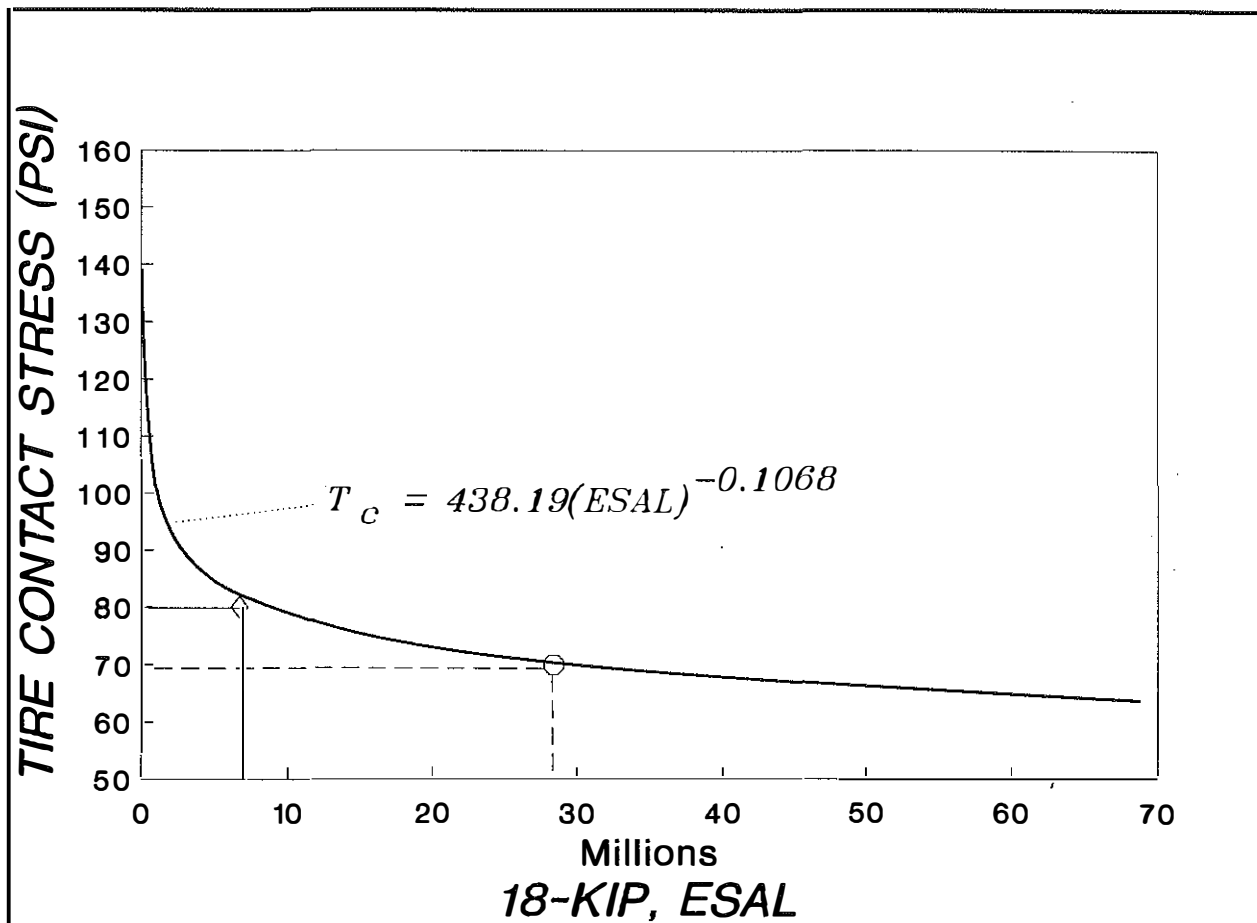


Figure 175. Relationship Between Tire Contact Stress and Predicted Values of ESAL.

To illustrate the effect of the variation of tire contact stress on the value of ESAL, values of ESAL were estimated using the relationship between ESAL and factor of safety given by Equation 262 and the factors safety appearing in Figure 174. This relationship is illustrated in Figure 175. As the tire contact stress increases above 80 psi, the value of ESAL decreases rapidly. For example, at a tire stress of 80 psi, the ESAL value is four million. If tire contact stress increases to 100 psi (20 percent increase), the value of ESAL decreases to 840,000 -- almost a fivefold decrease. Pavement life decreases rapidly (20 years to about 4.2 years). A slight decrease in tire contact stress significantly increases values of ESAL. Decreasing the contact stress from 80 psi to 70 psi (12.5%) increases ESAL values from four million to about 28.4 million (a sevenfold increase). Pavement life is extended very significantly, and future maintenance costs would decrease rapidly.

SUMMARY AND CONCLUSIONS

Based on the analysis presented herein, the following summary and conclusions are made:

- A generalized, mathematical bearing capacity model and computer program were developed for analyzing the mechanical behavior of pavements. The mathematical model and computer program may be used to analyze the bearing capacity of subgrades and flexible pavements containing multiple layers. The mathematical model is based on limit equilibrium and the theory of plasticity. The model is unique concerning pavement models currently in use since the factor of safety against failure of a flexible pavement consisting of multiple layers of different materials may be calculated. Additionally, the shear strength parameters, ϕ and c , obtained from triaxial tests are used in the mathematical bearing capacity model to define the shear strength of each layer of a pavement. Both total stress and effective stress analyses may be performed to determine the factor of safety against failure. The mathematical algorithms were programmed for the IBM 3091 computer (mainframe) and the PC[®] Computer using the FORTRAN Language.
- Derivations of the theoretical equations and a full description of the solution of these equations are presented. A Prandtl-type shear surface is used in the mathematical model to simulate the failure pattern of a pavement under tire loads. The potential failure mass is assumed to consist of a Rankine active wedge, a Prandtl central wedge (logarithmic spiral), and a Rankine passive wedge.
- Statistically, about 86 percent of Kentucky soils consist of clays, fat clays, and silts -- fine-grained soils. Most highways in Kentucky are constructed on soils of poor engineering quality. From a statistical viewpoint, approximately 40 percent of Kentucky soils have very low bearing strength when exposed to water -- that is, the soaked CBR is less than six. About 20 percent of Kentucky soils have soaked values of CBR that are less than three. Based on these data and reported observations, construction of subgrades and pavements is a major problem in Kentucky. Many pavement problems have developed during and after construction because of the low bearing strength of Kentucky soils.
- Although Kentucky soils have large bearing strengths when initially compacted, the bearing strengths of a high percentage of these soils decrease dramatically when exposed to water. The bearing strength initially may be adequate during and after construction to support traffic loadings. When these compacted soils are exposed to water, the bearing strengths may decrease to such a state that the pavement layers cannot be compacted adequately to meet standards; premature pavement failures may occur shortly after construction. Many of these soil types swell when exposed to water, increase in volume and moisture content, and lose bearing strength. Although a given soil type may be compacted to 95 percent of maximum dry density and near optimum moisture, there is no assurance that this initial compactive state will exist after compaction (and construction) if the soil is exposed to water. Both laboratory and field data support this conclusion.

- The principle of effective stress as proposed by Terzaghi (1943) is very useful in visualizing and explaining the mechanical behavior of soil subgrades and pavements under tire stresses. The proposed mathematical model described herein embraces this very important principle.
- Although a pavement may be designed, the issue of whether the pavement may be constructed has often been ignored. Usually, the subgrade is the weakest structural member of a pavement. Ignoring this fact leads to premature pavement failures and failures during construction.
- The credibility and reasonableness of solutions obtained from the HOPKIB bearing capacity model and computer program were established by solving three classes of bearing capacity problems. Solutions obtained from the proposed model of these problems were compared to theoretical and semi-theoretical solutions obtained from other mathematical or empirical models. These classes of problems included:
 - subgrade problems involving one homogeneous bearing medium,
 - pavement construction problems involving two different layers of materials, and
 - case studies of actual pavement failures that occurred during or after construction that involved multiple layers of materials.
- Bearing capacity factors, N_c and N_q , calculated from the HOPKIB model compared very well with values of N_c and N_q obtained from equations developed by Prandtl (1921). The ratio of N_c factors obtained from the proposed model to N_c factors proposed by Prandtl ranged from about 96 to 75 percent for ϕ values ranging from zero to 45 degrees. When values of N_c from Prandtl's equation are inserted into the HOPKIB model, factors of safety ranging from about 0.98 to 0.94 were obtained for values of ϕ ranging from zero to 45 degrees. Similar results were obtained when N_q factors obtained from the proposed model were compared to N_q factors obtained from Prandtl's classical bearing capacity equation.
- Values of N_γ , the bearing capacity factor, obtained from the HOPKIB model generally ranged from 116 to 146 percent higher than values of N_γ proposed by Vesic' (cf. Winterhorn and Fang 1975). However, the N_γ values obtained from the proposed model are in much better agreement with N_γ factors determined from experimental model footing tests reported by de Beer and Ladanyi and Vesic' than N_γ values proposed by Vesic', Terzaghi, Caquot and Kerisel, Feda, and de Mello.
- The minimum undrained shear, c , of a soil subgrade required to support anticipated contact stresses of construction traffic may be obtained from the HOPKIB model. The minimum strengths required to avoid failure, as determined from the HOPKIB model using a tire contact stress of 68 psi, ranges from about 1,662 pounds per square foot (factor of safety equal to 1.0) to 2,527 pounds per square foot (factor of safety equal to 1.5). For other tire contact stresses, the strengths required to avoid failure may be obtained from relationships presented herein.
- A relationship between the undrained shear strength and CBR was developed. The correlation was developed from theoretical considerations of conditions in the CBR test -- that is, values of c may be calculated from the CBR test and correlated to CBR values. This correlation was

checked by comparing this theoretical correlation with a correlation published by Thompson (1988). Additionally, unconfined compression tests and CBR tests were performed on a typical clay; the data were compared to the proposed correlation. Good agreement among the data obtained in the three different manners was obtained.

- Minimum CBR strengths required to avoid failure during construction were obtained from the HOPKIB model. At a factor of safety of 1.0 and for a tire contact stress of 68 psi, the minimum CBR strength of the subgrade should be 5.6. At a factor of 1.5, the CBR strength should be 8.3. Therefore, to avoid failure during construction, the minimum CBR strength should be equal to or greater than 5.6 - 8.3. For higher values of tire stresses, minimum CBR strengths may be obtained from relationships presented herein. These conclusions are supported by field data published by Thompson (1988) which showed that CBR strengths should be on the order of 5.3 to 8.5 for tire inflation pressures ranging from 50 to 80 pounds per square inch. These CBR values limit tire sinkage to about 0.25 inches.
- Minimum values of dynamic subgrade modulus of elasticity were established from the HOPKIB model. At a ground contact stress of 68 psi and for a factor of safety of 1.0, the dynamic elastic modulus is about 11,700 psi. At a factor of safety of 1.5, the dynamic modulus is about 16,679 psi. To avoid failure of the subgrade, the dynamic modulus of elasticity must be equal to or greater than about 12,000 - 17,000 psi.
- The dynamic cone penetrometer is a useful and simple means of characterizing the bearing strengths of newly constructed subgrades. Minimum dynamic cone penetrometer values were established from the HOPKIB model. For a contact tire stress of 68 psi and a factor of safety equal 1.0, the maximum dynamic cone penetrometer (DCP) value is 41 mm per blow. If the DCP value is greater than 41 mm per blow, then the subgrade is unstable. At a factor of safety of 1.5, the DCP value is 29. To be stable, the DCP value of a soil subgrade should be less than about 29-41 mm per blow. For other contact tire stresses, values of DCP necessary to insure subgrade stability may be obtained from relationships presented herein.
- Bearing capacity analyses of two-layered problems were analyzed. The first situation involved a granular base resting on a clayey subgrade. Comparisons of thicknesses obtained from the HOPKIB model and thicknesses obtained from a method proposed by Vesic' (cf. Winterhorn and Fang 1975) show that similar results are obtained from the two different approaches for CBR values ranging from one to six. Both approaches show that for very low values of CBR (≤ 3) granular thicknesses must be some 17 to 60 inches to avoid failure under typical construction traffic loadings. The second situation involved construction of a chemically-treated layer on an untreated layer. For subgrade CBR values ranging from one to six, the thickness of the treated layer should be approximately 17-23 inches (CBR = 1) to about seven to 8 inches (CBR = 6), respectively, to withstand typical construction traffic and to prevent undesirable deformations and subgrade shoving and pushing. Thickness of the treated layer should be designed using the methods presented herein. The third situation involves the construction of "full-depth" asphalt on a soil subgrade. Results of the HOPKIB analysis of this situation emphasize the need to analyze placement temperatures of asphalt lifts and CBR values of the subgrade at the time of construction of the first lift of asphalt pavement to insure safe and stable

construction. The analyses show that when the asphalt temperature approaches 140° F (surface temperature) and when the subgrade CBR is less than six, the factor of safety against failure of the first lift of asphalt pavement is less than or equal to 1.0 -- a failure condition. At a factor of safety of 1.5 and an asphalt pavement temperature of 140 ° F, the subgrade CBR must be about 9 to insure stable construction.

- Two case studies involving failures of partially completed flexible pavements were analyzed extensively using the HOPKIB computer model. Results generally show that the model yields factors of safety near or below 1.0. Moreover, in these cases, the factors of safety of the planned pavement sections were frequently near or below 1.0. The HOPKIB model appears to be a good predictor of the stability of a flexible pavement.
- Analyses of the 1981 Kentucky flexible pavement design curves were performed using the newly proposed bearing capacity model. CBR curves ranging from two to 12 were analyzed. Results of the analyses show that for low-bearing soils (CBR equal to two or 3), factors of safety equal to or less than 1.0 were obtained. For example, when the CBR of the subgrade is equal to two and values of EAL range from 10^3 to 5×10^5 , the factors of safety range from 0.30 to 1.07, respectively, for pavement thicknesses ranging from six to 23 inches. Other low values of factor of safety are obtained for certain combinations of thickness and values of EAL are obtained when the subgrade CBR is less than six. The situation is more critical when the tire contact stress increases from 80 psi to 105 psi. Based on these analyses, certain design thicknesses may be obtained from the design curves that may be unstable if constructed. This situation is not trivial since hundreds of miles of highways in Kentucky exist on soil subgrades that have CBR strengths of two or three.
- A relationship between (weighted) 18-kip equivalent single-axle load applications (ESAL) and factor of safety obtained from the HOPKIB bearing capacity computer program was established by analyzing 237 pavement sections of the AASHO Road Test (1962). The slope of this relationship rises sharply up to a factor of safety of about 1.3 (ESAL = one million) and tends to flatten when the ESAL value exceeds one million. At a factor of safety of 1.5 or greater, the value of ESAL generally was eight million or greater. These analyses indicate that flexible pavements should not be designed for a factor of safety below about 1.2 or 1.3 no matter how small the value of ESAL may be.
- Increasing the tire contact stress from 68 psi to 105 psi causes significant decreases in the values of ESAL that a pavement may sustain. That is, the life of the pavement decreases significantly. Decreasing the tire contact stress from 67.5 psi to 50 psi causes an increase in the values of ESAL and therefore increases significantly the life of pavements.
- For low values of ESAL ($< \approx 100,000$), the AASHO Road Test equation may yield pavement thicknesses that have factors of safety near 1.0 or lower.
- In cases where the subgrade CBR value is below about six, slight decreases in the bearing strength may cause a large decrease in the factor of safety against failure and the life of the pavement. For example, the average CBR strength of the AASHO Roadbed soils (loop 4, lane

1) recorded in the spring of 1960 was 3.6. During the summer of 1957, the CBR strength was 5.7. Based on an analysis using the HOPKIB model, the average factor of safety of loop 4 (lane 1) pavement sections was 1.64 when a CBR value of 5.7 was used for the roadbed. When a CBR value of 3.6 was used in the analyses, the average factor of safety was 1.21 -- a difference of some 27 percent. Based on Equations 262, which relates values of ESAL and factor of safety, the average value of ESAL obtained when the factor of safety (CBR - 3.6) is inserted into this Equation is 295,262. Using the average factor of safety of 1.65 (CBR - 5.7), the average predicted ESAL value of the sections of loop 4 (lane 1) is 6,728,755 -- some 23 times larger than the average ESAL value when the CBR of the subgrade soils is equal to 3.6. Increasing the strength of the subgrade results in an increase in the factor of safety and extends pavement life.

RECOMMENDATIONS AND IMPLEMENTATION

Based on the analysis and conclusions presented herein, the following recommendations and suggestions are made for consideration:

- The concept of designing a pavement should involve more than merely obtaining "the total thickness of the pavement" and the thicknesses of individual layers. The issue of constructability should be addressed during the design phase. For example, the stability of the subgrade subjected to the maximum anticipated construction traffic stresses should be analyzed to avoid failure of the subgrade during construction. Bearing capacity failures during construction build in weakened shear zones that may lead to premature pavement failures after construction. The stability of each lift of pavement (especially during the construction of the first lift of the pavement structure) should be analyzed to insure that each structural lift will not fail and to insure that each structural lift can be adequately compacted (note: This recommendation was partially implemented during this study). The proposed model (HOPKIB) may be used conveniently to analyze the different construction stages. The computer program requires nominal training for others to use.
- When the value of CBR of the subgrade soils is less than six, the subgrade should either be modified or stabilized to increase its bearing strength (Hopkins 1987 - note: this recommendation has been carried out). The CBR value should be increased to a minimum value of about nine to 10, or greater. The thickness of the modified or stabilized layer should be designed. Both the shear strengths (or bearing strengths) of the treated and untreated layers must be considered in the analysis. The HOPKIB computer model can conveniently be used for this design analysis. Construction of "full-depth[®]" asphalt pavements or granular bases on soil subgrades should not be permitted when the CBR value of the subgrade is less than about nine. Preferably, the soil subgrade CBR should be 9-10, or greater, to avoid failure or serious deformations.
- Flexible pavement thicknesses obtained from the 1981 Kentucky design curves should receive a critical review when the factor of safety is less than about 1.3 (as determined from the HOPKIB model), or when the subgrade is below a CBR value of six. Consideration should be given to revising the design curves for CBR values below six. To insure the factor of safety of

a given pavement design is not below 1.3 or near 1.0, the design should be checked using the model proposed herein.

- Tire contact stresses, or unit stresses of tires, at the AASHO Road Test (1962) averaged about 68 psi, although different types of loaded vehicles were used in the test. Consideration should be given to studying the tire contact stresses of vehicles currently operating on highways since significant changes may have occurred in the design of tires from 1962 to 1991. These data are needed to assess current design practices and policies and to assess likely damage to a given pavement.
- The test method currently used in Kentucky to obtain the CBR of a given soil should be revised. The test should be performed so that dry density and moisture content of the laboratory remolded CBR specimen is commensurable with dry density and moisture content of the Department of Highways' standard specifications. That is, if the standard specifications require that the subgrade soils be compacted to 95 percent of maximum dry density and (+) 2 percent of optimum moisture, then the laboratory CBR specimen should be remolded to reflect these conditions. As noted herein, dry densities of laboratory CBR specimens obtained when the current method is used generally are much larger than dry densities obtained from the AASHTO Test Method (T 99) or the ASTM Test Method (D 698). CBR values generally obtained from the current standard are larger than values of CBR obtained from the ASTM procedure (March 1988). The method may be revised using methods described by Hopkins, et al. in 1988. It is recommended that the method of soaking a CBR specimen as described in the KYCBR procedure be retained.

REFERENCES

American Society for Testing Materials (ASTM); March 1988, "Soil and Rock, Building Stones; Geotextiles," Volume 04.08, Section 4.

Baker, R.F. and Drake, W.B.; (1948), "Investigation of Field and Laboratory Methods for Evaluating Subgrade Support in the Design of Highway Flexible Pavements", Proceedings, Highway Research Board.

Bishop, A.W.; and Henkel, D.J.; (1957), "The Measurement of Soil Properties in the Triaxial Test," Edward Arnold (Publishers) LTD., London, England.

Bishop, A.W.; (1955), "The Use of the Slip Circle in the Stability Analysis of Slopes", Geotechnique, Vol. 5.

Bohn, A.; Ullidtz, P.; Stubstad, R.; and Sorenson, A.; (1982), (1972), "Danish Experiments with the French Falling Weight Deflectometer", Proceedings, 3rd International Conference on the Structural Design of Asphalt Pavements, University of Michigan, Ann Arbor, Vol. 1.

Brown, J.D.; and Meyerhof, G.G.; (1969); "Experimental Study of Bearing Capacity in Layered Clays,"

Proceedings of the Seventh International Conference on Soil Mechanics and Foundation Engineering, Mexico City.

Buisman, A.S.K.; (1940), "Groundmechanica," Waltman, Deft.

Burmister, D.M.; (1943), "The Theory of Stresses and Displacements in Layered Systems and Applications to the Design of Airport Runways," Highway Research Board, Proceedings, Volume 23.

Button, S.J.; (1953), "The Bearing Capacity of Footings on a Two-Layer Cohesive Subsoil," Proceedings of the Third International Conference on Soil Mechanics and Foundation Engineering, Switzerland.

Caquot, A.; and Kerisel, J.; (1953), "Ultimate Bearing Capacity of a Foundation on the Surface of a Cohesionless Soil," Proceedings of the Third International Conference on Soil Mechanics and Foundation Engineering, Switzerland.

Ching, R.K.H.; and Fredlund, D.G.; (1983), "Some Difficulties Associated with the Limit Equilibrium Method of Slices," Canadian Geotechnical Journal, Vol. 10, No. 4, National Research Council Canada.

Daehn, W.W. and Hilf, J.W.; (1951), "Implications of Pore Pressure in Design and Construction of Rolled Earth Dams," International Congress on Large Dams, 4, Transactions, Vol. 1, New Delhi.

de Mello, V.F.B.; (1969), "Foundations of Buildings in Clay," Proceedings of the Seventh International Conference on Soil Mechanics and Foundation Engineering.

DeBeer, E.E.; and Ladanyi, B.; (1961), "Etude Experimentale de la Capacite Portante du Sable sous des Foudations Etablies en Surface," Proceedings of the 5th International Conference on Soil Mechanics and Foundation Engineering.

Drake, W.B. and Havens, J. H. ; (June 1959), "Kentucky Flexible Pavement Design Studies," Engineering Experiment Station Bulletin No. 52, University of Kentucky.

Feda, J.; (1961), "Research on the Bearing Capacity of Loose Soil," Proceedings of the 5th International Conference on Soil Mechanics and Foundation Engineering.

Fredlund, D.G.; (August 1985), "Soil Mechanics Principles that Embrace Unsaturated Soils," Proceedings of the Eleventh International Conference on Soil Mechanics and Foundation Engineering, San Francisco, California.

Fredlund, D.G.; and Rahardji, H.; (February 1985), "Theoretical Context for Understanding Unsaturated Residual Soil," First International Conference on Geomechanics in Tropical Lateritic and Saprolitic Soils, Brazilian Society for Soil Mechanics, Vol. 1.

Hammitt, G.M.; (1970), "Thickness Requirements for Unsurfaced Roads and Airfields -- Bare Base Support", Technical Report S-70-5, U.S. Army Engineer Waterways Experiment Station, Vicksburg,

Mississippi.

Hardin, B.O. and Hardin, K. O.; (September 1984), "A New Statically Consistent Formulation for Slope Stability Analysis," Proceedings of the IV International Symposium on Landslides.

Havens, J. H.; Deen, R. C.; and Southgate, H. F.; (August 1981), "Development of a Thickness Design Guide for Bituminous Concrete Pavement Structures," University of Kentucky Transportation Center, College of Engineering, Research Report UKTRP-81-17.

Heukelom, W.; and Klomp, A. J. G.; (1962), "Dynamic Testing as a Means of Controlling Pavements during and after Construction," Proceedings of International Conference on the Structural Design of Asphalt Pavements, Ann Arbor, Michigan.

Heukelom, W.; and Foster, C.R.; (February 1960), "Dynamic Testing of Pavements," ASCE Journal of the Structural Division, No. SM 1, 86.

Hopkins, T. C.; (January 1986); "A Generalized Slope Stability Computer Program: User's Guide for HOPK-I," Research Report UKTRP-86-2, University of Kentucky Transportation Center, College of Engineering.

Hopkins, T. C.; (1991). "Computer Program for Analysis of embankments with Tensile Elements," University of Kentucky Transportation Center, College of Engineering (Research Study in progress; publication pending).

Hopkins, T. C.; (January 1988), "Shear Strength of Compacted Shales," University of Kentucky Transportation Center, College of Engineering, Research report UKTRP-88-1.

Hopkins, T. C.; and Hunsucker, D.; (November 1990), "Interim Design Guidelines for Modified Pavements," University of Kentucky Transportation Center, College of Engineering (Interim Report in Progress).

Hopkins, T. C.; (October 1987); "Lime Stabilization of Kentucky Soils," University of Kentucky Transportation Center, College of Engineering, Oral presentation to the National Lime Conference, Lexington, Kentucky.

Hopkins, T. C.; (August 1984), "Relationship Between Kentucky CBR and Slake Durability", University of Kentucky Transportation Center, College of Engineering, Research Report UKTRP 84-24.

Hopkins, T. C. and Sharpe, G. W.; (March 1985) "Unstable Subgrade I 65, Hardin County (I 65-5(17)92); FSP 047-0065-091-094-0396", University of Kentucky Transportation Center, College of Engineering, Research Report UKTRP 85-9.

Hopkins, T. C. and Allen, D.L.; (October 1986), "Lime Stabilization of Pavement Subgrade Soils of Section AA-19 of the Alexandria-Ashland Highway," University of Kentucky Transportation Center, Research Report UKTRP 86-24.

Hopkins, T. C.; Hunsucker, D.; and Sharpe, G. W.; (1988), "Highway Field Trials of Chemically Stabilized Soil Subgrades, Proceedings of the Ohio River Valley Soils Seminar XIX, Lexington, Kentucky.

Hopkins, T. C.; (1970), Relationship Between Soil Support Value and Kentucky CBR," Research Report 297, Division of Research, Kentucky Department of Highways, Lexington, Kentucky.

Hopkins, T. C.; Hunsucker, D. Q.; and Sharpe, G. W.; (October 1988), "Highway Field Trials of Chemically Stabilized Soil Subgrades," Proceedings, Nineteenth Annual Ohio River Valley Soils Seminar (ORVSS), Lexington, Kentucky.

Hopkins, T. C.; Tollner, N. W.; and Phalzer, B.; (1991- publication pending; study in progress), "Geotechnical Engineering Data", University of Kentucky Transportation Center, College of Engineering.

Janbu, N.; (1954), "Application of Composite Slip Surface for Stability Analysis, European Conference on Stability of Earth Slopes," European Conference on Stability of Earth Slopes, Stockholm, Sweden.

Kentucky Methods Manual; (1987), Division of Materials, Kentucky Department of Highways, Frankfort, Kentucky.

Lambe, T. W.; and Whitman, R. V.; (1969), "Soil Mechanics," John Wiley and Sons, Inc., New York.

Lee, I. K.; White, W.; and Ingles, O. G.; (19), "Geotechnical Engineering," Pitman Publishing Company, Boston, Massachusetts.

McLeod, N. W.; (1953), "Some Basic Problems in Flexible - Pavement Design," Highway Research Board, Proceedings, Thirty-Second Annual Meeting.

Michelow, J.; (September 1963), "Analysis of Stresses and Displacements in an n-Layered Elastic System Under a Load Uniformly Distributed on a Circular Area," unpublished, California Research Corporation, Chevron Oil Company, Richmond, CA.

Morgenstern, N. R. and Price, V. E.; (1965), "The Analysis of the Stability of General Slip Surfaces", Geotechnique, Vol. 15.

Peattie, K. R.; (1965, "Discussion" on a paper presented by G.M. Dormon and C.T. Metcalf entitled "Design Curves for Flexible Pavements Based on Layered System Theory," Highway Research Record 71, Flexible Pavement Design 1963 and 1964, Highway Research Board; Washington, D.C.

Prandtl; (1921), "Hautaufsatze Uber die Eindringungsfestigkeit (Harte) plastischer Baustoffe und die Festigkeit von Schneiden," Zeitschrift Fur Angewandte, Mathematik und Mechanik, Vol. 1, No. 1.

Reissner, H.; (1924), Zum Erddruckproblem, Proceedings, First International Conference on Applied Mechanics, Delft.

Sharpe, G. W.; (July 1988), "Pavement Investigation, AA-Highway, Mason and Bracken Counties," Memorandum Report, University of Kentucky Transportation Center, College of Engineering,

Sharpe, G. W. and Deen, R. C.; (September 1987), "Pavement Failure, Ky 461, Pulaski County", Memorandum Report, University of Kentucky Transportation Center, College of Engineering.

Skempton, A.W.; (1954), "The Pore Pressure Coefficients A and B," *Geotechnique*, Vol. 4, No. 4.

Skempton, A.W.; (1964), "Long-Term Stability of Clay Slopes," *Geotechnique*, Vol. 14.

Smith, D.; (1989 -- Geotechnical Engineer, Division of Materials, Geotechnical Branch, Kentucky Department of Highways); Private communication concerning pavement subgrade problems in Kentucky.

Southgate, H. F. and Deen, R. C.; (1969), "Temperature Distribution Within Asphalt Pavements and Its Relationship to Pavement Deflection," Highway Research Board, HRB-291, Washington, D.C.

Southgate, H. F.; Deen, R. C.; and Havens, J. H.; (November 1981), "Development of a Thickness Design System for Bituminous Concrete Pavements," University of Kentucky Transportation Center, College of Engineering, Research Report UKTRP-81-20.

Southgate, H. F.; Sharpe, G. W.; Deen, R. C.; and Havens, J. H.; (August 1982), "Structural Capacity of In-Place Asphaltic Pavements from Dynamic Deflections," Fifth International Conference on the Structural Design of Asphalt Pavements, Proceedings, Vol. 1, The Delft University of Technology, The Netherlands.

Southgate, H. F. and Deen, R. C.; (1975), "Temperature Distributions in Asphaltic Concrete Pavements," TRB-549, Transportation Research Board, Washington, D.C.

Spencer, E.; (1967), "A Method of Analysis of the Stability of Embankments Assuming Parallel Inter-Slice Forces," *Geotechnique*, Vol 17.

Spencer, E.; (1973), "Thrust Line Criterion in Embankment Stability Analysis", *Geotechnique*, Vol. 23.

Taylor, D. W.; (1948), "Fundamentals of Soil Mechanics," John Wiley and Sons, Inc., New York.

Terrel, R. L.; Epps, J. A.; Barenberg, E. J.; Mitchell, J. K.; and Thompson, M. R.; (1979), "Soil Stabilization in Pavement Structures -- A users Manual," FHWA-IP-80-1, Department of Transportation, Federal Highway Administration, Washington, D.C. (Volumes 1 and 2).

Terzaghi, K.; (1943), "Theoretical Soil Mechanics," John Wiley and Sons, Incorporated, New York, NY.

The AASHO Road Test (May 1962), Proceedings, Special Report 73, Publication No. 1012, National Academy of Sciences - National Research Council, Washington, D.C.

Thompson, M. R.; (October 1988), "Admixture Stabilization of Subgrades", *Proceedings, Nineteenth Annual Ohio River Valley Soils Seminar (ORVSS)*, Lexington, Kentucky.

Traylor, M.L. and Thompson, M. R.; (1977), "Sinkage Prediction-Subgrade Stability," *Civil Engineering Studies, Transportation Engineering Studies, Transportation Engineering Series No. 17, Illinois Cooperative Highway and Transportation Series No. 168, Department of Civil Engineering, University of Illinois at Urbana-Champaign.*

TRB Committee Number 2B05 on Strength and Deformation Characteristics of Pavement Sections; (September 1990), "Research Problem Statements; Design and Construction of Transportation Facilities," Problem Statement Number 81, Transportation Research Board/National Research Council, Number 363.

Vesic', A.S. and Johnson, W. H.; (1963), "Model Studies of Beams Resting on a Silt subgrade," *Proceedings, ASCE Journal of the Soil Mechanics and Foundations Division*, 89, No. SM1.

Vesic', A.S. and Saxena, S. K.; (1970), "Analysis of Structural Behavior of AASHO Road Test Rigid Pavements," Report 97, National Cooperative Highway Research Program, National Academy of Science, Washington, D.C.

Winterhorn, H. F. and Fang, H. Y.; (1975), *Foundation Engineering Handbook*, Von Nostrand Reinhold Company, New York.

Yoder, E. J.; and Witczak, M. W.; (1975), "Principles of Pavement Design," Second Edition, John Wiley and Sons, Inc., New York.

Yoder, E. J.; (1969), "Selection of Soil Strength Values for the Design of Flexible Pavements," *Highway Research Record* 276.

APPENDIX A

**SUMMARY OF FACTORS OF SAFETY
OF PAVEMENT SECTIONS OF THE
AASHO ROAD TEST (1962)**

Table 1A. Summary of AASHO Road Test Data for Loop 3 (Flexible Pavement) Lane 1 and 2 and 12-kip Load Applications

Stress = 65.7 psi					CBR = 2.7			
Section Number	THICKNESS OF PAVEMENT				Ratio of AC/Total	12-Kip Load	F. S. * (140 deg)	F. S. ** (77 deg)
	Total 1 (in.)	A.C. (in.)	Base (in.)	Subbase (in.)				
107	10	3	3	4	.300	89578	.969	1.250
109	11	3	0	8	.273	101054	1.008	1.285
111	16	2	6	8	.125	728448	1.196	1.374
113	5	2	3	0	.400	69576	.625	0.959
115	10	3	3	4	.300	89578	.969	1.250
117	9	3	6	0	.333	89578	.93	1.226
119	4	4	0	0	1.000	78434	.875	1.294
121	15	4	3	8	.267	623094	1.235	1.587
123	14	4	6	4	.286	1103300	1.191	1.518
125	6	2	0	4	.333	5356	.661	0.978
127	8	2	6	0	.250	77502	.743	1.046
129	14	3	3	8	.214	568022	1.142	1.414
131	13	3	6	4	.231	598804	1.902	1.353
133	10	2	0	8	.200	77502	.909	1.107
135	9	2	3	4	.222	73270	.799	1.068
137	3	3	0	0	1.000	77502	.639	1.105
139	18	4	6	8	.222	1103300	1.374	1.731
141	8	4	0	4	.500	79512	.874	1.349
143	10	2	0	8	.200	71492	.909	1.107
145	7	4	3	0	.571	82856	.933	1.333
147	6	3	3	0	.500	72616	.725	1.149
149	10	4	6	0	.400	108396	1.039	1.396
151	11	4	3	4	.364	108396	1.067	1.431
153	12	4	0	8	.333	108396	1.113	1.469
155	17	3	6	8	.176	1103300	1.271	1.551
157	12	2	6	4	.167	93240	.993	1.189
159	13	2	3	8	.154	90718	1.041	1.228
161	10	4	6	0	.400	180876	1.039	1.396
163	7	3	0	4	.429	89578	.856	1.156
165	2	2	0	0	1.000	69576	.533	0.964

Table 2A. Summary of AASHO Road Test Data for Loop 4 (Flexible Pavement), Lane 1 and 18-lip Load Applications

STRESS = 67.5 psi		CBR = 3.7						
Section Number	THICKNESS OF PAVEMENT				Ratio of AC/Total	18 Kip Load (100's)	F. S. * (140 deg)	F. S. ** (77 deg)
	Total (in.)	A.C. (in.)	Base (in.)	Subbase (in.)				
569	15	3	0	12	.200	1143	1.152	1.381
571	15	3	0	12	.200	852	1.152	1.381
573	14	3	3	8	.214	845	1.129	1.335
575	19	4	3	12	.211	11109	1.387	1.654
577	18	4	6	8	.222	11027	1.347	1.584
579	12	5	3	4	.417	1320	1.180	1.509
581	23	5	6	12	.217	11027	1.623	1.903
583	8	4	0	4	.500	787	0.992	1.293
585	13	3	6	4	.231	806	1.087	1.319
587	13	5	0	8	.385	1123	1.196	1.533
589	15	4	3	8	.267	985	1.206	1.495
591	19	5	6	8	.263	11027	1.426	1.722
593	20	5	3	12	.250	5992	1.461	1.766
595	14	4	6	4	.286	957	1.177	1.438
597	15	4	3	8	.267	1128	1.206	1.495
599	10	3	3	4	.300	752	0.995	1.214
601	21	3	6	12	.143	11027	1.418	1.609
603	16	4	0	12	.250	4452	1.243	1.521
605	9	5	0	4	.556	944	1.092	1.431
607	11	3	0	8	.273	740	1.022	1.245
615	15	5	6	4	.333	6216	1.277	1.576
617	18	3	3	12	.167	5888	1.299	1.473
619	12	4	0	8	.333	1073	1.119	1.384
621	17	5	0	12	.294	6853	1.357	1.667
623	17	3	6	8	.176	976	1.257	1.460
625	22	4	6	12	.182	11027	1.519	1.752
627	11	4	3	4	.364	885	1.075	1.359
629	15	5	6	4	.333	6479	1.277	1.576
631	16	5	3	8	.313	5914	1.298	1.627
633	7	3	0	4	.429	26	0.845	1.142
570	15	3	0	12	.200	1140	1.152	1.381

Table 3A. Summary of AASHO Road Test Data for Loop 4 (Flexible Pavement), Lane 2 and 32-kip Load Applications

Stress = 69.5 psi					CBR = 3.7			
Section Number	THICKNESS OF PAVEMENT				Ratio of AC/Total	32-Kip Load (100's)	F. S. *	F. S. **
	Total (in.)	A.C. (in.)	Base (in.)	Subbase (in.)			(140 deg)	(77 deg)
570	15	3	0	12	.200	1140	1.218	1.437
572	15	3	0	12	.200	1066	1.218	1.437
574	14	3	3	8	.214	872	1.165	1.420
576	19	4	3	12	.211	8005	1.471	1.726
578	18	4	6	8	.222	11025	1.395	1.659
580	12	5	3	4	.417	1532	1.211	1.571
582	23	5	6	12	.217	11025	1.715	2.016
584	8	4	0	4	.500	859	1.026	1.327
586	13	3	6	4	.231	832	1.128	1.372
588	13	5	0	8	.385	1311	1.242	1.598
590	15	4	3	8	.267	1532	1.268	1.563
592	19	5	6	8	.263	11025	1.527	1.827
594	20	5	3	12	.250	11025	1.552	1.876
596	14	4	6	4	.286	1201	1.215	1.494
598	15	4	3	8	.267	1404	1.268	1.563
600	10	3	3	4	.300	756	1.017	1.274
602	21	3	6	12	.143	6186	1.511	1.725
606	9	5	0	4	.556	1049	1.125	1.494
608	11	3	0	8	.273	756	1.056	1.312
616	15	5	6	4	.333	6243	1.327	1.640
618	18	3	3	12	.167	5995	1.345	1.553
620	12	4	0	8	.333	1049	1.153	1.441
622	17	5	0	12	.294	8534	1.422	1.752
624	17	3	6	8	.176	5849	1.308	1.526
626	22	4	6	12	.182	11025	1.617	1.864
628	11	4	3	4	.364	913	1.114	1.420
630	15	5	6	4	.333	7349	1.327	1.640
632	16	5	3	8	.313	7542	1.383	1.720
634	7	3	0	4	.429	139	0.938	1.190

Table 4A. Summary of AASHO Road Test Data for Loop 5 (Flexible Pavement), Lane 1 and 22.4-kip Load Applications

Stress = 66.4 psi					CBR = 3			
Section Number	THICKNESS OF PAVEMENT				Ratio of AC/Total	22.4-kip Load (100's)	F. S. * (140 deg)	F. S. ** (77 deg)
	Total (in.)	A.C. (in.)	Base (in.)	Subbase (inc.)				
411	11	4	3	4	.364	707	.802	1.143
413	16	3	9	4	.188	839	.915	1.183
415	18	3	3	12	.167	897	1.04	1.234
417	21	4	9	8	.190	4956	1.183	1.414
419	17	3	6	8	.176	761	1.008	1.211
421	16	5	3	8	.313	1065	1.076	1.38
423	15	5	6	4	.333	1004	1.055	1.337
425	22	4	6	12	.182	6257	1.248	1.461
427	26	5	9	12	.192	11010	1.446	1.704
429	18	3	3	12	.167	772	1.04	1.234
437	17	4	9	4	.235	1015	1.056	1.293
439	12	5	3	4	.417	785	.972	1.274
441	24	3	9	12	.125	11010	1.287	1.444
443	19	4	3	12	.211	1037	1.114	1.378
445	23	5	6	12	.217	11010	1.316	1.555
449	13	3	6	4	.231	755	.891	1.098
451	14	3	3	8	.214	738	.93	1.127
453	18	4	6	8	.222	1015	1.09	1.328
469	19	5	6	8	.263	6514	1.185	1.443
471	20	3	9	8	.150	940	1.136	1.295
473	14	4	6	4	.286	817	.972	1.216
475	18	5	9	4	.278	6360	1.138	1.419
477	25	4	9	12	.160	11010	1.338	1.583
479	20	5	3	12	.250	7552	1.206	1.462
481	15	4	3	8	.267	846	1.005	1.252
483	18	5	9	4	.278	6149	1.138	1.419
485	10	3	3	4	.300	700	.826	1.025
487	21	3	6	12	.143	4451	1.147	1.339

Table 5A. Summary of AASHO Road Test data for Loop 5 (Flexible Pavement), Lane 2 and 40-kip Load Applications

Stress = 66.4 psi					CBR = 3			
Section Number	THICKNESS OF PAVEMENT				Ratio of AC/Total	40-kip Load (100's)	F. S. * (140 deg)	F. S. ** (77 deg)
	Total (in.)	A.C. (in.)	Base (in.)	Subbase (in.)				
412	11	4	3	4	.364	661	.802	1.143
414	16	3	9	4	.188	843	.915	1.183
416	18	3	3	12	.167	1075	1.04	1.234
418	21	4	9	8	.190	4089	1.183	1.414
420	17	3	6	8	.176	777	1.008	1.211
422	16	5	3	8	.313	1303	1.076	1.38
424	15	5	6	4	.333	1164	1.055	1.337
426	22	4	6	12	.182	5698	1.248	1.461
428	26	5	9	12	.192	10936	1.446	1.704
430	18	3	3	12	.167	843	1.04	1.234
438	17	4	9	4	.235	1164	1.056	1.293
440	12	5	3	4	.417	957	.972	1.274
442	24	3	9	12	.125	6547	1.287	1.444
444	19	4	3	12	.211	1015	1.114	1.378
446	23	5	6	12	.217	10936	1.316	1.555
448	22	5	9	8	.227	10936	1.274	1.554
450	13	3	6	4	.231	767	.891	1.098
452	14	3	3	8	.214	750	.93	1.127
454	18	4	6	8	.222	5862	1.09	1.328
470	19	5	6	8	.150	1045	1.136	1.295
472	20	3	9	8	.150	1045	1.136	1.295
474	14	4	6	4	.286	861	.972	1.216
476	10	5	9	4	.278	6270	1.138	1.419
478	25	4	9	12	.160	10936	1.338	1.583
480	20	5	3	12	.250	10936	1.206	1.462
482	15	4	3	8	.267	861	1.005	1.252
484	18	5	9	4	.278	6254	1.138	1.419
486	10	3	3	4	.300	50	.826	1.025
488	21	3	6	12	.143	5862	1.147	1.339

Note: * 140 Deg. ----> Top Pavement

** 77 Deg. ----> Throughout Pavement

Table 6A. Summary of AASHO Road Test Data for Loop 6 (Flexible Pavement), Lane 1 and 2 and 48-kip Load Applications

Stress = 68.8 psi					CBR = 3.9				
Section Number	THICKNESS OF PAVEMENT				Ratio of AC/Total	48-kip Load (100's)	F. S. * (140 deg)	F. S. ** (77 deg)	Elapsed Time (days)
	Total (in.)	A.C. (in.)	Base (in.)	Subbase (in.)					
253	26	4	6	16	.154	6105	1.519	1.678	163
255	25	6	3	16	.240	10788	1.537	1.215	755
257	24	6	6	12	.250	10788	1.482	1.740	755
259	19	5	6	8	.263	1041	1.269	1.531	183
261	20	5	3	12	.250	4127	1.294	1.548	438
263	23	6	9	8	.261	10788	1.435	1.737	755
265	30	5	9	16	.167	10788	1.701	1.916	755
267	25	4	9	12	.160	7250	1.455	1.640	576
269	15	4	3	8	.267	823	1.093	1.315	147
271	23	6	9	8	.261	10788	1.435	1.737	755
297	17	6	3	8	.353	5754	1.240	1.554	513
299	19	4	3	12	.211	5694	1.226	1.411	513
301	28	6	6	16	.214	10788	1.645	1.923	755
303	18	4	6	8	.222	3814	1.120	1.409	417
305	23	5	6	12	.217	6352	1.417	1.648	539
307	23	5	6	12	.217	5908	1.417	1.648	524
309	29	4	9	16	.138	10788	1.621	1.838	755
311	27	6	9	12	.222	10788	1.622	1.888	755
313	22	5	9	8	.227	6174	1.352	1.586	529
315	24	5	3	16	.208	6402	1.456	1.688	544
317	23	4	3	16	.174	6079	1.379	1.558	526
319	16	5	3	8	.313	1068	1.166	1.429	178
321	21	4	9	8	.190	1572	1.293	1.489	237
323	22	4	6	12	.182	1015	1.330	1.549	176
325	20	6	6	8	.300	2663	1.331	1.623	329
327	27	5	6	16	.185	7980	1.589	1.786	605
329	23	4	3	16	.174	1041	1.379	1.558	183
331	26	5	9	12	.192	7162	1.536	1.767	572
333	31	6	9	16	.194	10788	1.777	2.101	755
335	21	6	3	12	.286	4973	1.388	1.658	479

Note: * 140 Deg. ----> Top Pavement

** 77 Deg. ----> Throughout Pavement

Table 7A. Summary of AASHO Road Test Data for Loop 6 (Flexible Pavement) Lane 1 and 2 and 48-kip Load Applications

Stress = 69.8 psi					CBR = 3.9				
	THICKNESS OF PAVEMENT								
Section Number	Total (in.)	A.C. (in.)	Base (in.)	Subbase (in.)	Ratio of AC/Total	48-kip Load (100's)	F. S. * (140 deg)	F. S. ** (77 deg)	Elapsed Time (days)
254	26	4	6	16	.154	6105	1.519	1.678	163
256	25	6	3	16	.240	10788	1.537	1.815	755
258	24	6	6	12	.250	10788	1.482	1.740	755
260	19	5	6	8	.263	1041	1.269	1.531	183
262	20	5	3	12	.250	4127	1.294	1.548	438
264	23	6	9	8	.261	10788	1.435	1.737	755
266	30	5	9	16	.167	10788	1.701	1.916	755
268	25	4	9	12	.160	7250	1.455	1.640	576
270	15	4	3	8	.267	823	1.093	1.315	147
272	23	6	9	8	.261	10788	1.535	1.737	755
298	17	6	3	8	.353	5754	1.240	1.554	513
300	19	4	3	12	.211	5694	1.226	1.411	513
302	28	6	6	16	.214	10788	1.645	1.923	755
304	18	4	6	8	.222	3814	1.120	1.409	417
306	23	5	6	12	.217	6352	1.417	1.648	539
308	23	5	6	12	.217	5908	1.471	1.648	524
310	29	4	9	16	.318	10788	1.621	1.838	755
312	27	6	9	12	.222	10788	1.622	1.888	755
314	22	5	9	8	.227	6174	1.352	1.586	529
316	24	5	3	16	.208	6402	1.456	1.688	544
318	23	4	3	16	.174	6079	1.379	1.558	526
320	16	5	3	8	.313	1068	1.166	1.429	178
322	21	4	9	8	.190	1572	1.293	1.489	237
324	22	4	6	12	.182	1015	1.330	1.549	176
326	20	6	6	8	.300	2663	1.331	1.623	329
328	27	5	6	16	.185	7980	1.589	1.786	605
330	23	4	3	16	.174	1041	1.379	1.558	183
332	26	5	9	12	.192	7162	1.536	1.767	572
334	31	6	9	16	.194	10788	1.777	2.010	755
336	21	6	3	23	.286	4973	1.388	1.658	479

Note: * 140 Deg. ----> Top Pavement

** 77 Deg. ----> Throughout Pavement